



**Targeting the phosphatidylinositol-3-kinase (PI3K) and
mitogen-activated protein kinase (MAPK) pathways to
enhance chemoradiotherapy responsiveness in colorectal
cancer.**

Aoife Carr, BSc

Department of Medical Oncology

**A thesis submitted to the School of Postgraduate Studies, Faculty of
Medicine and Health Sciences, Royal College of Surgeons in Ireland, in
fulfilment of the degree of Doctor of Philosophy**

May 2020

**Supervisors: Prof. Bryan Hennessy,
Dr. Sinead Toomey,
Dr. Simon Furney,
Prof. Elaine Kay,
Dr. Brian O'Neill**

Candidate Thesis Declaration

I declare that this thesis, which I submit to RCSI for examination in consideration of the award of a higher degree of Doctor of Philosophy, is my own personal effort. Where any of the content presented is the result of input or data from a related collaborative research programme this is duly acknowledged in the text such that it is possible to ascertain how much of the work is my own. I have not already obtained a degree in RCSI or elsewhere on the basis of this work. Furthermore, I took reasonable care to ensure that the work is original, and, to the best of my knowledge, does not breach copyright law, and has not been taken from other sources except where such work has been cited and acknowledged within the text.

Signed  (Aoife Carr)

Student number 14130521

Date 2020

Table of contents

Chapter 1 Introduction	33
1.1. Colon and rectum: An overview.	34
1.2. Histology	34
1.2.1. Mucosa	34
1.2.2. Submucosa	36
1.2.3. Muscularis externa / propria	36
1.2.4. Serosa/adventitia	36
1.2.5. Recto-anal junction	36
1.3. Colorectal cancer	37
1.3.1. Colorectal polyps	37
1.3.2. Polyp formation	38
1.3.3. Symptoms of colorectal cancer	38
1.3.4. Testing for colorectal cancer	38
1.3.5. Staging and differentiation of colorectal cancer	39
1.3.6. Treatment	40
<i>Chemotherapy</i>	41
<i>Radiation therapy</i>	41
<i>Surgery: Total mesorectal excision (TME)</i>	43
1.3.7. How radiation affects cellular survival	43
1.3.8. Radiation resistance	43
1.3.9. Radiation resistance and the hallmarks of cancer	43
1.3.10. The role of the immune system in cancer	47
1.3.11. Recurrences	47
1.3.12. Survival	48
1.4. Circulating tumour cells and their role in tumour metastasis	49
1.5. Human genome	51
1.5.1 Structure of DNA	51
1.5.2. Transcription and translation of DNA	52
1.6. Mutations in the human genome	54

1.6.1. Point mutations	54
1.6.2. Transition and Transversion point mutations.....	55
1.6.3. Frameshift mutations	55
1.7. The role of genomic aberrations and the mutator phenotype in the development of CRC.	57
1.7.1. Chromosomal instability (CIN)	58
1.7.2. Mismatch repair (MMR)	58
1.7.3. CpG Island Methylator Phenotype (CIMP) pathway	60
1.7.4. Causes of DNA damage	61
1.8. Mutational signatures	65
1.9. The role of the PI3K and MAPK signalling pathways in cancer	69
1.9.1. PI3K signalling pathway.....	69
PIK3CA.....	70
1.9.2. Mutations in PI3K / MAPK pathways.....	73
1.9.3. PI3K pathway mutations	73
1.9.4. The MAPK signalling pathway.....	74
1.9.5. MAPK pathway mutations.....	75
1.9.6. Co-occurrence of PI3K/MAPK pathway mutations.	77
1.10. Inhibition of the PI3K and MAPK pathways.....	78
1.10 .1. Copanlisib / BAY80-6946 / Aliqopa	78
1.10.2. Refametinib / BAY86-9766 / RDEA119	81
Aims	82
Chapter 2 Materials and methods.....	83
2.1. Materials and methods utilised in aim 1 to determine the full spectrum of somatic genetic aberrations that activates the PI3K and related signalling pathways in LARC and how they are modulated by treatment.....	84
2.1.1. Human rectal cancer tumour samples.....	84
2.1.2. DNA extraction from normal and tumour samples.....	85
2.1.3. Whole exome sequencing.....	86
2.1.4. DNA quantification	86
2.1.5. Determination of quality of DNA.....	87

2.1.6. Whole-exome sequencing	89
2.2.1. TRI-LARC (ICORG 12-38) clinical trial	90
<i>Inclusion criteria</i>	90
<i>Exclusion criteria</i>	91
<i>Treatment regimens</i>	91
2.2.2. Blood collection.....	92
2.2.3. Processing of plasma samples	94
2.2.4. Tumour tissue collection	94
2.2.5. Whole blood for circulating tumour cell (CTC) analysis	95
<i>Histological staining of ScreenCell filters</i>	97
<i>Identification of circulating tumour cells</i>	97
<i>Statistical analysis</i>	97
2.3. Materials and methods utilised in aim 3 to determine if in-vitro inhibition of the PI3K and related kinase signalling pathways augments rectal cancer chemoradiotherapy sensitivity.....	98
2.3.1. Colorectal cancer cell lines	100
2.3.2. Proliferation assays	102
<i>Statistics</i>	103
2.3.3. Clonogenic assays.....	104
2.3.4. Optimisation of clonogenic cell volume	104
2.3.5. Colony fixation and crystal violet staining technique	104
2.3.6. Quantification of cellular growth in clonogenic assays	105
2.3.7. Optimisation of drug concentrations.....	105
2.4. Materials and methods utilised in aim 4 to determine in vivo if inhibition of the PI3K and related kinase signalling pathways augments the chemoradiotherapy sensitivity of genetically defined rectal cancer models.	110
2.4.1. In vivo training	111
2.4.2. Husbandry	111
2.4.3. Preparation of cells for subcutaneous implantation	111
2.4.4. Subcutaneous implantation of tumour cells.....	112
2.4.5. Monitoring of mice	112

2.4.6. Drug treatments for mice	113
2.4.7. Intravenous injection	114
2.4.8. Intraperitoneal mouse injection.	114
2.4.9. Radiation of mice	115
2.4.10. Culling of mice	116
2.4.11. Harvesting organs.....	116
2.4.12. Processing of organs	117
2.4.13. Haematoxylin and eosin staining:	118
Chapter 3 To determine the full spectrum of somatic genetic aberrations that activates the PI3K and related signalling pathways in LARC and how they are modulated by treatment.	120
3.1. Introduction.....	121
3.1.1. Mutations within the human genome.....	121
3.1.2. Oncogenic pathways associated with colorectal cancer	121
3.1.3. Mutations within the PI3K and MAPK pathways.....	122
3.2. Results:.....	124
3.2.1. Whole exome sequencing study from an Irish cohort of LARC patients.	124
3.2.2. Mutational frequency of synonymous and non-synonymous, somatic mutations in pre-treatment LARC biopsy samples	129
3.2.3. Genes most commonly mutated in our LARC sample cohort	135
3.2.4. Somatic mutations in pre-treatment LARC biopsies associated with response to NACRT	136
3.2.5. Heterogeneity in tumour samples using variant allele frequency.....	139
3.2.6. Mutational signatures.....	143
3.3. Whole exome sequencing study from an American cohort of LARC patients. 144	
3.3.1. Mutational frequency of synonymous and non-synonymous, somatic mutations in pre-treatment LARC biopsy samples	148
3.3.2. Genes most commonly mutated in our LARC sample cohort	154
3.3.3. Somatic mutations in pre-treatment LARC biopsies associated with response to NACRT	156
3.3.4. Intra-tumour heterogeneity in pre-treatment biopsies from LARC patients ...	159

3.3.5. Mutational signatures.....	167
3.3.6. Mutations of interest from pre-treatment LARC samples	168
3.4. Discussion	169
3.4.1. Tumour mutational burden.....	169
3.4.2. PI3K/MAPK pathway mutations	171
3.4.3. Most commonly mutated genes	173
3.4.4. Mutations associated with patient response to NACRT	175
3.4.5. Heterogeneity	177
3.4.6. Mutational signatures.....	177
Chapter 4 To determine the impact of neoadjuvant chemoradiotherapy on circulating tumour DNA and circulating tumour cells as potential biomarkers of treatment response in LARC patients	178
4.1. Introduction.....	179
4.1.1. Tumour metastasis as a result of circulating tumour cells	179
4.1.2. Circulating tumour cells.....	179
4.1.3. Isolation and identification of circulating tumour cells from peripheral blood.	180
4.1.4. Circulating tumour DNA (ctDNA).....	180
4.2. Results.....	182
4.2.1. Clinicopathological characteristics of TRILARC study population.....	182
4.2.2. Increased volumes of circulating rectal tumour cells are shed into the periphery during neoadjuvant chemoradiation therapy.....	186
4.2.3. Mutations in rectal tumours and matched ctDNA	193
4.2.4. Mutational variations between pre-treatment and post-chemoradiation therapy surgical specimens isolated from ctDNA and tumour tissue samples from LARC patients.....	196
4.2.5. Intra-tumour mutational alterations as a result of NACRT treatment	200
4.2.6. Mutational characteristics identified in metastatic LARC patients.....	203
4.3. Discussion	208
Chapter 5 Determination in-vitro if inhibition of the PI3K and MAPK signalling pathways augments rectal cancer chemoradiotherapy sensitivity.	212
5.1. Introduction.....	213
5.1.1. Current treatment of colorectal cancer	213

5.1.2. Chemoradiotherapy resistance within colorectal cancer patients	213
5.1.3. PI3K pathway mutations associated with colorectal cancer	213
5.1.4. PI3K inhibitor, Copanlisib	214
5.1.5. MAPK pathway mutations associated with colorectal cancer	214
5.1.6. MEK inhibitor, Refametinib	215
5.1.7. Copanlisib and Refametinib targeting the PI3K and MAPK pathways.	215
5.2. CRC cell line anti-proliferative response to copanlisib and/or refametinib in vitro is dependent on their PI3K and MAPK pathway mutational status.	220
5.2.2. Determination of copanlisib and refametinib sensitivity in a panel of colorectal cancer cell lines via MTS proliferation assays.....	222
5.2.3 PI3K and MAPK pathway mutations determine the anti-proliferative abilities of copanlisib, refametinib and 5-FU chemotherapy in CRC cell lines in clonogenic assays.	230
5.2.4. Copanlisib and refametinib used together as a standard of care for locally advanced rectal cancer increase the chemoradiation sensitivity of colorectal cancer (CRC) cell lines with PI3K and MAPK pathway mutations in clonogenic assays.	235
5.3. Discussion.....	243
Chapter 6 Inhibition of the PI3K signalling pathway increases chemoradiotherapy sensitivity of genetically defined colorectal cancer mouse models.	247
6.1. Introduction	248
6.1.1. Overview.....	248
6.1.2. PI3K inhibitor, Copanlisib.....	248
6.1.3. Our preliminary in vitro study (chapter 5)	248
6.1.4. Previous in vivo studies of copanlisib.....	249
6.1.5. Clinical trials involving copanlisib	249
6.2. Results.....	251
6.2.1 Colorectal cancer response to treatment in vivo is dependent on the mutational status of the tumour.	251
6.2.2. Effects of treatment on survival in xenograft models	256
6.2.3. Tolerability of copanlisib chemoradiotherapy in vivo.	265
6.2.4. Macroscopic variability between tumours based on their mutational status and treatment regimens.....	270

6.2.5. Microscopic variability between tumours based on their mutational status and treatment regimens.....	277
6.3. Discussion	286
6.4. Overview of results chapters.....	289
Discussion	290
Future directions.....	300
References	302
Appendices.....	331

Abbreviations

#

3D-CRT: 3-D Chemoradiation Therapy

5-FU: 5-Fluorouracil

A

A: Adenine

AFAP: Attenuated Familial Adenomatous Polyposis

AJCC: American Joint Committee on Cancer

AKT: Protein Kinase B

APC: Adenomatous polyposis coli

ARF: ADP ribosylation factor

ASH1L: ASH 1 like Histone Lysine Methyltransferase

ASPA: Animals Scientific Procedures Act

ATCC: American Type Culture Collection

B

Bad: Bcl-2-Associated Death Promoter

BALB/C: Bagg Albino

Bax: Bcl-2-Like Protein 4

BCL10: B cell lymphoma/leukaemia 10

BIRC6: Baculoviral IAP Repeat Containing 6

BSA: Bovine serum albumin

C

C: Cytosine

CACNA1I: Calcium Voltage-Gated Channel Subunit Alpha1 I

CACNA2D3: Calcium Voltage-Gated Channel Auxiliary Subunit Alpha2 Delta3

CBCT: Cone Beam Computed tomography

CCDC141: Coiled-Coil Domain Containing 141

CEA: Carcinoembryonic Antigen

CEP112: Centrosomal Protein 112

CIMP: CpG Island Methylator Phenotype

CIN: Cervical intraepithelial neoplasia

COL27A1: Collagen type XXVII Alpha 1 Chain

CR: Conserved region

CRC: Colorectal cancer

CREB: cAMP Response Element Binding

CRM: Circumferential Resection Margin

CRT: Chemoradiotherapy

CT: Computed tomography

CTC: Circulating Tumour Cell

CTNNB1: Catenin beta 1

D

DCC: Deleted in colorectal cancer

DDX23: DEAD-box helicase 23

DMEM: Dulbecco's Modified Eagle's Medium

DMMR: Defective MMR

DMSO: Dimethylsulfoxide

DNA: Deoxyribonucleic acid

DRE: Digital Rectal Exam

DRIM: Down Regulated In Metastasis

DSMZ: Deutsche Sammlung Von Mikroorganismen und Zellkulturen

E

ECOG: Eastern Cooperative Oncology Group (ECOG)

EDTA: Ethylenediaminetetraacetic acid

EGFR: Epidermal Growth Factor Receptor

EMEM: Eagle's Minimum Essential Medium

EpCAM: Epithelial Cell Adhesion Molecule

ERK: Extracellular Signal-regulated Kinase

F

FAP: Familial Adenomatous Polyposis

FBC: Full blood count

FBS: Foetal Bovine Serum

FBXW7: F-box and WD repeat domain containing 7

FC2: ScreenCell fixed cells dilution buffer

FDR: False Discovery Rate

FF: Fresh Frozen

FFPE: Formalin-Fixed Paraffin-Embedded

G

G: Guanine

GABRD: Gamma-Aminobutyric Acid Type A Receptor Delta Subunit

GALT: Gut-associated lymphoid tissue

GAP: GTPase activating protein

GDP: Guanosine-5'-diphosphate

GEF: Guanine Nucleotide Exchange Factor

Grb2: Growth Factor Receptor-Bound Protein 2

GTP: Guanosine-5'-triphosphate

Gy: Gray

H

H&E: Haematoxylin and Eosin

HCl: Hydrochloric acid

Hmlh1: Human mutL homolog 1

HNPCC: Hereditary Nonpolyposis Colorectal Cancer

I

IBD: Inflammatory bowel disease

IBS: Irritable Bowel Syndrome

ICGC: International Cancer Genome Consortium

ICH-GCP: International Conference on Harmonisation – Good Clinical Practice

ICORG: All-Ireland Cooperative Oncology Research Group

IGRT: Image-Guided Radiation Therapy

IMRT: Intensity-Modulated Radiation Therapy

IP: Intra-peritoneal

IRS1: Insulin receptor substrate 1

iSH2: Inter-SH2

IV: Intravenous

K

KCLB: Korean Cell line Bank

KCNA3: Potassium Voltage-Gated Channel Subfamily A Member 3

KDR: Kappa Delta Rho

KRAS: Kirsten Rat Sarcoma

L

LAMA1: Laminin Subunit Alpha 1

LAMA5: Laminin Subunit Alpha 5

LARC: Locally Advanced Rectal Cancer

LFT: Liver Function Test

LINAC: Linear Accelerator

LOH: Loss of heterozygosity

M

MAP: MYH-Associated Polyposis

MAPK: Mitogen-activated protein kinase

MAN1B1: Mannosidase Alpha Class 1B Member 1

MEK: Mitogen-Activated Protein Kinase Kinase

MgCl₂: Magnesium chloride

MGMT: O-6-Methylguanine-DNA Methyltransferase

MiRNA: MicroRNA

MLH1: MutL homolog 1

MLH3: MutL homolog 3

mM: Millimolar

MMR: Mismatch Repair

MRI: Magnetic Resonance Imaging

mRNA: Messenger RNA (ribonucleic acid)

MSH2: MutS protein homolog 2

MSH3: MutS Homolog 3

MSH5: MutS Homolog 5

MSH5-SAPCD1: MutS Homolog 5 – Suppressor APC Domain-Containing Protein
1 read-through

MSH6: MutS homolog 6

MSI: Microsatellite instable

MTM-1: Myotubularin 1 gene
mTOR: Mammalian Target Of Rapamycin
MUC16: Mucin 16
MUC20: Mucin 20
MutL: Mutator L
MutS: Mutator S
MV: Megavoltage
MXRA5: Matric Remodelling Associated 5
Myc: Avian Myelocytosis Viral Oncogene Homolog
MYH: Myosin heavy chain
MYO6: Myosin VI

N

NA 3V04: Sodium orthovanadate
NaCl: Sodium chloride
NACRT: Neoadjuvant Chemoradiation Therapy
NADH: Nicotinamide adenine dinucleotide
NADPH: Nicotinamide adenine dinucleotide phosphate
NCRI: National Cancer Registry Ireland
NF- κ B: Nuclear Factor-Kappa B
NFW: Nuclease-free water
nM: Nanomolar
NRAS: Neuroblastoma RAS Viral Oncogene
NUP155: Nucleoporin 155

P

PADI3: Peptidyl arginine deiminase 3
PBS: Phosphate buffered saline
PCDHA12: Protocadherin Alpha-12
PCNA: Proliferating cell nuclear antigen
pCR: Pathological Complete Response
PCR: Polymerase Chain Reaction
PDS5B: PDS5 Cohesion Associated Factor B
PEG3: Paternally Expressed Gene 3
PEG400: Polyethylene glycol 400

PEN/STREP: Penicillin/Streptomycin

PET: Positron Emission Tomography

PHLPP: PH Domain and Leucine Repeat Protein Phosphatase

PI3K: Phosphatidylinositol 3 Kinase

PIK3CA: Phosphatidylinositol-4, 5-Bisphosphate 3-Kinase Catalytic Subunit Alpha

PIK3CB: Phosphatidylinositol-4, 5-Bisphosphate 3-Kinase Catalytic Subunit beta

PIK3CD: Phosphatidylinositol-4, 5-Bisphosphate 3-Kinase Catalytic Subunit delta

PIK3CG: Phosphatidylinositol-4, 5-Bisphosphate 3-Kinase Catalytic Subunit
gamma

PIK3R1: Phosphoinositide-3-Kinase Regulatory Subunit 1

PIK3R2: Phosphoinositide-3-Kinase Regulatory Subunit 2

PIP2: Phosphatidylinositol-4,5-Bisphosphate

PIP3: Phosphatidylinositol-3,4,5-Triphosphate

pMMR: Proficient MMR

POGZ: Pogo Transposable Element with ZNF Domain

POLE: DNA polymerase Epsilon

PPIG: Peptidylprolyl Isomerase G

P/S: Penicillin-Streptomycin

PtdIns: Phosphatidylinositol

PtdIns(3)P: Phosphatidylinositol-3-phosphate

PTEN: Phosphatase and Tensin Homolog

Q

QC: Quality control

R

RAF: Rapidly accelerated fibrosarcoma

RAN: RAS related nuclear protein

RAS: Rat sarcoma

RC: Rectal cancer

RC Path: Royal College of pathologists

REV3L: REV3 Like, DNA Directed polymerase Zeta Catalytic Subunit

RFC: Replication factor C subunit

Rheb: Ras Homolog Enriched in Brain

Rho: Rhodopsin

RIZ: Retinoblastoma interacting zinc finger
RNA: Ribonucleic acid
RPA: Replication protein A
RPMI: Roswell Park Memorial Institute medium
RTK: Receptor Tyrosine Kinases

S

S6K: S6 kinase
SCID: Severe combined immune deficiency
SDC2: Syndecan 2
SDS: Sodium dodecyl sulfate
SHIP-1: SH2 domain-Containing Inositol 5-Phosphatase 1
SHIP-2: SH2 domain-Containing Inositol 5-Phosphatase 2
SM: Somatic mutation
SMAD: Acronym for the Caenorhabditis Elegans Sma genes fused with the Drosophila Mad (mothers against decapentaplegic) proteins
SOS: Son of Sevenless
SPHKAP: Sphingosine Kinase type-1 Interacting Protein
STS: Sequence Tagged Site
SYNJ1: Synaptojanin 1
SYNE1: Spectrin Repeat Containing Nuclear Envelope Family Member 1
SYNE3: Spectrin Repeat Containing Nuclear Envelope Family Member 3

T

T: Thymine
TBE: Tris borate EDTA
TCF4: Transcription factor 4
TCGA: The Cancer Genome Atlas
TCTE1: T-Complex-Associated Testis Expressed 1
TFA: Trifluoroacetic acid
TGFB: Transforming growth factor beta
TGFBR2: Transforming growth factor beta receptor 2
TME: Total Mesorectal Excision
TNM: Tumour size, Node, Metastasis
TP53: Tumour Protein 53

TRIS: Trisaminomethane

TSC22D1: Transforming Growth Factor Beta-Stimulated Protein TSC-22

TTN: Titin

U

U: Uracil

U/E: Urea and Electrolytes

uM: Micromolar

UV: Ultraviolet

V

VAF: Variant Allele Frequency

VAV2: Vav 2 oncogene

W

Wnt: Wingless Integrated

WT: Wild-type

Z

ZNF441: Zinc Finger protein 441

ZNF638: Zinc Finger protein 638

Figures:

Figure 1.1: Eukaryotic chromosomal structure (46).....	51
Figure 1.2: Transcription and translation of DNA (47).	52
Figure 1.3: Transcription and translation of DNA into a protein.	53
Figure 1.4: Sixty-four nucleotide combinations which form 20 amino acids and 3 stop codons.....	53
Figure 1.5: Transition and transversion mutations in DNA.	55
Figure 1.6: Types of mutations, comparing a) normal DNA; point mutations: b) synonymous, c) missense, d) nonsense; frameshift: e) insertion and f) deletion mutations.	56
Figure 1.7: Ninety-six mutational trinucleotide possibilities located along the horizontal axis of mutational signatures.	66
Figure 1.8: The MAPK and PI3K pathway interactions.....	72
Figure 2.1: ScreenCell Cyto filtration method (172).....	96
Figure 2.2: Chemical structure of tetrazolium MTS compound and its formazan by-product (177).	102
Figure 2.3: Method for clonogenic assays.....	109
Figure 2.4: In vivo treatment regimens.....	113
Figure 2.5: Radiation of mice	115
Figure 3.1: Relationship between age and patient response to NACRT.....	126
Figure 3.2: Relationship between TRG status and patient response.	127
Figure 3.3: Relationship between lymph node positivity and patient response to NACRT.	128
Figure 3.4: Tumour mutational burden for non-synonymous somatic mutations per pre-treatment biopsy sample.....	132

Figure 3.5: Percentile distribution of non-synonymous somatic mutations per individual pre-treatment biopsy sample.	133
Figure 3.6: Mutations associated with positive lymph nodes.	134
Figure 3.7: Frequently mutated genes in the pre-treatment biopsies of patients who had good or poor response to NACRT.	137
Figure 3.8: Frequently mutated genes in the pre-treatment biopsy samples of non-responders (intermediate and poor responders).	138
Figure 3.9: Variant allele frequency (VAF) in good responders.	140
Figure 3.10: Variant allele frequency (VAF) in intermediate responders.	141
Figure 3.11: Variant allele frequency (VAF) in poor responders.	142
Figure 3.12: Mutational signatures.	143
Figure 3.13: Relationship between age and patient response to NACRT.	145
Figure 3.14: Relationship between TRG status and patient response.	146
Figure 3.15: Relationship between lymph node positivity and patient response to NACRT.	147
Figure 3.16: Tumour mutational burden for non-synonymous somatic mutations per pre-treatment biopsy sample.	151
Figure 3.17: Percentile distribution of non-synonymous somatic mutations per individual pre-treatment biopsy sample.	152
Figure 3.18: Associated with lymph node positivity	154
Figure 3.19: Commonly mutated genes in LARC patients.	155
Figure 3.20: Frequently mutated genes in the pre-treatment biopsy samples of good and poor responders.	157
Figure 3.21: Frequently mutated genes in the pre-treatment biopsy samples of non-responders (intermediate and poor responders).	158
Figure 3.22: Intra-tumour heterogeneity in pre-treatment biopsies taken from two spatially separated regions of the primary tumour from intermediate responder MDA-5.	160

Figure 3.23: Intra-tumour heterogeneity in pre-treatment biopsies taken from two spatially separated regions of the primary tumour from intermediate responder MDA-8.	161
Figure 3.24: Intra-tumour heterogeneity in pre-treatment biopsies taken from two spatially separated regions of the primary tumour from intermediate responder MDA-10.	162
Figure 3.25: Intra-tumour heterogeneity in pre-treatment biopsies taken from two spatially separated regions of the primary tumour from intermediate responder MDA-15.	163
Figure 3.26: Intra-tumour heterogeneity in pre-treatment biopsies taken from two spatially separated regions of the primary tumour from poor responder MDA-4.	164
Figure 3.27: Intra-tumour heterogeneity in pre-treatment biopsies taken from two spatially separated regions of the primary tumour from poor responder MDA-12.....	165
Figure 3.28: Intra-tumour heterogeneity in pre-treatment biopsies taken from two spatially separated regions of the primary tumour from poor responder MDA-13.....	166
Figure 3.29: Mutational signatures.....	167
Figure 4.1: Clinicopathological characteristics of TRILARC cohort (a) composition of TRGs according to radiation arm, (b) composition of TRG grades according to gender, (c) comparison of patient age group per gender (d) age group respective of TRG status...	185
Figure 4.2: Circulating tumour cells (CTCs) isolated from blood samples. White blood cells are scattered throughout samples and primarily trapped in membrane pores.	186
Figure 4.3: (a) Bar chart represents the percentage of patients with blood samples positive for CTCs (b) Scatter plot depicts the number of CTCs identified per patient sample.....	189
Figure 4.4: The relationship between serial circulating tumour cell (CTC) counts and TRG status (A) Percentage of samples positive for CTCs according to time-point and pCR status. (B) Number of CTCs identified in 3mls blood per sample in patients who achieved pCR (black), and those who did not (TRG2-5) (blue).	190
Figure 4.5: The effects of the type of radiation treatment on circulating tumour cells (CTCs) in LARC patients. (A) Percentage of patients with blood samples positive for CTCs according to time-point and the type of radiation therapy, (B) Number of CTCs identified in 3mls blood per patient sample in (i) 3-DCRT and (ii) IMRT arms.	191
Figure 4.6: The relationship between circulating tumour cells (CTCs) and gender (A) Percentage of patient blood samples positive for CTCs at each time-point by gender. (B)	

Number of CTCs identified in 3mls blood per sample in (i) males and (ii) females at each time-point.....	192
Figure 4.7: Mutational profiles obtained from (A) ctDNA and (B) tumour tissue samples from LARC patients participating in the TRILARC clinical trial, before during and after NACRT treatment.	194
Figure 4.8: KRAS ^{G12D} mutations.....	195
Figure 4.9: Mutations identified in pre-treatment tumour tissue and ctDNA samples from LARC patients enrolled in the TRILARC clinical trial, and divided according to TRG status.	198
Figure 4.10: Mutations identified in surgical resection tumour tissue and ctDNA samples from LARC patients enrolled into the TRILARC clinical trial.	199
Figure 4.11: Overview of mutational status before and post-NACRT treatment.	201
Figure 4.12: Overview of mutational status identified in tumour tissue samples before and post-NACRT treatment.	202
Figure 4.13: Mutations identified in ctDNA of eight LARC patients who developed recurrent rectal cancer.....	205
Figure 4.14: Mutations identified in tumour tissue of eight LARC patients who developed recurrent rectal cancer.....	206
Figure 4.15: Mutations identified in ctDNA of eight LARC patients who developed recurrent rectal cancer.....	207
Figure 5.1: Representation of the effects of PIK3CA, RAS, RAF and PIK3CA/RAS mutations within the cells, and how PI3K inhibitors alter the signalling pathways.....	216
Figure 5.2: Representation of the effects of PIK3CA, Ras, Raf and PIK3CA/Ras mutations within the cells, and how MEK inhibitors alter the signalling pathways.....	217
Figure 5.3: Representation of the effects of PIK3CA, Ras, Raf and PIK3CA/Ras mutations within the cells, and how a combination of PI3K and MEK inhibitors alter the signalling pathways.....	218
Figure 5.4: Efficacy of copanlisib in a panel of CRC cell lines with varying PI3K and MAPK pathway mutations, consisting of (a) Wild-type, (b) BRAF ^{mut} , (c) KRAS ^{mut} , (d) PIK3CA ^{mut} , (e) PIK3CA-KRAS ^{co-mut}	224

Figure 5.5: Efficacy of refametinib in a panel of CRC cell lines with varying PI3K and MAPK pathway mutations, consisting of (a) Wild-type, (b) BRAF ^{mut} , (c) KRAS ^{mut} , (d) PIK3CA ^{mut} , (e) PIK3CA-KRAS ^{co-mut} .	225
Figure 5.6: Efficacy of the combination of copanlisib and refametinib in a panel of CRC cell lines with varying PI3K and MAPK pathway mutations, consisting of (a) Wild-type, (b) BRAF ^{mut} , (c) KRAS ^{mut} , (d) PIK3CA ^{mut} , (e) PIK3CA-KRAS ^{co-mut} .	226
Figure 5.7: Efficacy of Copanlisib (●), Refametinib (■), and a combination of copanlisib and refametinib (▲), in a panel of CRC cell lines, with the mean values for (a) Wild-type, (b) BRAF ^{mut} , (c) KRAS ^{mut} , (d) PIK3CA ^{mut} , (e) PIK3CA-KRAS ^{co-mut} .	227
Figure 5.8: Clonogenic assays for BRAF ^{mut} (LS-411N = ■), PIK3CA-KRAS ^{mut} (DLD-1 = ■), PIK3CA ^{mut} (SNU-C4 = ■), KRAS ^{mut} (LS-1034 = ■) and wild-type (Caco-2 = ■) colorectal cancer (CRC) cell lines treated with the PI3K inhibitor copanlisib.	232
Figure 5.9: Clonogenic assays for BRAF ^{mut} (LS-411N = ■), PIK3CA-KRAS ^{mut} (DLD-1 = ■), PIK3CA ^{mut} (SNU-C4 = ■), KRAS ^{mut} (LS-1034 = ■) and wild-type (Caco-2 = ■) colorectal cancer (CRC) cell lines treated with the MEK inhibitor refametinib.	233
Figure 5.10: Clonogenic assays for BRAF ^{mut} (LS-411N = ■), PIK3CA-KRAS ^{mut} (DLD-1 = ■), PIK3CA ^{mut} (SNU-C4 = ■), KRAS ^{mut} (LS-1034 = ■) and wild-type (Caco-2 = ■) colorectal cancer (CRC) cell lines treated with 5-fluorouracil (5-FU) chemotherapy.	234
Figure 5.11: Cellular growth of PIK3CA-KRAS ^{mut} DLD-1 cells treated with DMSO/DMSO-TFA vehicle control (C), 5-FU chemoradiotherapy (5R), copanlisib and chemoradiotherapy (P5R), refametinib and chemoradiotherapy (M5R) and copanlisib, refametinib and chemoradiotherapy (PM5R) in clonogenic assays.	238
Figure 5.12: Cellular growth of KRAS ^{mut} LS-1034 treated with DMSO/DMSO-TFA vehicle control (C), 5-FU chemoradiotherapy (5R), copanlisib and chemoradiotherapy (P5R), refametinib and chemoradiotherapy (M5R) and copanlisib, refametinib and chemoradiotherapy (PM5R) in clonogenic assays.	239
Figure 5.13: Cellular growth of BRAF ^{mut} LS-411N treated with DMSO/DMSO-TFA vehicle control (C), 5-FU chemoradiotherapy (5R), copanlisib and chemoradiotherapy (P5R), refametinib and chemoradiotherapy (M5R) and copanlisib, refametinib and chemoradiotherapy (PM5R) in clonogenic assays.	240
Figure 5.14: Cellular growth of PIK3CA ^{mut} SNU-C4 treated with DMSO/DMSO-TFA vehicle control (C), 5-FU chemoradiotherapy (5R), copanlisib and chemoradiotherapy	

(P5R), refametinib and chemoradiotherapy (M5R) and copanlisib, refametinib and chemoradiotherapy (PM5R) in clonogenic assays.	241
Figure 5.15: Cellular growth of wild-type Caco-2 CRC cell lines treated with DMSO/DMSO-TFA vehicle control (C), 5-FU chemoradiotherapy (5R), copanlisib and chemoradiotherapy (P5R), refametinib and chemoradiotherapy (M5R) and copanlisib, refametinib and chemoradiotherapy (PM5R) in clonogenic assays.	242
Figure 6.1: Mean tumour growth in wild-type (Caco-2), PIK3CA (SNU-C4), KRAS (LS-1034) and PIK3CA-KRAS (DLD-1) xenograft models.	253
Figure 6.2: Mean tumour growth in wild-type (Caco-2), PIK3CA (SNU-C4), KRAS (LS-1034) and PIK3CA-KRAS (DLD-1) xenograft models during days 1-10 of treatment. ...	254
Figure 6.3: Scatter plot depicting the mean number of days per xenograft tumour to reach 400mm ³ . Tumours were divided into wild-type (Caco-2), PIK3CA ^{mut} (SNU-C4), KRAS ^{mut} (LS-1034) and PIK3CA-KRAS ^{co-mut} (DLD-1) mutations.....	259
Figure 6.4: Kaplan-Meier survival curves for mice implanted with wild-type (Caco-2), PIK3CA ^{mut} (SNU-C4), KRAS ^{mut} (LS-1034) and PIK3CA-KRAS ^{mut} (DLD-1) tumours	263
Figure 6.5: Mean body weight alterations over the course of the study.....	266
Figure 6.6: Spleen mass in wild-type (Caco-2 = ▲), KRAS ^{mut} (LS-1034 = ○), PIK3CA ^{mut} (SNU-C4 = ■) and PIK3CA-KRAS ^{mut} (DLD-1 = ◇) xenograft mice at the time of sacrifice.	267
Figure 6.7: Scatter plot depicting lung mass (mg) excised from wild-type (Caco-2 = ▲), KRAS ^{mut} (LS-1034 = ○), PIK3CA ^{mut} (SNU-C4 = ■) and PIK3CA-KRAS ^{mut} (DLD-1 = ◇) xenograft models.	268
Figure 6.8: Scatter plot depicting liver mass (mg) excised from wild-type (Caco-2 = ▲), KRAS ^{mut} (LS-1034 = ○), PIK3CA ^{mut} (SNU-C4 = ■) and PIK3CA-KRAS ^{mut} (DLD-1 = ◇) xenograft models.	269
Figure 6.9: Scatter plot depicting primary tumour mass (mg) excised from wild-type (Caco-2 = ▲), KRAS ^{mut} (LS-1034 = ○), PIK3CA ^{mut} (SNU-C4 = ■) and PIK3CA-KRAS ^{mut} (DLD-1 = ◇) xenograft models.....	271
Figure 6.10: Macroscopic view of wild-type tumours from mice after sacrifice.....	273
Figure 6.11: Macroscopic view of PIK3CA ^{mut} tumours from mice after sacrifice.	274

Figure 6.12: Macroscopic view of KRAS ^{mut} tumours from mice after sacrifice.	275
Figure 6.13: Macroscopic view of PIK3CA-KRAS ^{mut} tumours from mice after sacrifice.	276
Figure 6.14: Microscopic view of Caco-2 (WT) primary tumours. (A) H&E of a necrotic core with mass inflammatory cell infiltration (x20). (B) H&E of numerous necrotic cores (pink) surrounded by tumour tissue (purple) (4x), (C) H&E of a well-differentiated tumour (10x). (D) Ki67 staining of proliferative glandular tumour epithelium surrounding necrotic cores (20x).	277
Figure 6.15: Microscopic view of DLD-1 (PIK3CA-KRAS ^{mut}) xenograft tissues (A) H&E of primary tumour (10x), (B) Ki67 stain of proliferative tumour islands amongst necrotic tissue (10x), (C) H&E of large secondary lung metastasis (20x), (D) Ki67 stain of large secondary lung metastasis (20x), (E) Ki67 positive cluster in lung tissue (10x) (F) Ki67 positive scattered cells in spleen (4x).	278
Figure 6.16: Microscopic view of LS-1034 (KRAS ^{mut}) xenograft tissues. (A) H&E of primary tumour tissue with necrotic cores (20x), (B) H&E of primary tumour tissue with inflammatory cell infiltration into necrotic core (20x), (C) Ki67 staining of primary tumour (x20), (D) Ki67 staining of primary tumour (x20), (E) H&E of secondary tumour metastasis in lung (x10), (F) Ki67 staining of proliferative clusters in spleen (x10).....	279
Figure 6.17: Microscopic view of SNU-C4 (PIK3CA ^{mut}) xenograft tissues. (A) H&E of primary tumour, with islands of glandular epithelium amongst necrotic tissue (x10), (B) Ki67 staining of proliferative islands of cellular growth (x10), (C) H&E stain of secondary metastatic tumour in lung (20x), (D) Ki67 stain of secondary metastatic tumour in lung (20x).....	280

List of tables:

Table 1.1: The stages of colorectal cancer. (11).....	39
Table 1.2: Relative 1 and 5-year survival rates (12).	48
Table 1.3: Genetic adenomatous polyp syndromes.....	62
Table 1.4: Cancer locations and proposed aetiology for mutational signatures (90).	68
Table 1.5: Clinical trials for copanlisib treatments worldwide.	79
Table 1.6: Clinical trials for copanlisib treatments worldwide, continued.....	80
Table 1.7: Clinical trials involving refametinib (170).....	81
Table 2.1: List of reagents used for whole-exome sequencing study, their names, suppliers and product codes.	84
Table 2.2: List of reagents used for TRILARC study, their names, suppliers and product codes.....	90
Table 2.3: ECOG grading system (171).	91
Table 2.4: Time-points for collection of blood and tissue samples during TRILARC clinical trial.	93
Table 2.5: List of reagents used for in vitro study, including their names, suppliers and product codes.	98
Table 2.6: Colorectal cancer cell lines, and their corresponding PI3K/MAPK pathway mutations, growth medium requirements, tissue type and morphology.	101
Table 2.7: Combination index values and corresponding Chou-Talalay definition for levels of synergism within a sample.....	103
Table 2.8: Optimised incubation times, cell volume and drug concentrations for PI3K inhibitor (copanlisib), MEK inhibitor (refametinib), and 5-FU chemotherapy, for 5 colorectal cancer cell lines for varying mutations within the PI3K and MAPK pathways.	106
Table 2.9: Drug treatment regimens for clonogenic assays.....	107
Table 2.10: List of reagents used for in vivo study, including their names, suppliers and product codes.	110

Table 2.11: Colorectal cancer cell lines subcutaneously implanted in SCID BALB/C mice.	112
Table 2.12: Days mice were treated by copanlisib, 5-FU chemotherapy and radiation.	116
Table 3.1: Clinicopathological data for patients in whole exome sequencing study	124
Table 3.2: Tumour purity and ploidy for whole exome sequencing study	125
Table 3.3: Single nucleotide variant (SNV) and insertion/deletion (indel) mutations in LARC biopsies from good, intermediate and poor responders to NACRT.	130
Table 3.4: Non-synonymous, somatic mutations in LARC biopsies from good, intermediate and poor responders to NACRT.	131
Table 3.5: Mutations frequently identified in hypo-mutated samples.....	134
Table 3.6: Single nucleotide variant (SNV) and insertion/deletion (indel) mutations in LARC biopsies from good, intermediate and poor responders to NACRT.	149
Table 3.7: Non-synonymous, somatic mutations in LARC biopsies from good, intermediate and poor responders to NACRT.	150
Table 3.8: Mutations frequently identified in hypo-mutated samples.....	153
Table 3.9: Intra-tumour heterogeneity in two pre-treatment biopsy samples taken from two regions within the primary tumour.	159
Table 4.1: Mandard tumour regression grade (TRG) system (240).	182
Table 4.2: Patient demographics of TRILARC study population.	184
Table 4.3: Patient demographics of TRILARC study population who progressed onto metastatic disease.	204
Table 5.1: Mutation status of the colorectal cancer cell lines included in the study.	221
Table 5.2: The IC ₅₀ s of copanlisib and refametinib inhibitors in combination compared to the IC ₅₀ of each drug as a single agent, and combination index (CI) values at ED50, ED75 and ED90 for the combination of copanlisib and refametinib.....	228
Table 5.3: IC75 values of cell lines treated in clonogenic assays with Copanlisib, Refametinib and 5-fluorouracil (5-FU) chemotherapy.....	231
Table 5.4: Survival fraction and p-values of clonogenic assays.....	237

Table 6.1: P-values for tumour growth (days 2-10) for wild type, PIK3CA, KRAS and PIK3CA-KRAS xenografts.	255
Table 6.2: Mean number of days for xenografted tumours to reach 400mm ³	257
Table 6.3: Overall survival. F value, F-crit and p-values for the mean number of days it took for tumours to reach 400mm ³ , comparing control vs. chemoradiotherapy (C: 5R); control vs. copanlisib-chemoradiotherapy (C: P5R); and chemoradiotherapy vs. copanlisib-chemoradiotherapy (P5R) treatment regimens in wild-type, PIK3CA ^{mut} , KRAS ^{mut} and PIK3CA-KRAS ^{mut} xenograft models.	258
Table 6.4: Mean, median, range and standard deviation values for survival times in mice bearing wild-type, PIK3CA, KRAS and PIK3CA-KRAS mutant xenografts by treatment cohort (untreated control (C), chemoradiotherapy (5R) and copanlisib chemoradiotherapy (P5R)).	260
Table 6.5: Survival fractions at 10, 20, 30 and 40 days post commencement of treatment.	262
Table 6.6: Log-rank (Mantel-Cox) test used to determine significant differences in survival curves.	264
Table 6.7: P-values for variation in tumour mass for wild type, KRAS, PIK3CA and PIK3CA-KRAS tumours, depending on the treatment regimen.	272
Table 6.8: Ki67 quantification in tumour samples.	282
Table 6.9: Ki67 quantification in spleen samples.	283
Table 6.10: Ki67 quantification in liver samples.	284
Table 6.11: Ki67 quantification of lung samples	285

Appendices:

Supplementary figure 1: The relationship between serial circulating tumour cell (CTC) counts and TRG status (A) Percentage of samples positive for CTCs according to time-point and TRG grade. (B) Number of CTCs identified in 3mls blood per sample in (i) TRG1, (ii) TRG2, (iii) TRG3, (iv) TRG4, and (v) TRG5 patients.	335
Supplementary figure 2: Cellular growth of PIK3CA ^{mut} SNU-C4 cell line in clonogenic assays.	336
Supplementary figure 3: Cellular growth of PIK3CA-KRAS ^{mut} DLD-1 cell line in clonogenic assays.	337
Supplementary figure 4: Cellular growth of KRAS ^{mut} LS-1034 cell line in clonogenic assays.	338
Supplementary figure 5: Cellular growth of wild-type Caco-2 CRC cell line in clonogenic assays.	339
Supplementary figure 6: Cellular growth of BRAF ^{mut} LS-411N in clonogenic assays..	340
Supplementary figure 7: Tumour growth for each wild-type (Caco-2), PIK3CA (SNU-C4), KRAS (LS-1034) and PIK3CA-KRAS (DLD-1) xenograft model.	341
Supplementary figure 8: Scatter plot depicting tumour mass (mg) excised from wild-type (Caco-2 = ▲), KRAS mutated (LS-1034 = ○), PIK3CA mutated (SNU-C4 = ■) and PIK3CA-KRAS mutated (DLD-1 = ◇) xenograft models.	342
Supplementary figure 9: Scatter plot depicting spleen mass (mg) excised from wild-type (Caco-2 = ▲), KRAS mutated (LS-1034 = ○), PIK3CA mutated (SNU-C4 = ■) and PIK3CA-KRAS mutated (DLD-1 = ◇) xenograft models.	343
Supplementary figure 10: Scatter plot depicting lung mass (mg) excised from wild-type (Caco-2 = ▲), KRAS mutated (LS-1034 = ○), PIK3CA mutated (SNU-C4 = ■) and PIK3CA-KRAS mutated (DLD-1 = ◇) xenograft models.	344
Supplementary figure 11: Scatter plot depicting liver mass (mg) excised from wild-type (Caco-2 = ▲), KRAS mutated (LS-1034 = ○), PIK3CA mutated (SNU-C4 = ■) and PIK3CA-KRAS mutated (DLD-1 = ◇) xenograft models.	345

Summary

Purpose: Late-stage colorectal cancer (CRC) is currently treated with neoadjuvant chemoradiation therapy (NACRT), however, responses are not uniform. The PI3K and MAPK pathways have been implicated in tumourigenesis, poor patient outcomes and resistance to chemoradiation therapy (CRT).

Methods: Whole-exome sequencing and mutational analysis were carried out on pre-treatment tumour biopsies from locally advanced rectal cancer (LARC) patients (n=26). LARC patients (n=66) were monitored for circulating tumour cells (CTCs) and mutational variations in blood and tissue samples taken before, during and post-NACRT. A panel of *PI3K/MAPK^{mut}* CRC cell lines were treated with the PI3K inhibitor copanlisib, and/ MEK inhibitor refametinib in proliferation assays; and treated with various combinations of radiation, 5-FU chemotherapy, copanlisib and/or refametinib in clonogenic assays. BALB-C mice were implanted with CRC cell lines (n=4) and treated with copanlisib, and / CRT, and monitored for tumour growth.

Results: Whole-exome sequencing detected PI3K and MAPK pathway mutations in 88.5% of samples, including *KRAS* (15.4%), *BRAF* (11.5%) and *PIK3CA* (11.5%); with *BRAF* and *PIK3CA* mutations identified exclusively in non-responders. CTCs increased during CRT, with CTCs detected in 40% and 38.1% of samples at week 3 and final week of CRT respectively, compared to 17.1% of pre-treatment samples. In vitro, copanlisib and refametinib were most effective in the *PIK3CA^{mut}* (IC₅₀=28nm), and *KRAS^{mut}* (IC₅₀=36nm) cell lines respectively. The copanlisib-refametinib combination resulted in a synergistic response in 8/10 cell lines. In 3D clonogenic assays, CRC cell growth was significantly reduced when treated with copanlisib-CRT (*KRAS^{mut}*), refametinib-CRT (*KRAS^{mut}*) and copanlisib-refametinib-CRT (*WT*, *KRAS^{mut}*, *BRAF^{mut}* and *PIK3CA-KRAS^{mut}*) compared to CRT alone. In vivo, copanlisib-CRT significantly reduced tumour growth and increased overall survival in *KRAS^{mut}*, *PIK3CA^{mut}* and *WT* xenografts compared to untreated controls.

Conclusion: Our results suggest that kinase signalling pathway mutations may modulate treatment responsiveness and clinical outcomes in CRC. Furthermore, treatment with PI3K/MEK inhibitors may enhance CRC patient responsiveness to CRT.

Acknowledgements

I would like to thank my funding bodies, the Irish Cancer Society, St. Luke's Radiation Oncology Network, Cancer trials Ireland, Science Foundation Ireland (SFI) and the Northeast Cancer Research Education Trust (NECRET) without whom, this project would not have been possible.

I would like to thank my supervisors Prof. Bryan Hennessy, Dr. Sinead Toomey, Dr. Simon Furney, Prof. Elaine Kay and Dr. Brian O'Neill for all their help and support throughout the past four years. I would like to give a special acknowledgement to Prof. Bryan Hennessy for entrusting me with a project of this calibre. Over the past four years, Prof. Hennessy has guided and trained me to become the researcher I am today. Furthermore, I am also grateful to Dr. Sinead Toomey, for her direction and assistance throughout my time in RCSI, particularly concerning Sequenom analysis of the TRILARC patient samples. In addition, I would like to thank Dr. Simon Furney and Scott Piraino, for performing the biostatistical analysis of the whole-exome sequencing data, which aided in the interpretation of my results.

I would like to acknowledge the past and present medical oncology staff that I have had the pleasure to work with over the duration of my time in RCSI. Their support and guidance are greatly appreciated. I would like to give special recognition to Dr. Angela Farrelly, Julie Workman and Dr. Alex Eustace for their help throughout my project, particularly with their training in cell culture, and help with continuing the TRILARC clinical trial whilst I was undertaking the in vivo study in Belfast.

Furthermore, I would like to express my gratitude to all of the molecular medicine research groups. Their support and friendship throughout my time in RCSI made working in the ERC building a pleasure. I would like to give a special thank you to Dr. Olive McCabe for her organisation and help throughout my project.

I would like to acknowledge the staff in St. Luke's Radiation Oncology Network. I would like to thank the staff of the Beaumont facility including Shirley Bradshaw, Lydia O'Sullivan and Ravikumar Venkateshappa for their participation in the

TRILARC clinical trial, including the collection of samples as well as treating and caring for all of the patients involved in the clinical trial. Furthermore, I would like to acknowledge the staff in Rathgar including Prof. Brendan McClean, Dr. Peter McBride, Dr. Laura Shields, and Dr. Allen Curran for providing the necessary equipment and taking time out of their busy schedules to help with radiation of my clonogenic experiments.

I would like to thank Dr. Jonathan Coulter for welcoming me into his lab at Queens University, Belfast for the duration of my in vivo study. I am profoundly grateful for his continued guidance and help throughout the study. Furthermore, I would like to thank all of the staff in Queens University and BSU, particularly Dr. Nermeen Moustafa, Lindsey Bennie and Lynda Collins for their continued training and support throughout the in vivo study.

I would like to thank RCSI and the school of postgraduate studies for their guidance and assistance throughout the process of the PhD.

Finally, I would like to give a special recognition to my family, particularly my parents, and three sisters, Deirdre, Siobhan and Sinead; friends and boyfriend, Louis Bowers for their endless support and understanding throughout the duration of my PhD.

Dedication

I would like to dedicate this project to my parents, Martin and Angela Carr who have always encouraged me to pursue my dreams and never give up.

Poster presentations:

- 12/03/2015: RCSI research day, RCSI, Dublin
- 09/03/2017: RCSI research day, RCSI, Dublin
- November 2016: Breast Predict, UCD, Dublin.
- 24/10/2017: Beaumont Hospital Translational Research Awards. Beaumont hospital. Targeting the PI3K and MAPK pathways in LARC.
- 22 – 23 /02/2018: IACR (Irish Association of Cancer Research): Crowne Plaza Hotel, Santry, Dublin. Targeting the phosphatidylinositol-3-kinase (PI3K) and mitogen activated protein kinase (MAPK) pathways to enhance chemoradiation therapy in locally advanced rectal cancer patients.

Oral presentations:

- Annual PhD viva examinations
- 22-23 October 2015: 8th annual meeting of the Irish Epithelial Physiology Group (IEPG). Newpark Hotel, Kilkenny. The role of kinase related somatic mutations in locally advanced rectal cancer.
- 25/02/2016: RCSI research day

Courses:

- March 2016: LAST Ireland (rodent module), Trinity, Dublin.

Conferences and symposiums attended:

- May 2015: 3D modelling of breast cancer, Charterhouse Square, London
- March 2016: Presenting your research at conferences
- Monthly ERC symposiums in RCSI, Beaumont.
- June 2018: Association for radiation research / Irish radiation research society annual meeting, Queens University, Belfast.

Memberships / certifications

- ASPA UK cert

Papers published

‘Genomic and transcriptomic correlates of response to neoadjuvant chemoradiation therapy in locally advanced rectal cancer’. Submitted to JCO Precision Oncology.

Introduction

1.1. Colon and rectum: An overview.

The large intestine is a dense, muscular tube spanning five to six foot in length and a diameter of approximately 7.5cm. It consists of the cecum, colon (ascending (right), transverse, descending (left), sigmoid), rectum and anus. The majority of the large intestine is confined within the peritoneal cavity where it can move relatively freely. The rectum, meaning 'straight' in Latin, joins the sigmoid colon to the anus. It ranges from ten to twenty cm in length and approximately six cm in diameter. Unlike the rest of the large intestine, the rectum cannot move and is instead bound to the intraperitoneal, retroperitoneal and extraperitoneal cavities via ligaments and muscles (1,2).

1.2. Histology

The colon and rectum are composed of four concentric layers; the mucosa, submucosa, muscularis externa (propria) and serosa or adventitia. The mucosa and submucosa are thrown into folds producing rugae, which increase surface area, optimising its ability for the absorption of nutrients, and to facilitate post-prandial extension.

1.2.1. Mucosa

The outermost layer of the intestinal tract, the mucosa is a dense mucous membrane which is essential to protect the cells from digestive enzymes, hydrochloric acid and harmful bacteria. The mucosa consists of the epithelium, lamina propria, and the muscularis mucosa (2).

Epithelium

The epithelial layer is composed of simple columnar epithelium lined with a brush border. Straight, unbranched tubular glands known as crypts of Lieberkühn open at the epithelial luminal surface and extend as far as the muscularis mucosae. There are approximately 10 million highly proliferative crypts in the GIT, each crypt is lined with:

- a) Pericryptal fibroblast sheaths: Consisting of continuously regenerating population of fibroblasts and myofibroblasts.
- b) Stem cells: Highly proliferative, multipotent stem cells are primarily located along the base of crypts. As they migrate towards the lumen, they

differentiate into enterocytes, goblet, secretory or endocrine cells; a process which takes 3-8 days for completion.

- c) Absorptive enterocytes: Water and electrolytes are absorbed from the colon (primarily in the ascending colon), and filtered into the bloodstream. Absorptive enterocytes are composed of columnar epithelium with basal nuclei and eosinophilic cytoplasm which predominate the luminal surface.
- d) Goblet cells: The colonic walls are lined with mucus secreting cells which protect against the bacterial fermentation process. Fermentation and gut microflora convert remaining undigested waste into faeces. Fibre is broken down in the descending colon, releasing butyrate, propionate and acetate, which are essential for the cells lining the colon. Goblet cells are typically located along the base of the glands, and have small, condensed nuclei which are pushed to the side as a result of mucin accumulation, giving them their distinctive 'bubble appearance'.
- e) Enteroendocrine cells: The gastrointestinal tract has earned the title as 'the largest endocrine organ in the body' (3), generating over thirty different hormones. Enteroendocrine cells are scattered throughout the mucosal lining of the colon and rectum. They contain luminal nuclei and are typically located along the base of the crypts. They contain small, eosinophilic granules with secretory proteins, which are released at the basal surface. These cells secrete numerous hormones including serotonin, somatostatin, peptide tyrosine tyrosine, glucagon-like peptide 1 and 2, glicentin and oxyntomodulin. These hormones are crucial for intestinal secretions, appetite, gastric emptying, enterocyte proliferation, and colonic peristalsis.

Lamina propria

The lamina propria is composed of loose connective tissue which surrounds and supports the glands. It contains blood and lymphatic vessels, collagen, plasma cells, leukocytes, and inflammatory cells. The capillaries are ubiquitous whilst the lymphatic vessels run parallel to the muscularis mucosa. Lymphoid nodules are known as gut-associated lymphoid tissue (GALT) extend from the lamina propria to the submucosa. GALT is the largest lymphoid organ in the body (4).

Muscularis mucosa

The muscularis mucosa is a thin band of smooth muscle and elastic fibres, composed of inner circular and outer longitudinal layers. It is essential for ruggae movement.

1.2.2. Submucosa

The submucosa consists of loose connective tissue containing blood and lymphatic vessels and neural tissue (submucosal plexus of Meissner, parasympathetic motor neurons, nerve fibres and sensory neurons). The submucosal plexus of Meissner is essential for regulation and coordination of the smooth muscle layer contractions and digestive glandular secretions.

1.2.3. Muscularis externa / propria

The muscularis externa is a thick band of smooth muscle consisting of inner circular and outer longitudinal fibres. The latter is arranged into 3 bands known as the teniae coli. The muscles interact with the intramural enteric nervous system resulting in peristaltic movements to agitate substances through the digestive tract. These are made of autonomic reflexes, mainly controlled by the myenteric plexus which is located between the circular and longitudinal smooth muscle layers.

1.2.4. Serosa/adventitia

The outermost layer of the large intestine differs between the serosa (intraperitoneal) and adventitia (retroperitoneal). The serosa is composed of a monolayer of simple squamous mesothelial cells and adjacent fibroelastic tissue. Whereas the adventitia is a thick network of collagen fibres and loose connective tissue which adhere the large intestine to adjacent structures.

1.2.5. Recto-anal junction

The epithelium at the recto-anal junction changes from simple columnar to keratinized stratified squamous epithelium. Crypts decrease in size, eventually disappearing, as does the muscularis mucosae, resulting in the lamina propria

adhering to the submucosa. There is an abundance of submucosal veins in the skeletal and smooth muscle for the anal sphincters.

1.3. Colorectal cancer

Colorectal cancer (CRC) accounts for 12.4% of all invasive cancer cases in Ireland, rendering it the second most common cancer nationally (5). Furthermore, CRC has the second highest mortality rate in Ireland, constituting 11% of all cancer deaths (5). Despite efforts to combat cancer worldwide, CRC cases are on the rise, with a reported 2,775 cases per annum (5), compared to with 1,752 cases reported in 1994 (6).

The rectum accounts for a mere 9% of the entire length of the large intestine, however rectal cancer (RC) accounts for 37% of all CRC cases in Ireland (7,8). Furthermore, between 1994 and 2010, there was a 1.8% increase per annum in the number of cases diagnosed and a 4.5% increase in the number of deaths per annum. This has been largely denoted as a result of increasing population size and age (6).

1.3.1. Colorectal polyps

Chromosomal damage can cause CRC. This can occur as a germline genetic defect which affects every cell in the body, as in hereditary CRC, or acquired (sporadic) whereby the damage is localized within the affected cells in the tumour or polyp.

Adenomatous polyps are the leading cause of CRC. The risk of sporadic polyp formation increases with age, with ~33% of individuals over 50 years harbouring a minimum of 1 colonic polyp (9). Factors predicting prognosis include the amount and size of the polyps and histology; with villous adenomas being the most aggressive form. The second most common form of colonic polyps is hyperplastic polyps. These typically do not progress into malignancies, however, there are increased risks if they are located in the ascending colon, have serrated histology, or if the individual has a genetic predisposition to CRC. Other colonic polyps include hamartomatous, juvenile and inflammatory polyps.

Polyp removal occurs through sigmoidoscopy or colonoscopy. Subsequent histological examination is carried out to determine the histological subtype of the

polyp if it is benign or malignant, and genetic testing may be carried out to determine if other family members are at increased risk.

1.3.2. Polyp formation

Chromosomal alterations (either genetic or acquired) accumulate within the epithelial cells lining the intestine. These mutations alter the cells apoptotic and maturation abilities, whilst processes such as cellular proliferation remain unscathed. This results in the production of a localised mass of mutated cells, known as a benign polyp. If chromosomal damage continues to occur, additional mutations may result in cell destabilisation, whereby a benign polyp may transition into a malignant tumour with deregulated proliferative abilities, and potentially gain the ability to spread and metastasise throughout the body.

1.3.3. Symptoms of colorectal cancer

Precancerous polyp formation and early stages of CRC are typically asymptomatic. As a result, CRC can be present for years prior to diagnosis. Symptoms of CRC include changes in bowel movement (e.g. constipation or diarrhoea), a feeling of incomplete evacuation, abdominal pain, discomfort and bloating, trapped wind, shortness of breath, weight loss, malaise, fatigue, iron deficiency (hypochromic microcytic) anaemia, bright red rectal bleeding or blood in stools. However, many of these symptoms may also be associated with other bowel disorders such as Irritable Bowel Syndrome (IBS), peptic ulcers, diverticulitis, Crohn's disease or ulcerative colitis.

1.3.4. Testing for colorectal cancer

Initial examinations for CRC include a rectal exam, collection of stool samples for faecal occult blood, and blood tests for anaemia. This may be followed up by further specialised testing such as a sigmoidoscopy, proctoscopy, colonoscopy, CT colonography and pelvic MRI. Full staging of the cancer can be further carried out by CT or PET scanning (with the former used more commonly) (10). Whilst molecular testing is carried out to detect mutations in mismatch repair proteins and microsatellite instability genes.

1.3.5. Staging and differentiation of colorectal cancer

Differentiation of RC is based on histological subtype and staging of the disease. Histologically over 95% of RCs are adenocarcinomas, which originate in the intestinal glandular epithelium. The remaining 5% consists of squamous cell carcinomas, lymphomas and sarcomas (1). Rare forms of adenocarcinomas include signet ring (1-2%) and mucinous tumours (1). Signet ring carcinomas have a large amount of mucus within the cell, causing the nucleus to be displaced and squashed to the side (periphery) of the cell, giving it its classic signet ring appearance.

Although the majority of CRCs are a result of polyp formation, a small subset of CRCs forms in the colonic walls. These are known as non-polyposis CRCs, they are typically more difficult to identify and treat, resulting in an increased chance of metastasis. HNPCC is an example of a genetic disorder which can result in cancer with few or no polyps. 80% of people identified with HNPCC develop CRC, typically at a younger age than their counterparts.

Tumour staging is based upon the TNM grading system which classifies the tumour based on tumour size (T), the number of positive lymph nodes adjacent to the tumour (N), and whether it has metastasised (M). The stages of CRC range from 0-4, as described below in Table 1.1.

	T	N	M	
Stage 0	Tis	N0	M0	The tumour is contained entirely within the mucosa (in situ).
Stage 1	T1/ T2	N0	M0	The cancer has breached through the mucosal wall (T1), or mucosal and submucosal walls (T2) of the colon or rectum.
Stage 2	T3 / T4	N0	M0	The cancer has spread through the muscularis externa (T3), and possibly adjacent tissue (T4).
Stage 3	Any	N+	M0	The cancer has metastasised to 1 or more local lymph nodes (N1-3)
Stage 4	Any	Any	M+	Distant metastasis of the cancer to other organs and, or lymph nodes (M1)

Table 1.1: The stages of colorectal cancer. (11)

The majority of RC patients present with locally advanced rectal cancer (LARC), defined by T3 or T4 stage, and/or lymph node-positive status (8). There has been a steady increase in the numbers of patients presenting with stage II and III cancer in the rectosigmoid junction and rectum, with 46% of patients presenting with stage II or III between 1995-1999, compared to 52% of patients between 2005 and 2009 (12).

1.3.6. Treatment

RC patients typically present with late-stage disease, locally advanced cancer (8). The standard treatment for LARC patients is Neoadjuvant chemoradiation therapy (NACRT), whereby the patient undergoes radiation therapy and 5-fluorouracil (5-FU) or Capecitabine combined chemoradiotherapy for 6-8 weeks, followed by surgical resection of the tumour.

A study carried out by the National Cancer Registry Ireland (NCRI) analysed alterations in CRC treatment regimens between 1995 and 2009. It found a decrease in treatment with surgery alone from 1995-1999 in both stage 2 (52.5%) and stage 3 (37.9%), in comparison to 2005-2009 (stage 2 = 37.7%, stage 3 = 16.8%). More strikingly however was the increase in the combination of chemotherapy, radiation and surgery between 1995-1999 (stage 2 = 2.7%, stage 3 = 1.1%) and 2005-2009 (stage 2 = 23.2%, stage 3 = 28.7%). The use of pre-operative radiotherapy (NACRT) in rectal cancer patients (stage II/III), has significantly increased between from 5% of cases between 1995-1999, up to 38% of cases between 2005 and 2009 (12).

In 2004, the German Rectal Cancer Trial which was carried out on 823 LARC patients, found a direct correlation between NACRT and reduced local relapse rates and improved patient survival rates in comparison to postoperative treatment (13,14). Its benefits are most marked when a pathologic complete response (pCR) is achieved (i.e. when no remaining tumour is identified upon pathological examination in the subsequent surgical specimen). Currently, only 15-27% of all LARC patients achieve pCR (15). The remainders have residual disease, varying from a few scattered tumour cells to large islands of resistant tumour. As a result, these patients have subsequent high relapse and death rates (16).

Chemotherapy

Chemotherapy kills cancer cells with cytotoxic drugs which circulate throughout the bloodstream. The 2 forms of chemotherapy given for rectal cancer are 5 fluorouracil (5-FU) and Capecitabine. Both drugs are anti-metabolites which prevent cells from making and repairing DNA.

Side effects associated with both forms of chemotherapy include fatigue; lethargy; loss of appetite; nausea; vomiting; increased risk of infection; diarrhoea; breathlessness; thinning or total loss of hair; arrhythmia; pain, erythema (redness) and desquamation (peeling skin) of palms and soles of feet; thrombocytopenia resulting in bruising, bleeding nose or gums; sores and ulcers in the mouth; headaches; problems with eyes include epiphora (excessive tear production), dry, itchy skin and brittle nails.

5-FU chemotherapy inhibits the thymidylate synthase enzyme, thereby switching off pyrimidine nucleotide synthesis. It can be given via a bolus or IV infusion. Patients are more likely to achieve higher acute toxicity if treated with a long course chemoradiation therapy (18.2%) in comparison to short-course therapy (3.2%). Additional side effects associated with 5-FU chemotherapy include low blood pressure problems with the eyes including pain or nystagmus (rapid eye movements); loss of fertility; and increased levels of uric acid in the blood resulting in inflamed joints;

Capecitabine is functionally similar to 5-FU, however, it is given orally twice a day. Additional side effects associated with Capecitabine include anaemia; insomnia; pain in the arms, legs, abdomen back and joints; fever; deep vein thrombosis; depression; conjunctivitis and skin sensitivity to sunlight.

Radiation therapy

A linear accelerator (LiNac) emits high energy x-rays which can be customized to each patient's needs, depending on the size, depth and shape of the tumour, thereby reducing damage to healthy tissue. LiNac machines are used for oncologic radiation therapy. When the radiation enters the body it kills both cancerous and healthy tissue. Normal tissue can regrow, but cancerous tissue cannot. Furthermore, cancerous cells become increasingly sensitive to radiation

due to their high proliferative rates (17). Currently, there are 2 forms of radiation typically being used for colorectal cancer; Intensity-modulated radiotherapy (IMRT) and three-dimensional conformal radiotherapy (3-DCRT).

3DCRT is carried out by composing a 3D image of the tumour by compiling images from a minimum of one of the following scans: computed tomography (CT), magnetic resonance imaging (MRI), positron emission tomography (PET) or PET-CT. The oncology team manually adjust the radiation beams intensity, volume, shape and direction; whilst the computer software adjusts dose distribution. These parameters ensure the radiation beams target the exact shape of the tumour, thereby minimising damage to adjacent healthy tissue and organs. Conventional radiation methods previously targeted the region of tissue to the exact width and height of the tumour. 3DCRT is directed to the shape of the tumour itself, thereby minimising damage to the surrounding tissue. This, therefore, allows increased levels of radiation to be used, thereby maximising its effectiveness.

Intensity-modulated radiation therapy (IMRT) targets the tumour directly. 3D scans are taken to locate the tumour and a virtual reality simulation is composed and used to establish a treatment plan. IMRT has significantly lower side effects compared to standard radiation therapy. Conversely to 3-DCRT, the oncology team enter the dose distribution, whilst the computer software generates beam intensity levels required. IMRT can target the tumour more accurately than that of 3-DCRT by altering the radiation beam intensity levels into several smaller fractions. This results in increased radiation being emitted to the tumour, whilst reducing radiation to the surrounding tissue and organs.

Side effects to radiation therapy include nausea; fatigue; lethargic; fibrosis which may result in affected structures adhering to each other; bowel incontinence; rectal irritation resulting in diarrhoea, haematochezia (blood in stool) and painful bowel movements; proctitis (inflammation of rectum); extended wound healing post-surgery; skin irritation resulting in erythema (redness), desquamation (peeling skin) and blistering; weaker pelvic bones; sexual problems; bladder irritation resulting in increased urge to urinate, dysuria (painful urination) or haematuria (blood in urine) or vitamin B12 deficiency.

Surgery: Total mesorectal excision (TME)

Any residual tumour in LARC patients post chemoradiation therapy is removed via total mesorectal excision (TME). This involves removal of the rectum, surrounding mesorectum, pararectal lymph nodes, whilst preserving all organs outside of the rectal fasciation (i.e. bladder, vagina / prostate).

1.3.7. How radiation affects cellular survival

Radiation therapy consists of x-rays targeted at the cancer. This triggers single and double stranded breaks which alter the structure of DNA, oxidative stress, the production of free radicals and reactive oxygen species (ROS) in targeted cancer cells, ultimately resulting in cell death. Furthermore, radiation can affect non-irradiated cells nearby through the 'bystander effect'. This occurs as a result of signal transduction through gap junctions, and release of factors into the growth media from the irradiated cells.

1.3.8. Radiation resistance

Radiation therapy resistance occurs when the tumour cells mutate to overcome the effects of radiation. 15-27% of rectal cancer patients respond fully to chemoradiation therapy. The remaining 73-85% have remaining tumour varying in size from single scattered cells to large islands of resistant tumour, and are associated with high relapse and death rates (16).

1.3.9. Radiation resistance and the hallmarks of cancer

Hanrahan et al identified ten anti-cancer functions which are altered in the majority of cancers. These were termed the hallmarks of cancer and consisted of:

- 1) Self-sufficiency in growth signals: Normal cells are reliant on growth signals from transmembrane receptors for proliferation. However many cancer cells possess the ability to mimic these growth signals, thereby reducing its reliance on the extracellular signals. Furthermore, cancer cells can increase the volume of extracellular receptors which induce growth, or are in a permanently active state(18) . Several pro-survival signalling pathways can be induced during radiation including the MAPK and PI3K signalling pathways.

- 2) Insensitivity to anti-growth signals: Anti-growth signals from molecules including TGF- β and p53, inhibit cellular growth and maturation. Cancer cells become desensitised and bypass these signals to facilitate uncontrolled growth.
- TGF- β is an anti-growth signal which prevents cell cycle progression. However cancer cells can be deficient in, or contain mutated TGF- β receptors on their surface. Furthermore, TGF- β can induce epithelial-to-mesenchymal transition (EMT) in late stage tumours, whereby cancer cells obtain stem-cell like properties which are resistant to radiation therapy (19).
- p53 is an anti-growth signal which is involved in cell cycle arrest and apoptosis. Typically DNA damage (including radiation) induces p53 accumulation, thereby triggering apoptosis. However if the tumour contains mutations in p53, then apoptosis and tumour suppression is reduced. p53 mutations are associated with radiation resistance (20,21)
- 3) Tissue invasion and metastasis: Our bodies consist of epithelial (adherent sheets) and mesenchymal (single cells capable of migration) cells. Cell-cell adhesion molecules (CAMs) and integrins are essential for adherence of cells to the extracellular matrix (ECM). Cancer cells can undergo epithelial to mesenchymal transition (EMT), whereby they transition from epithelial cells into mesenchymal cells. Matrix degrading proteases are upregulated whilst protease inhibitors are down regulated to degrade the ECM and cellular adhesion proteins. This facilitates cellular detachment from the ECM, transition into and migration throughout the circulatory system. When the cell attaches in its final location, it transitions back to an epithelial cell and continues to proliferate. This is a process typically intended for embryonic development; however cancer cells also possess this ability, whereby the detached mesenchymal stem cell is referred to as a circulating tumour cell (CTC). Cancer stem cells or CTCs are undifferentiated, appear resistant to chemotherapy, other drug therapies and apoptosis, and have been associated with increased metastatic risk post chemoradiation therapy.
- 4) Limitless replicative potential: Normal cells can proliferate a limited number of times. Each round of proliferation removes 50-100 nucleotides of telomeric DNA. After 40-60 proliferative cycles the telomeres have degraded so much they are unable to protect the chromosomal DNA from

DNA damage, thereby triggering the cell into senescence. In contrast, cancer cells telomeres do not shorten, instead they produce large volumes of telomerases which adds telomeric DNA to the ends of the chromosomes, thereby preventing cellular senescence and resulting in limitless replicative potential (22). Telomeres are particularly sensitive to DNA damage via oxidative stress due to DNA repair being less effective on telomeric DNA (23,24). However, radiation induces telomerase activity, thereby aiding with radiation resistance rather than tumour death (25,26). Inhibition of telomerase activity radiosensitises cancer cells. Interestingly, the PI3K/AKT pathway regulates telomerase activity, therefore targeting this pathway may be beneficial.

- 5) Sustained angiogenesis: All cells require a constant supply of nutrients and oxygen, including cancer cells. Therefore, cancer cells have constant angiogenic production. They reduce angiogenesis inhibitor production, whilst oncoproteins e.g. RAS increase production of vascular endothelial growth factor (VEGF). However, blood vessels in tumours grow in a disorganised manner, and tumour cells may grow faster than its angiogenic ability, resulting in hypoxic regions within the tumour. Since oxygen is a radiosensitiser, hypoxic tumour cells are more resistant to radiation than oxygenated cells.
- 6) Evading apoptosis: The PI3K and MAPK pathways can activate apoptosis. However they can also activate DNA damage repair. If these pathways are mutated in cancer, DNA damage repair may be enhanced, resulting in the repair of radiation induced DNA damage, and ultimately evade apoptosis (27). Mutations within these pathways are associated with resistance to both chemotherapy and radiation therapy (28,29).
- 7) Avoiding immune destruction: The body's innate immune system can recognise and remove cancer cells. However, the innate immune system can also induce tumour-promoting inflammation which drives early tumour growth. Tumours can produce cytokines, chemokines and metabolic pathway modulators which trigger macrophages to induce angiogenesis and tissue architecture remodelling, thereby promoting tumour growth and metastasis. NFκB is important for modulating the immune response to tumour, including its response to inflammation, cytokine and chemokine release and influencing the innate/adaptive immune systems. However,

NFκB is also associated with radiation resistance. Other inflammatory markers associated with radiation resistance include HIF-1, STAT-3 and PGHS-2.

- 8) Tumour-promoting inflammation: During inflammation, leucocytes are attracted to the injury site. Neutrophils are typically the first leucocytes attracted, they engulf microbes and release reactive oxygen species (ROS). ROS simultaneously kill microbes and healthy surrounding cells. During chronic inflammation, macrophages are also recruited, and tissue damaged by ROS is replaced by fibrosis. Tumour cells secrete cytokines and chemokines during tumour development, which change macrophages into tumour associated macrophages (TAMs). TAMs produce growth factors, secrete VEGF for angiogenesis, degrade the ECM to facilitate metastasis, and suppress the immune system to prevent tumour cell apoptosis. Cancer patients which have TAMs have a worse prognosis than patients who do not and are associated with resistance to chemotherapy and radiation therapy (30,31).
- 9) Genome instability and mutations: Genomic instability is a hallmark of aggressive cancers, including CRC. It is driven by chromosomal instability (loss of tumour suppressor genes), microsatellite instability (defects in DNA mismatch repair) or the CpG island methylator phenotype (CIMP). Oxidative stress from genotoxic agents has been shown to induce genomic instability. Furthermore, ionizing radiation damages and mutates DNA. This DNA typically undergoes DNA repair or cellular death. However if the cells are deficient in essential DNA repair genes (e.g. XRCC2, XRCC3) then the cells cannot repair the damage induced by the radiation, then radiation induced genomic instability may ensue.
- 10) Deregulating cellular energetics: Normal cells break glucose down to pyruvate and 32 ATP molecules with carbon dioxide waste expelled (aerobic respiration). In reduced oxygen levels, anaerobic respiration breaks glucose down to pyruvate and 2 ATP molecules and produces lactic acid. Cancer cells metabolism is altered to facilitate tumour growth. Cancer cells require 20 times as much glucose as normal cells, however they use the less efficient form of glycolysis (anaerobic respiration) for accumulation of its by-products. In addition, cancer cells can create ATP at a faster rate than normal cells. The PI3K pathway is commonly mutated in cancer and

can activate HIF which is important for changing the metabolic pathways in cancer cells, altering them from aerobic to anaerobic respiration. Alterations in metabolism, particularly glucose metabolism can result in radiation resistance (23,24).

1.3.10. The role of the immune system in cancer

Cancer occurs through alterations in the immune system, known as 'immunoediting', of which there are 3 phases.

- 1) Elimination: The body's innate immune system (T cells, macrophages and natural killer (NK) cells) identify and eliminate cancer cells. Tumour associated antigens are then excreted and presented to the adaptive (CD4+ and CD8+ T cells) immune system for production of immunological memory.
- 2) Equilibrium: Some tumour cells can become resistant to the immune system due to genomic instability. These tumour cells have evaded cell death, however they are monitored by the adaptive immune system, and kept under control or in equilibrium.
- 3) Escape: If the tumour continues to mutate, it may gain the ability to escape immune detection. Tumours do this by recruiting immunosuppressive cells and reducing the volume of antigens present.

Radiation affects the tumour cells and its surrounding tumour environment, inducing endothelial cell permeability, platelet aggregation, inflammation, separation from the basement membrane and cell death. This results in further inflammation and fibrosis. Dying and dead cells release pro-inflammatory mediators known as damage associated molecular patterns (DAMPs). These include chemokines, cytokines (e.g. TGF- β , TNF- α), heat shock proteins, interleukins, ROS and tumour antigens. DAMPs can then be recognised by dendritic cells, whilst tumour antigens are presented to T cells, thereby enhancing the immune response.

1.3.11. Recurrences

Recurrences can occur up to 10 years after the original diagnosis of RC, with the risk of recurrence decreasing over time. RC recurrences typically occur at a

different site to its original diagnosis. Progression of RC results in invasion of the submucosa, which contains blood and lymphatic vessels, facilitating possible metastasis. Venous blood flows from the mesenteric vein to the hepatic portal and external iliac veins. Therefore, RC typically metastasises to the liver, but other recurrence locations may include the bones, peritoneum, locoregional or distant lymph node, or lungs (32).

1.3.12. Survival

Over the past 20 years, there have been significant improvements in rectal cancer patient outcomes, with a decrease in RC incidence, local recurrence and mortality, and an increase in quality of life. Furthermore, relative 1 and 5-year survival rates have increased in recent years (Table 1.2). However the volume of CRC cases in Ireland has increased due to the growing population, and the stage of diagnosis has increased, this is believed to be a result of better staging techniques (8).

Table 1.2: Relative 1 and 5-year survival rates (12).

	1994-1998 (%)	2004-2008 (%)
Stage 1 – 1yr	92	96
5yr	82	92
Stage 2 – 1 yr.	82	88
5 yr.	58	70
Stage 3 – 1 yr.	85	90
5 yr.	45	64
Stage 4 – 1 yr.	35	51
5 yr.	7	10

1.4. Circulating tumour cells and their role in tumour metastasis.

Despite NACRT treatment, 25-50% of LARC patients relapse as a result of an undiagnosed metastasis. This high recurrence rate suggests that either the metastatic process was undiagnosable during previous treatment (33), or that the treatment itself increases the likelihood of metastasis (34,35) either through resection, chemotherapy or radiation therapy (36).

Every tumour comprises of genetically mutated cells which proliferate at an uncontrollable rate. As the primary tumour matures, some cancerous cells may detach and circulate in the patients' peripheral blood or lymphatic systems. These are referred to as circulating tumour cells (CTCs). Some CTCs may ultimately adhere to tissue at a distant site and result in metastasis.

The concept of CTCs has circulated throughout the world of science since they were first described in 1829 by Recamier. It is estimated that on average, there is only one CTC for every $10^6 - 10^8$ haematopoietic cells (37). This has resulted in difficulty detecting CTCs, until recent years. Currently, there are two main methods for detecting CTCs:

1. Immuno-magnetic antigen-dependent techniques: Detects CTCs by membrane protein expression e.g. CellSearch. However, this method can miss tumour cells if they lose their epithelial markers during epithelial-mesenchymal transition (EMT). CellSearch detects CTCs by their EpCAM positive status. Most CRC cells are strongly EpCAM positive; however, there are a fraction, especially patients with Lynch syndrome who do not express EpCAM. Therefore, the CellSearch technique would rule out all of these samples. Furthermore, since CTCs are heterogeneous, identification of CTCs via cell surface antigens (e.g. EpCAM) or designated RNA sequences may be limiting the identification of positive results, ultimately running the risk of false negatives.
2. Filtration techniques are based on the large size of CTCs compared to other cellular components within the blood. CTCs vary in size from 9 - 30 μ m, compared to platelets (2 - 3 μ m), erythrocytes (6 - 8 μ m) and leukocytes (6 - 12 μ m). The size-selective filters allow smaller cells and debris to pass through, whilst retaining the remaining CTCs, e.g. ScreenCell.

Detection of CTCs in the peripheral blood is relatively non-invasive and has been termed a 'liquid biopsy' or 'real-time tumour biopsy'. It is hoped to serve as a useful diagnostic tool for staging and prognostication in LARC by eliminating invasive monitoring techniques for patients. Furthermore, CTCs extracted from the patients' peripheral blood can undergo molecular testing to signify the primary tumours resistance profile, thereby aiding in a more personalised therapy regimen. Multiple studies in colorectal, breast and prostate cancers have shown that the presence of CTCs in the peripheral blood, particularly post-treatment, is indicative of a poor prognosis, reduced overall survival and recurrence-free survival in CRC patients](34,38–43). Studies have also shown that current treatment regimens reduce the volume of CTCs in the peripheral blood. However, the CTCs which remain are typically resistant to drug therapies (44,45). Furthermore, as peripheral CTCs do not replicate rapidly, it is believed they may not be affected by chemotherapy.

CRC treatment is aggressive and can subject the patient to toxic chemicals. Therefore we need to identify, in advance, patients who may potentially have a worse prognosis, and adapt therapies to the individual for a personalised treatment regimen. A minimally invasive procedure such as enumeration of CTCs throughout treatment through means of a liquid biopsy could be an ideal solution to this hurdle.

The role of genomic aberrations in LARC

1.5. Human genome

An adult body consists of an estimated 37.2 trillion cells. The vast majority of these cells possess a nucleus, each harbouring 23 pairs of chromosomes.

Chromosomes consist of DNA coiled around histones (protein). DNA is the hereditary material which forms an individual's genetic code.

1.5.1 Structure of DNA

The DNA double helix is composed of nucleotides. Each nucleotide consists of a sugar molecule, a phosphate molecule and a base (Figure 1.1). There are four bases which are divided into purines (adenine (A), and guanine (G)), and pyrimidines (cytosine (C) and thymine (T)). Purine and pyrimidine bases connect via hydrogen bonds to form base-pairs (A joins with T, and C with G). The complete set of human DNA sequences (human genome) comprises of approximately 3 billion bases. DNA is converted into RNA in a process known as transcription. DNA and RNA consist of exons (coding), and introns (non-coding), which are cleaved for protein production during translation.

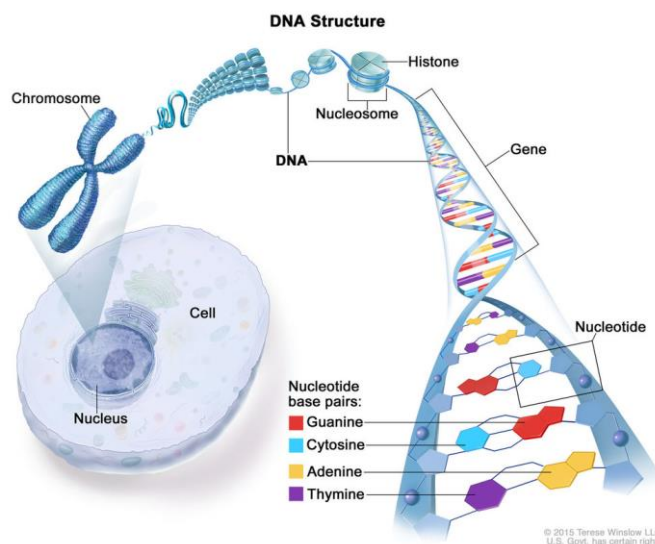


Figure 1.1: Eukaryotic chromosomal structure (46).

Chromosomes are composed of tightly wrapped supercoils and coils of histones bound by the DNA double helix.

1.5.2. Transcription and translation of DNA

Transcription occurs through three steps, initiation, elongation and termination.

Initiation: The enzyme RNA polymerase II attaches to the DNA upstream of the required gene at the promoter site, and begins to unravel the DNA double helix.

Elongation: RNA polymerase reads one of the DNA strands and forms a complementary single-stranded pre-messenger RNA strand, whereby T is substituted for U.

Termination: When RNA polymerase encounters a stop codon (UAA, UAG, UGA), it ceases transcription and cleaves the RNA strand product.

Splicing: The pre-messenger RNA strand contains both introns and exons. RNA polymerase II binds to the 5' and 3' ends of introns and forms a loop of excess DNA. Introns are subsequently removed, and the remaining exons are bound together to form a single strand.

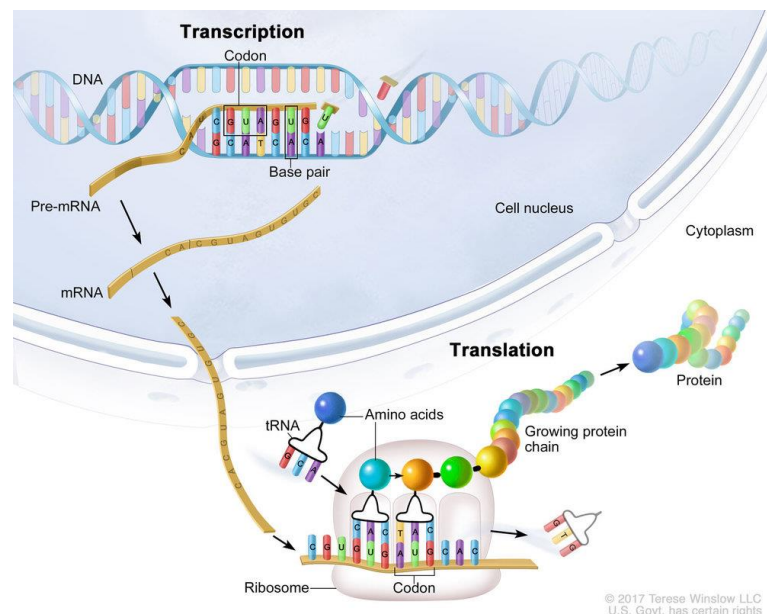


Figure 1.2: Transcription and translation of DNA (47).

This region of RNA is then used as a template and converted into messenger RNA (mRNA) (Figure 1.3). The mRNA strand is completed with a nucleotide cap and poly(A) tail (~100-200 adenine nucleotides in length). Multiple combinations may be formed via splicing in a process known as alternative splicing. mRNA leaves the nucleus through nuclear pores and enters the endoplasmic reticulum. The mRNA template then produces proteins through translation. Within the mRNA, there are codons (set of 3 nucleotides), each of these encodes for a specific amino acid or stop signal during protein synthesis (Figure 1.3).

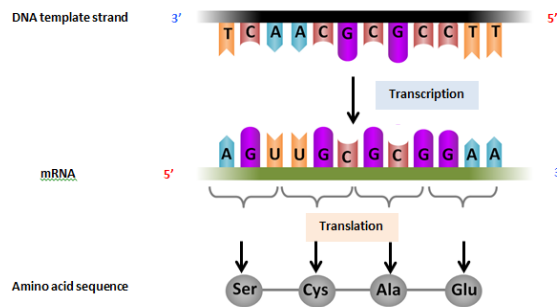


Figure 1.3: Transcription and translation of DNA into a protein.

Overall there are 61 possible codon combinations which form 20 amino acids, and 3 combinations which form stop codons. Therefore, there is an overlap between the majority of codons for the same amino acid (Figure 1.4).

		Second letter									
		T		C		A		G			
First letter	T	TTT	Phe	TCT	Ser	TAT	Tyr	TGT	Cys	T	Third letter
		TTC		TCC		TAC		TGC		C	
		TTA	Leu	TCA		TAA	Stop	TGA	Stop	A	
		TTG		TCG		TAG		TGG	Trp	G	
	C	CTT		CCT	Pro	CAT	His	CGT	Arg	T	
		CTC		CCC		CAC		CGC		C	
		CTA		CCA		CAA	Gin	CGA		A	
		CTG		CCG		CAG		CGG		G	
	A	ATT	Lle	ACT	Thr	AAT	Asn	AGT	Ser	T	
		ATC		ACC		AAC		AGC		C	
		ATA		ACA		AAA	Lys	AGA	Arg	A	
		ATG		ACG		AAG		AGG		G	
	G	GTT	Val	GCT	Ala	GAT	Asp	GGT	Gly	T	
		GTC		GCC		GAC		GGC		C	
		GTA		GCA		GAA	Glu	GGA		A	
		GTG		GCG		GAG		GGG		G	

Figure 1.4: Sixty-four nucleotide combinations which form 20 amino acids and 3 stop codons.

1.6. Mutations in the human genome

The human body is made up of approximately 37.2 trillion cells, with billions of cells being replaced on a daily basis. During this process, the body makes tens of thousands of mistakes every day, with the majority of these mistakes being identified and corrected as follows. Copying errors during DNA replication or transcription into RNA can cause alterations in the sequence of bases which constitute the genetic code. If the error is located within an intron (non-coding region), it is typically removed during splicing and its results are void. However, if the mistake is located within an exon (coding region), or results in intron retention, cancer may ensue.

The vast majority of errors within exons are identified and corrected at checkpoints throughout the replication process. However, if an error evades the body's checkpoints or has the ability to divide independently from the checkpoints, a tumour is formed. These tumours can be benign or malignant. The growth of benign tumours is contained within the tissue where it originated and lacks the ability to shed cells into the periphery. On the contrary, malignant cancer cells do have this ability, thereby facilitating metastasis.

CRC may be acquired (somatic), or inherited (germline). Copying errors can be further classified into point mutations which affect one or a few nucleotides (e.g. synonymous, missense and nonsense mutations); and frameshift mutations which result in an alteration in the reading frame (e.g. insertions and deletions).

1.6.1. Point mutations

- a) Synonymous (silent) mutations are point mutations which alter the gene sequence without changing the encoded protein. In general, if the mutation occurs in the codons third nucleotide, the same amino acid will be produced; such is the case with synonymous mutations. For this reason, synonymous mutations were believed to be passenger mutations. However recent findings suggest that certain synonymous mutations may act as driver mutations, thereby increasing their significance (48,49).
- b) Missense or nonsynonymous mutations occur when a single base-pair is substituted, resulting in the synthesis of an alternate amino acid, which may affect protein function.

c) Nonsense or stop-gain mutations substitute an amino acid coding codon with a stop codon (UAG, UAA or UGA). This results in a premature stop in the translation of the messenger RNA (mRNA), thereby forming a shorter, incomplete, truncated protein which is generally non-functional.

1.6.2. Transition and Transversion point mutations

DNA base sequences can be disrupted as a result of point mutations, leading to transitional or transversional mutations (Figure 1.5). The former is a substitution of a base with one possessing the same chemical properties, i.e. purine>purine, or pyrimidine>pyrimidine. Conversely, a transversional mutation is the replacement of a base with one of the alternate chemical properties i.e. purine>pyrimidine, pyrimidine>purine. Although there are twice as many transversion combinations as transition, these are less likely to occur due to the differences between the chemical structures of the bases.

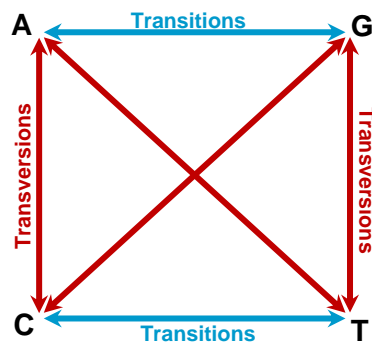
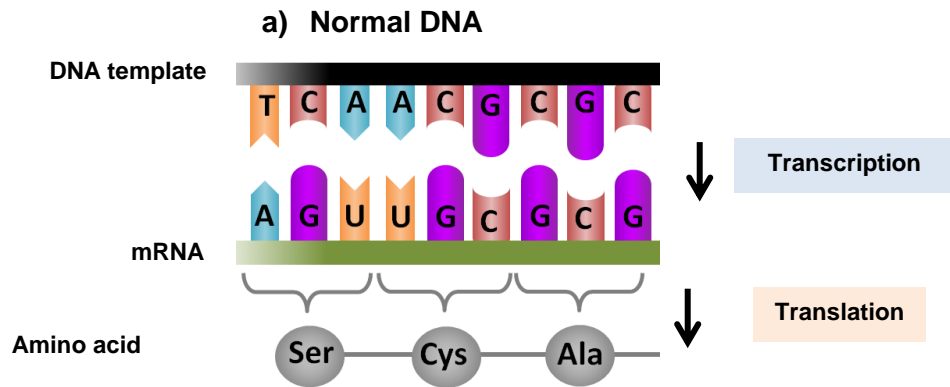


Figure 1.5: Transition and transversion mutations in DNA.

A transition is the substitution of a base with the same chemical properties e.g. purine>purine, or pyrimidine>pyrimidine. A transversion is the replacement of a base with a base of the alternate chemical properties e.g. purine>pyrimidine or pyrimidine>purine

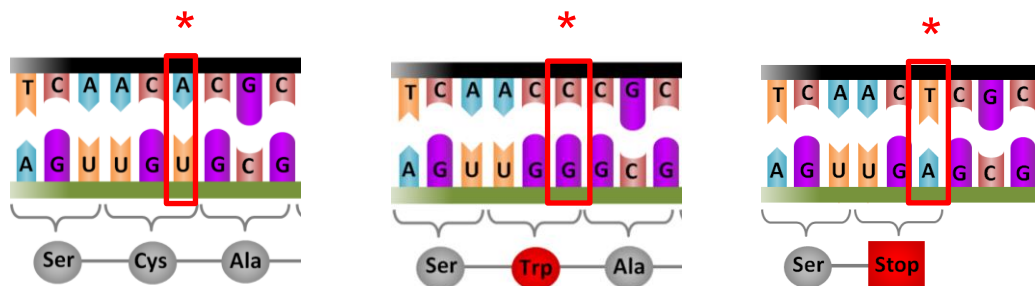
1.6.3. Frameshift mutations

Frameshift or indel mutations are caused by an insertion or deletion which alters the reading frame. During translation, each codon of three nucleotides is read at a time. When a nucleotide is inserted or deleted, this results in the affected codon and every subsequent codon to be affected. Thus an abnormal protein is synthesised



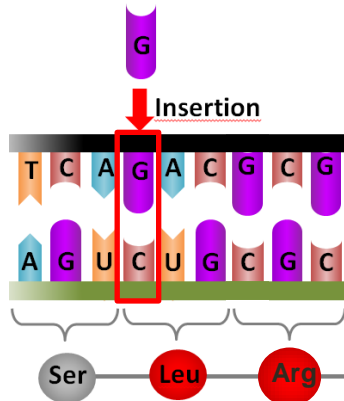
Point mutations

b) Synonymous mutation c) Missense mutation d) Nonsense mutation



Frame-shift mutations

e) Insertion



f) Deletion

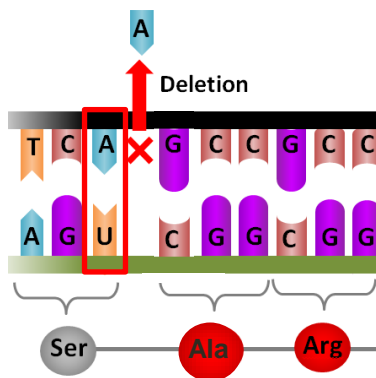


Figure 1.6: Types of mutations, comparing a) normal DNA; point mutations: b) synonymous, c) missense, d) nonsense; frameshift: e) insertion and f) deletion mutations.

1.7. The role of genomic aberrations and the mutator phenotype in the development of CRC.

Fearon and Vogelstein first hypothesised the “adenoma-carcinoma sequence” in 1990. This model suggested that CRC occurs as a result of a multistep process of events, whereby normal epithelium becomes adenomatous and eventually transitions into adenocarcinoma. They theorised that initiation of this pathway occurred through inactivation of the *APC* tumour suppressor gene in normal colonic epithelium. Subsequent activation of *KRAS* would then ensue, leading to an accumulation of mutations in *TGFB*, *PIK3CA* and *TP53* pathways. They proposed a minimum of 7 mutations were necessary for CRC to occur (50). Although there have been many alterations to this model over the past 28 years, the basis of this hypothesis still stands true.

Numerous genetic alterations are required for tumour initiation and progression. Genomic instability is a hallmark in the majority of aggressive cancers and is believed to be a driving force in CRC initiation.

However, Loeb et al noted that normal functioning cells have far lower mutational frequencies than that required for, or identified in human cancers. Therefore he hypothesised that cancer cells possess a ‘mutator phenotype’ which facilitates their increased mutational abilities (51). Loeb theorised that mutations occur in genes which alter cells genetic stability (i.e. apoptosis, checkpoints, chromosome segregation, telomere dysfunction etc.), thereby triggering a mutational cascade (51).

There are 3 pathways associated with genomic instability resulting in CRC pathogenesis:

- i. Chromosomal instability (CIN): Mutations occur at chromosomal separation during mitosis resulting in loss of tumour suppressor genes. Constitutes 65% of all CRC cases.
- ii. Microsatellite instability: Defects within the DNA mismatch repair genes, resulting in an accumulation of mutations in microsatellite regions resulting in hypermutated tumours and microsatellite instability (MSI) (51). Constitutes 15% of all CRC cases

- iii. CpG island methylator phenotype (CIMP) / Serrated methylator pathway.
Constitutes 20% of CRC cases.

1.7.1. Chromosomal instability (CIN)

The majority (~65%) of sporadic CRCs occur as a result of chromosomal instability (CIN); The CIN pathway largely resembles that of Fearon and Vogelstein's adenoma-carcinoma sequence hypothesis. CIN is partial or total loss or gain of a chromosome, resulting in karyotypic abnormalities. It is characterised by loss of heterozygosity (LOH), aneuploidy (chromosome number imbalance), genomic amplification of chromosomal regions, and an accumulation of specific oncogenes and tumour suppressor gene mutations. These mutations activate pathways which are essential for CRC (52).

CIN tumours have an accumulation of 5 tumour suppressor genes and 3 oncogenes, which are vital in activating the oncogenic pathway in CRC. The tumour suppressor gene mutations include APC (5q21), TP53 (17p13), SMAD2 (18q21), SMAD4 (18q21) and DCC (18q21), whilst the oncogenes comprise of KRAS (12p12), CTNNB1 (3p22) and PIK3CA (3q26) (52).

1.7.2. Mismatch repair (MMR)

Throughout the DNA replication process, numerous mistakes occur. A proficient DNA MMR system removes base-pair mismatches and insertion-deletion loops. Base-pair mismatches involve single base substitutions, whilst insertion-deletion loops are a result of DNA polymerase slippage during DNA replication which results in short repeat units in microsatellites.

In a proficient MMR system, MutS related proteins identify and bind to these mismatched bases. MSH-2 dimerises with either MSH-6 or MSH-3, to form MutS α and MutS β respectively. MutS α (MSH-2/MSH-6 heterodimer) is responsible for detecting and binding base: base mismatches (particularly G:T), and small insertion or deletion mismatch loops (up to 12 unpaired bases in length) (53–56). MutS β (MSH-2/MSH-3 heterodimer) is crucial for rectifying large insertion and deletion mismatch loops (57–59).

This dimerisation results in recruitment of MutL related proteins. MLH1 dimerises with PMS1 to form a complex which increases MutS related proteins ability to detect mismatches (54,60). MLH1/PMS1 further binds to the MutS β heterodimer complex. MLH1 binds with PMS2 for the repair of MutS β pathway insertions and deletions (61). The MLH1/PMS2 heterodimer removes the mismatched DNA and synthesises a new DNA strand.

When the MutS and MutL heterodimer complexes bind to the identified DNA mismatch site, an incision is made in the DNA 1-2 kilobases prior to mismatch site. Exonuclease mediated degradation occurs along the DNA strand until the area of interest is removed. DNA polymerase δ supplements this region with the correct nucleotide sequence.

Multiple other proteins are required for MMR, including replication protein A (RPA), replicating factor C (RFC), DNA polymerase δ , exonuclease 1, RAD27, and proliferating cell nuclear antigen (PCNA) (62).

The human genome contains over 100,000 regions of short tandem repeat sequences, in which a genetic sequence of one to five base-pairs in length is consecutively repeated fifteen to thirty times. These are referred to as microsatellites. Microsatellites are particularly susceptible to 'slippage' during the DNA replication process; therefore a proficient MMR system is vital in these regions. Slippage results in the formation of a loop of the nascent or template DNA strand. Slippage in MSI tumours are frequently found at polyA or poly(C) regions and near diploid genomes. A proficient MMR (pMMR) system can detect and rectify this process. However, when there is a defect in the mismatch repair system, the loops of DNA strands go undetected, resulting in the formation of alleles of inconsistent lengths during the subsequent replication process. These mutations accumulate at the microsatellite regions, initiating the "hypermutator phenotype" and ultimately results in MSI. Tumours with a deficient MMR system have mutation rates of 100-1000 fold that of proficient cells (63,64). When a tumour becomes MMR deficient, every nucleotide repeat sequence in the genome (both intronic and exonic) is susceptible to insertion and deletion mutations.

The majority of microsatellites are located in introns. However, frameshift mutations can result in truncation, inactivation or constitutive activation of proteins essential for DNA proliferation, repair, apoptosis, cell signalling and growth. This is particularly true in the promoter regions of the MMR genes including *BAX*, *BCL10*, *Caspase5*, *IGFRII*, *PTEN* and *TGFBRII* (65). Mutations in these genes have been found to facilitate carcinogenesis. Frameshift mutations in MSI CRCs typically occur in tumour suppressors (*TGFBRII*, *IGFIIR*, *PTEN*, *RIZ*), DNA MMR (*MSH-3*, *MSH-6*), apoptosis promoter (*Bax*), transcription factor (*TCF4*), Wnt signalling (*AXIN2*), and DNA glycosylase (*MBD4*).

MSI is identified in ~90% of all HNPCC cases (germline inactivation of MMR), and 10-15% of sporadic CRC cases. Both have a diploid or nearly diploid karyotypes, conversely, the majority of CRCs are aneuploid. Knudson has hypothesised that both MMR gene alleles must be inactivated for MSI to occur (66). Sporadic defective MMR (dMMR) typically results from epigenetic alterations, particularly silencing of the hMLH1 promoter methylation gene, resulting in MLH1 silencing. This can occur sporadically or as a result of the CpG island methylator phenotype (CIMP) pathway.

There is a growing link to suggest that MMR deficient CRCs (both germline and sporadic) undertake an alternative pathway to that of the conventional adenoma-carcinoma pathway. Inactivation of the MMR genes results in the classical “mutator phenotype” associated with these tumours.

1.7.3. CpG Island Methylator Phenotype (CIMP) pathway

CpG islands are regions of DNA (typically 500-1500bp) which have a high frequency (>0.6) of cytosine-guanine bases. The human genome contains an estimated 30,000 CpG islands. They are generally located along the 5' end of promoter sites, where they are shielded from methylation, in contrast to all other CpG regions which are methylated. CpG methylation is involved in the regulation of transcription and translation.

Alterations in methylation can result in inactivation of tumour suppressor genes, and initiation of genomic instability. In cancer, the CpG islands in the promoter regions can become methylated, thereby reversing the standard methylation

process within the cells; converting unmethylated promoter regions into a state of hypermethylation, and removing methyl groups from all remaining cells. These are referred to as CpG methylator phenotype (CIMP) tumours.

CIMP tumours account for 9-23% of rectal cancers (63, 64). They were first hypothesised in colorectal cancer by Toyota et al in 1999 (67). The majority of sporadic MSI tumours simultaneously contain CIMP pathway mutations. CIMP tumours display gene silencing as a result of hypermethylation of CpG islands. CIMP tumours are divided into CIMP-high and CIMP-low, associated with a high frequency of BRAF and KRAS mutations respectively (68). They are significantly associated with old age, females, sporadic MSI tumours, BRAF and KRAS mutations, and poor differentiation. The most frequently used CIMP markers are P16, MINT1, MINT2, MINT31 and MLH1.

1.7.4. Causes of DNA damage

Mutations are a direct result of DNA damage from either endogenous or exogenous factors, and affect vital cellular functions such as cell cycle checkpoints, apoptosis, cellular growth, telomere dysfunction, chromosomal segregation, invasion and metastasis (51).

Endogenous factors that can affect mutation accumulation include:

- Genetic predisposition: Family history accounts for 20% of cases, with the remaining 80% consisting of sporadic cases. Hereditary CRC diseases result from inheriting a cancer-causing genetic defect from one or both parents. An individual's risk of developing CRC increases two or three-fold if they have a first degree relative with CRC (69). Genetic predisposition accounts for approximately 10% of all CRC cases, and can lead to syndromes such as familial adenomatous polyposis (FAP), attenuated familial adenomatous polyposis (AFAP), MYH-associated polyposis (MAP) and hereditary nonpolyposis colorectal cancer (HNPCC); which all result in an increased risk of developing cancers including CRC. These syndromes are further discussed in Table 1.3.

Syndrome	Vol of colonic polyps	Average age at which cancer develops	Risk of other cancers	Associated with mutations in	Autosomal	Note
FAP (Familial adenomatous polyposis)	100's-1000's	40's.	Thyroid, stomach, ampulla, benign desmoid tumours	APC gene	Autosomal dominant	>80% of individuals with FAP develop CRC.
AFAP (Attenuated FAP)	<100		Gastric and duodenal polyps	5' or 3' region of the APC gene	Autosomal recessive	16-40% of patients with AFAP carry bi-allelic inactivation of MUTYH based excision repair gene.
MAP (MUTYH associated polyposis)	10-100	40's		MYH gene	Mutation occurs sporadically but may be seen in siblings.	
HNPCC (Hereditary non-polyposis colon cancer) / Lynch syndrome	Colon polyps + cancer	30's-40's	Stomach, ovaries, ureters, bile ducts, endometrium.	MMR components (95% of mutations are found in hMLH1 or hMSH2)	Autosomal dominant	Usually in the right side of the colon.
						Usually react better to treatment than sporadic tumours.

Table 1.3: Genetic adenomatous polyp syndromes

Mismatch repair (MMR) proteins identify and correct base pair alterations and small insertion loops. Deficiencies within the MMR genes can therefore lead to an accumulation of somatic mutations within tumours and ultimately result in genomic instability and the mutator phenotype. dMMR proteins are unable to identify and remove oxidative damage or induce apoptosis.

- **Metabolic alterations:** Metabolic rates can be altered within tumours as a result of reduced nutrient and oxygen supply and pH levels within the tumour microenvironment. This can lead onto genomic instability within the tumour (70). Furthermore, reactive oxygen species (ROS) are produced during endogenous metabolism. However, prolonged exposure to ROS (i.e. during chronic stress), can result in inflammation, cellular damage, formation of somatic mutations, and has been linked to carcinogenesis (71).
- **Oxidative damage:** Oxidative stress is caused by an imbalance between free radicals (including ROS) and anti-oxidants within the body, resulting in cellular damage. Oxidative damage which occurs during base hydrolysis or metabolism can result in single strand DNA breaks, and accounts for 75% of mutations. Double strand breaks can occur as a result of multiple single strand breaks, however these occur less often, but are more dangerous. Hydrogen peroxide is a genotoxin produced under oxidative stress, which cause DNA strand breaks in colonocytes, particularly in basal crypt cells (72). Proliferating cells at the base of the crypts have high proliferation and metabolic rates. They are believed to have increased oxidation levels (73), are more sensitive to DNA damage (72) and have increased potential to become cancerous. Oxidative stress markers are increased in patients with FAP and colorectal cancer.
- **Inflammation:** During inflammation, phagocytotic cells including leukocytes produce reactive oxygen (ROS) and nitrogen species (RNS). Both ROS and RNS form peroxynitrite which is mutagenic and results in DNA damage in proliferating cells. Continued exposure of cells (particularly proliferating cells) to ROS and RNS can result in genomic aberrations (74,75). Chronic inflammation of the bowel can result in CRC. This is evident in

long-standing inflammatory bowel diseases (IBD), such as Crohn's disease or ulcerative colitis which are known risk factors for CRC, contributing to 10-15% of all IBD patient deaths (76,77). The latter is a chronic inflammatory disease of the large intestine. Patients with long-standing ulcerative colitis are shown to have an increased risk of CRC from 8-10 years post-onset, with this risk continuing to increase over time (2.5% at 20 years, 7.6% in 30 years and 10.8% in 40 years) (76). However ulcerative colitis patients who develop CRC typically have better outcomes than CR patients without ulcerative colitis. This is believed to be a result of early detection methods and different genetic mutation profiles. In order to detect CRC early, patients with ulcerative colitis in excess of 8 years have annual examinations for precancerous changes in the large intestine. Furthermore, anti-inflammatory drugs and aspirin are associated with a reduced risk of CRC (78–81).

- Increasing age is associated with increased risk of cancer, particularly greater than 60 years (unless there is an underlying genetic condition). 87.9% of males and 86.3% of females diagnosed with CRC between 1995 and 2009 were over 55 years of age (82). Increased age is linked to increased volumes of free radicals and oxidation.

Exogenous factors that can affect mutation accumulation:

- Heterocyclic amines: Diets high in fats and low in fibre, alcohol abuse and obesity are all risk factors for CRC. Every 5kg/m² increase in an individual's body mass index (BMI) results in an 18% increased risk of developing CRC (83). Haemoglobin from red meat potentially increases colonic oxidative damage resulting in increased DNA mutations (84). Furthermore, heterocyclic amines which are found in cooked meat and fish are associated with increased risk of cancer.
- Obesity: Adipose tissue is an endocrine organ which produces and secretes hormones (adipokines) which are associated with inflammation, coagulation and dyslipidaemia. One such adipokine is leptin, which has pro-inflammatory, pro-angiogenic and anti-apoptotic properties. Furthermore, leptin receptors activate the PI3K and MAPK pathways.

Obesity is related to chronic inflammation, increased production of acute phase proteins (incl CRP) and abnormal production of cytokines. An increase in adipokines results in chronic low-grade inflammation, and the activation of pro-inflammatory signalling pathways e.g. NFκB, JNK and IKKβ whose activity increases with adiposity. This leads to the production of reactive oxygen species, pro-inflammatory cytokines and adipokines, and a reduction in anti-inflammatory adipokines. Adiposity is associated with the release of pro-inflammatory cytokines e.g. TNF-α, CRP and IL-6. Cytokines and growth factors secreted from adipose tissue may have pro-tumourigenic properties in the gastrointestinal tract. Macrophages are important in adipose tissue secretions and are the main source of inflammatory cytokines e.g. TNFα and IL-6.

Furthermore, men typically have higher volumes of visceral fat compared to women. This has therefore been linked to the higher frequency of colorectal cancers in males compared to females.

1.8. Mutational signatures

Somatic mutations are present in all cancer genomes; however, our knowledge of their impact is limited. As a result, many studies focus on combining information to gain a greater knowledge of the human body's response to mutational triggers. These studies have shown that varying mutational processes which occur as a result of both endogenous and exogenous mutagens can result in the formation of distinctive somatic mutational sequences or imprints on the cancer genome. These imprints are classified as 'mutational signatures', and each signature is based on the type of mutational process, its duration and intensity of exposure (85,86).

At present, there are 30 validated mutational signatures. These have been established from whole-genome sequencing of 1,048 samples, and exome sequencing of 10,952 samples from 40 different types of human cancers. This meta-analysis was based on data from the International Cancer Genome Consortium (ICGC), The Cancer Genome Atlas (TCGA), and numerous other peer-reviewed publications (86–89).

Signature profiles are determined using the 6 base substitution groups, starting

with the pyrimidines for each base-pair (C>A, C>G, C>T, T>A, T>C, T>G). Each of these substitution groups are further divided into 12 subgroups, depending on the bases immediately 5' and 3' to the mutated base. This results in 96 potential mutational trinucleotide possibilities (6 base substitutions * 4 possible 5' bases * 4 possible 3' bases) (Figure 1.7):

Preceding nucleotide		Altered nucleotide						Subsequent nucleotide
		C>A	C>G	C>T	T>A	T>C	T>G	
A	{	A C A	A C A	A C A	A T A	A T A	A T A	A
		A C C	A C C	A C C	A T C	A T C	A T C	C
		A C G	A C G	A C G	A T G	A T G	A T G	G
		A C T	A C T	A C T	A T T	A T T	A T T	T
C	{	C C A	C C A	C C A	C T A	C T A	C T A	A
		C C C	C C C	C C C	C T C	C T C	C T C	C
		C C G	C C G	C C G	C T G	C T G	C T G	G
		C C T	C C T	C C T	C T T	C T T	C T T	T
G	{	G C A	G C A	G C A	G T A	G T A	G T A	A
		G C C	G C C	G C C	G T C	G T C	G T C	C
		G C G	G C G	G C G	G T G	G T G	G T G	G
		G C T	G C T	G C T	G T T	G T T	G T T	T
T	{	T C A	T C A	T C A	T T A	T T A	T T A	A
		T C C	T C C	T C C	T T C	T T C	T T C	C
		T C G	T C G	T C G	T T G	T T G	T T G	G
		T C T	T C T	T C T	T T T	T T T	T T T	T

Figure 1.7: Ninety-six mutational trinucleotide possibilities located along the horizontal axis of mutational signatures.

The majority of mutations in a tumour are passenger mutations, which have a relatively low mutational type probability and can lead to a uniform depiction (signatures 3 and 5). However, the majority of pathways are defined by a few dominant 'driver' mutations (e.g. signatures 10, 15, 27) which form distinctive spikes within the signatures. Different signatures have been associated with varying causes i.e. age, MMR deficiency etc.

The majority of cancer samples have numerous mutational processes co-occurring simultaneously. This results in an amalgamation of multiple signatures, with as many as 6 signatures per sample found in uterine, stomach and liver

cancers (88). Colorectal cancers have an average of 3 signatures per sample (88). This amalgamation can result from multiple subclonal populations which arise from varying mutagens, or heterogeneity within the tumour. This ultimately results in signatures which cannot be clearly defined to any one category by eye. Therefore, further computer analysis is required.

Signatures 1, 6 and 10 are the signatures most commonly associated with CRC (88). Signature 6 is characterised by an overwhelming dominance of C>T mutations at NpCpG, i.e. where the mutated cytosine (underlined) is flanked 5' by any nucleotide, and 3' by a guanine, and connected by phosphate (p) groups. Samples which possess signature 6 have an abundance of small indels and substitutions at nucleotide repeats as a result of defective DNA mismatch repair and result in microsatellite instable (MSI) tumours (88). Signature 10 is associated with mutations within POLE, which is involved in DNA replication and repair.

Some mutational signatures can be linked to endogenous or exogenous sources. Endogenous sources include Age (signature 1), inflammation (signatures 2, 13), retrotransposon jumping (signatures 2, 13), defective DNA mismatch repair (signatures 6, 15, 20, 26), polymerase η (signature 9) and altered POLE mutations (signature 10). Whilst exogenous sources include viral infection (signatures 2, 13), tobacco smoking (signature 4), chewing tobacco (signature 29), ultraviolet (UV light), alkylating agents (signature 11) and aflatoxin exposure (signature 24).

The mutational signatures are constantly being updated with new samples to gain a greater understanding of these signatures, and which cancer types they affect most. New signatures may also be identified in the future.

Signature	Identified in	Proposed aetiology
Signature 1	All types of cancers	Increasing age
Signature 2	22 types of cancer, predominantly bladder and cervical	Inflammation, viral infection or retrotransposon jumping. Associated with cytidine deaminase AID/APOBEC family.
Signature 3	Pancreatic, ovarian and breast cancer	Failure of dsDNA repair by homologous recombination. Associated with somatic and germline BRCA 1/2 mutations.
Signature 4	Lung, oesophageal, liver, head and neck cancer	Smoking tobacco
Signature 5	All types of cancers	Unknown
Signature 6	17 types of cancer, predominantly colorectal and uterine	Defective DNA mismatch repair and MSI tumours
Signature 7	Skin cancer	Exposure to ultraviolet (UV) light
Signature 8	Medulloblastoma and breast cancer	Unknown
Signature 9	Malignant B-Cell lymphoma, chronic lymphocytic leukaemia	polymerase η , involved in cytidine deaminase AID family
Signature 10	6 types of cancer, predominantly colorectal and uterine	Altered POLE activity. These cancers are ultra-hypermutators
Signature 11	Glioblastoma and melanoma	Alkylating agents
Signature 12	Liver cancer	Unknown
Signature 13	22 types of cancer, predominantly bladder and cervical	Inflammation, viral infection or retrotransposon jumping. Associated with cytidine deaminase AID/APOBEC family.
Signature 14	Uterine cancer and glioma	Unknown
Signature 15	Stomach and small cell lung carcinoma	Defective DNA mismatch repair
Signature 16	Liver cancer	Unknown
Signature 17	Oesophagus, stomach, lung, liver, breast cancer, melanoma and B-cell lymphoma	Unknown
Signature 18	Neuroblastoma, breast and stomach cancer	Unknown
Signature 19	Pilocytic astrocytoma	Unknown
Signature 20	Breast and stomach cancer	Defective DNA mismatch repair
Signature 21	Stomach cancer	MSI tumours. Only in tissues also possessing signatures 15 and 20
Signature 22	Urothelial and liver cancer	Unknown
Signature 23	Liver cancer	Unknown
Signature 24	Liver cancer	Aflatoxin exposure
Signature 25	Hodgkin lymphoma	Unknown
Signature 26	Stomach, cervical, breast, uterine cancer	Defective DNA mismatch repair
Signature 27	Clear cell kidney cancer	Unknown
Signature 28	Stomach cancer	Unknown
Signature 29	Gingivo-buccal oral squamous cell carcinoma	Chewing tobacco
Signature 30	Breast cancer	Unknown

Table 1.4: Cancer locations and proposed aetiology for mutational signatures (90).

1.9. The role of the PI3K and MAPK signalling pathways in cancer

Within the body, many cellular processes occur through signalling pathways. Two such pathways are the phosphatidylinositol-3-kinase (PI3K) and mitogen-activated protein kinase (MAPK) pathways. These are kinase signalling cascades which are regulated by phosphorylation and dephosphorylation of their substrates. Under normal physiological conditions, these pathways are involved in activation and regulation of vital cellular functions such as proliferation, differentiation, apoptosis, transcription and intracellular trafficking. Somatic genetic alterations (e.g. PIK3CA, KRAS and BRAF mutations) that activate the pro-oncogenic PI3K and MAPK signalling pathways have been linked to multiple forms of cancers, including rectal cancer (15–17). My mentor Prof. Hennessy, and others have shown that these alterations are associated with resistance to chemotherapy and radiation therapy, and poor patient outcomes (93). Although there are numerous pathways involving both PI3K and MAPK, this report will focus on the Ras/Raf/MEK/MAPK (ERK) and PI3K/AKT/mTOR pathways.

1.9.1. PI3K signalling pathway

The PI3K molecule consists of a p85 α regulatory subunit which is transcribed from one of two genes (*PIK3R1* or *PIK3R2*) and a p110 α catalytic subunit which is transcribed from 1 of 4 genes (*PIK3CA*, *PIK3CB*, *PIK3CD*, *PIK3CG*). In its inactive state, p85 is bound to p110. Activation of the PI3K pathway can occur through binding to a receptor tyrosine kinase (RTK), G-protein coupled receptor (GPCR), extracellular growth factor or active membrane-bound RAS (Figure 1.8). Upon activation, class I PI3Ks are recruited to the plasma membrane, where p110 separates from p85, allowing the p85 subunit to interact with tyrosine phosphates on the activated receptors, or to adaptor proteins associated with the receptors.

The activated p110 subunit phosphorylates the 3'hydroxyl group of phosphatidylinositol-4, 5-bisphosphate (PIP2) thereby converting it to phosphatidylinositol-3, 4, 5-triphosphate (PIP3). PIP3 activates the proto-oncoprotein Akt, resulting in a conformational change. This, in turn, activates Akt dependent and independent downstream signalling pathways, which can regulate apoptosis (Bax), translocation (Rheb, mTOR and S6K) and transcription (NF- κ B, CREB and p53).

Negative regulatory molecules for the PI3K pathway are phosphatases. These include PHLPP which disables Akt; and SHIP-1, SHIP-2 and PTEN, all of which inactivate PIP3. The lipid phosphatase PTEN, hydrolyses PIP3, reverting it back to PIP2 via dephosphorylation of the 3' phosphate group of PIP3, thereby deactivating the PI3K signalling pathway. Inactivating mutations in these phosphatases or activating mutations (e.g. in PI3K or Akt) can result in tumour initiation and progression (94–96).

PIK3CA

PI3Ks are lipid kinases which are triggered by growth factors, cytokines etc., and result in intracellular signalling cascades which are responsible for cell growth, proliferation, metabolism, cell cycle progression, survival and motility. There are three classes of PI3Ks based on structure, function and corresponding substrates; with the most studied being Class I PI3Ks.

Class I

Class I PI3K isoforms are divided into class IA (PI3K α , PI3K β and PI3K δ) and class IB (PI3K γ). All PI3K Class I catalytic isoforms possess an N-terminal RAS-binding domain which facilitates interacting and binding to members of the RAS family and RAS GTPases.

Class IA

Class IA PI3Ks are lipid kinases which form heterodimers. They are composed of a highly homologous p110 catalytic subunit and a p85 regulatory subunit. The p110 subunit can be found in 3 isoforms (p110 α , p110 β , p110 δ), which are encoded by PIK3CA, PIK3CB and PIK3CD respectively. The latter is almost exclusively expressed in the immune system, whilst p110 α and p110 β are ubiquitously expressed. p110 α and β are similar in structure and some functions, however, p110 α is involved in vascular endothelial growth signalling and angiogenesis, whereas β does not (97). The p85 subunit can be found in 5 isoforms and are encoded by one of three genes PIK3R1 (p85 α , p55 α , p50 α), PIK3R2 (p85 β), or PIK3R3 (p85 γ).

Class IB

Class IB PI3Ks are heterodimers consisting of a p110 γ catalytic subunit, and a p101 or p87 regulatory subunit, encoded by PIK3CG, PIK3R5 or PIK3R6 respectively.

Class II

Class II PI3Ks are monomers, consisting of 3 isoforms, PI3K-C2 α , PI3K-C2 β and PI3K-C2 γ , which are encoded by PIK3C2A, PIK3C3B and PIK3C2G respectively. Class II PI3K monomers convert PtdIns to PtdIns(3)P.

Class III

Class III PI3Ks are composed of a catalytic subunit Vps34 (encoded by PIK3C3), which couples with its regulatory subunit Vps15 (encoded by PIK3R4). This results in the formation of PtdIns(3)P which is responsible for autophagy and regulating intracellular trafficking. The family of myotubules (MTM1 and MTMR1) act as negative regulators for the class II and II PI3Ks, by dephosphorylating the 3' phosphate group of PtdIns(3)P.

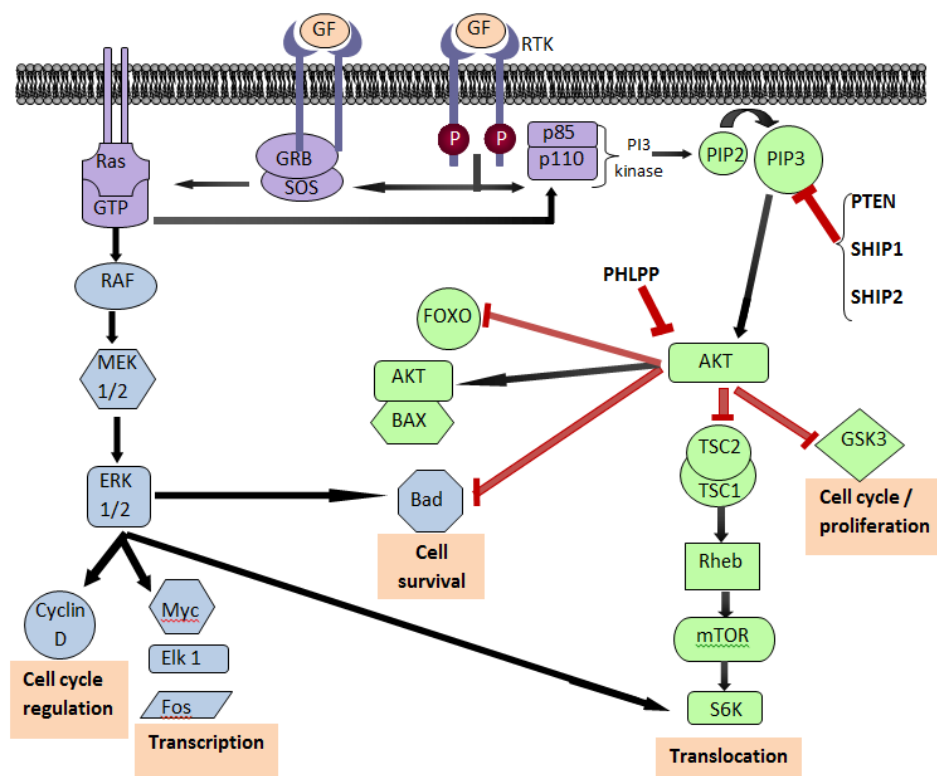


Figure 1.8: The MAPK and PI3K pathway interactions

Initiation of the MAPK pathway (depicted in red) occurs through the binding of a ligand to, and dimerisation of two receptor tyrosine kinases (RTKs), resulting in phosphorylation. This creates a docking site for GRB2 and SOS, to which Ras binds, thereby activating it. Ras activation can trigger multiple signaling cascades, such as the PI3K or MAPK pathways. In the latter, a phosphorylation cascade ensues, resulting in activation of RAF which phosphorylates MEK1/2, thereby activating MAPK (ERK1/2). MAPK can activate multiple other factors involved in transcription (Myc, ELK1, Fos), cell cycle regulation (cyclin D), and cell survival (Bad).

The PI3K pathway (depicted in black) is activated via an RTK, and extracellular growth factor, or binding to active membrane-bound RAS. The PI3K complex phosphorylates phosphatidylinositol-4, 5-bisphosphate (PIP2) into phosphatidylinositol-3, 4, 5-triphosphate (PIP3). PIP3 then activates the proto-oncoprotein Akt, which can regulate apoptosis (Bax), translocation (Rheb, mTOR, and S6K) and transcription (NF- κ B, CREB and p53). Negative regulatory molecules for the PI3K pathway are phosphatases. These include PTEN, SHIP-1 and SHIP-2 which all act on PIP3, or PHLPP which acts on Akt. Inactivating mutations in these phosphatases or activating mutations (e.g. in PI3K or Akt) can result in tumour initiation and progression (94–96).

1.9.2. Mutations in PI3K / MAPK pathways

Cancer cell growth is dependent on signalling pathways. Due to proto-oncogenic mutations and loss of function in tumour suppressor genes, cancer cells have autonomous control over cellular growth and non-compliance to apoptotic or cellular growth-inhibitory signals.

Somatic genetic alterations (e.g. *PIK3CA*, *KRAS* and *BRAF* mutations) that activate the pro-oncogenic PI3K and MAPK signalling pathways are common in rectal cancer. My mentor, Prof. Hennessy, and others have shown that these alterations are associated with resistance to chemotherapy and radiation therapy, and poor outcomes (93). Therefore, it is possible that inhibition of the PI3K and MAPK pathways may increase treatment effectiveness in LARC.

1.9.3. PI3K pathway mutations

In RC, the vast majority of PI3K pathway aberrations are a result of upregulation of RTKs, mutations in, or overexpression of the proto-oncogene *PIK3CA* and/or inactivation of the tumour suppressor gene *PTEN*.

Somatic mutations in *PIK3CA*

Somatic missense mutations, deletions and amplifications in *PIK3CA* have been linked to CRC, and other cancers (95,98). *PIK3CA* gene mutations are present in 8-20% of all CRC cases (23–25, 36), with the majority of these mutations (80%), occurring in two hotspots in the helical domain of exon 10 (codons 542 and 545) and the kinase domain of exon 21 (codon 1047)(92). All three hotspot mutations are known to be oncogenic and increase PI3K activity. Mutations within the helical domain reduce p85's ability to inhibit p110 α or allow direct interaction between p110 α and the insulin receptor substrate 1 (IRS1). Kinase domain mutations increase p110 α interactions with lipid membranes.

PIK3CA mutations in exon 10 are associated with loss of O-6-methylguanine-DNA methyltransferase (MGMT) expression (required for DNA repair), increased levels of CpG island methylator phenotypes (CIMP) and the co-occurrence of *KRAS* mutations (100). Mutations in exon 21 are associated with microsatellite instable (MSI) tumours (100). In general, patients with *PIK3CA* mutations are less likely to

achieve pCR (93) and have a higher risk of local recurrence with a more rapid onset than patients who are wild-type for *PIK3CA* (99).

Somatic alterations in the *PIK3R1* and *PIK3R2* regulatory subunits are commonly found in cancer, resulting in decreased inhibition of p110. Somatic *PIK3R1* mutations are commonly inframe insertions, deletions or substitutions within the inter-SH2 (iSH2) domain of p85 α , which is the interaction point between p85 α and p110. Many of these mutations result in reduced ability to inhibit p110, thereby increasing PI3K activity.

PIK3CB, *PIK3CD* and *PIK3CG* are not typically mutated in cancers but are commonly overexpressed or amplified.

Somatic mutations in *PTEN*

PTEN is a negative regulatory molecule for the PI3K pathway, therefore its loss results in upregulation of this pathway. Mutations within the *PTEN* gene occur in 5-14% of all CRC cases, with the higher frequency found in MSI tumours (101,102). Little research has been carried out on *PTEN* mutations within CRC due to limited identification techniques for *PTEN*. However, it is known that a loss of *PTEN* expression is associated with decreased overall survival (103).

1.9.4. The MAPK signalling pathway

MAPK pathway activation occurs through the binding of a ligand to and dimerisation of two receptor tyrosine kinases (RTKs) (Figure 1.8). This creates a docking site for GRB2, and SOS, to which inactive Ras proteins (HRAS KRAS, NRAS) bind, thereby activating it. A phosphorylation cascade results in activation of Raf (ARAF, BRAF, CRAF), which phosphorylates MEK1/2, thereby activating MAPK (ERK 1/2). ERK1/2 can activate multiple other factors involved in transcription (Myc, ELK1, Fos), cell cycle regulation (cyclin D) and cell survival (Bad) (94,95).

RAS

There are over 150 RAS-like genes in the RAS superfamily, with scientists having contrasting beliefs of what should be included. The 5 subfamilies include (*Ras*,

Rho/Rac, Rab, Ran and Arf). All members of the RAS superfamily have the ability to catalyse and hydrolyse guanine nucleotides and have similar structures. Ras proteins are small GTPases, of which there are 3 (HRAS, KRAS and NRAS). Ras can be active (bound to GTP), or inactive (bound to GDP). Activation and deactivation of Ras occurs as a result of guanine nucleotide exchange factors (GEFs), and GTPase activating proteins (GAPs), respectively. GEFs catalyse GDP-bound RAS, to replace it with GTP-bound RAS. RAS proteins have a small amount of GTPase activity; however, GAPs increase hydrolysis of GTP by 100,000 fold. Ras activation can trigger multiple signalling cascades, such as the PI3K pathway or the MAPK pathway.

RAF (Rapidly Accelerated Fibrosarcoma)

There are three RAF mammalian isoforms; A-Raf, B-Raf and C-Raf, all of which are products of 3 different genes. The majority of work was carried out on C-Raf as it was the first to be discovered. However, this shifted in 2002 when Davies et al identified B-Raf in multiple tumour types (91). All forms of Raf have 3 conserved regions (CR), CR1, CR2 and CR3. CR1 has the Ras-binding domain (essential for Ras interactions and membrane recruitment), and cysteine-rich domain (secondary Ras binding domain, and for Raf auto-inhibition). CR2 has inhibitory phosphorylation domains for negative regulation of Ras binding and Raf activation. CR3 phosphorylation is essential for kinase activation.

1.9.5. MAPK pathway mutations.

Within the MAPK pathway, the most common mutations in CRC are *KRAS* (35-47%) (93,104,105), and *BRAF* (<5%, 5-10%) (93,105–107). *RAS* mutations can affect both the MAPK and PI3K pathways. Therefore, inhibition of the PI3K and MAPK pathways may increase treatment effectiveness in LARC.

Somatic mutations in KRAS

KRAS gene mutations alter its ability to hydrolyse GTP to GDP, retaining *KRAS* in an active GTP-bound state thereby resulting in a permanently activated *KRAS* protein, to which downstream effectors (i.e. BRAF, PIK3CA) can interact. 95% of *KRAS* mutations occur within exon 2, codons 12 (80%) and 13 (15%). The glycine residues in positions 12 and 13 of *KRAS* are vital docking sites for *KRAS* to interact with GAPs. Consequently, these mutations have been linked to

resistance to anti-EGFR therapy, poor recurrence-free survival and overall survival (93), [34], [35]. CRC patients with Dukes' stage C combined with a somatic *KRAS*^{G12V} mutation have been shown to have a significantly reduced overall survival and disease-free survival (110,111), whilst *KRAS* mutations in codon 13 did not have any significant effect.

KRAS mutations are also commonly located in codons 61 and 146. The glutamine residue in position 61 is essential for the hydrolysis of GTP. *KRAS* mutated CRCs are less inclined to have MSI than wild-type *KRAS* tumours. Elevated levels of *KRAS* mutations are associated with increased CEA (carcinoembryonic antigen) levels and transformation of the colonic epithelium from monolayer to numerous layers (112).

Somatic mutations in *BRAF*

Mutations in *BRAF* were first discovered in 2002 when they were identified in ~66% of malignant melanoma samples from the Cancer Genome Project (91). Histologically, *BRAF* tumours tend to be mucinous, poorly differentiated and serrated.

Studies have shown that *BRAF* mutated CRCs have a worse prognosis, are significantly more inclined to be found in females over 70 years, located in the proximal (right side) colon, identified at a higher grade, increased lymph node involvement and peritoneal metastasis, more inclined to have MSI and decreased overall survival and disease-free survival than their wild-type *BRAF* counterparts (113,114). Furthermore, patients with non-curative metastatic *BRAF* mutated CRC have a median survival of 33-50% of that of their wild-type *BRAF* counterparts. Over 100 different *BRAF* mutations have been identified in exons 11 and 15 of chromosome 7, with the most prevalent being a V600E mutation. *BRAF*^{V600E} mutations are present in ~10% of all CRC cases and constitute 80-90% of all *BRAF* mutations (115), and are indicative of a poor prognosis, particularly in microsatellite stable CRCs. V600E mutations occur when a thymidine (T) is substituted for an adenine (A) at position 1799, resulting in valine being substituted for a glutamate at position 600. The valine residue at position 600 in *BRAF* proteins is essential for retaining *BRAF* in an inactive conformation when it is not bound to *KRAS*. Therefore, mutations at this site result in a constantly active

BRAF, with the ability to phosphorylate and activate its downstream effectors. Consequently, incessant activation and downstream signalling of the MAPK pathway and EGFR-independent cellular proliferation occurs.

Tumours with *BRAF* mutations in codons 594 and 596 differ from other *BRAF* mutated tumours. These tumours have different pathological and molecular characteristics, and patient outcomes (116).

Multiple studies have shown a different response to BRAF inhibitors in different tissue types. This is particularly true for melanoma and CRC, where varying levels of resistance have been noted between the two. CRC resistance to BRAF inhibitors has been linked to reactivation of EGFR via a feedback loop (117,118). The activated EGFR then phosphorylates and activates CRAF and RAS. This particular feedback loop appears to be limited to CRC. Melanomas only express a few, if any EGFR receptors. Therefore BRAF inhibitors need to be combined with MEK inhibitors to achieve a significant effect on the tumour. However, resistance to this combination frequently develops.

1.9.6. Co-occurrence of PI3K/MAPK pathway mutations.

BRAF, *KRAS* and *NRAS* mutations are nearly always mutually exclusive. However, *PIK3CA* mutations often co-occur with these mutations. Mutations in *KRAS* and *BRAF* can result in upregulation of COX-2 (119), which promotes tumour growth, proliferation, and is associated with resistance to chemotherapy and radiation therapy (120,121).

1.10. Inhibition of the PI3K and MAPK pathways.

1.10 .1. Copanlisib / BAY80-6946 / Aliqopa

Copanlisib is a potent, small-molecule pan-class 1 PI3K α/δ inhibitor from Bayer. It is the chemical compound 2-amino-N-(7-methoxy-8-(3-morpholinopropoxy)-2,3-dihydroimidazo(1,2-c)quinazolin-4-yl)pyrimidine-5-carboxamide and has the molecular formula $C_{23}H_{28}N_8O_4$. It has a molecular weight of 480.529g/mol.

Copanlisib primarily targets the PI3K α and δ isoforms, whilst simultaneously targeting the β and γ isoforms to a lesser degree, and has a mild inhibitory effect on mTOR (122). On 14th September 2017, the U.S. Food and Drugs Administration (FDA) accelerated copanlisib approval, due to the overall response rates (59%) seen in the Phase II CHRONOS-1 (NCT01660451) clinical trial. This trial was carried out on 104 patients with relapsed follicular B-cell non-Hodgkin's lymphoma, who failed to respond to a minimum of 2 other systemic therapies. The study also resulted in a complete response in 14% of patients. As a result, copanlisib (Aliqopa) was the first intravenous PI3K α/δ inhibitor to be approved by the FDA.

Copanlisib is administered via an hour-long intravenous infusion on an intermittent dosing schedule (days 1, 8 and 15 of a 28 day treatment cycle). Side effects include hypertension, hyperglycaemia, infections (particularly pneumonia), embryo-foetal toxicity, leukopenia, neutropenia, thrombocytopenia, diarrhoea, nausea and cutaneous reactions; with 26% of patients in the CHRONOS II trial reporting serious adverse reactions (123).

Copanlisib has been shown to have pro-apoptotic and anti-tumorigenic properties both in vivo and in vitro (122,124–126). It is currently in several clinical trials for cancers including HER2 positive breast cancer (phase 1), Endometrial endometrioid adenocarcinoma (phase 2), Non-Hodgkin's lymphoma (phase 3) (Table 1.5).

Furthermore, copanlisib has been used as a successful monotherapy in a phase II clinical trial; however, it is believed that this drug will work best in combination therapies. Therefore, my research aimed to determine if combining copanlisib with chemoradiotherapy can increase chemoradiotherapy responsiveness in LARC.

Condition	Phase	Treatment	Locations	NCT identifier	Ref
Lymphoma, Non-Hodgkin's	1	Copanlisib	China	NCT03498430	(127)
Lymphoma, Non-Hodgkin's	1	Copanlisib	Belgium	NCT02155582	(128)
Lymphoma, Non-Hodgkin's	1	Copanlisib, Itraconazole, Rifampin	U.S.A	NCT02253420	(129)
Lymphoma (stage III/IV), metastatic malignant solid neoplasm	1	Copanlisib, Nivolumab	U.S.A	NCT03502733	(130)
Advanced cancer	1	Copanlisib, Gemcitabine, Cisplatin	U.S.A	NCT01460537	(131)
Advanced cancer	1	Copanlisib + Refametinib	U.S.A	NCT01392521	(132)
Neoplasms	1	Copanlisib	U.S.A	NCT00962611	(133)
Advanced cancer	1	Copanlisib, Paclitaxel	U.S.A	NCT01411410	(134)
Healthy Volunteers	1	Copanlisib, Metformin	U.S.A	NCT03655301	(135)
Healthy Volunteers	1	Copanlisib	Netherlands	NCT02119221	(136)
Endometrial, Ovarian, Peritoneal, fallopian tube cancer	1	Copanlisib, Niraparib	U.S.A.	NCT03586661	(137)
Hepatic Insufficiency	1	Copanlisib	Germany	NCT03172884	(138)
Advanced or metastatic solid tumour	1	Copanlisib, Rogaratinib	U.S.A	NCT03517956	(139)
Lymphoma	1, 2	Ibrutinib, Copanlisib	U.S.A	NCT03581942	(140)
Lymphoma, Non-Hodgkin's	1, 2	Copanlisib	Japan	NCT02342665	(141)
Breast cancer	1, 2	Copanlisib	U.S.A	NCT03128619	(142)
Breast cancer, HER2 Positive	1,2	Copanlisib, Trastuzumab	Ireland	NCT02705859	(143)
Carcinoma, Squamous Cell of Head and Neck	1, 2	Copanlisib, Cetuximab	France	NCT02822482	(144)
Mature T-Cell and NK-Cell Neoplasm	1, 2	Copanlisib, Gemcitabine	Korea	NCT03052933	(145)
Unresectable or Metastatic Microsatellite Stable (MSS) Solid Tumour Along With Microsatellite Stable (MSS) Colon Cancer	1, 2	Copanlisib, Nivolumab	U.S.A	NCT03711058	(146)

Table 1.5: Clinical trials for copanlisib treatments worldwide.

Condition	Phase	Treatment	Locations	NCT identifier	Ref
Non-small Cell Lung Cancer (NSCLC), Head and Neck Squamous Cell Carcinoma (HNSCC), Colorectal Cancer (CRC), Hepatocellular Carcinoma (HCC)	1, 2	Copanlisib, Nivolumab	Canada, U.S.A.	NCT03735628	(147)
Mixed Tumour, Malignant	1, 2	Copanlisib	U.S.A	NCT03458728	(148)
Lymphoma, Non-Hodgkin's	2	Copanlisib	U.S.A	NCT01660451	(149)
Lymphoma, Diffuse, large B-cell	2	Copanlisib	Australia	NCT02391116	(150)
Lymphoma, Marginal zone	2	Copanlisib	Germany	NCT03474744	(151)
Lymphoma, Non-Hodgkin's / Follicular	2	Copanlisib, Rituximab	U.S.A	NCT03789240	(152)
Lymphoma	2	Copanlisib, Nivolumab	U.S.A.	NCT03484819	(153)
Lymphoma, Mantle-Cell	2	Copanlisib	U.S.A	NCT02455297	(154)
Endometrioid Adenocarcinoma	2	Copanlisib	U.S.A	NCT02728258	(155)
Biliary Carcinoma, Gall Bladder Carcinoma, Cholangiocarcinoma, Gastrointestinal tumour	2	Copanlisib, Gemcitabine, Cisplatin	U.S.A	NCT02631590	(156)
Breast cancer, Oestrogen Receptor-Positive, HER2/Neu Negative, Progesterone Receptor-Positive	2	Copanlisib, Fulvestrant, Palbociclib	U.S.A	NCT03377101	(157)
Lymphoma, Non-Hodgkin's	3	Copanlisib, Rituximab	U.S.A	NCT02367040	(158)
Lymphoma, Non-Hodgkin's	3	Copanlisib	Brazil	NCT02369016	(159)
Lymphoma, Non-Hodgkin's	3	Copanlisib, Rituximab, Cyclophosphamide, Doxorubicin, Vincristine, Bendamustine, Prednisone	U.S.A	NCT02626455	(160)

Table 1.6: Clinical trials for copanlisib treatments worldwide, continued.

1.10.2. Refametinib / BAY86-9766 / RDEA119

Refametinib is a potent, highly selective, allosteric, small-molecule MEK 1 and 2 inhibitors from Bayer. It binds to an allosteric target in the MEK 1 and 2 enzymes, thereby inhibiting tumour proliferation and growth factor-mediated cell signalling. Refametinib has been involved in 10 phase I/II clinical trials worldwide. These clinical trials were used for a range of tumours, particularly hepatocellular, pancreatic and advanced-stage tumours, along with combinations of drugs such as Sorafenib, Gemcitabine, Regorafenib and Copanlisib (Table 1.7). However, during the course of this project, BAYER has decided to cease further studies using Refametinib due to toxicity concerns.

Conditions	Phase	Treatment	Location	NCT identifier	Ref
Neoplasms	1	Refametinib	China	NCT01764828	(161)
Neoplasms	1	Refametinib	Japan	NCT01179295	(162)
Neoplasms	1	Refametinib, Copanlisib	U.S.A	NCT01392521	(132)
Neoplasms	1	Refametinib, Regorafenib	U.S.A	NCT02168777	(163)
Drug Interactions	1	Refametinib	U.S.A	NCT01925638	(164)
Pancreatic Neoplasms	1, 2	Refametinib, Gemcitabine	U.S.A, Europe	NCT01251640	(165)
Advanced Cancer	1,2	Refametinib, Sorafenib	U.S.A	NCT00785226	(166)
Hepatocellular carcinoma	2	Refametinib, Sorafenib	China, Korea, Singapore, Taiwan	NCT01204177	(167)
Hepatocellular carcinoma	2	Refametinib	U.S.A	NCT01915589	(168)
Hepatocellular carcinoma	2	Refametinib, Sorafenib	U.S.A	NCT01915602	(169)

Table 1.7: Clinical trials involving refametinib (170)

Aims

Response rates between colorectal cancer patients vary significantly. Kinase signalling pathway mutations have been implicated in tumourigenesis, resistance to chemoradiotherapy and poor patient outcomes. We thus hypothesise that inhibition of these pathways may increase sensitivity to chemoradiotherapy in rectal cancer. I worked on the following four aims in the hope of testing this hypothesis:

Aim 1

To determine the full spectrum of somatic genetic aberrations that activates the PI3K and related signalling pathways in LARC and how they are modulated by treatment.

Aim 2

To determine the impact of neoadjuvant chemoradiotherapy on circulating tumour cells in LARC patients.

Aim 3

Determination in-vitro if inhibition of the PI3K and related kinase signalling pathways augments rectal cancer chemoradiotherapy sensitivity.

Aim 4

Determination in-vivo, if inhibition of the PI3K and related kinase signalling pathways augments the chemoradiotherapy sensitivity of genetically defined rectal cancer models.

Materials and methods

2.1. Materials and methods utilised in aim 1 to determine the full spectrum of somatic genetic aberrations that activates the PI3K and related signalling pathways in LARC and how they are modulated by treatment.

Table 2.1: List of reagents used for whole-exome sequencing study, their names, suppliers and product codes.

Reagent	Supplier	Product code
All Prep DNA / RNA mini kit	Qiagen	80204
QIAamp DNA mini kit	Qiagen	51304
Qubit dsDNA BR assay kit	Life technologies	Q32853
HotStarTaq Plus Master mix kit	Qiagen	203643, 203645, 203646
Agarose	Sigma	A9539
Trizma base	Sigma	T1503
Boric acid	Sigma	B7901
Ethylenediaminetetraacetic acid, anhydrous, >98.5% titration	Sigma	E6758
Sybr Safe DNA gel stain	Invitrogen	S33102
GeneRuler 1kb DNA ladder, ready-to-use, 0.1ug/ul	Thermo scientific	SM0313

2.1.1. Human rectal cancer tumour samples

Fresh frozen pre-treatment tumour biopsies, and matched normal samples were collected at endoscopy and surgery from 26 patients who presented with locally advanced rectal cancer (LARC). Samples were obtained from the Beaumont hospital bio-bank (Dublin, Ireland) (n=10) and MD Anderson cancer centre, Houston, Texas (n=16), using an ethics committee-approved protocol. All patients were treated with neoadjuvant chemoradiation therapy (NACRT), and the cohort was stratified by response to NACRT treatment. Response was defined by the volume of tumour remaining upon surgery post-NACRT treatment, according to the RC Path guidelines. Samples were separated into good (RC Path1 – no remaining tumour) (n=5), intermediate (RC Path 2 – some remaining tumour) (n=11) and poor (RC Path 3 – a large quantity of remaining tumour) (n=10) responders to treatment. Extensive pathology reviews were carried out by a trained pathologist to ensure there was adequate tumour content within the frozen biopsies, and that no remaining tumour was present in the normal samples.

2.1.2. DNA extraction from normal and tumour samples

DNA was extracted from the normal tissue or blood, and tumour tissue samples using an All Prep DNA/RNA mini kit (Qiagen).

Principle

The All Prep DNA/RNA mini kit purifies genomic DNA and RNA from biological samples. Extracted DNA is on average 15-30kb in length. Samples are homogenised and lysed by a denaturing guanidine-isothiocyanate-salt containing buffer (Buffer RLT Plus) which is used to inactivate DNAses for isolation of DNA. The lysate is passed through an All Prep DNA spin column which binds genomic DNA. A range of wash buffers are used (Buffer AW1, AW2 and EB). AW1 is a stringent wash containing a low concentration of guanidine hydrochloride salts to denature proteins to facilitate sample filtration. AW2 is a Tris-ethanol based solution used to remove salts. Buffer EB is an elution buffer consisting of 10mM Tris-HCl, pH 8.5, which releases DNA from the sample. The slightly basic pH stabilises the acidic DNA, enabling optimal dissolution into the buffer.

Protocol:

30mg of tissue was homogenised in 60ml buffer RLT Plus. The lysate was centrifuged at maximum speed for 3 minutes. The supernatant was transferred to All Prep DNA spin column, contained in a 2ml collection tube, and centrifuged at 10,000rpm for 30 seconds. The spin column was transferred to a new 2ml collection tube. Buffer AW1 (500µl) was added to spin column and centrifuged at 10,000rpm for 15 seconds. Flow-through was discarded. Buffer AW2 (500µl) was added to the column and centrifuged at full speed for 2 minutes. The spin column was transferred to a new 1.5ml collection tube. Buffer EB (100µl) was added directly to the membrane, incubated at room temperature for 1 minute, and centrifuged at 10,000rpm for 1 minute.

2.1.3. Whole exome sequencing

Beaumont hospital cohort:

Exome capture sequencing was carried out on 2µg of DNA using the Agilent SureSelect Human All Exome V3 kit. A mean coverage of 83x was achieved, using 91bp paired end reads from the Illumina HiSeq 2000.

MD Anderson cohort:

500ng of Biorupter Ultrasonicator (Diagenode)-sheared genomic DNA was processed with a Kapa hyper library preparation kit (Kapa Biosystems) to form an illumina compatible indexed library. The TapeStation High Sensitivity DNA kit (Agilent Technologies) was used to assess the quality of the library.

NimbleGenSeqCap EZ Exome kit V3.0 (Roche Nimblegen) was used to carry out exome capture of the library pool. The HiSeq3000 Sequencer (Illumina Inc., San Diego) was used to carry out sequencing using the 76nt paired end format.

2.1.4. DNA quantification

Principle

The Qubit fluorometer is a benchtop device used to quantify DNA and RNA using fluorescence-based assays. The Qubit dsBR reagent is highly selective at detecting double-stranded DNA, with the ability to detect a broad range of DNA, varying from 100pg/µl, up to 1,000ng/µl. The qubit assay is incubated for 2 minutes to maximise its fluorescence signal, which is then stable for up to 3 hours.

Procedure

DNA was quantified using the Qubit dsDNA BR assay kit (Invitrogen). A 1:200 working stock solution (dsDNA BR reagent: dsDNA BR buffer) was made, and vortexed. Samples and standards were diluted in the working solution, 1:200 and 1:20 respectively, with a final volume of 200µl per tube. Samples were vortexed and incubated at room temperature for 2 minutes. Samples were measured on the Qubit fluorometer (Invitrogen).

2.1.5. Determination of quality of DNA

300bp β -globin PCR

Principle of PCR

Polymerase chain reactions (PCRs) consist of four primary steps, initial denaturation followed by repeated denaturation, annealing and extension cycles. Initial denaturation: The PCR mix is incubated at 95°C initially to activate DNA polymerase and to convert double-stranded DNA molecules into single-stranded DNA.

Denaturation: Occurs at 95°C to remove all hydrogen bonds between complementary DNA bases, further ensuring only single-stranded DNA is present prior to amplification process.

Annealing: The temperature is reduced to 5°C below the primer melting temperature. This promotes primer binding to the complementary single-stranded DNA sequence.

Extension: The temperature is increased to 72°C which is the optimal temperature for DNA polymerase activity. This facilitates the extension of hybridised primers.

Cycles are typically repeated several times to maximise amplification of the end product.

Preparation of samples

Verification of DNA quality was carried out using a 300bp β -globin PCR, using the Qiagen Quality HotStarTaq Plus Master Mix kit. The master mix was made using the following:

Solution	μ l per sample
2x Taq master mix buffer	10
β -globin primer	2
Coral load concentrate 10x	2
Nuclease-free water (NFW)	4
DNA (5ng)	2

The 2 x master mix buffer consists of 1-part β -globin forward primer (5'-GGG TTT GAA GTC CAA CTC CTA AG-3'), and 1 part β -globin reverse primer (5'-CAA CTT CAT CCA CGT TCA CCT-3').

18ul of master mix and 2ul of DNA was added to per well. Positive and negative controls consisted of DNA control and nuclease-free water (NFW) respectively. Samples were covered, vortexed and centrifuged at 3,500rpm for 1 minute. Samples were run on a 300bp β -globin programme, with the following PCR cycle:

Process	Temperature	Time	Number of cycles
Incubation	95°C	5 minutes	} 35
Denaturation	95°C	30 seconds	
Annealing	30.5°C	20 seconds	
Extension	72°C	60 seconds	
	72°C	10 minutes	

Electrophoresis gel

PCR products were subsequently analysed on an electrophoresis gel. Agarose and 1 x Tris Borate EDTA (TBE) were mixed and heated in a microwave for 2 minutes, or until the solution was fully dissolved. 10ul of Sybr Safe were added, the solution was mixed and poured into a gel case, and allowed to set. The composition of 1X TBE and the 1.5% agarose gel are displayed below:

Composition of 1X TBE solution:

Reagent / solution	Volume
Tris-base	10.8g
Boric acid	5.5g
EDTA	0.93g
Distilled water	Fill up to 1L

Composition of 1.5% agarose gel:

Solution	Per 1.5% gel
Agarose	1.5g
1 x TBE	100ml
Sybr Safe	10ul

The 1.5% agarose gel was subsequently placed in an OWL separation system box, which was filled with 1x TBE buffer. 8 μ l of 1Kb ladder and 12 μ l of the sample were loaded into wells. Electrophoresis gel was run for 10 minutes at 260 volts. Gels were scanned to check for bands to ensure the quality of DNA prior to exome sequencing.

2.1.6. Whole-exome sequencing

3µg genomic DNA was sent to BGI Tech for exome sequencing. Targeted exome capture was performed using an Agilent SureSelect Human all Exome V3 kit. Samples were sequenced to a minimum of 50X coverage using 91bp paired end reads on the Illumina HiSeq2000.

Whole-exome sequencing data analysis

The quality of Fastq files generated was determined using FastQC, and adapter and primer sequences and low quality 3' end reads were trimmed off using Trimmomatic. Remaining reads (with a minimum length of 90 bases) were aligned to the hg19 reference genome using BWA. Alignments with mapping quality score <10 were removed. Picard was used to sort and index BAM files and remove PCR duplicates. Local realignment, base quality score recalibration, variant and indel calling and filtering were carried out using the Genome analysis toolkit. To identify somatic mutations, variants from tumour and matched normal samples were compared and variants coming up in both were removed. Varscan and Mutect were used for SNV and indel calling. Excavator was used for calling copy number alterations. Identified somatic variants were annotated using ANNOVAR and variants within the targeted capture genes were kept for further analysis. Based on functional annotations the variant was considered non-silent if it was annotated as non-synonymous. SIFT and Polyphen2 predictor databases were used to enrich for variants with deleterious/damaging effects. To identify the significantly mutated genes, Fisher's exact test was used to compare the gene mutation results against the background mutation rate estimated previously. Data analysis was done in collaboration with Dr. Simon Furney and Scott Piraino.

Prism software (GraphPad) was used to calculate the statistical significance for tumour mutational burden. Whereby I used the unpaired 2-tailed t-test with Welch's correction with a confidence interval of 95%. P-values ≤ 0.05 were indicative of a result of statistical significance.

2.2. Materials and methods utilised in aim 2 to determine the impact of neoadjuvant chemoradiotherapy on circulating tumour cells in LARC patients.

Table 2.2: List of reagents used for TRILARC study, their names, suppliers and product codes.

Reagent	Supplier	Product code
CYTO kit	ScreenCell	CY 4FC
Phosphate buffered saline tablet	Sigma	P4417
Nuclease-free water	Sigma	3098
Papanicolaou's solution 1b haematoxylin solution S	Merck	109254
Eosin Y solution	Sigma Aldrich	318906
Faramount aqueous mounting medium ready-to-use	Dako	S3025

2.2.1. TRI-LARC (ICORG 12-38) clinical trial

The TRI-LARC phase II clinical trial (ICORG 12-38) is the first pre-operative Irish rectal cancer trial. This prospective randomised control trial aims to compare two forms of radiation therapies in 240 LARC patients. The two arms include treatment using traditional 3-D confocal radiotherapy (3-DCRT), and the novel Intensity-Modulated Radiotherapy (IMRT). The trial is currently open in three clinical centres, St. Luke's hospital, Beaumont; St. Luke's hospital, Rathgar and St. James' hospital, Dublin. This study was approved by the ethics committee and informed written consent in line with the ICH-GCP guidelines was obtained from all patients prior to the undertaking of any clinical trial procedures.

Inclusion criteria

Inclusion criteria for the trial included a minimum age of 18 years, no evidence of metastatic disease and an Eastern Cooperative Oncology Group (ECOG) performance status of 0-2. The latter is a scale which records patients levels of functioning (i.e. physical and self-care abilities), which is further discussed in Table 2.3.

Table 2.3: ECOG grading system (171).

*All patients enrolled in the trial had histologically confirmed rectal adenocarcinoma, with any of the following stages according to AJCC Version V: cT3/4 N0-2
cT(any) N1-2
cT (any) N (any) where the Circumferential Resection Margin (CRM) is at risk.
All patients gave written informed consent in line with ICH-GCP guidelines.*

ECOG grade	ECOG performance status
0	Fully active, able to carry on all pre-disease performance without restriction.
1	Restricted in physically strenuous activity but ambulatory and able to carry out work of a light or sedentary nature.
2	Ambulatory and capable of self-care but unable to carry out any work activities; up and about more than 50% of waking hours.
3	Capable of only limited self-care; confined to bed or chair more than 50% of waking hours.
4	Completely disabled; cannot carry out any self-care; totally confined to bed or chair.
5	Dead

Exclusion criteria

Patients were excluded from taking part in the TRILARC clinical trial if they had any of the following: previously received radiotherapy treatment to the pelvic region, induction chemotherapy was given prior to chemoradiotherapy, history of inflammatory bowel disease, previous hip replacement or bowel surgery, patients with other conditions associated with increased radiosensitivity, any other co-existing malignancies within the past 5 years (excluding non-melanoma skin cancer), pregnant or lactating.

Treatment regimens

Prior to study enrolment, imaging and staging of the tumour were carried out via an MRI scan and CT scan of the thorax and abdomen. Other baseline assessments included a Digital Rectal Exam (DRE), rigid sigmoidoscopy and an

array of blood tests (Full blood count (FBC), Urea and Electrolytes (U/E), Liver Function Test (LFT) and Carcinoembryonic Antigen (CEA)).

Continuous intravenous (IV) infusion of 5-FU chemotherapy (225mg/m²) was given daily for the duration of radiotherapy. 28 fractions of external-beam pelvic radiotherapy (50.4Gy) were delivered using a Linear Accelerator (LINAC) with ≥ 6 MV energy and an Image-Guided Radiation Therapy (IGRT) capacity for improved accuracy and precision. Patients received 5 fractions of either 3DCRT or IMRT per week, for 6-8 weeks, with a minimum inter-fractionation interval of 6 hours. During radiation therapy treatment, patients were immobilised, and with the aid of Cone Beam CT (CBCT) scans, they were set in a supine position for IGRT. Completion of the course of radiation was followed by Total Mesorectal Excision (TME), and adjuvant chemotherapy. Acute toxicities were assessed weekly during radiotherapy and at 2 and 4 weeks post-treatment. Late toxicities were assessed at 3, 6, 9, 12, 18 and 24 months post-treatment and will be assessed annually up to 10 years.

2.2.2. Blood collection

Peripheral blood was collected at various time-points before, during and after therapy, and after surgery (see Table 2.4) from patients enrolled in the TRI-LARC (ICORG 12-38) clinical trial. 9mls of peripheral blood was collected in ScreenCell K2-EDTA tubes for analysis of circulating tumour cells; whilst a further 15mls of blood was collected in two EDTA vacutainer tubes (9mls and 6mls) for plasma. Blood tubes were inverted a minimum of 10 times immediately after drawing blood. Samples were taken pre-treatment, week 3 on radiotherapy, last week on radiotherapy, 4 weeks after radiotherapy, after surgical procedure and 6 months - 1 year follow up.

Table 2.4: Time-points for collection of blood and tissue samples during TRILARC clinical trial.

Peripheral blood was collected at the following time-points before, during and after therapy, and after surgery from patients enrolled in the TRI-LARC (ICORG 12-38) clinical trial. Blood was collected by clinical staff in St. Luke's hospital, Beaumont; St. Luke's hospital, Rathgar and St. James' hospital, Dublin. Blood for plasma and circulating tumour cells (CTCs) were collected in EDTA vacutainer tubes and ScreenCell K2-EDTA tubes respectively. Blood tubes were inverted a minimum of 10 times immediately after drawing blood.

Time-point	Pre-treatment	Week 3 on RT	Last week on RT	4 weeks after RT	Surgical procedure	After surgical procedure
Plasma (15mls)	Sample 1	Sample 2	Sample 3	Sample 4		Sample 5
CTC blood (9mls)	Sample 1	Sample 2	Sample 3	Sample 4		Sample 5
Tissue	FFPE 1	FF (optional)			FFPE 2 FF 1	

RT = Radiation therapy

SM= somatic mutation

CTC = circulating tumour cells

FFPE = formalin-fixed, paraffin-embedded tissue

FF = fresh frozen tissue

2.2.3. Processing of plasma samples

Blood (15mls) was processed to plasma by centrifuging at 1000g for 15 minutes at 4°C. This resulted in the fractionation of the sample into 3 phases; a lower phase containing erythrocytes, buffy coat containing leukocytes and platelets, and an upper phase consisting of the plasma. Plasma was removed and divided into 1.5ml tubes and centrifuged at 15,000rpm for 10 minutes at 4°C. 1ml aliquots of plasma were transferred into cryovials and stored at -80 °C. Circulating DNA in the plasma was analysed by Dr. Sinead Toomey using the ultra-sensitive mutation detection technique, UltraSEEK (Agena Biosciences).

2.2.4. Tumour tissue collection

The RCSI bio-bank collected pre-treatment formalin-fixed paraffin-embedded (FFPE) and fresh frozen (FF) tumour tissue, and an FFPE and fresh frozen sample at the surgical procedure. An optional FF biopsy was also collected at week 3 of radiotherapy treatment. FF tumour tissue was frozen immediately in liquid nitrogen and stored at -80C. Tissue for FFPE blocks were fixed in buffered formalin.

2.2.5. Whole blood for circulating tumour cell (CTC) analysis

Principle:

For every 1ml of blood, there are approximately 4.5 - 11 million leukocytes, 150 - 400 million platelets and 4.2 - 6.1 billion erythrocytes per millilitre of blood.

Therefore identification of a single CTC can often be masked and can be highly challenging to detect. ScreenCell have developed a filtration device to capture CTCs from human blood using a ScreenCell CY device.

Prior to filtration, blood is mixed with ScreenCell fixed cells (FC2) dilution buffer, which is composed primarily of paraformaldehyde and saponin. This causes erythrocytic lysis to occur within the sample, whilst still preserving the integrity of all other remaining cells. The resulting solution is filtered using a disposable, size-selective ScreenCell CY device which has a track-etched poly(C)arbonate microporous filter. This filter has a pore size of 7.5µm, since platelets are ~2µm, these too are automatically eliminated. The filter is further rinsed with phosphate-buffered saline (PBS) to ensure removal of all erythrocytic debris. This process removes an average of 99.9% of cells from the blood sample, thereby leaving us with the 0.01% of cells which may be of interest.

Protocol:

Isolation of CTCs was carried out on peripheral blood within 4 hours of sample collection (blood was kept at 4°C before filtration) (Figure 2.1). 3mls of whole blood was diluted in 4mls of ScreenCell FC2 dilution buffer (pH 6.7-7), tubes were inverted a minimum of 5 times, and incubated at room temperature for 8 minutes. Post incubation, the solution was poured into module A of the ScreenCell cyto filtration unit. The protective membrane was removed and a fresh EDTA tube was attached to module B, facilitating filtration. When the blood: buffer solution reached the yellow line on module A, 1.6mls of phosphate-buffered saline (PBS) was added. When there was no solution remaining in the cyto filtration unit, module A was removed, and the attached filter was released onto Whatman paper and air-dried for 15 minutes.

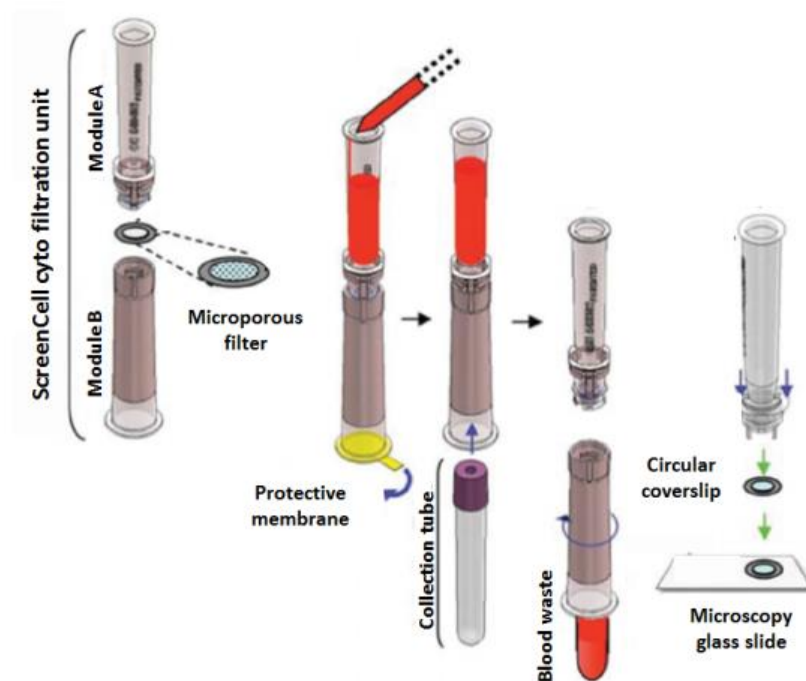


Figure 2.1: ScreenCell Cyto filtration method (172).

9mls of peripheral blood was collected into a ScreenCell K2-EDTA tube.

Isolation of CTCs was carried out on less than 4hours after sample collection (blood was kept at 4°C before filtration). 3mls of the blood was diluted in 4mls of ScreenCell FC2 dilution buffer (pH 6.7-7), tubes were inverted a minimum of 5 times, and incubated at room temperature for 8 minutes. Post incubation, the solution was poured into module A in the ScreenCell cyto filtration unit. The protective membrane was removed and a fresh EDTA tube was attached to module B, facilitating filtration. When the blood: buffer solution reached the yellow line on module A, 1.6mls of phosphate-buffered saline (PBS) was added. When there is no solution remaining in the cyto filtration unit, module A was removed, and the attached filter was released onto Whatmann paper and air-dried for 15 minutes. Filter was stained with haematoxylin and eosin and analysed microscopically for the presence of CTCs.

Histological staining of ScreenCell filters

Filters were stained with haematoxylin and eosin to assess for the presence of CTCs in the blood. Haematoxylin (70µl) was applied to the CY filter for 1 minute at room temperature. Using a forceps, the filter was rinsed vertically in a water bath. Excess water was removed, and eosin (70µl) was applied for 30 seconds at room temperature. CY filter was rinsed vertically in a water bath and left to air dry for 15 minutes at room temperature. Filters were attached to a microscope slide and mounted with an 8mm diameter circular coverslip using Faramount mounting medium.

Identification of circulating tumour cells

ScreenCell filters were analysed microscopically for the presence of CTCs. The following cytomorphological criteria were used for identification of CTCs, whereby a minimum of 4 of the following was required for positive identification (173–175):

Anisonucleosis (ratio >0.5)

Nucleus size >16µm

Irregular nuclei

3-D sheets

High (>2.1) nuclear/cytoplasmic ratio.

Statistical analysis

Statistical data analysis was carried out using the Prism software (GraphPad). The unpaired 2-tailed t-test with Welch's correction was used to determine statistical significance for variations between patient cohorts (gender, age, treatment) and for the volume of CTCs detected at each time-point. A confidence interval of 95% was used and p-values ≤ 0.05 were indicative of a result of statistical significance.

2.3. Materials and methods utilised in aim 3 to determine if in-vitro inhibition of the PI3K and related kinase signalling pathways augments rectal cancer chemoradiotherapy sensitivity.

Table 2.5: List of reagents used for in vitro study, including their names, suppliers and product codes.

Reagent	Supplier	Product code
DLD-1	ATCC	ATCC CCL-221
LS-174T	ATCC	ATCC CL-188
LS-513	ATCC	ATCC CRL-2134
LS-1034	ATCC	ATCC CRL-2158
LS-411N	ATCC	ATCC CRL-2159
Colo-205	ATCC	ATCC CCL-222
C2BBel	ATCC	ATCC CRL-2102
CL-14	DSMZ	ACC-504
Caco-2	ATCC	ATCC HTB-37
SNU-C4	KCLB	0000C4
RPMI-1640 medium	Sigma Aldrich	R8758
Dulbecco's modified eagle medium – high glucose	Sigma Aldrich	D6429
DMEM and HAMS F12	Sigma Aldrich	D8062
Eagle minimum essential medium	Sigma Aldrich	M0325
Transferrin human	Sigma-Aldrich	T8158
FBS, Qualified (Foetal bovine serum)	Gibco	10270-106
Penicillin Streptomycin	Gibco	15070-063
Copanlisib	BAYER	S2802
Refametinib	BAYER	S1089
Dimethylsulfoxide (DMSO)	Sigma-Aldrich	D2650
TFA	Sigma-Aldrich	T6580
CellTiter96 AQueous one solution cell proliferation assay (MTS)	Promega	G3582
Crystal violet solution, 1% aqueous solutionSigmaV5265	Sigma-Aldrich	V5265
Acetic acid	Sigma-Aldrich	27225
0.25% Trypsin-EDTA (1x)	Gibco	25200-056
Phosphate buffered saline tablet	Sigma-Aldrich	P4417
Methanol	Sigma-Aldrich	34680
5-Fluorouracil	Sigma-Aldrich	F6627
1% Triton X-100	Sigma-Aldrich	T8787
50mM HEPES	Sigma-Aldrich	H3375
150nM NaCl	Sigma-Aldrich	S7653
1.5nM MgCl ₂	Sigma-Aldrich	M2670
1mM EGTA	Sigma-Aldrich	E3889
100mM NaF	Sigma-Aldrich	S7920

Reagent	Supplier	Product code
10% glycerol	Sigma-Aldrich	G5516
Protease inhibitor	Roche Applied Science	11836153001
Phos-Stop phosphatase inhibitor	Roche Applied Science	4906845001
8% SDS	Sigma-Aldrich	L3771
0.25M Tris-HCl (ph6.8)	Sigma-Aldrich	RES3098T-B7
Biorad DC protein assay - reagent A	Biorad	500-0113
Biorad DC protein assay - reagent B	Biorad	500-0114
Biorad DC protein assay - reagent S	Biorad	500-0115

2.3.1. Colorectal cancer cell lines

We acquired the following colorectal cell lines DLD-1, LS-174T, LS-513, LS-1034, LS-411N, Colo-205, Caco-2 and C2BBE1 from ATCC; CL-14 was obtained from DSMZ and SNU-C4 from the KCLB (Table 2.6). Fingerprinting was carried out on all cell lines to confirm their identity by Source BioScience, LifeSciences, Nottingham, UK. The cell lines DLD-1, LS-513, LS-1034, LS-411N, SNU-C4 and Colo-205 were all cultured in RPMI-1640 media. C2BBE1 was grown in Dulbecco's modified eagle medium (DMEM), supplemented with 0.01mg/ml human transferrin (Sigma-Aldrich). CL-14 was cultured in DMEM and HAMS F12, and LS-174T and Caco-2 required eagle minimum essential medium (EMEM). All media was obtained from Sigma-Aldrich. All cell lines were maintained at 37°C with 5% CO₂, and supplemented with 10% foetal bovine serum (FBS) (with the exception of CL-14 and Caco-2 where 20% FBS was used), and 1% penicillin/streptomycin (P/S) (P/S free media was used during drug treatments).

Cell lines were screened for mutations within the PI3K and MAPK pathways using the Agena MassArray system and publically available data from the cancer cell line encyclopaedia (CCLE) (176). Cell lines were subdivided into 5 groups according to their mutational subtype: wild-type (C2BBE1, CL-14, Caco-2), KRAS mutated (LS-513, LS-1034), BRAF mutated (LS-411N, Colo-205), PIK3CA mutated (SNU-C4) and PIK3CA and KRAS mutated (DLD-1, LS-174T).

Table 2.6: Colorectal cancer cell lines, and their corresponding PI3K/MAPK pathway mutations, growth medium requirements, tissue type and morphology.

Cell line	Mutations	Media	Tissue type	Morphology
DLD-1 (ATCC CCL-221)	PIK3CA: E545K KRAS: G13D	RPMI + 10% FBS	Colon, Dukes type C, colorectal adenocarcinoma	Epithelial
LS-174T (ATCC CL-188)	PIK3CA: H1047R KRAS: G12D	EMEM + 10% FBS	Colon, Dukes type B, colorectal adenocarcinoma	Epithelial
Colo-205 (ATCC CCL-222)	BRAF: V600E	RPMI + 10% FBS	Colon, Dukes type D, Colorectal adenocarcinoma.	Epithelial
LS-411N (ATCC CRL-2159)	BRAF: V600E	RPMI + 10% FBS	Cecum, Dukes type B, colorectal carcinoma	Epithelial
LS-513 (ATCC CRL-2134)	KRAS: G12D	RPMI + 10% FBS	Cecum, Dukes type C, colorectal adenocarcinoma	Epithelial
LS-1034 (ATCC CRL-2158)	KRAS: A146P	RPMI + 10% FBS	Cecum, Dukes type C, colorectal carcinoma	Epithelial
CL-14 (ACC 504)	WT	DMEM and HAMS F12 + 20% FBS	Colon, carcinoma	Epithelial
C2BBel (ATCC CRL-2102)	WT	DMEM with 0.01mg.ml human transferrin + 10% FBS	Colonic enterocyte, colorectal carcinoma	Epithelial
Caco-2 (ATCC HTB-37)	WT	EMEM + 20% FBS	Colorectal adenocarcinoma	Epithelial
SNU-C4 (KCLB 0000C4)	PIK3CA: E545G	RPMI + 10% FBS	Colon, Colorectal adenocarcinoma	Epithelial

2.3.2. Proliferation assays

Principle

The CellTiter96 Aqueous One solution cell proliferation assay (Promega) is a colourimetric assay used for determination of the number of viable cells in culture. It contains a tetrazolium compound [3-(4, 5-dimethylthiazol-2-yl)-5-(3-carboxymethoxyphenyl)-2-(4-sulfophenyl)-2H-tetrazolium, inner salt; MTS] and an electron coupling reagent (phenazine ethosulfate; PES). Metabolically active cells contain dehydrogenase enzymes which release NADH and NADPH. This results in bioreduction of the tetrazolium MTS compound into a blue formazan by-product which is soluble in tissue culture medium. The absorbance reads the volume of formazan produced, which is directly proportional to the number of viable cells in the culture (177).

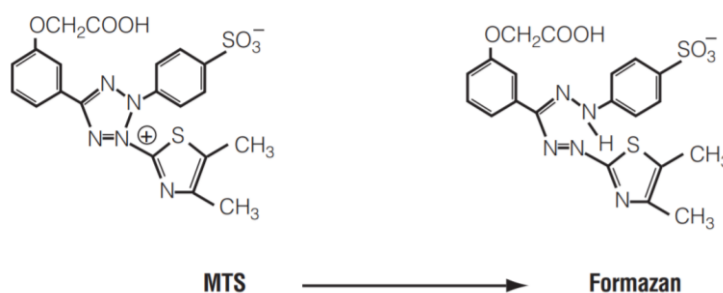


Figure 2.2: Chemical structure of tetrazolium MTS compound and its formazan by-product (177).

Metabolically active cells contain dehydrogenase enzymes which release NADH and NADPH. This results in bioreduction of the tetrazolium MTS compound into a blue formazan by-product which is soluble in tissue culture medium. The absorbance reads the volume of formazan produced, which is directly proportional to the number of viable cells in the culture.

Procedure

The novel PI3K inhibitor Copanlisib / BAY-806946 (5mM) and the MEK inhibitor Refametinib / RDEA-119 / BAY-86-9766 (10mM) were acquired from Bayer. Cells were plated in triplicate at 1×10^4 cells/ml in 96 well plates (100ul per well), and incubated at 37°C with 5% CO₂ for 24 hours. Media was subsequently removed, and 100ul drug-containing media was added to each well. For the semi-adherent cell line, Colo-205, the drug-containing media was added directly to the cell

suspension. Cells were treated with serial 1:2 dilutions of the MEK inhibitor refametinib (2 μ M - 7.8nM) or DMSO control, the PI3K inhibitor copanlisib (200nM – 0.78nM) or DMSO/TFA control, or copanlisib-refametinib combination (200nM – 0.78nM and 1mM – 3.9nM respectively). 200 μ l of sterile PBS was added to the outside wells of the plates to prevent the plate from drying out. Cells were incubated at 37°C with 5% CO₂ for 5 days. 20 μ l of MTS reagent (40 μ l for Colo-205) was added to each well and incubated at 37°C with 5% CO₂ for 2 hours. Absorbance was read at 490nm using a 96-well plate reader.

Statistics

Proliferation assays were run in biological triplicates. CalcuSyn software (Biosoft) was used to calculate IC₅₀ and combination index (CI) values, which is based on the Chou-Talalay quantification method (Table 2.7). Error bars were used in charts to represent the standard deviation between samples. P-values ≤ 0.05 were indicative of a result of statistical significance.

Table 2.7: Combination index values and corresponding Chou-Talalay definition for levels of synergism within a sample.

CI range	Chou-Talalay definition
<0.1	very strong synergism
0.1-0.3	strong synergism
0.3-0.7	synergism
0.7-0.85	moderate synergism
0.85-0.9	slight synergism
0.9-1.1	nearly additive
1.1-1.2	slight antagonism
1.2-1.45	moderate antagonism
1.45-3.3	antagonism
3.3-10	strong antagonism
>10	very strong antagonism

2.3.3. Clonogenic assays

Clonogenic assays were used to enable combination treatment of chemoradiation therapy and the PI3K and MEK inhibitors.

Principle

Clonogenic assays are a method of determining if a single cell has the ability to form a colony in vitro. By plating very low levels of single cells, each cell is required to proliferate, thereby testing the whole population. If cells are treated with cytotoxic drugs, cell proliferation rates may be affected as a result. Therefore, a cluster of cells must contain a minimum of 50 cells to be classified as a colony.

Background

Cells were grown in clonogenic assays to facilitate chemoradiation therapy (CRT), and to determine if a single cell has the ability to form a colony in vitro.

Preliminary work for the clonogenic assays included optimisation of cell volume, length of the experiment (weeks) and optimisation of drug concentrations for each cell line.

2.3.4. Optimisation of clonogenic cell volume

Cells were plated at 50, 100, 200, 400, 800, 1200, 1600, 2000, 2500 cells per well in a 6 well plate for all mutated cell lines (PIK3CA = SNU-C4, KRAS = LS-1034, BRAF = LS-411N, PIK3CA-KRAS = DLD-1). For the wild-type cell line, Caco-2, 1000, 1500, 2000, 3000, 4000, 5000, 10000 and 20000 cells were plated per well. Plates were incubated at 37°C, with 5% CO₂ for 2 weeks. Cells were fixed and stained with 0.1% crystal violet. Optimised cellular volumes are shown in Table 2.8.

2.3.5. Colony fixation and crystal violet staining technique

Media was carefully removed from well / flask. Fresh media (1ml/ well / 6 well plate, or 3mls/T25 flask) was slowly added to the side of the well / flask to avoid lifting colonies. Media was removed and plates / flasks were washed with PBS. PBS was removed and 1:4 acetic acid: methanol mix (4°C) (2ml/ well / 6 well plate, or 5mls/T25 flask) was added to cells, and incubated at room temperature

for 30 minutes. Acetic acid: methanol mix was removed and cells were rinsed with water. Cells were stained with 0.1% crystal violet (2ml/ well / 6 well plate, or 5mls/T25 flask) for 30 minutes, and plates were subsequently rinsed with water.

2.3.6. Quantification of cellular growth in clonogenic assays

As colony size varied widely between treatment regimens, counting colonies of over 50 cells did not fully represent the cellular response to treatment. Therefore we determined the crystal violet staining intensity via a colourimetric assay, whereby the crystal violet intensity is directly proportional to the volume of cells within a flask / well.

30% acetic acid was added to each well (2mls/well/6 well plate) or T25 flask (5mls) and incubated at room temperature for 20 minutes on a shaker. Samples were diluted 1:5 with water. 250µl of the diluted crystal violet solution was added to 96-well plate (each well / flask was carried out in triplicate) and measured on a plate reader at 595nm.

2.3.7. Optimisation of drug concentrations

Cells were plated in 6 well plates at optimised cellular concentrations from 2.3.4 (2mls per well) and incubated at 37°C with 5% CO₂ for 24hours. Media was subsequently removed, and 2mls drug-containing media was added to each well. Cells were treated with serial 1:2 dilutions of the MEK inhibitor refametinib (2µM – 0.24nM), PI3K inhibitor copanlisib (200nM – 0.024nM) or 5-FU chemotherapy (250µM – 0.03µM), or vehicle controls (DMSO for refametinib and 5-FU chemotherapy, or DMSO/TFA for copanlisib). Cells were incubated at 37°C with 5% CO₂ for 2 weeks. Colonies were subsequently fixed, stained and quantified via methods 2.3.5 and 2.3.6. Experiments were run in triplicate and error bars were representative of standard deviations. IC₇₅ values were calculated for each cell line per drug, and are represented in Table 2.8.

Table 2.8: Optimised incubation times, cell volume and drug concentrations for PI3K inhibitor (copanlisib), MEK inhibitor (refametinib), and 5-FU chemotherapy, for 5 colorectal cancer cell lines for varying mutations within the PI3K and MAPK pathways.

Cellular volume was optimised for each cell line, depending on colony formation during a two-week incubation period at 37°C, with 5% CO₂. Drug concentrations for copanlisib, refametinib and 5-FU chemotherapy are representative of IC75 values for each cell line treated with varying concentrations of each drug.

	Wild type	BRAF mutated	PIK3CA mutated	KRAS mutated	PIK3CA & KRAS mutated
	Caco-2	LS-411N	SNU-C4	LS-1034	DLD-1
Volume of cells seeded per T25 flask	50,000 cells	5,000 cells	2,000 cells	3,000 cells	1,000 cells
IC50 for Copanlisib (nm)	6.1	100	3.1	8.6	50
IC50 for Refametinib (nm)	250	4.6	4.4	33.25	500
IC75 for 5-FU chemotherapy (nm)	130	290	56	60	730
Incubation period	2 weeks	2 weeks	2 weeks	2 weeks	2 weeks

2.3.8. Clonogenic assays of PI3K and/or MEK inhibition in combination with chemoradiation therapy

Cells (cellular concentration determined from section 2.3.4, see Table 2.8) were seeded in T25 flasks and incubated at 37°C in 5% CO² for 24 hours. Following incubation, cells were treated with drug-containing media (drug concentrations determined from section 2.3.7, see Table 2.8). Overall there were 15 treatment arms, and 2 controls, which are outlined in Table 2.9. Cells were radiated 1-hour post drug treatment (as per section 2.3.9) and incubated until colony formation (Table 2.8). Colonies were fixed and stained as per method 2.3.5 and quantified as per method 2.3.6. The clonogenic assays are described in Figure 2.3.

Table 2.9: Drug treatment regimens for clonogenic assays

Vehicle	Refametinib;
Vehicle and transport	Refametinib and chemotherapy;
5-FU chemotherapy	Refametinib and radiation
Radiation	Refametinib and chemoradiation
Chemoradiation	Copanlisib and Refametinib
Copanlisib;	Copanlisib, refametinib and chemotherapy;
Copanlisib and chemotherapy	Copanlisib, refametinib and radiation;
Copanlisib and radiation;	Copanlisib, refametinib and chemoradiation.
Copanlisib and chemoradiation	

2.3.9. Radiation of T25 flasks

Based on results from a previous study (178). The cancer cell lines were irradiated in T25 culture flasks (Corning) which were placed in a Perspex phantom. This was subsequently placed under slabs of water equivalent plastic to position the cells at a depth of 10cm, which was 100cm from the radiation source, to mimic a clinically relevant tumour depth. Up to 8 flasks were radiated at a time in a perspex phantom. All irradiations performed used a 6MV photon beam produced by an Elekta Precise LINAC with an 80 leaf multi-leaf collimator. A nominal dose rate of 400MU/min and a dose of 2Gy were delivered to the base of the in-field culture flasks using a 10 x 15cm² field. Radiation was carried out in collaboration with Prof. Brendan McClean, Dr. Peter McBride, Dr. Laura Shields, and Dr. Allen Curran St. Luke's hospital, Rathgar.

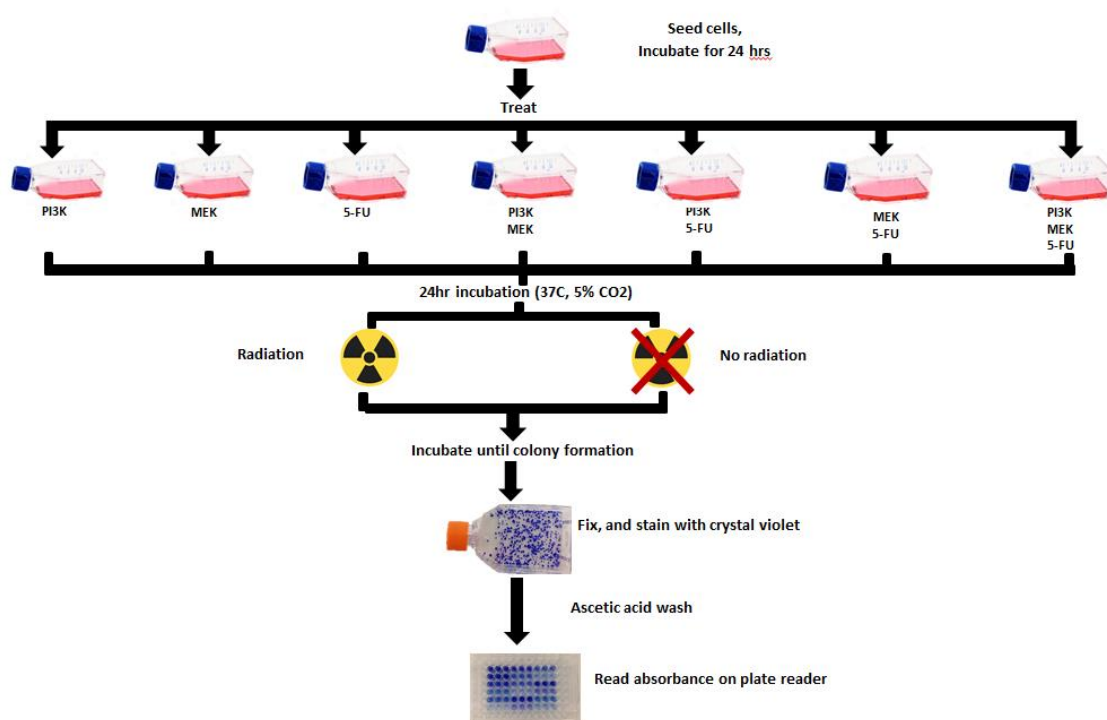


Figure 2.3: Method for clonogenic assays

Cells (LS-411N = 1,000 cells; DLD-1 = 200 cells; SNU-C4 = 400 cells; LS-1034 = BH-600 cells and Caco-2 = 10,000 cells) were plated in 6 well plates (2mls per well) and incubated for 24 hours. Cells were treated with serial 1:2 dilutions of the PI3K inhibitor Copanlisib (200nm - 0.025nm), and a DMSO/TFA control (200nm). Cells were incubated until colony formation (2 weeks for mutated cell lines, and 5 weeks for wild-type cell line). Cells were fixed and stained with 0.1% crystal violet. Wells were rinsed with 1ml acetic acid to remove crystal violet, which was subsequently diluted (1:5), and the staining intensity was read on a plate reader at 595nm. Error bars represent the standard deviation, with experiments run in triplicate.

2.3.10. Statistical analysis

CalcuSyn software (Biosoft) was used to calculate IC_{75} values required for drug concentrations for the clonogenic study via an automated median-effect plot (Chou plot). Prism software (GraphPad) was used to for the generation of graphs and to calculate the statistical significance between various treatment cohorts. The unpaired 2-tailed t-test with Welch's correction was used with a confidence interval of 95%. Data are representative of the mean and standard deviation of 3 independent experiments. P-values ≤ 0.05 were indicative of a result of statistical significance.

2.4. Materials and methods utilised in aim 4 to determine in vivo if inhibition of the PI3K and related kinase signalling pathways augments the chemoradiotherapy sensitivity of genetically defined rectal cancer models.

Table 2.10: List of reagents used for in vivo study, including their names, suppliers and product codes.

Reagent	Supplier	Product code
DLD-1	ATCC	ATCC CCL-221
LS-1034	ATCC	ATCC CRL-2158
Caco-2	ATCC	ATCC HTB-37
SNU-C4	KCLB	0000C4
RPML-1640 medium	Sigma Aldrich	R8758
Dulbecco's modified eagle medium - high glucose	Sigma Aldrich	D6429
DMEM and HAMS F12	Sigma Aldrich	D8062
Eagle minimum essential medium	Sigma Aldrich	M0325
FBS, Qualified (Foetal bovine serum)	Gibco	10270-106
Copanlisib	BAYER	S2802
Refametinib	BAYER	S1089
Dimethylsulfoxide (DMSO)	Sigma-Aldrich	D2650
0.25% Trypsin-EDTA (1x)	Gibco	25200-056
Phosphate buffered saline tablet	Sigma	P4417
5-Fluorouracil	Sigma-Aldrich	F6627
EURodent Diet 14%	Lab Supply	5LF2
Gamma Irradiated DietGel Recovery	Clear H2O	72-06-5022
Polyethylene glycol	Sigma	p-3140
NaCl	Sigma-Aldrich	S7653
Xylene (500ml bottle)	Sigma-Aldrich	534056-500ml
Paraffin	Sigma-Aldrich	1496904
Hydrochloric acid	Sigma-Aldrich	H1758
Monoclonal mouse anti-human Ki-67 antigen clone MIB-1	Dako	M7240

2.4.1. In vivo training

Prior to initiation of the in vivo study, appropriate training was undertaken for handling, carrying out procedures and culling of mice. Theoretical training was carried out through the LAST Ireland 2-day training programme. Manual training was carried out in animal housing units in Beaumont hospital and Queens University by trained personnel. Training included handling of mice, measuring tumours with callipers, IV and IP injections, radiation, and culling. LAST Ireland and ASPA certificates were obtained prior to initiation of the project.

2.4.2. Husbandry

Mice were bred in house, and housed in individually ventilated cage racks, thereby minimising the risk of cross-contamination of animal-related pathogens. Personal protective equipment was worn at all times; this included a face mask, 2 pairs of gloves, scrubs, hat, gown and shoes specific to the area.

2.4.3. Preparation of cells for subcutaneous implantation

Cells were grown to 80-90% confluency (Table 2.11). Growth medium was removed, and cells were washed with PBS. Cells were detached using 3mls trypsin and incubated at 37°C for 5-10 minutes, or until the cells detached. Trypsinisation was neutralised with 5mls growth media. Cells were pelleted by centrifugation for 5 minutes at 1000rpm. Cells were washed twice with PBS and counted using a haemocytometer. Cells were resuspended in fresh PBS to a concentration of 2.5×10^6 cells/100ul for PIK3CA, KRAS and PIK3CA-KRAS mutated cell lines, and 3.5×10^6 cells/100ul for the wild-type. Cell-PBS suspension was stored on ice until implantation.

Table 2.11: Colorectal cancer cell lines subcutaneously implanted in SCID BALB/C mice.

	Mutations	Media	Tissue type	Morphology
DLD-1 (ATCC CCL-221)	PIK3CA: E545K KRAS: G13-D	RPMI + 10% FBS	Colon, Dukes type C, colorectal adenocarcinoma	Epithelial
LS-1034 (ATCC CRL-2158)	KRAS: A146P	RPMI + 10% FBS	Cecum, Dukes type C, colorectal carcinoma	Epithelial
Caco-2 (ATCC HTB-37)	WT	EMEM + 20% FBS	Colorectal adenocarcinoma	Epithelial
SNU-C4 (KCLB 0000C4)	PIK3CA: E545G	RPMI + 10% FBS	Colon, Colorectal adenocarcinoma	Epithelial

2.4.4. Subcutaneous implantation of tumour cells

6-8 week old mice were weighed and their right flank shaved. All protocols were carried out using sterile instruments using aseptic techniques in a class II biosafety cabinet. Mice were anaesthetised via inhalation of isofluorane gas. Inoculation area was sterilised with ethanol. Cells were mixed for even distribution, and 100ul of cell/PBS suspension was injected into the right flank of BALB/C SCID mouse using a 26 gauge needle. Mice were clipped on the ears for identification purposes whilst under anaesthetic. Mice were monitored postoperatively for 30 minutes to ensure no unwanted side effects occurred as a result of the anaesthetic or implantation procedures.

2.4.5. Monitoring of mice

Mice were weighed a minimum of every 3 days. Mice were put on a high fat diet supplement 'DietGel' during the week of treatment, or if their weight dropped by 10% from their initial starting weight. If their weight continued to drop to below 20% of their initial starting weight, mice were culled humanely. Tumours were measured with callipers a minimum of every 3 days. Tumour diameters were calculated by the formula: length x width x height x 0.52.

2.4.6. Drug treatments for mice

Tumours were measured with callipers when they became palpable. Drug treatments began when mice tumours reached 100mm^3 (Figure 2.4). Treatment arms for mutated tumours included untreated (n= 8), vehicle (n=5), copanlisib (n=5), chemoradiation (n=8) and copanlisib-chemoradiation (n=8). Because Caco-2 tumour growth was slow, in this group, treatment arms were restricted to vehicle (n=5), chemoradiation (n=5) and copanlisib-chemoradiation (n=5).

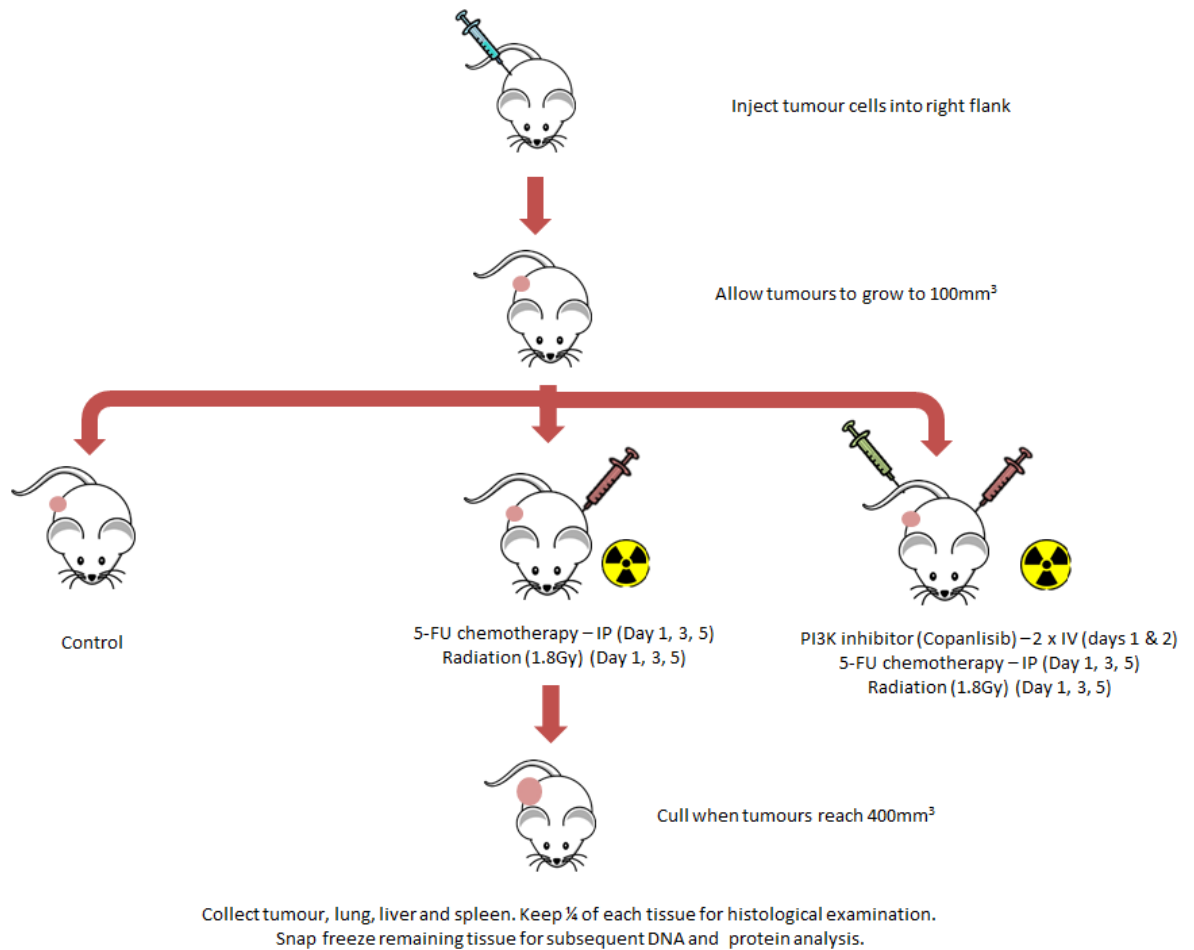


Figure 2.4: In vivo treatment regimens

Tumour cell lines were implanted into 6-8 week old mice. When tumours reached 100mm^3 , mice were divided into control; vehicle; copanlisib; chemoradiotherapy or copanlisib-chemoradiotherapy treatment groups. Copanlisib (7mg/kg) was administered intravenously twice a day on days 1 and 2. 5-FU chemotherapy (20mg/kg) was administered intraperitoneally, and mice were radiated in a Faxitron CP 160 x-ray generator at 1.8Gy on days 1, 3 and 5. Mice were sacrificed when tumours reached 400mm^3 . Tumours, lungs, livers and spleens were excised for histological examination, and the remaining tissue was snap-frozen.

2.4.7. Intravenous injection

Mice were weighed to calculate appropriate drug volume (7mg/kg). Mice were placed in a heat box for 2-3 minutes (until the tail veins have dilated) and subsequently inserted into a sterile restraint chamber. Prior to injection, needles were assessed for air bubbles. Copanlisib was administered with an insulin needle into one of the lateral tail veins, with a maximum dose of 200ul. A sterile swab was placed over the injection site for ~20 seconds, or until the tail has ceased bleeding. Copanlisib was administered as an intravenous bolus twice a day on day 1 and 2 of treatment, and mice were allowed to recover for a minimum of 2 hours between injections. Copanlisib stock was dissolved in PEG400: 0.1N HCl (20:80). This was further diluted 1:40 in 0.9% NaCl. Mice tail veins were punctured a maximum of 3 times / vein / day.

2.4.8. Intraperitoneal mouse injection.

Mice were weighed to calculate the correct drug dosage of 5-FU chemotherapy (20mg/kg). Mice were restrained by scuffing behind the ears and along the back. Mice were tilted in a downward position, thereby minimising organ injury. The needle was inserted on the right-hand side, near the teat, at a 30° angle. A maximum dose of 200ul was injected. 5-FU chemotherapy was administered on days 1, 3 and 5 of treatment. 5-FU chemotherapy was dissolved in DMSO, and diluted (1:100) with 0.9% NaCl prior to injection.

2.4.9. Radiation of mice

Mice were placed in a plastic holding fixture and covered with a lead dose shield (Figure 2.5) to minimise radiation exposure to the remaining body. Mice were radiated in a Faxitron CP 160 x-ray generator at 1.8Gy (160KV for 2.2minutes). Mice were radiated on days 1, 3 and 5 of treatment. Mice were given a minimum recovery time of 1 hour between IV/IP injections and radiation.



Figure 2.5: Radiation of mice

6-8 week old SCID mice were implanted with cancer cell lines (WT, KRAS mutated, PIK3CA mutated and PIK3CA-KRAS mutated). When tumours reached 100mm³, mice were separated into control; vehicle; copanlisib; chemoradiotherapy or copanlisib-chemoradiotherapy treatment regimens. Copanlisib (7mg/kg) was administered intravenously twice a day on days 1 and 2. 5-FU chemotherapy (20mg/kg) was administered intraperitoneally, and subsequently radiated. Mice were placed in a holding fixture and covered with a lead dose shield. They were subsequently radiated in a Faxitron CP 160 x-ray generator at 1.8Gy (160KV for 2.2minutes). Mice were radiated on days 1, 3 and 5 of treatment.

Table 2.12: Days mice were treated by copanlisib, 5-FU chemotherapy and radiation.

Days mice were treated are represented as red, whilst days untreated are represented as grey.

	1	2	3	4	5
Copanlisib					
5-FU chemotherapy					
Radiation					

2.4.10. Culling of mice

Mice were sacrificed humanely when tumours quadrupled in size from treatment initiation. For this, mice were placed in a clean and aired out carbon dioxide chamber. 100% of carbon dioxide was slowly released at a flow rate of 11-15% of the chamber volume/minute. Mice were retained in the chamber for 5 minutes and subsequently removed. Mice were assessed for loss of consciousness and indications of death. Cervical dislocation was carried out to ensure mice were appropriately culled.

2.4.11. Harvesting organs

A vertical midline incision was made with scissors. Primary tumour, lungs, liver and spleen were removed using a scalpel and scissors. Tumour and organs were subsequently weighed and dissected into quarters. $\frac{3}{4}$ of the organs were snap-frozen in liquid nitrogen for subsequent DNA and proteomic analysis in future studies, whilst the remaining $\frac{1}{4}$ was placed in formalin for further histological examination.

2.4.12. Processing of organs

Principle:

Fixation: Tissues are submerged in a fixation solution (typically formalin), which slowly penetrates the specimen, resulting in chemical and physical alterations which solidify and preserve the tissue, whilst simultaneously protecting it from subsequent steps in the processing of the sample.

Dehydration: Specimens will ultimately be embedded in melted paraffin wax which is a hydrophobic substance. Therefore all water within the specimen must be removed to facilitate wax infiltration throughout the tissue. This is carried out by dehydration of the tissue through ascending grades of ethanol solutions.

Clearing: Paraffin wax is also immiscible with alcohol; therefore tissues must be submerged in a clearing solution (typically xylene) which removes the ethanol and any fat within the tissue which may hinder wax infiltration.

Wax infiltration: Tissues infiltrated with paraffin wax, and cooled to solidify.

Procedure:

Sections of organs were fixed in formalin (15mls) for 24-48 hours. Following fixation, specimens were placed in labelled cassettes and processed on a VIP processor under the following programme:

Solution	Time (minutes)	Temperature
10% buffered formalin	25	37°C
10% buffered formalin	60	
70% alcohol	75	
94% alcohol	75	
94% alcohol	75	
Absolute alcohol	75	
Absolute alcohol	90	
Xylene	75	
Xylene	105	
Xylene	105	
Wax	60	60°C
Wax	60	
Wax	90	
Wax	60	

After processing, specimens were placed in embedding cassettes, orientated in the appropriate plane, infiltrated with paraffin wax and left on a cooling plate (-4°C) to solidify. Sections were cut at 4µm thickness and subsequently placed on glass

slides for haematoxylin and eosin (H&E) processing or superfrost glass slides for Ki67 staining.

2.4.13. Haematoxylin and eosin staining:

Principle:

Haematoxylin contains alum which acts as a mordant, staining basophilic structures e.g. nuclei, blue. Sections are subsequently differentiated in acid, which turns the haematoxylin red. Blueing in water reverts stained tissue into an insoluble blue colour. Eosin is used as a counterstain. It is an acidic dye which stains basic cellular components within the tissues, such as cytoplasm pink, red blood cells, and collagen.

Procedure:

Sections were stained in a Thermo Shandon Varistain Gemini automated slide stainer. Whereby slides were deparaffinised twice in xylene (10minutes each), followed by two rehydration steps in 100% alcohol (5 minutes each), 95%, 80% and 70% alcohol (2 minutes each). Sections were rinsed in water and stained with haematoxylin solution for 8 minutes. Samples were rinsed in water, differentiated in 1% acid alcohol for 30 seconds and rinsed again. Slides were blued in water for 5 minutes, followed by 95% alcohol (10 seconds). Sections were counterstained with eosin for 1 minute, and dehydrated in alcohol (95%, 100%, 100% for 5 minutes each), and finally cleared in xylene (twice for 5 minutes each). Slides were subsequently coverslipped using a xylene based mounting medium.

2.4.14. Statistical analysis

Prism software (GraphPad) was used for generation of graphs and statistical analysis. Variations in tumour growth between various treatment cohorts was analysed using the one way ANOVA Kruskal-Wallis test (did not assume Gaussian distributions), and the Dunns test, using a confidence interval of 95%.

Overall survival, and variations between organ / tumour mass between groups was analysed using the unpaired 2-tailed t-test with Welch's correction and a confidence interval of 95%.

Survival was calculated using Kaplan-Meier survival curves, and p-values were calculated using the log-rank (Mantel-Cox) test. The Bonferroni method was used to calculate the statistical significance for the p-value, assuming a significant value of 0.05. Error bars are representative of standard deviations in each treatment group. Mice whose survival rates were above or below the mean $\pm 2 \times$ s.d. were removed from the analysis.

To determine the full spectrum of somatic genetic aberrations that activates the PI3K and related signalling pathways in LARC and how they are modulated by treatment.

3.1. Introduction

3.1.1. Mutations within the human genome

Tens of thousands of errors occur daily during the cell replication process. Mistakes located in introns (non-coding) regions of the DNA are removed during transcription of DNA into RNA. Whilst the majority of remaining errors are removed by the body's checkpoints. A proficient DNA mismatch repair (MMR) system removes base-pair mismatches and insertion-deletion loops. If errors evade all precautionary steps, a tumour may ensue. Many of these mutations are synonymous or silent mutations, whereby the mutation alters the gene sequence without altering the encoded protein. Remaining mutations include point mutations which can affect single base-pairs i.e. missense (single base-pair substitution, resulting in the synthesis of an alternate amino acid) or nonsense (formation of a premature stop codon) mutations; or frame-shift mutations whereby an insertion or deletion alters the entire reading frame.

3.1.2. Oncogenic pathways associated with colorectal cancer

The adenoma-carcinoma sequence was first hypothesised by Fearon and Vogelstein in 1990. This theory suggests that CRC is a result of a multi-step process of events whereby normal epithelium becomes adenomatous and eventually transitions into adenocarcinoma. *APC* mutations typically trigger the pathway, followed by *KRAS* mutations, and subsequent *TGFB*, *PIK3CA* and *TP53* mutations. The 3 mechanisms now known to be associated with CRC include:

1. Loss of DNA mismatch repair genes, resulting in microsatellite instability (MSI) (15% of CRC cases). When a tumour becomes MMR deficient, every nucleotide repeat sequence in the genome (both intronic and exonic) is susceptible to insertion and deletion mutations. Frameshift mutations in MSI CRCs typically occur in tumour suppressors (*TGFBRII*, *IGFIIR*, *PTEN*, and *RIZ*), DNA MMR genes (*MSH3*, *MSH6*), apoptosis promoter (*Bax*), and transcription factor (*TCF4*), Wnt signalling (*AXIN2*), and DNA glycosylase (*MBD4*).

2. Chromosomal instability (CIN), (65% of CRC cases). CIN cancers are associated with loss of tumour suppressor genes, and are characterised by loss of heterozygosity (LOH) and aneuploidy (chromosome number imbalance), karyotypic abnormalities, genomic amplifications of chromosomal regions, and an accumulation of specific oncogenes and tumour suppressor gene mutations. CIN tumours have an accumulation of mutations which are vital in activating the oncogenic pathway in CRC. These mutations are in both tumour suppressor genes (*APC* (5q21), *TP53* (17p13), *SMAD2* and *SMAD4* (18q21), *DCC* (18q21)), and oncogenes (*KRAS* (12p12), *CTNNB1* (3p22) and *PIK3CA* (3q26)).
3. CpG island methylator phenotype (CIMP) / Serrated methylator pathway (20% of CRC cases). CIMP tumours display gene silencing as a result of hypermethylation of CpG islands. CIMP tumours are divided into CIMP-high (high frequency of *BRAF* mutations) and CIMP-low (high frequency of *KRAS* mutations). They are significantly associated with old age, females, sporadic MSI tumours, *BRAF* and *KRAS* mutations, and poor differentiation. The most frequently used CIMP markers are P16, MINT1, MINT2, MINT31 and MLH1.

3.1.3. Mutations within the PI3K and MAPK pathways

Somatic genetic alterations (e.g. *PIK3CA*, *KRAS* and *BRAF* mutations) that activate the pro-oncogenic PI3K and MAPK signalling pathways are common in rectal cancer. These alterations are associated with resistance to chemotherapy and radiation therapy, and poor patient outcomes (93).

In RC, the vast majority of PI3K pathway aberrations are a result of upregulation of RTKs, mutations in, or overexpression of the proto-oncogene *PIK3CA* and/or inactivation of the tumour suppressor gene *PTEN*. Somatic missense mutations, deletions and amplifications in *PIK3CA* have been linked to CRC, and other cancers (95,98). *PIK3CA* gene mutations are present in 8-20% of all CRC cases (89,99,100).

Within the MAPK pathway, the most common mutations in CRC are *KRAS* (35-47%) (93,104,105), and *BRAF* (<5%, 5-10%) (93,105–107). 95% of *KRAS* mutations occur within exon 2, codons 12 (80%) and 13 (15%). These mutations have been linked to resistance to anti-EGFR therapy, poor recurrence-free survival and poor overall survival (93,108,109). *BRAF^{mut}* CRCs have a worse prognosis, are significantly more inclined to be found in females over 70 years, located in the proximal (right side) colon, identified at a higher grade, more inclined to have MSI and decreased overall survival than their *BRAF^{wild-type}* counterparts (113). *BRAF^{mut}* patients have been shown to have a higher grade, increased lymph node involvement, peritoneal metastasis, decreased disease-free survival, and overall survival post-recurrence. Furthermore, patients with non-curative metastatic *BRAF^{mut}* CRC have a median survival of 33-50% of that of their *BRAF^{wild-type}* counterparts. V600E mutations are present in ~10% of all CRC cases and 80-90% of all *BRAF* mutations (115). It is indicative of a poor prognosis, particularly in microsatellite stable CRCs.

The objectives of this chapter include:

1. Analysis of tumour mutational burden within CRC
2. To determine if the number and type of mutations determine patient response to NACRT.
3. To identify mutations associated with patient response to NACRT.
4. To analyse intra-tumour heterogeneity to identify potential driver mutations.
5. To identify mutational signatures in LARC samples, and see if mutational signatures determine response to NACRT.

3.2. Results:

3.2.1. Whole exome sequencing study from an Irish cohort of LARC patients.

Whole-exome sequencing was carried out on DNA extracted from fresh frozen pre-treatment tumour biopsies and matched normal tissue or blood samples from 11 patients who presented with locally advanced rectal cancer (LARC) and were treated with neoadjuvant chemoradiation therapy (NACRT) in Ireland. Patient biopsy samples were stratified into good (n = 3), intermediate (n = 5) and poor (n = 3) responders to NACRT treatment. Resulting data for the somatic synonymous and non-synonymous mutations from each sample was analysed to determine mutational frequencies, intra-tumour heterogeneity and mutational signatures; to see if we could identify any biomarkers which may predict patient response to NACRT treatment.

Table 3.1: Clinicopathological data for patients in whole exome sequencing study

Age at diagnosis (years)		Good (n=3)	Intermediate (n=5)	Poor (n=3)
Average		49	64.6	73.3
Range		42-60	52-79	70-76
Median		45	65.7	74.1
Gender				
Male		2 (66.6%)	3 (60%)	2 (66.6%)
Female		1 (33.3%)	2 (40%)	1 (33.3%)
TNM status				
T	T0	3	0	0
	T1	0	1	0
	T2	0	0	0
	T3	0	3	3
	T4	0	1	0
N	N0	3	3	2
	N+	0	2	1

Table 3.2: Tumour purity and ploidy for whole exome sequencing study

	Sample	Purity	Ploidy
Good responders	BH-610	0.366	3.791
	BH-634	0.250	3.479
	BH-643	0.611	2.342
Intermediate responders	BH-600	0.539	3.151
	BH-601	0.177	1.791
	BH-607	0.415	2.007
	BH-614	0.195	1.975
	BH-659	0.300	2.201
Poor responders	BH-608	0.355	3.398
	BH-612	0.997	2.054
	BH-644	0.535	4.299

Although there was a trend towards poorer prognosis with increasing age within our cohort, there was no significant difference between any of the groups.

All patients with a good response had a TNM stage 0, whereby the tumour was contained entirely within the mucosa. Intermediate and poor responders ranged from TNM stages 2-4 whereby the tumour had spread through the muscularis mucosa (stage 2) up to the local lymph nodes (stage 4). No statistical significance was identified between the TNM stages and patient response.

Lymph node positivity did not determine patient response to NACRT between intermediate and poor responders to NACRT.

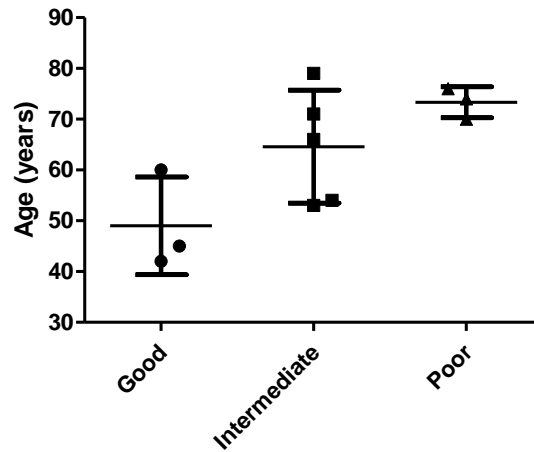


Figure 3.1: Relationship between age and patient response to NACRT.

Whole-exome sequencing was carried out on DNA extracted from tumour biopsies of LARC patients with good (n = 3), intermediate (n = 5) and poor (n = 3) response to NACRT. Data was run through a bioinformatics pipeline described in section 2.1.6 and Fishers exact test was used to identify significantly mutated genes. An unpaired 2-tailed t-test, using Welch's correction was carried out to determine if there was any significance between groups. A confidence interval of 95% was used.

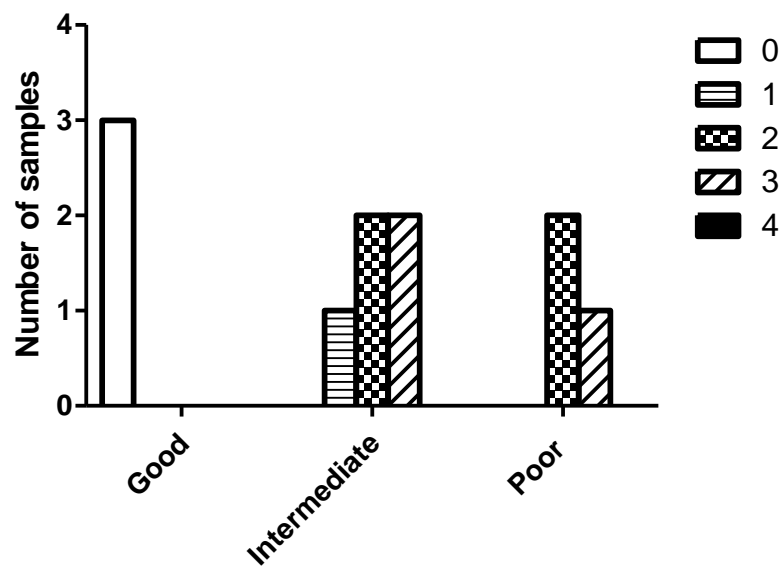


Figure 3.2: Relationship between TRG status and patient response.

Whole-exome sequencing was carried out on DNA extracted from tumour biopsies of LARC patients with good (n = 3), intermediate (n = 5) and poor (n = 3) response to NACRT. Each bar is representative of the 5 TNM stages, (stage 0 = the tumour is contained within the mucosa, stage 1 = the cancer has breached through the mucosa, stage 2 = the cancer has spread through the muscularis mucosa, stage 3 = cancer has metastasised to 1 or more lymph nodes, stage 4 = distant metastasis). Data was run through a bioinformatics pipeline described in section 2.1.6 and Fishers exact test was used to identify significantly mutated genes. A 2 way ANOVA test, using the Bonferroni post-test was used to calculate statistical significance.

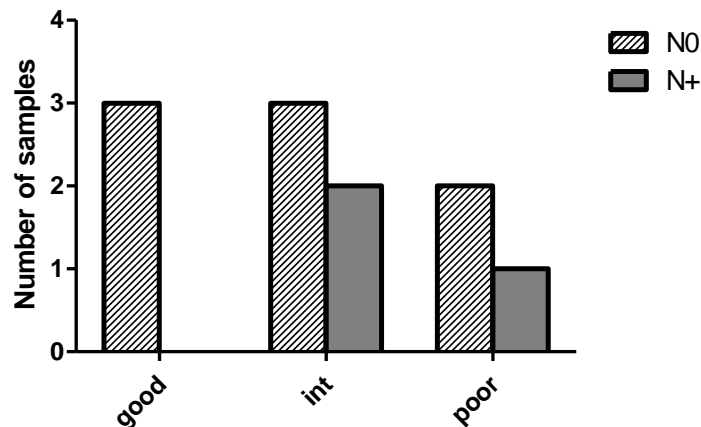


Figure 3.3: Relationship between lymph node positivity and patient response to NACRT.

Whole-exome sequencing was carried out on DNA extracted from tumour biopsies of LARC patients with good ($n = 3$), intermediate ($n = 5$) and poor ($n = 3$) response to NACRT. Data was run through a bioinformatics pipeline described in section 2.1.6 and Fishers exact test was used to identify significantly mutated genes. A 2-way ANOVA was carried out to determine statistical significance between groups.

3.2.2. Mutational frequency of synonymous and non-synonymous, somatic mutations in pre-treatment LARC biopsy samples

The pre-treatment patient biopsy samples from the 11 LARC patients yielded 5,518 synonymous and 1,474 non-synonymous mutations. These mutations were sub-divided according to their mutation type, and are represented in Table 3.3 or Table 3.4 and Figure 3.4 for non-synonymous mutations.

There were large variations in tumour mutational burden between samples and response groups, with the lowest mutational frequency identified in poor responders (total mean = 94.3 mutations, non-synonymous mean = 43.3 mutations), compared to good (total mean = 523.3 mutations, non-synonymous mean = 72 mutations), or intermediate responders (total mean = 1027.8 mutations, non-synonymous mean = 225.6 mutations). However, this was partly due to a select few hyper-mutated samples which skewed results. As a result, the tumour mutational burden did not alter significantly between the three groups (good vs intermediate, total $p = 0.43$, non-synonymous $p = 0.26$; good vs poor, total $p = 0.32$, non-synonymous $p = 0.33$; intermediate vs poor, total $p = 0.13$, non-synonymous $p = 0.20$).

Table 3.3: Single nucleotide variant (SNV) and insertion/deletion (indel) mutations in LARC biopsies from good, intermediate and poor responders to NACRT.

Whole-exome sequencing was carried out on DNA extracted from tumour biopsies of LARC patients with good (n = 3), intermediate (n = 5) and poor (n = 3) response to NACRT. Data was run through a bioinformatics pipeline described in section 2.1.6 and Fishers exact test was used to identify significantly mutated genes. Somatic non-synonymous mutations were divided into types of mutations and their response to NACRT.

	Sample	SNVs	Indels
Good	BH-610	261	9
	BH-634	1168	6
	BH-643	119	7
Intermediate	BH-600	65	6
	BH-601	2499	26
	BH-607	556	137
	BH-614	75	5
	BH-659	1757	13
Poor	BH-608	124	8
	BH-612	23	5
	BH-644	107	16

Since synonymous mutations do not alter the encoded protein and are therefore known as silent mutations, we will primarily focus on non-synonymous mutations for the remainder of this chapter.

Our study identified 1,474 non-synonymous somatic mutations in 1,275 genes. These mutations were further classified into mutational type (Table 3.7, Figure 3.16). Percentile frequency analysis of the somatic non-synonymous mutations showed a predominance of missense (n = 1,129, 76.6%), and frameshift (n = 172, 11.7%), mutations, and to a lesser degree splicing (n = 84, 5.7%), inframe deletions (n = 36, 2.4%) and nonsense (n = 32, 2.2%) mutations (Figure 3.17). The remaining 1.4% consisted of inframe insertions, lost start and stop codons, retained stop codons, mature miRNA and 3' untranslated region (UTR) variants. This pattern occurred throughout the majority of samples; however this fluctuated in the hypo-mutated sample BH-612 due to the low volume of mutations, and the

hyper-mutated sample BH-607 had an increased volume of frameshift mutations at 47.1%.

Table 3.4: Non-synonymous, somatic mutations in LARC biopsies from good, intermediate and poor responders to NACRT.

Whole-exome sequencing was carried out on DNA extracted from tumour biopsies of LARC patients with good (n=3), intermediate (n=5) and poor (n=3) response to NACRT. Data was run through a bioinformatics pipeline described in section 2.1.6 and Fishers exact test was used to identify significantly mutated genes. Somatic non-synonymous mutations were divided into types of mutations and their response to NACRT.

	Good responders	Intermediate responders	Poor responders	Total
Missense	160	873	96	1129
Frameshift	23	129	20	172
Nonsense	6	17	9	32
Splicing	13	67	4	84
Inframe deletion	11	25	0	36
Inframe insertion	2	8	1	11
Incomplete terminal codon	1	0	0	1
Stop-retain	0	3	0	3
3' prime UTR variant	0	1	0	1
Stop-lost	0	3	0	3
Start-lost	0	2	0	2
Total	216	1128	130	1474

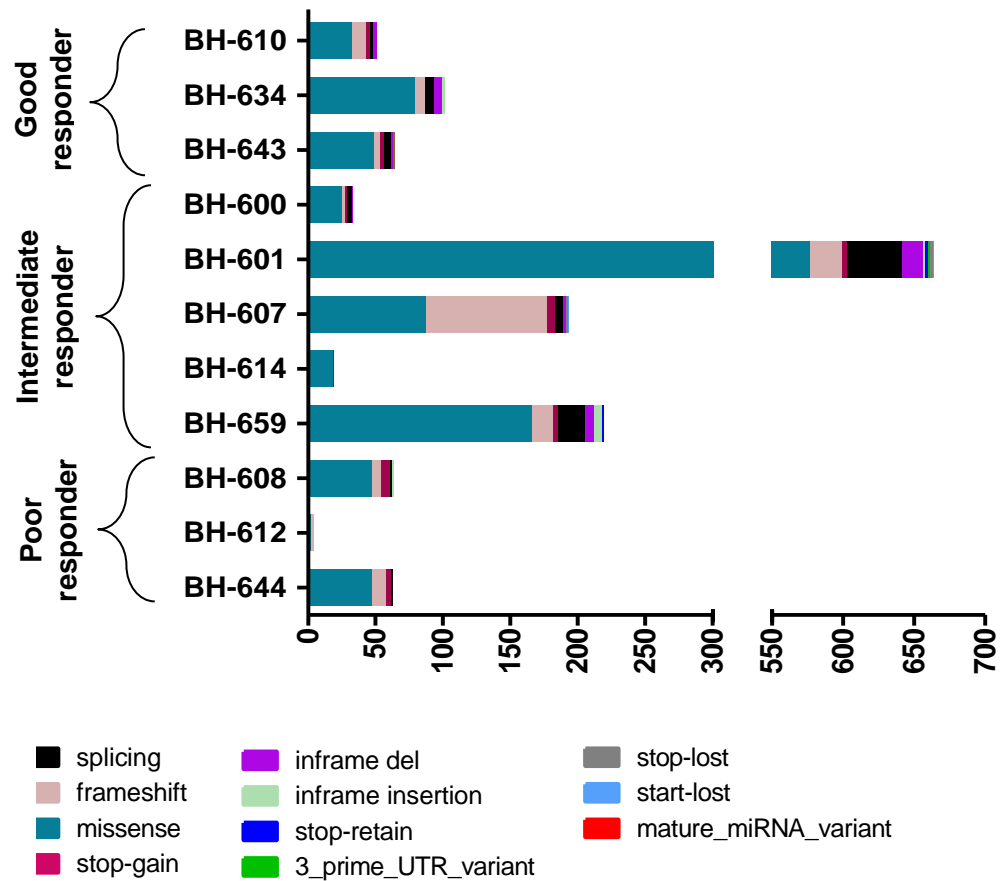


Figure 3.4: Tumour mutational burden for non-synonymous somatic mutations per pre-treatment biopsy sample.

Whole-exome sequencing was carried out on DNA extracted from tumour biopsies of LARC patients with good ($n=3$), intermediate ($n=5$) and poor ($n=3$) response to NACRT. Data was run through a bioinformatics pipeline described in section 2.1.6 and Fishers exact test was used to identify significantly mutated genes. Somatic non-synonymous mutations were divided into types of mutations and their response to NACRT.

Sample numbers, grouped according to NACRT response are represented along the Y-axis. Composition and frequency of mutations in individual samples are represented along the X-axis. A colour-coded system was used to illustrate mutational type frequency per sample.

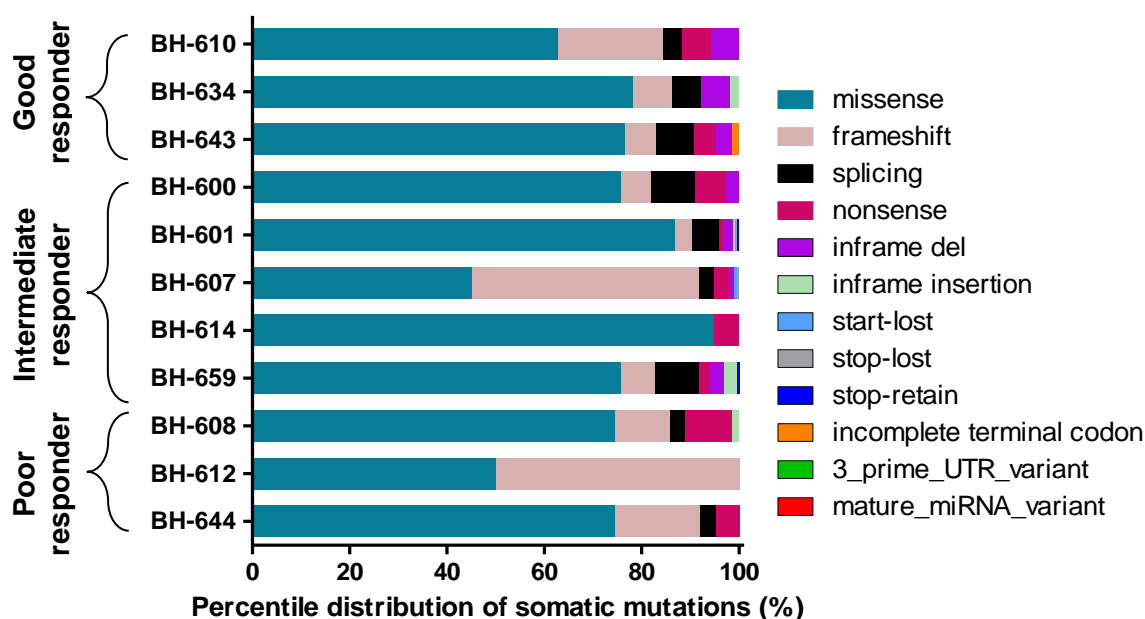


Figure 3.5: Percentile distribution of non-synonymous somatic mutations per individual pre-treatment biopsy sample.

Whole-exome sequencing was carried out on DNA extracted from tumour biopsies of LARC patients with good ($n=3$), intermediate ($n=5$) and poor ($n=3$) response to NACRT. Data was run through a bioinformatics pipeline described in section 2.1.6 and Fishers exact test was used to identify significantly mutated genes. Somatic non-synonymous mutations were divided into types of mutations and their response to NACRT.

Sample numbers, grouped in according to NACRT response are represented along the Y-axis. Composition and frequency of mutations in individual samples are represented along the X-axis. A colour-coded system was used to illustrate mutational type frequency per sample.

Hyper-mutated samples BH-601 (intermediate responder) had 664 somatic, non-synonymous mutations, however it did not show any genetic mutations associated with MSI tumours.

In contrast, less than 35 non-synonymous mutations were identified in 3 samples, all of which were non-responders to NACRT (intermediate responder, $n = 2$; poor responder, ($n = 1$) (Table 3.8). From these mutations, APC, ASH1L, HECW1 and TP53 mutations were identified in a high frequency ($>66\%$ of samples) of hypo-

mutated tumours. ASH1L and HECW1 were only identifiable in tumours of a low mutational yield.

		Sample		
		BH-600	BH-612	BH-614
Mutation	APC			
	ASH1L			
	HECW1			
	TP53			

Table 3.5: Mutations frequently identified in hypo-mutated samples.

Whole-exome sequencing was carried out on DNA extracted from tumour biopsies of LARC patients with intermediate (n=2) and poor (n=1) response to NACRT. Data was run through a bioinformatics pipeline described in section 2.1.6 and Fishers exact test was used to identify significantly mutated genes. 3 patient samples had ≤ 35 non-synonymous, somatic mutations. Samples positive for the mutation are identified in red, whilst wild-type is represented as grey.

	BH-607	BH-644	BH-659
ADGB			
AHNAK2			
APC			
BRAF			
CACNA2D3			
DDX23			
DNAH5			
MBTPS2			
TP53			

Figure 3.6: Mutations associated with positive lymph nodes.

Whole-exome sequencing was carried out on DNA extracted from tumour biopsies of LARC patients with good (n=3), intermediate (n=5) and poor (n=3) response to NACRT. Data was run through a bioinformatics pipeline described in section 2.1.6 and Fishers exact test was used to identify significantly mutated genes. Colour intensity is representative of the volume of mutations identified within the sample. Mutated genes are represented as blue, whilst wild-type genes are represented as grey,

3.2.3. Genes most commonly mutated in our LARC sample cohort

From the 1,474 mutated genes, 6 genes were mutated at a high frequency ($n = \geq 3$ samples, $\geq 25\%$) throughout all samples (Figure 3.3). These included mutations within genes known to be frequently mutated in CRC, including *APC* ($n = 7/11$, 63.6%) and *TP53* ($n = 6/11$, 54.5%). However, we also identified a high frequency of lesser studied mutations in genes including *AHNAK2*, *MYO18B*, *SYNE1* and *TTN*, all of which were identified in 3/11 samples (27.3%).

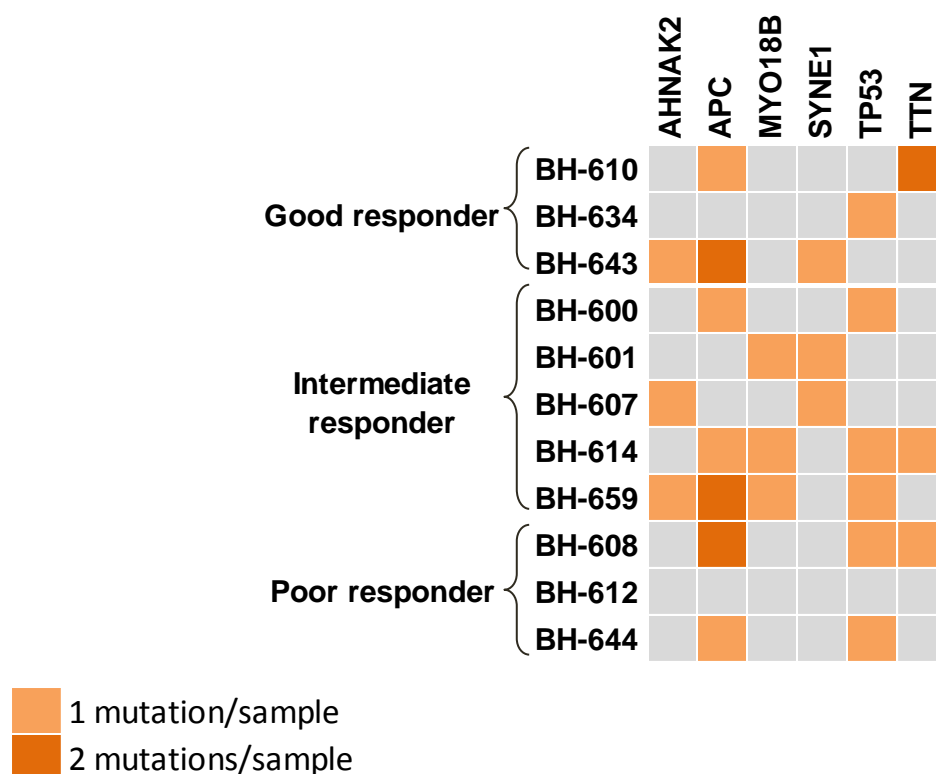


Figure 3. 3. Commonly mutated genes in LARC patients

Whole-exome sequencing was carried out on DNA extracted from tumour biopsies of LARC patients with good ($n=3$), intermediate ($n=5$) and poor ($n=3$) response to NACRT. Data was run through a bioinformatics pipeline described in section 2.1.6 and Fishers exact test was used to identify significantly mutated genes. Colour intensity is representative of the volume of mutations identified within the sample.

3.2.4. Somatic mutations in pre-treatment LARC biopsies associated with response to NACRT

An investigation into the molecular basis of tumours response to NACRT was performed by analysing mutations specific to good (n =3), poor (n = 3) and non-responders (intermediate, n = 5; poor, n = 3) to therapy.

Somatic mutations identified in pre-treatment biopsies of patients who had a good response to NACRT.

216 non-synonymous somatic mutations were identified in 205 genes from pre-treatment biopsy samples of patients who achieved pathological complete response (pCR), where there was no tumour remaining at the time of surgery (good responders). Mutations in 161 genes were only identified in patients who achieved a pCR, and were not identified in any of the non-responders (intermediate or poor responders). Of which, MUC16 was the only gene to be mutated in more than 1 sample ($\geq 66\%$) (Figure 3.7). Both mutations were C>A missense mutations. MUC16 is a gene responsible for the production of mucins, and increased expression of MUC16 in cancer is associated with poor prognosis.

Somatic mutations identified in the pre-treatment biopsies of patients who had a poor response to NACRT.

130 non-synonymous somatic mutations were identified in 123 genes in the pre-treatment LARC samples of poor responders. From the 123 mutated genes, 105 were mutated in poor responders only, of which only 2 genes were mutated in 2 or more poor responder patients ($\geq 66\%$) (figure 3.7, supplementary table 3). These genes included *PCDHA12* and *TCTE1*.

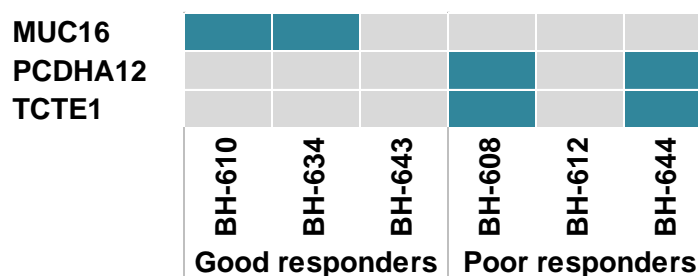


Figure 3.7: Frequently mutated genes in the pre-treatment biopsies of patients who had good or poor response to NACRT.

Whole-exome sequencing was carried out on DNA extracted from tumour biopsies of LARC patients with good ($n=3$), intermediate ($n=5$) and poor ($n=3$) response to NACRT. Data was run through a bioinformatics pipeline described in section 2.1.6 and Fishers exact test was used to identify significantly mutated genes.

In the mutation matrix chart, the horizontal bar chart displays the number of mutations identified per sample. The vertical bar chart displays the number of mutations identified per gene.

Somatic mutations identified in pre-treatment biopsies of patients who did not have a complete response to NACRT

1,258 non-synonymous, somatic mutations were identified in 1,094 genes in non-responders (intermediate and poor responders). Of which, 1,052 genes were identified in non-responders only and not in good responders. 58 genes were identified in 2 or more samples ($> 18\%$) (figure 3.8). 89.7% of these mutations were identified in the pre-treatment biopsies of intermediate responders, while 10.3% were identified in the biopsies from poor responders. The hyper-mutated sample, BH601 had 4 co-occurring mutations in the tumour suppressor *FAT2* gene and 3 co-occurring mutations in *WDFY4*. Other genes mutated in the non-responders include *ASH1L*, *BRAF*, *HECW1* and *MAPK4*, which have roles in transcription, cell growth, division, differentiation, adhesion and proliferation. Furthermore, *BRAF* and *MAPK4* are commonly known oncogenes in CRC and other cancers.

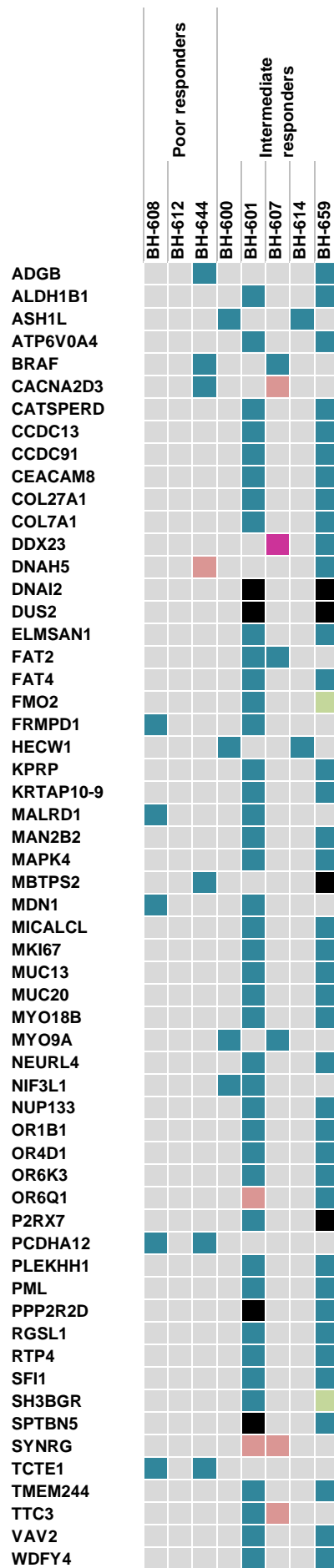


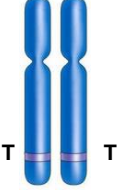
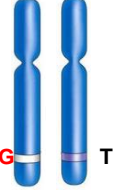
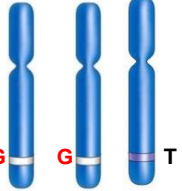

Figure 3.8: Frequently mutated genes in the pre-treatment biopsy samples of non-responders (intermediate and poor responders).

Whole-exome sequencing was carried out on DNA extracted from tumour biopsies of LARC patients with good ($n=3$), intermediate ($n=5$) and poor ($n=3$) response to NACRT. Data was run through a bioinformatics pipeline described in section 2.1.6 and Fishers exact test was used to identify significantly mutated genes.

1,052 mutated genes were identified in non-responders (intermediate and poor responders), and not good-responders. 58 of these genes were mutated in $\geq 18\%$ of pre-treatment biopsy samples from non-responders.

3.2.5. Heterogeneity in tumour samples using variant allele frequency

The variant allele frequency (VAF) of a sample depicts the rate of occurrence of an allele at a specific locus in a population, expressed as a percentage. Due to intra-tumour heterogeneity within samples and normal contamination, the VAF will usually differ slightly from these figures.

				
Status	Normal	T>G mutation	T>G mutation, and extra allele	T>G mutation and loss of allele
VAF %	0%	25%	33%	50%
Result	TT	GT	GGT	G

Clonality plots were carried out on Irish cohort samples from Beaumont hospital (good = 3, intermediate = 5, poor = 3) using Maftools software. Clustering of variant allele frequencies can show heterogeneity within tumour samples. We found a higher volume of tumour mutational clones within good (mean = 3.7 clones) and intermediate (mean = 3.8 clones) responders, compared to poor responders (mean = 1.6 clones) (Figures 3.9-3.11).

Mutant allele tumour heterogeneity (MATH) scores are quantitative values for intra-tumour heterogeneity which are calculated with the width of the VAF curve (180). Higher MATH scores are associated with worse patient outcome. Patients in our study who did not respond fully to NACRT had higher MATH scores (intermediate MATH score = 46.04, poor MATH score = 46.19) than that of good responders (MATH score = 39.36) (Figures 3.9-3.11).

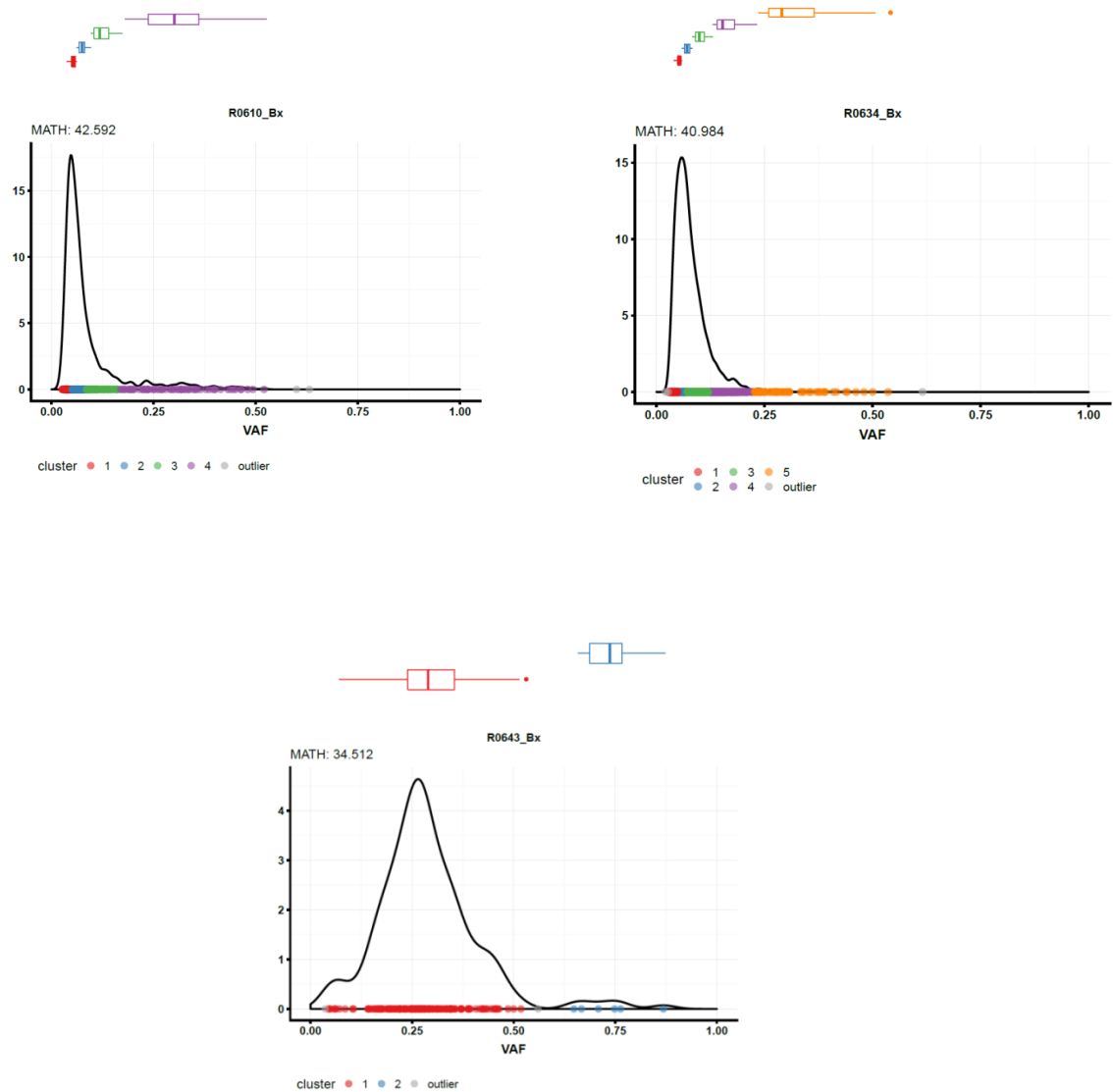


Figure 3.9: Variant allele frequency (VAF) in good responders.

Whole-exome sequencing was carried out on DNA extracted from tumour biopsies of LARC patients with good ($n=5$), intermediate ($n=11$) and poor ($n=10$) response to NACRT. Data was run through a bioinformatics pipeline described in section 2.1.6 and Fishers exact test was used to identify significantly mutated genes. Heterogeneity plots were created using Maftools software. Each boxplot above chart depicts a different clone. The chart has variant allele frequency (VAF) along the X-axis, percentages are represented as a fraction, with 1 = 100%. Peak size is representative of the importance of the clone. i.e. major / minor. Each dot is representative of a mutation, and the colour codes represent the various mutational clusters. MATH score = width of the VAF distribution. Higher MATH scores are associated with poor outcomes.

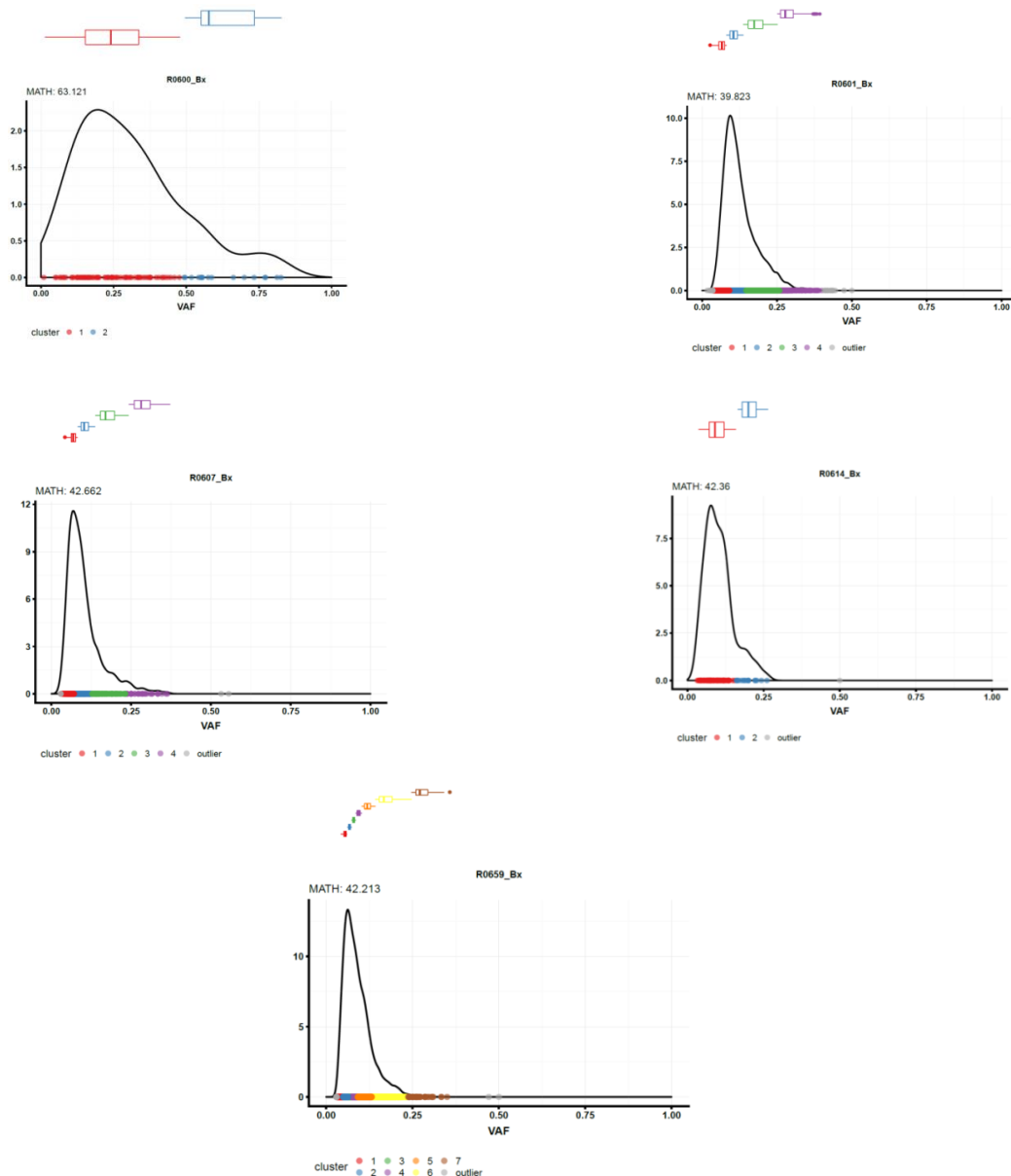


Figure 3.10: Variant allele frequency (VAF) in intermediate responders.

Whole-exome sequencing was carried out on DNA extracted from tumour biopsies of LARC patients with good ($n=5$), intermediate ($n=11$) and poor ($n=10$) response to NACRT. Data was run through a bioinformatics pipeline described in section 2.1.6 and Fishers exact test was used to identify significantly mutated genes. Heterogeneity plots were created using Maftools software. Each boxplot above chart depicts a different clone. The chart has variant allele frequency (VAF) along the X-axis; percentages are represented as a fraction, with 1 = 100%. Peak size is representative of the importance of the clone. i.e. major / minor. Each dot is representative of a mutation, and the colour codes represent the various mutational clusters. MATH score = width of the VAF distribution. Higher MATH scores are associated with poor outcomes.

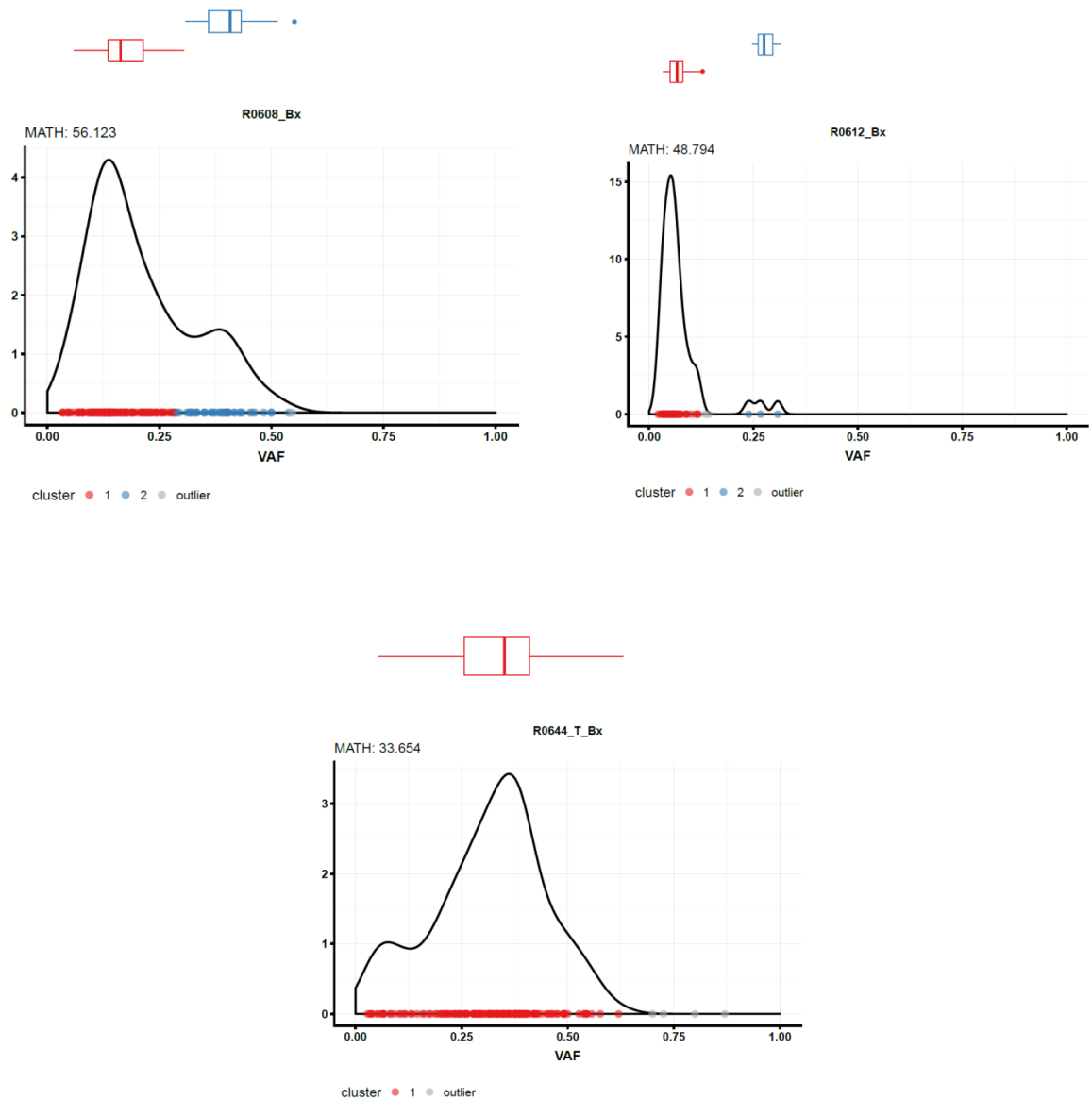


Figure 3.11: Variant allele frequency (VAF) in poor responders.

Whole-exome sequencing was carried out on DNA extracted from tumour biopsies of LARC patients with good ($n=5$), intermediate ($n=11$) and poor ($n=10$) response to NACRT. Data was run through a bioinformatics pipeline described in section 2.1.6 and Fishers exact test was used to identify significantly mutated genes. Heterogeneity plots were created using Maftools software. Each boxplot above chart depicts a different clone. The chart has variant allele frequency (VAF) along the X-axis, percentages are represented as a fraction, with 1 = 100%. Peak size is representative of the importance of the clone. i.e. major / minor. Each dot is representative of a mutation, and the colour codes represent the various mutational clusters. MATH score = width of the VAF distribution. Higher MATH scores are associated with poor outcomes.

3.2.6. Mutational signatures

Colorectal cancers have an average of 3 signatures per sample. Samples in our cohort had an increased volume of signatures in good (mean = 4.6), intermediate (mean = 5.4) and poor (mean = 4) responders, albeit some signatures were found at low frequencies. All samples (n = 11) had signature 1 mutations, with it being the most dominant signature in 10/11 samples. Signatures 12 (n = 5), 20 (n = 5), 5 (n = 4) and 6 (n = 4), were also common signatures throughout our cohort. Signatures 6, 15, 20 and 26 were all identified in sample BH-607, all 4 signatures are associated with defective DNA mismatch repair.

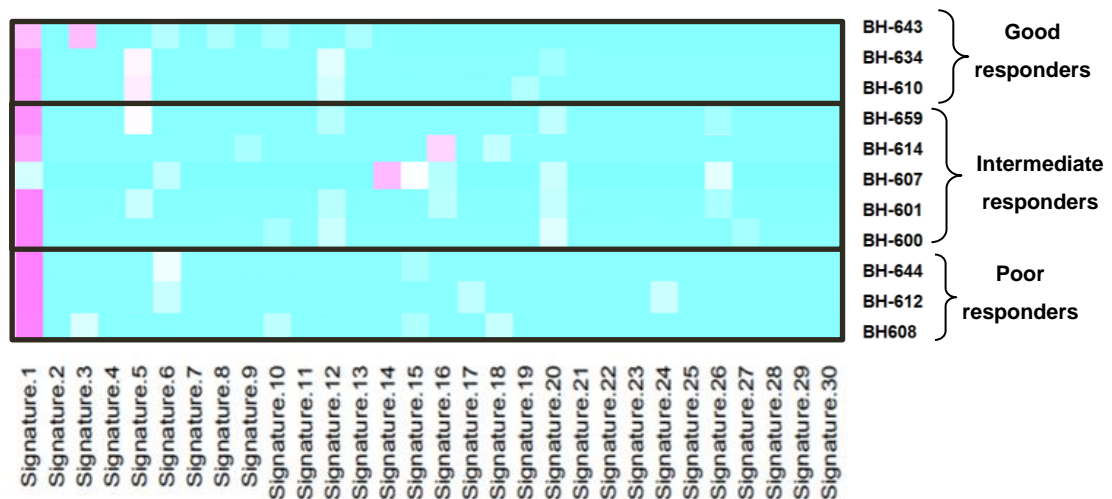


Figure 3.12: Mutational signatures

Whole-exome sequencing was carried out on DNA extracted from tumour biopsies of LARC patients with good (n=3), intermediate (n=5) and poor (n=3) response to NACRT. Data was run through a bioinformatics pipeline described in section 2.1.6 and Fishers exact test was used to identify significantly mutated genes.

3.3. Whole exome sequencing study from an American cohort of LARC patients.

Whole-exome sequencing was carried out on DNA extracted from fresh frozen pre-treatment tumour biopsies and matched normal tissue or blood samples from 15 patients who presented with locally advanced rectal cancer (LARC) and were treated with neoadjuvant chemoradiation therapy (NACRT). Patient biopsy samples were stratified into good (n = 2), intermediate (n = 6) and poor (n = 7) responders to NACRT treatment. Resulting data for the somatic synonymous and non-synonymous mutations from each sample was analysed to determine mutational frequencies, intra-tumour heterogeneity and mutational signatures; to see if we could identify any biomarkers which may predict patient response to NACRT treatment.

Clinicopathological data for patients in whole exome sequencing study

Age at diagnosis (years)		Good (n=2)	Intermediate (n=6)	Poor (n=7)
Average		46.4	55.9	51.5
Range		43-50	43-70	42-71
Median		46.4	57	47.2
Gender				
Male		1 (50%)	3 (50%)	2 (28.6%)
Female		1 (50%)	3 (50%)	5 (71.4%)
TNM status				
T	T0	2	0	0
	T1	0	2	2
	T2	0	3	4
	T3	0	1	1
	T4	0	0	0
N	N0	2	6	2
	N+	0	0	5
M	M-	2	6	7
	M+	0	0	0

No significant difference could be found in regards to age within our American cohort (Figure 3.13). However we did find that only patients who achieved pCR had tumours which were in situ (TNM stage 0). Whereas patients who did not achieve pCR had tumours which had breached through the mucosa (TRG stage 1) up to and including local lymph node involvement (TNM stage 4) (Figure 3.14). Of which,

only patients with a poor response to NACRT had metastatic spread to local lymph nodes (Figure 3.15).

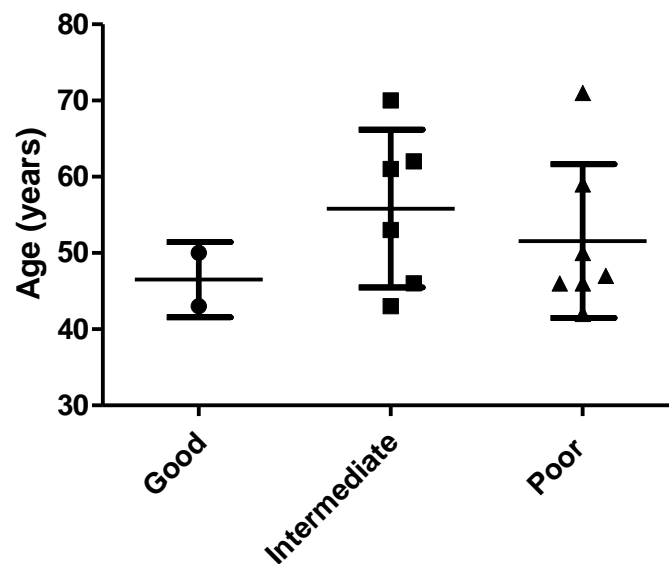


Figure 3.13: Relationship between age and patient response to NACRT.

Whole-exome sequencing was carried out on DNA extracted from tumour biopsies of LARC patients with good (n = 2), intermediate (n = 6) and poor (n = 7) response to NACRT. Data was run through a bioinformatics pipeline described in section 2.1.6 and Fishers exact test was used to identify significantly mutated genes. An unpaired 2-tailed t-test, using Welch's correction was carried out to determine if there was any significance between groups. A confidence interval of 95% was used.

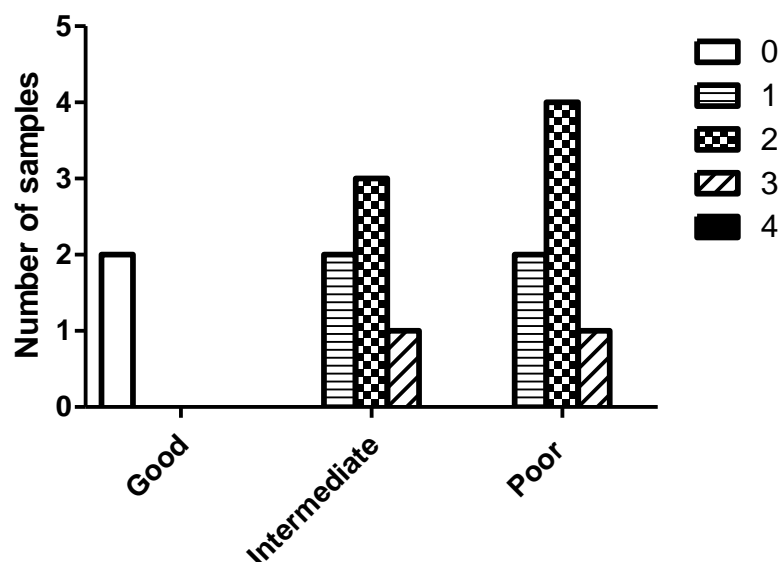


Figure 3.14: Relationship between TRG status and patient response.

Whole-exome sequencing was carried out on DNA extracted from tumour biopsies of LARC patients with good ($n = 2$), intermediate ($n = 6$) and poor ($n = 7$) response to NACRT. Each bar is representative of the 5 TNM stages, (stage 0 = the tumour is contained within the mucosa, stage 1 = the cancer has breached through the mucosa, stage 2 = the cancer has spread through the muscularis mucosa, stage 3 = cancer has metastasised to 1 or more lymph nodes, stage 4 = distant metastasis). Data was run through a bioinformatics pipeline described in section 2.1.6 and Fishers exact test was used to identify significantly mutated genes. A 2 way ANOVA test, using the Bonferroni post-test was used to calculate statistical significance.

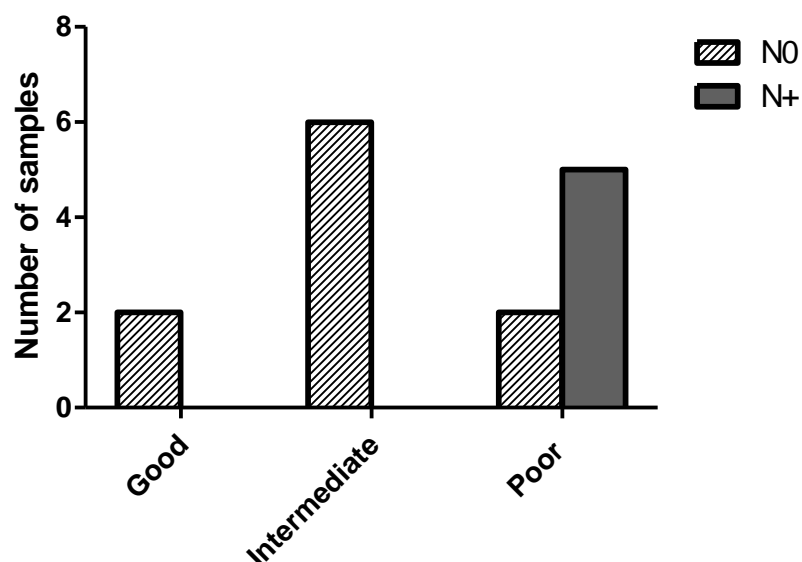


Figure 3.15: Relationship between lymph node positivity and patient response to NACRT.

Whole-exome sequencing was carried out on DNA extracted from tumour biopsies of LARC patients with good (n = 2), intermediate (n = 6) and poor (n = 7) response to NACRT. Data was run through a bioinformatics pipeline described in section 2.1.6 and Fishers exact test was used to identify significantly mutated genes. A 2-way ANOVA was carried out to determine statistical significance between groups.

3.3.1. Mutational frequency of synonymous and non-synonymous, somatic mutations in pre-treatment LARC biopsy samples

The pre-treatment patient biopsy samples from the 15 LARC patients yielded 11,634 synonymous and 1,684 non-synonymous mutations. These mutations were sub-divided according to their mutation type, and are represented in Table 3.6 or Table 3.7 and Figure 3.16 for non-synonymous mutations.

There were large variations in tumour mutational burden between samples and response groups, with the lowest mutational frequency identified in poor responders (total mean = 226.7 mutations, non-synonymous mean = 39.9 mutations), compared to good (total mean = 2130.5 mutations, non-synonymous mean = 524.5 mutations), or intermediate responders (total mean = 325.2 mutations, non-synonymous mean = 59.3 mutations). However, this was partly due to a select few hyper-mutated samples which skewed results. As a result, the tumour mutational burden did not alter significantly between the three groups (good vs intermediate, total $p = 0.52$, non-synonymous $p = 0.51$; good vs poor, total $p = 0.50$, non-synonymous $p = 0.49$; intermediate vs poor, total $p = 0.22$, non-synonymous $p = 0.30$).

Table 3.6: Single nucleotide variant (SNV) and insertion/deletion (indel) mutations in LARC biopsies from good, intermediate and poor responders to NACRT.

Whole-exome sequencing was carried out on DNA extracted from tumour biopsies of LARC patients with good (n = 2), intermediate (n = 6) and poor (n = 7) response to NACRT. Data was run through a bioinformatics pipeline described in section 2.1.6 and Fishers exact test was used to identify significantly mutated genes. Somatic non-synonymous mutations were divided into types of mutations and their response to NACRT.

	Sample	SNVs	Indels
Good	MDA-2	183	20
	MDA-3	2249	1809
Intermediate	MDA-5	248	10
	MDA-8	343	16
	MDA-10	576	21
	MDA-11	127	31
	MDA-15	365	17
	MDA-16	175	22
Poor	MDA-1	128	10
	MDA-4	264	16
	MDA-6	211	19
	MDA-7	237	17
	MDA-12	219	25
	MDA-13	341	16
	MDA-17	63	21

Since synonymous mutations do not alter the encoded protein and are therefore known as silent mutations, we will primarily focus on non-synonymous mutations for the remainder of this chapter.

Our study identified 1,684 non-synonymous somatic mutations in 1,480 genes. These mutations were further classified into mutational type (Table 3.7, Figure 3.16). Percentile frequency analysis of the somatic non-synonymous mutations showed a predominance of missense (n = 1081, 64.2%), and frameshift (n = 353, 21%), mutations, and to a lesser degree splicing (n = 116, 6.9%) and nonsense

(n = 105, 6.2%) mutations (Figure 3.17). The remaining 1.7 % consisted of inframe insertions and deletions, lost start and stop codons and mature miRNA variants. This pattern occurred throughout the majority of samples; however this fluctuated in the hypo-mutated sample (MDA-17) due to the low volume of mutations.

Table 3.7: Non-synonymous, somatic mutations in LARC biopsies from good, intermediate and poor responders to NACRT.

Whole-exome sequencing was carried out on DNA extracted from tumour biopsies of LARC patients with good (n=2), intermediate (n=6) and poor (n=7) response to NACRT. Data was run through a bioinformatics pipeline described in section 2.1.6 and Fishers exact test was used to identify significantly mutated genes. Somatic non-synonymous mutations were divided into types of mutations and their response to NACRT.

	Good responders	Intermediate responders	Poor responders	Total
Missense	621	264	196	1081
Frameshift	298	26	29	353
Nonsense	53	31	21	105
Splicing	65	26	25	116
Inframe deletion	7	4	5	16
Inframe insertion	0	3	1	4
Stop-lost	1	0	1	2
Start-lost	1	1	0	2
Mature miRNA variant	3	1	1	5
total	1049	356	279	1684

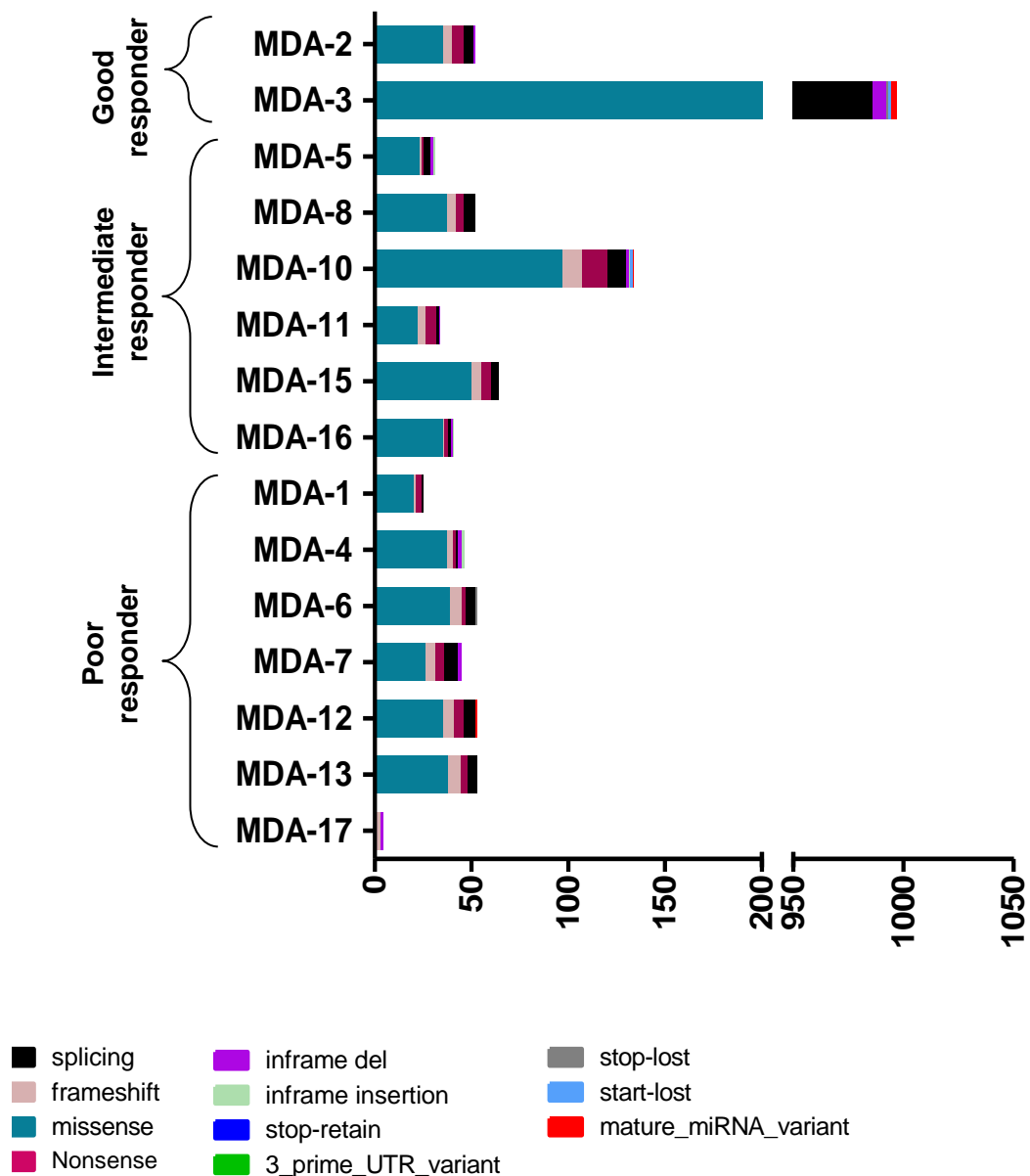


Figure 3.16: Tumour mutational burden for non-synonymous somatic mutations per pre-treatment biopsy sample.

Whole-exome sequencing was carried out on DNA extracted from tumour biopsies of LARC patients with good ($n = 2$), intermediate ($n = 6$) and poor ($n = 7$) response to NACRT. Data was run through a bioinformatics pipeline described in section 2.1.6 and Fishers exact test was used to identify significantly mutated genes. Somatic non-synonymous mutations were divided into types of mutations and their response to NACRT.

Sample numbers, grouped according to NACRT response are represented along the Y-axis. Composition and frequency of mutations in individual samples are represented along the X-axis. A colour-coded system was used to illustrate mutational type frequency per sample.

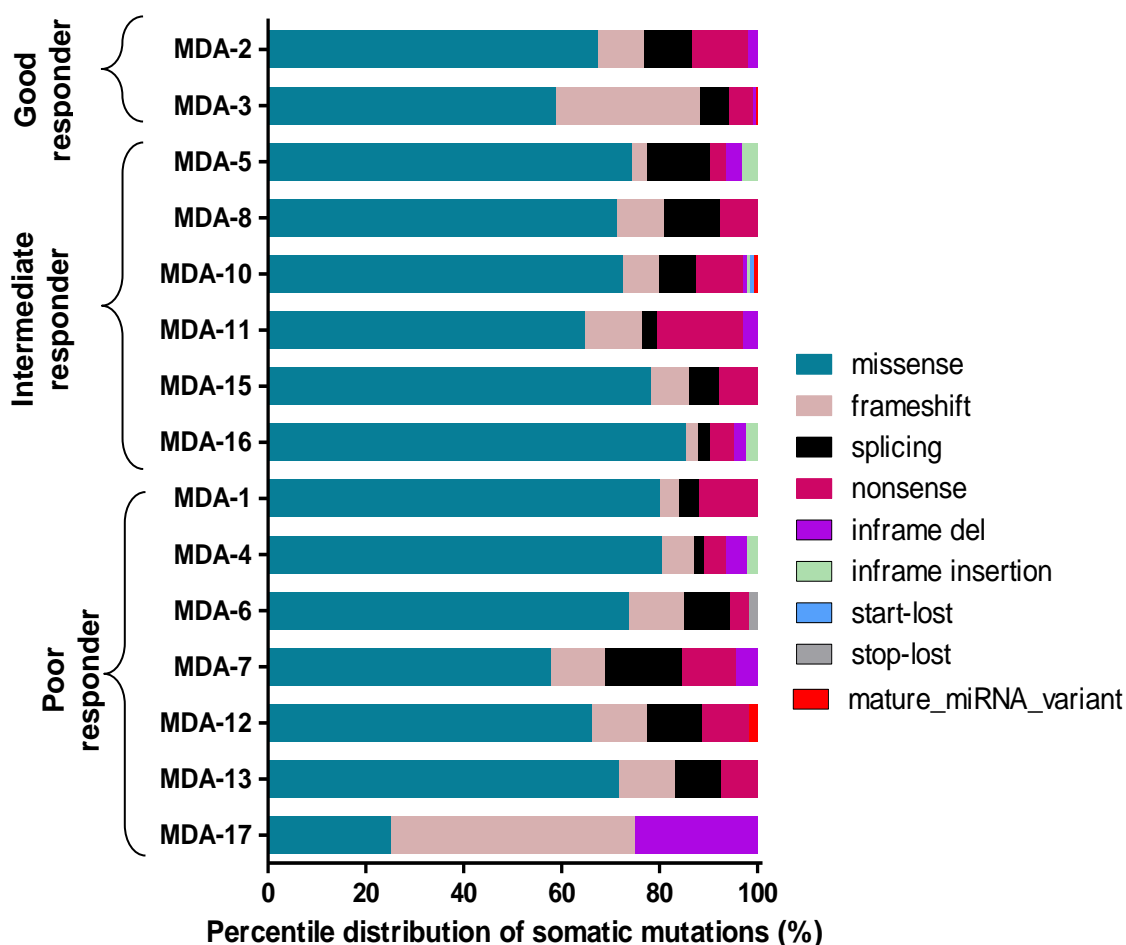


Figure 3.17: Percentile distribution of non-synonymous somatic mutations per individual pre-treatment biopsy sample.

Whole-exome sequencing was carried out on DNA extracted from tumour biopsies of LARC patients with good ($n = 2$), intermediate ($n = 6$) and poor ($n = 7$) response to NACRT. Data was run through a bioinformatics pipeline described in section 2.1.6 and Fishers exact test was used to identify significantly mutated genes. Somatic non-synonymous mutations were divided into types of mutations and their response to NACRT.

Sample numbers, grouped in according to NACRT response are represented along the Y-axis. Composition and frequency of mutations in individual samples are represented along the X-axis. A colour-coded system was used to illustrate mutational type frequency per sample.

Hyper-mutated samples included MDA-3 (good responder) had 997 somatic, non-synonymous mutations and was a microsatellite unstable (MSI) tumour with mismatch repair mutations in *Bax*, *MLH3*, *MSH3* and *TGFBR2*.

In contrast, less than 35 non-synonymous mutations were identified in 4 samples, all of which were non-responders to NACRT (intermediate responder, n = 2; poor responder, n = 2) (Table 3.8). From these mutations, APC, CD93, ELP2, FAM47A and TP53 mutations were identified in a high frequency (>50 % of samples) of hypo-mutated tumours. CD93 and ELP2 mutations were exclusively identified within tumours of a low mutational burden, with CD93 identified in poor responders only, and ELP2 in intermediate responders.

Table 3.8: Mutations frequently identified in hypo-mutated samples.

Whole-exome sequencing was carried out on DNA extracted from tumour biopsies of LARC patients with good (n=2), intermediate (n=6) and poor (n=7) response to NACRT. Data was run through a bioinformatics pipeline described in section 2.1.6 and Fishers exact test was used to identify significantly mutated genes. 4 patient samples had ≤35 non-synonymous, somatic mutations. Mutated genes are represented as red, whilst genes wild-type for the mutation are represented as grey.

	Intermediate responders		Poor responders	
	MDA-5	MDA-11	MDA-1	MDA-17
APC				
CD93				
ELP2				
FAM47A				
TP53				

	MDA-1	MDA-4	MDA-6	MDA-7	MDA-13
APC					
PIK3CA					
RANBP2					
TP53					
ZIC1					

Figure 3.18: Associated with lymph node positivity

Whole-exome sequencing was carried out on DNA extracted from tumour biopsies of LARC patients with good ($n = 2$), intermediate ($n = 6$) and poor ($n = 7$) response to NACRT. Data was run through a bioinformatics pipeline described in section 2.1.6 and Fishers exact test was used to identify significantly mutated genes. Mutated genes are represented as blue, whilst genes wild-type for the mutation are represented as grey.

3.3.2. Genes most commonly mutated in our LARC sample cohort

From the 1,684 mutated genes, 19 genes were mutated at a high frequency (≥ 3 samples, $\geq 20\%$) throughout all samples (Figure 3.19). These included mutations within genes known to be frequently mutated in CRC, including *APC* ($n = 14$, 93%), *TP53* ($n = 11$, 73%), *KRAS* ($n = 3$, 20%), and *PIK3CA* ($n = 3$, 20%). However, we also identified a high frequency of lesser studied mutations in genes including *LRP2* ($n = 4$, 27%), and *FBXW7* ($n = 4$, 27%).

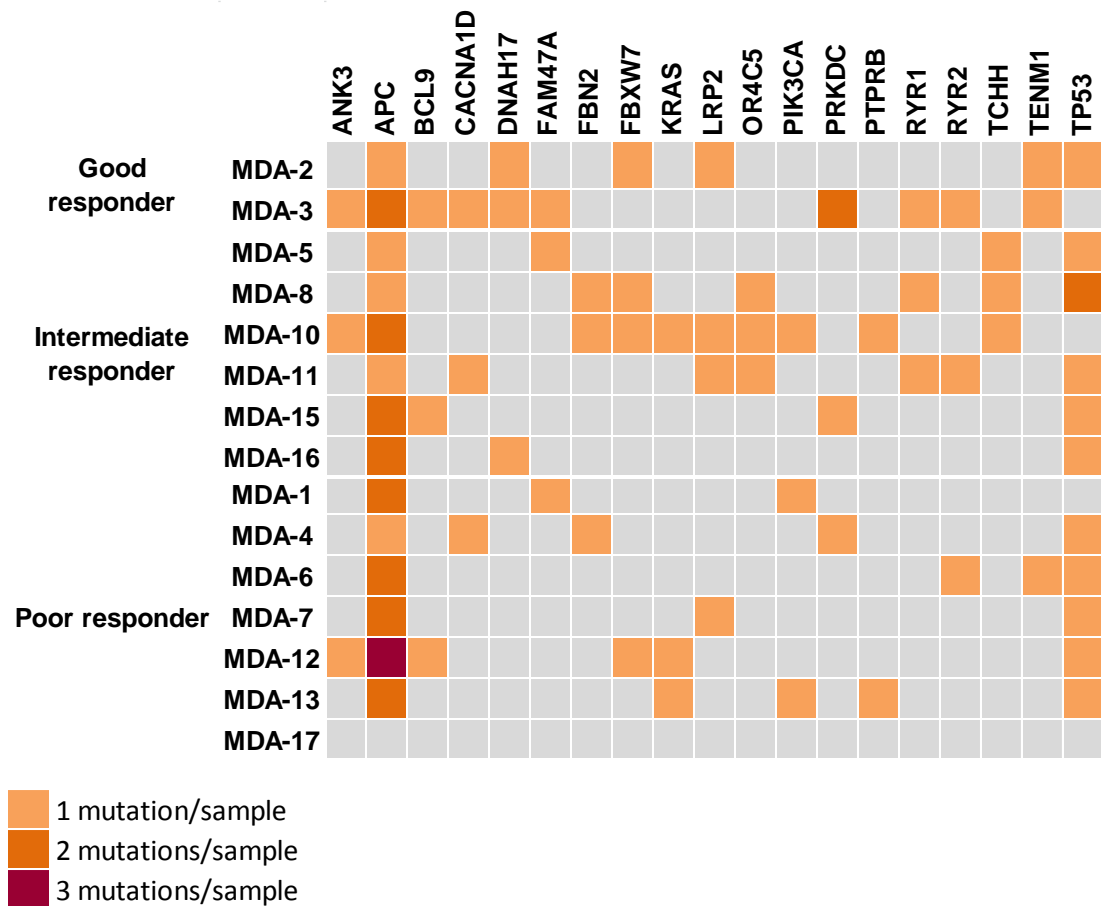


Figure 3.19. Commonly mutated genes in LARC patients

Whole-exome sequencing was carried out on DNA extracted from tumour biopsies of LARC patients with good ($n = 2$), intermediate ($n = 6$) and poor ($n = 7$) response to NACRT. Data was run through a bioinformatics pipeline described in section 2.1.6 and Fishers exact test was used to identify significantly mutated genes. Colour intensity is representative of the volume of mutations identified within the sample

3.3.3. Somatic mutations in pre-treatment LARC biopsies associated with response to NACRT

An investigation into the molecular basis of tumours response to NACRT was performed by analysing mutations specific to good (n = 2), poor (n = 7) and non-responders (intermediate, n = 6 ; poor, n = 7) to therapy.

Somatic mutations identified in pre-treatment biopsies of patients who had a good response to NACRT.

1,049 non-synonymous somatic mutations were identified in 990 genes from pre-treatment biopsy samples of patients who achieved pathological complete response (pCR), where there was no tumour remaining at the time of surgery (good responders). Mutations in 928 genes were only identified in patients who achieved a pCR, and were not identified in any of the non-responders (intermediate or poor responders). 5 genes (APC, DNAH17, KMT2C, TCF20 and TENM1) were mutated in both samples, whilst KMT2C and TCF20 were frequently mutated and identified exclusively in good responders. Both mutations are associated with vital cellular processes including transcription.

Both TCF20 and one KMT2C mutation were frameshift mutations, whilst the other KMT2C mutation was a G>A nonsense mutation.

Somatic mutations identified in the pre-treatment biopsies of patients who had a poor response to NACRT.

279 non-synonymous somatic mutations were identified in 249 genes in the pre-treatment LARC samples of poor responders. From the 249 mutated genes, 212 were mutated in poor responders only, of which 7 genes were mutated in 2 or more poor responder patients ($\geq 28\%$) (Figure 3.20). These genes included *APOB*, *CD93*, *IGHV3-11*, *PZP*, *RANBP2*, *TPD52L2* and *ZIC1*. MDA-4 and MDA-7 each had two co-occurring mutations in *ZIC1* and *TPD52L2*, respectively.

MDA-4 and MDA-7 had identical mutations in *CD93* (thymine insertion frameshift mutation T at chromosome 20, exon 1, codon 121) and *IGHV3-11* (ACC inframe deletion in chromosome 14, at position 106573362).

Other genes of interest include *PZP* and *ZIC1*, which have a role in proteinase inhibition and transportation respectively. *RANBP* mutations are associated with the MAPK signalling pathway.

	Good responders		Poor responders						
	MDA-2	MDA-3	MDA-1	MDA-4	MDA-6	MDA-7	MDA-12	MDA-13	MDA-17
APOB									
CD93									
IGHV3-11									
KMT2C									
PZP									
RANBP2									
TCF20									
TPD52L2									
ZIC1									

Figure 3.20: Frequently mutated genes in the pre-treatment biopsy samples of good and poor responders.

Whole-exome sequencing was carried out on DNA extracted from tumour biopsies of LARC patients with good ($n = 2$), intermediate ($n = 6$) and poor ($n = 7$) response to NACRT. Data was run through a bioinformatics pipeline described in section 2.1.6 and Fishers exact test was used to identify significantly mutated genes. 928 mutated genes were identified in good responders only, and not found in intermediate or poor responders. 2 of these genes were mutated in both good responder samples.

Somatic mutations identified in pre-treatment biopsies of patients who did not have a complete response to NACRT

635 genes were mutated in non-responders (intermediate and poor responders) only. Of which, 23 genes were mutated in more than 1 sample (Figure 3.21). This includes mutations within the PI3K and MAPK pathways such as MAP4 and PIK3CA.

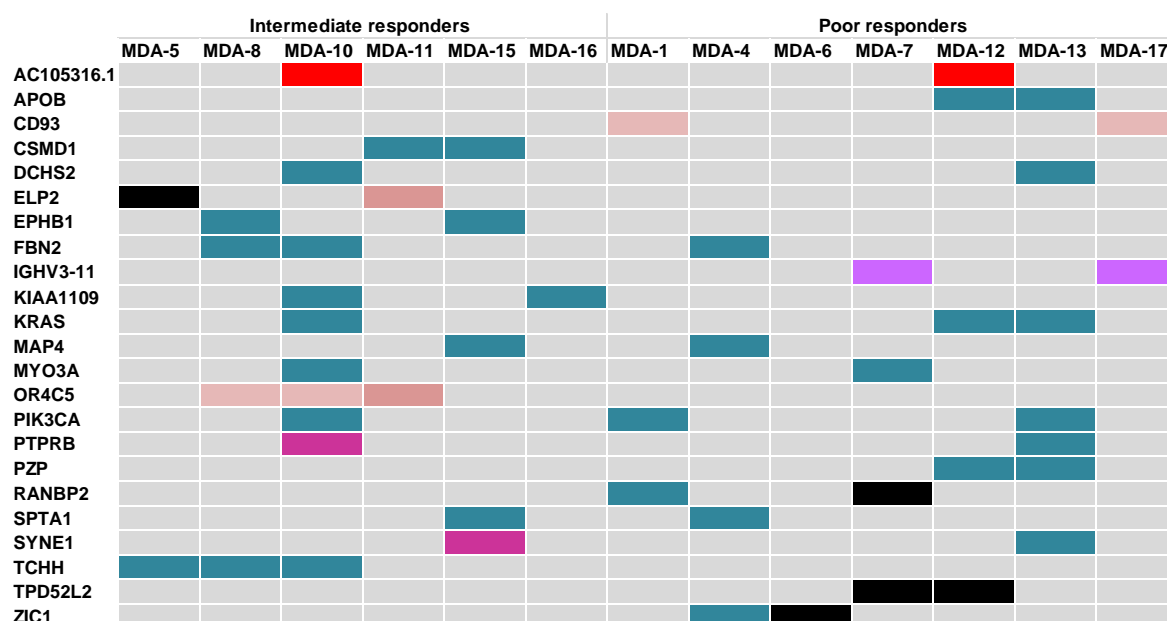


Figure 3.21: Frequently mutated genes in the pre-treatment biopsy samples of non-responders (intermediate and poor responders).

Whole-exome sequencing was carried out on DNA extracted from tumour biopsies of LARC patients with good ($n = 2$), intermediate ($n = 6$) and poor ($n = 7$) response to NACRT. Data was run through a bioinformatics pipeline described in section 2.1.6 and Fishers exact test was used to identify significantly mutated genes. 635 mutated genes were identified in non-responders (intermediate and poor responders), and not good-responders. 23 of these genes were mutated in $\geq 15\%$ of pre-treatment biopsy samples from non-responders. In the mutation matrix chart, the horizontal bar chart displays the number of mutations identified per sample. The vertical bar chart displays the number of mutations identified per gene.

3.3.4. Intra-tumour heterogeneity in pre-treatment biopsies from LARC patients

Intra-tumour heterogeneity was examined in a subset of our cohort, whereby analysis was carried out on two tumour biopsies taken from different regions within the primary tumour from patients ($n = 4$ intermediate and $n = 3$ poor responders). 50.5% % of mutations were identified in both tumour biopsies from all patients (intermediate (43%, mean = 30.5) and poor (64.5%, mean = 32.7) responders) (Table 3.9, Figure 3.22- Figure 3.28). However, some mutations were only identified in one of the biopsies in all patients, with a mean increase of 20.3 and 9 mutations identified per sample in intermediate and poor responders, respectively. The intermediate responders (MDA-5 (Figure 3.22) and MDA-10 (Figure 3.24)) had the highest mutational imbalance, with only 19% and 23% of total mutations identified in both samples respectively.

Table 3.9: Intra-tumour heterogeneity in two pre-treatment biopsy samples taken from two regions within the primary tumour.

Whole-exome sequencing was carried out on DNA extracted from tumour biopsies of LARC patients intermediate ($n = 4$) and poor ($n = 3$) response to NACRT. Data was run through a bioinformatics pipeline described in section 2.1.6 and Fishers exact test was used to identify significantly mutated genes.

Mutations were analysed for their presence in one or both biopsy samples per patient.

		Retained in both	Sample 1 only	Sample 2 only
Intermediate responders	MDA-5	6	8	17
	MDA-8	31	3	18
	MDA-10	47	58	32
	MDA-15	38	1	25
Poor responders	MDA-4	23	20	3
	MDA-12	38	8	7
	MDA-13	37	11	5

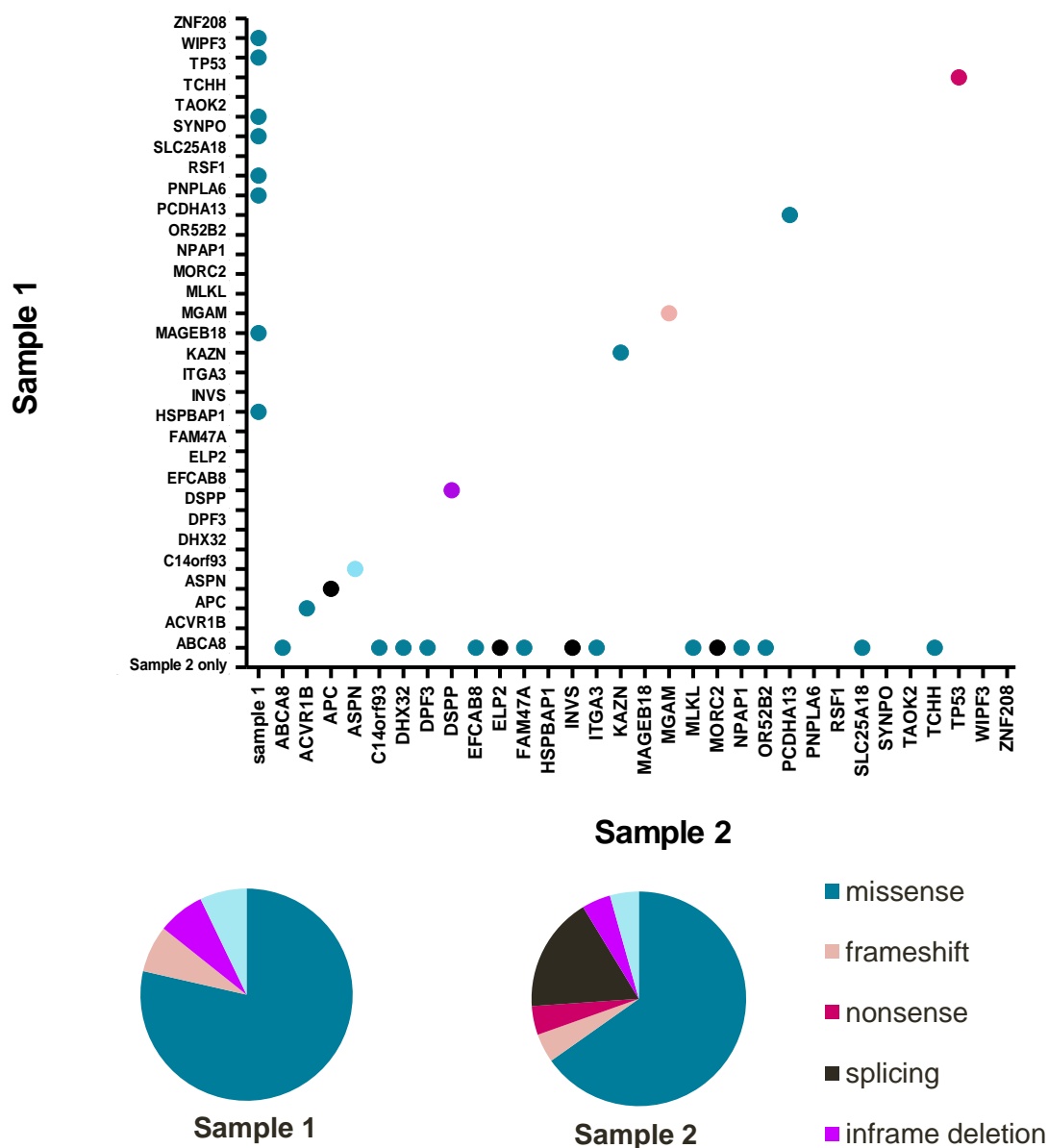


Figure 3.22: Intra-tumour heterogeneity in pre-treatment biopsies taken from two spatially separated regions of the primary tumour from intermediate responder MDA-5.

Whole-exome sequencing was carried out on DNA extracted from tumour biopsies of LARC patients with intermediate ($n = 4$) response to NACRT. Data was run through a bioinformatics pipeline described in section 2.1.6 and Fishers exact test was used to identify significantly mutated genes.

(A) Each dot on the scatter plot represents an individual mutation identified within the samples. Mutations identified in both biopsies ($n = 6$) can be seen along the diagonal line. Mutations found only in sample 1 ($n = 8$) are located along Y-axis, whilst mutations only located in sample 2 ($n = 17$) are located along the X-axis. Pie charts represent variations between mutation type in (B) sample 1, and (C) sample 2.

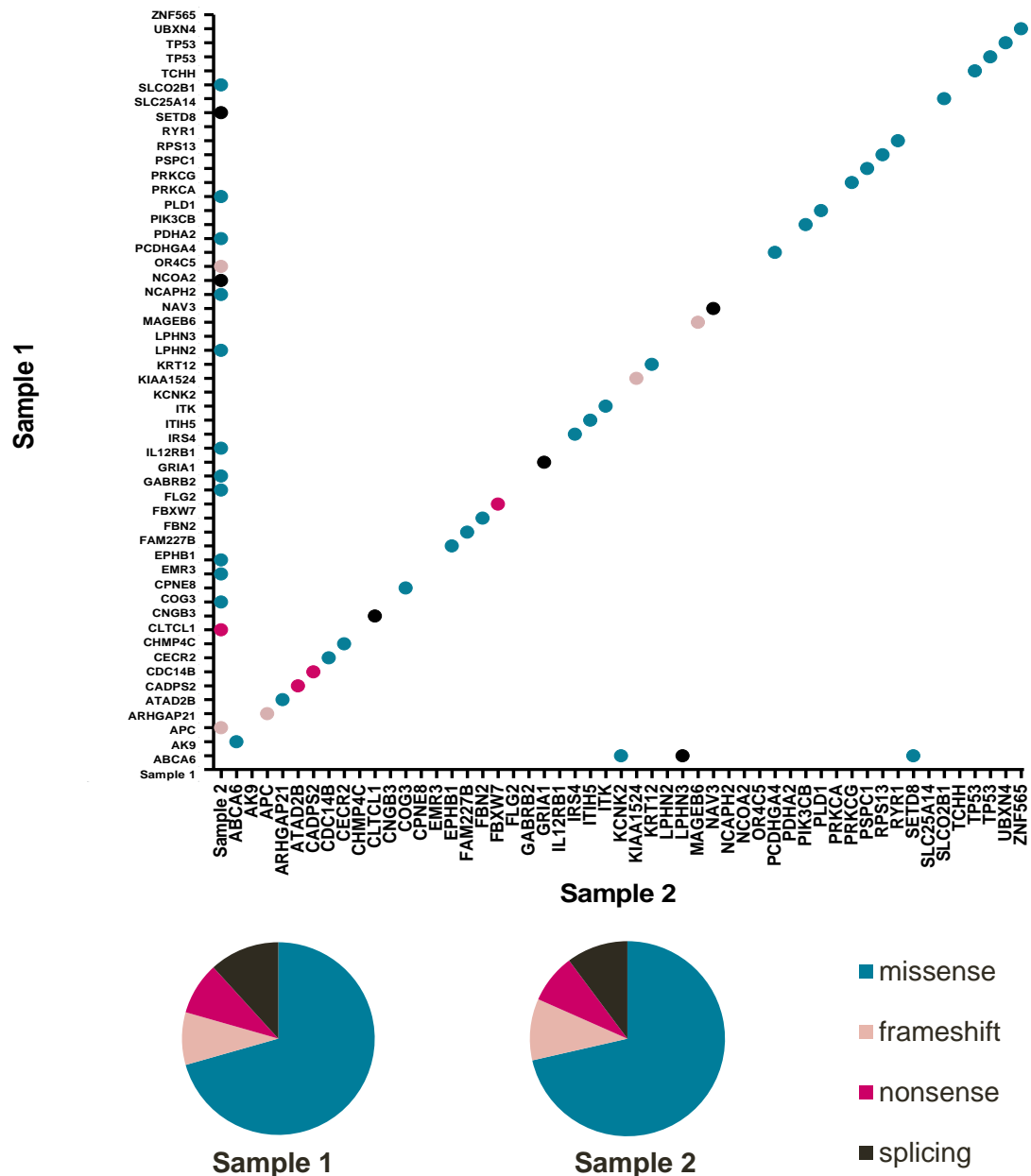


Figure 3.23: Intra-tumour heterogeneity in pre-treatment biopsies taken from two spatially separated regions of the primary tumour from intermediate responder MDA-8.

Whole-exome sequencing was carried out on DNA extracted from tumour biopsies of LARC patients with intermediate ($n = 4$) response to NACRT. Data was run through a bioinformatics pipeline described in section 2.1.6 and Fishers exact test was used to identify significantly mutated genes.

(A) Each dot on the scatter plot represents an individual mutation identified within the samples. Mutations identified in both biopsies ($n = 31$) can be seen along the diagonal line. Mutations found only in sample 1 ($n = 3$) are located along Y-axis, whilst mutations only located in sample 2 ($n = 18$) are located along the X-axis.

Pie charts represent variations between mutation type in (B) sample 1, and (C) sample 2.

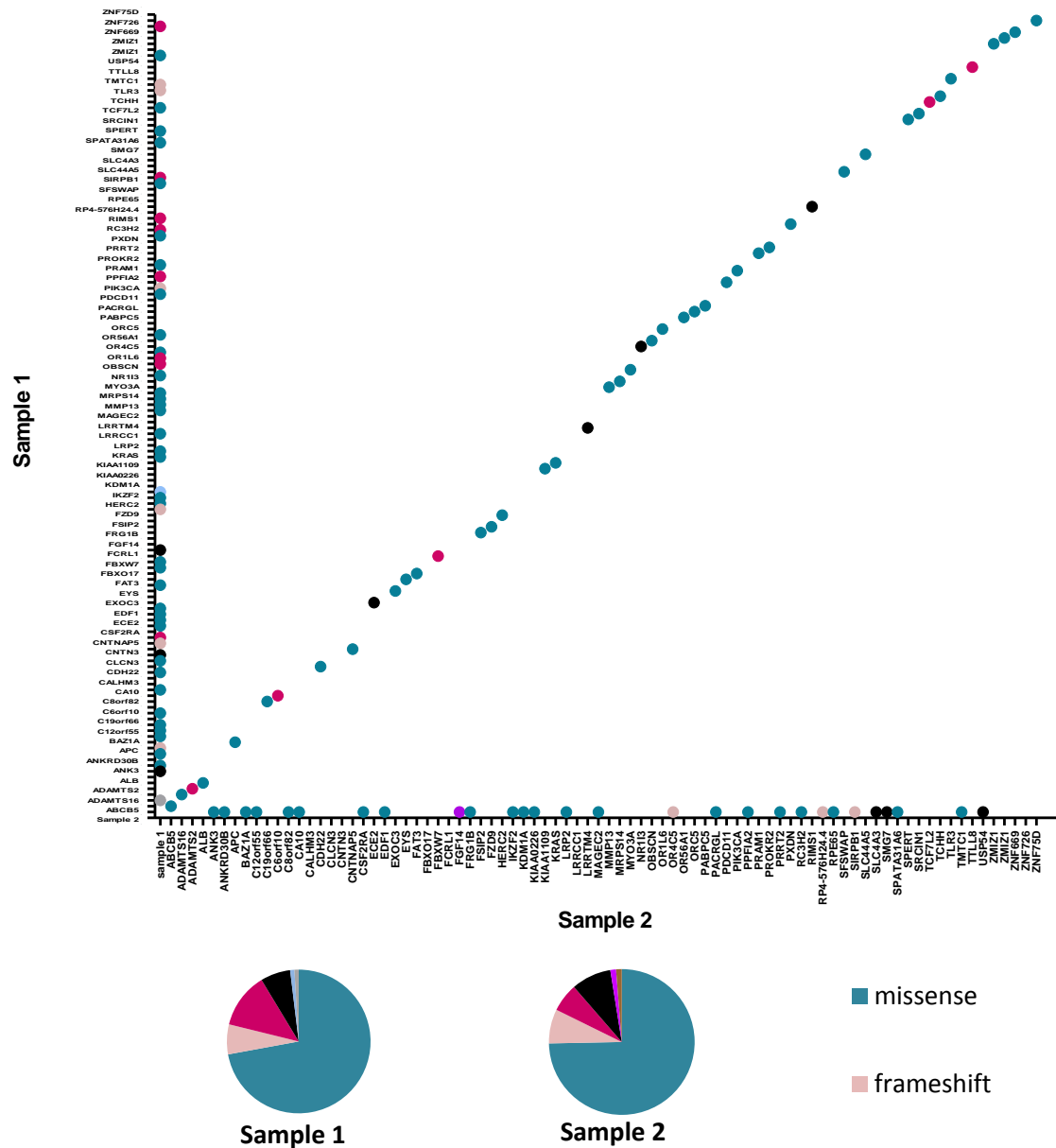


Figure 3.24: Intra-tumour heterogeneity in pre-treatment biopsies taken from two spatially separated regions of the primary tumour from intermediate responder MDA-10.

Whole-exome sequencing was carried out on DNA extracted from tumour biopsies of LARC patients with intermediate ($n = 4$) response to NACRT. Data was run through a bioinformatics pipeline described in section 2.1.6 and Fishers exact test was used to identify significantly mutated genes.

(A) Each dot on the scatter plot represents an individual mutation identified within the samples. Mutations identified in both biopsies ($n = 47$) can be seen along the diagonal line. Mutations found only in sample 1 ($n = 58$) are located along Y-axis, whilst mutations only located in sample 2 ($n = 32$) are located along the X-axis. Pie charts represent variations between mutation type in (B) sample 1, and (C) sample 2.

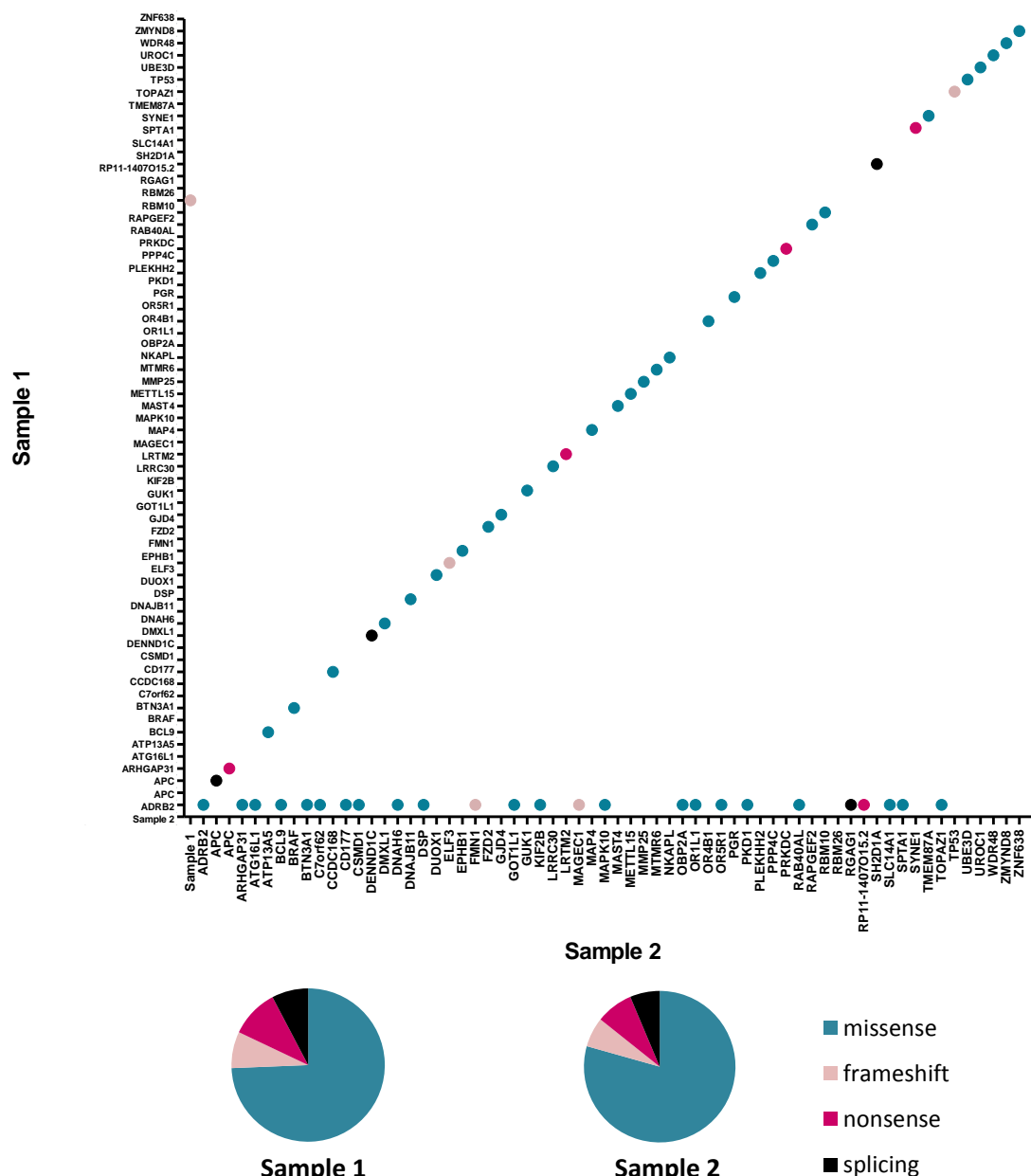


Figure 3.25: Intra-tumour heterogeneity in pre-treatment biopsies taken from two spatially separated regions of the primary tumour from intermediate responder MDA-15.

Whole-exome sequencing was carried out on DNA extracted from tumour biopsies of LARC patients with, intermediate ($n = 4$) response to NACRT. Data was run through a bioinformatics pipeline described in section 2.1.6 and Fishers exact test was used to identify significantly mutated genes.

(A) Each dot on the scatter plot represents an individual mutation identified within the samples. Mutations identified in both biopsies ($n = 38$) can be seen along the diagonal line. The mutation found only in sample 1 ($n = 1$) is located along Y-axis, whilst mutations only located in sample 2 ($n = 25$) are located along the X-axis.

Pie charts represent variations between mutation type in (B) sample 1, and (C) sample 2.

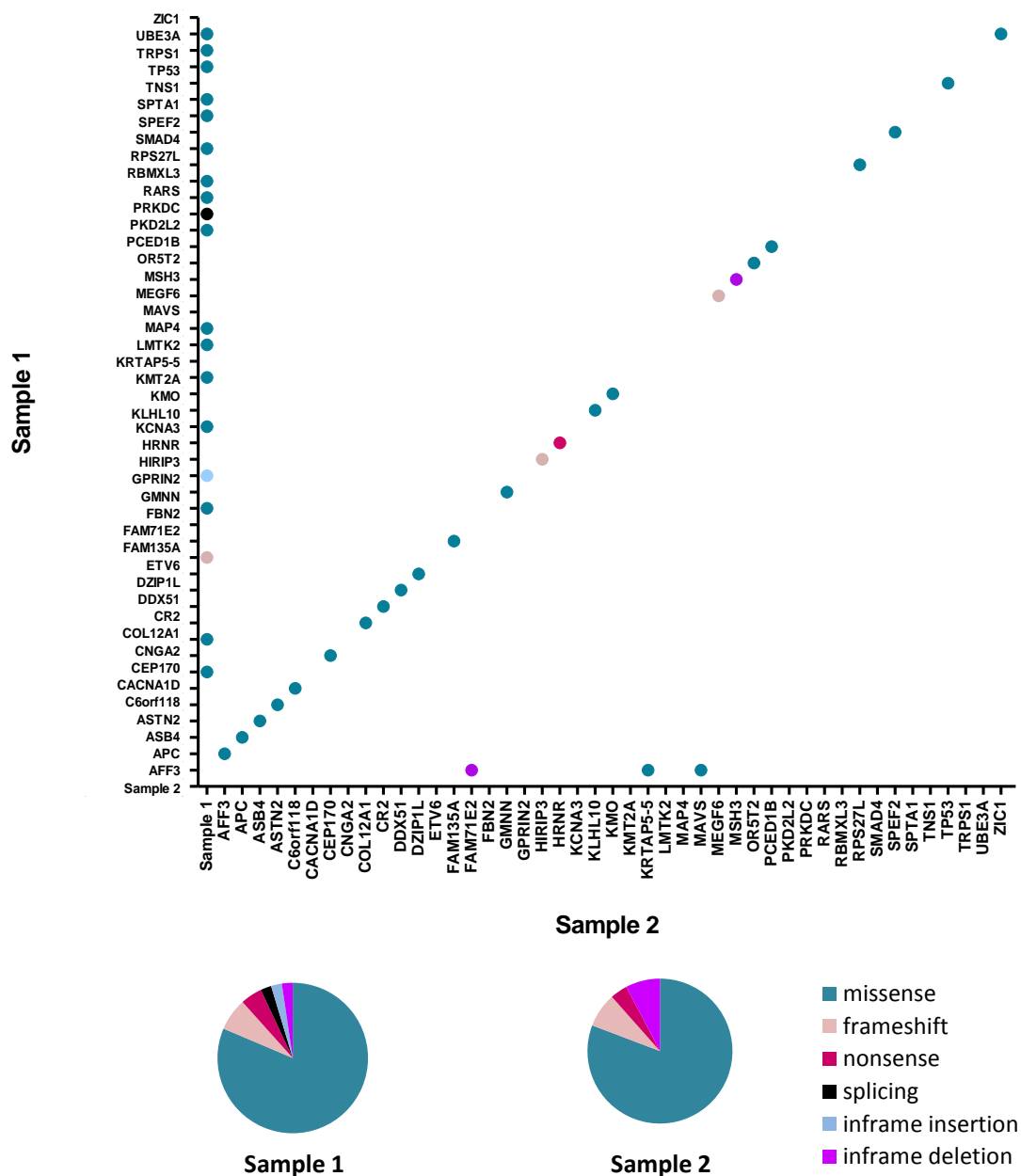


Figure 3.26: Intra-tumour heterogeneity in pre-treatment biopsies taken from two spatially separated regions of the primary tumour from poor responder MDA-4.

Whole-exome sequencing was carried out on DNA extracted from tumour biopsies of LARC patients with intermediate ($n = 4$) and poor ($n = 3$) response to NACRT. Data was run through a bioinformatics pipeline described in section 2.1.6 and Fishers exact test was used to identify significantly mutated genes.

(A) Each dot on the scatter plot represents an individual mutation identified within the samples. Mutations identified in both biopsies ($n = 23$) can be seen along the diagonal line. Mutations found only in sample 1 ($n = 20$) are located along Y-axis, whilst mutations only located in sample 2 ($n = 3$) are located along the X-axis.

Pie charts represent variations between mutation type in (B) sample 1, and (C) sample 2.

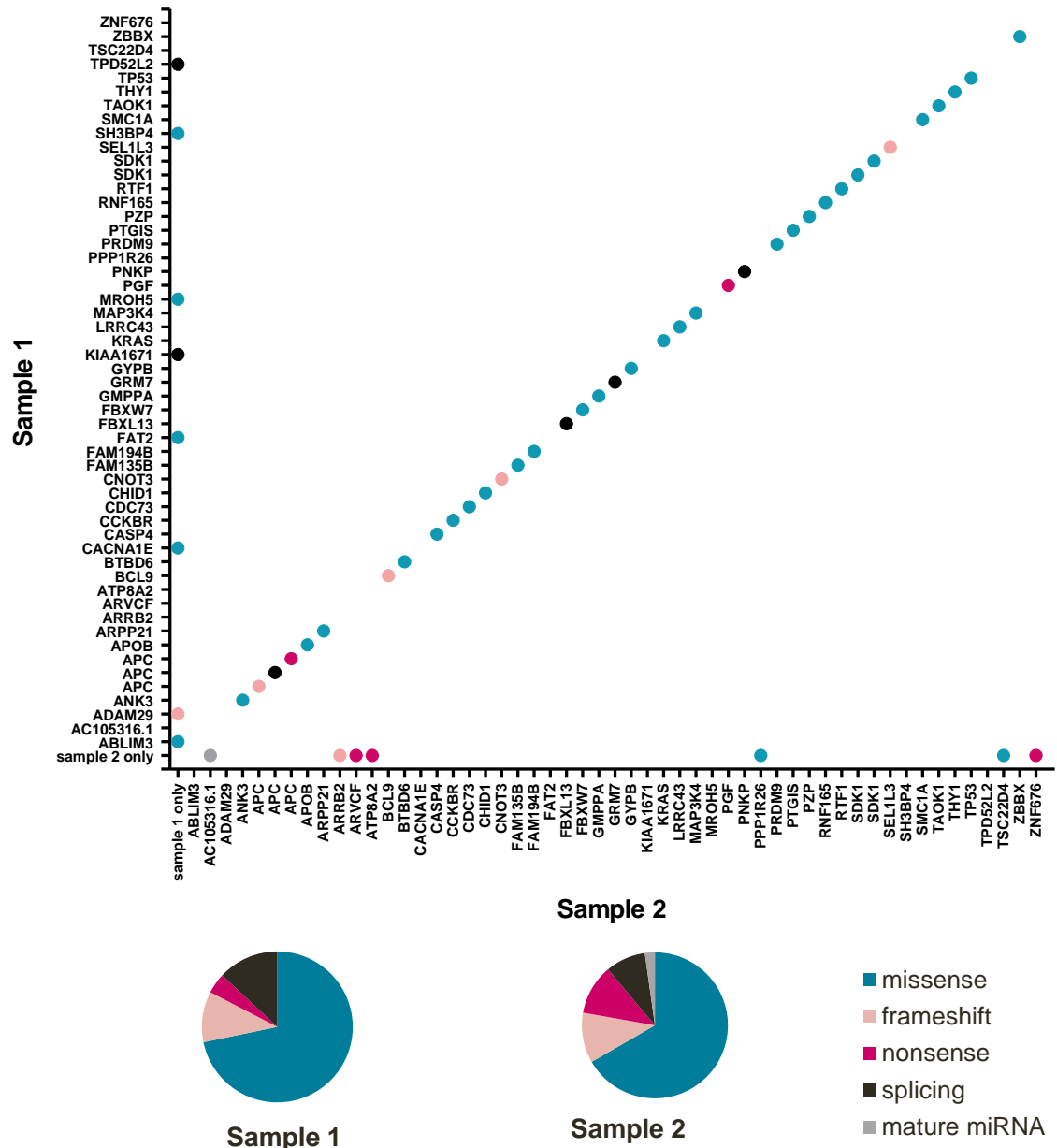


Figure 3.27. Intra-tumour heterogeneity in pre-treatment biopsies taken from two spatially separated regions of the primary tumour from poor responder MDA-12

Whole-exome sequencing was carried out on DNA extracted from tumour biopsies of LARC patients with intermediate ($n = 4$) and poor ($n = 3$) response to NACRT. Data was run through a bioinformatics pipeline described in section 2.1.6 and Fishers exact test was used to identify significantly mutated genes.

(A) Each dot on the scatter plot represents an individual mutation identified within the samples. Mutations identified in both biopsies ($n = 38$) can be seen along the diagonal line. Mutations found only in sample 1 ($n = 8$) are located along Y-axis, whilst mutations only located in sample 2 ($n = 7$) are located along the X-axis.

Pie charts represent variations between mutation type in (B) sample 1, and (C) sample 2.

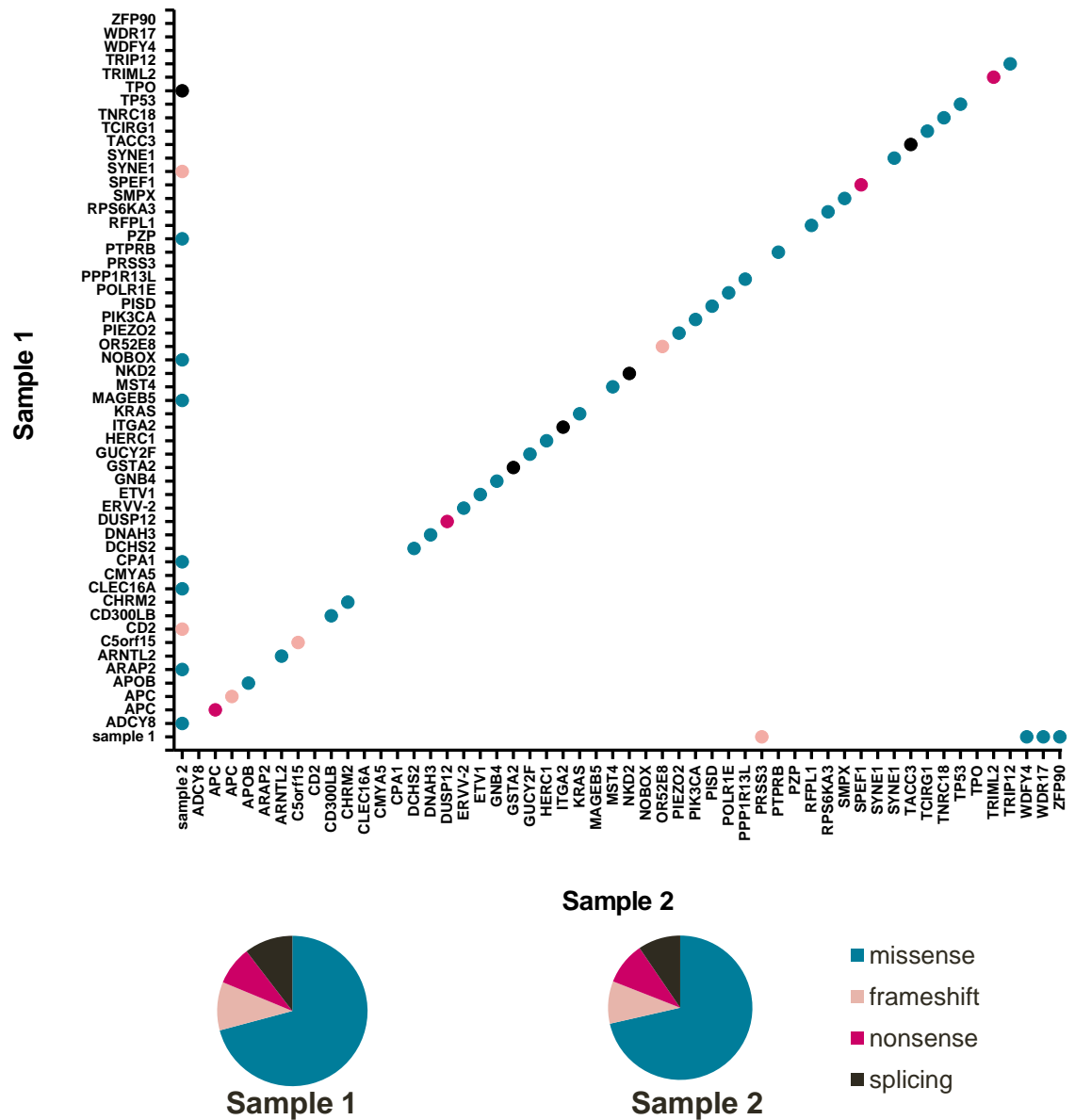


Figure 3.28: Intra-tumour heterogeneity in pre-treatment biopsies taken from two spatially separated regions of the primary tumour from poor responder MDA-13

Whole-exome sequencing was carried out on DNA extracted from tumour biopsies of LARC patients with intermediate ($n = 4$) and poor ($n = 3$) response to NACRT.

Data was run through a bioinformatics pipeline described in section 2.1.6 and Fishers exact test was used to identify significantly mutated genes.

(A) Each dot on the scatter plot represents an individual mutation identified within the samples. Mutations identified in both biopsies ($n = 37$) can be seen along the diagonal line. Mutations found only in sample 1 ($n = 11$) are located along Y-axis, whilst mutations only located in sample 2 ($n = 5$) are located along the X-axis.

Pie charts represent variations between mutation type in (B) sample 1, and (C) sample 2.

3.3.5. Mutational signatures

Colorectal cancers have an average of 3 signatures per sample. Samples in our cohort had an increased volume of signatures in good (mean = 6), intermediate (mean = 7) and poor (mean = 7.7) responders, albeit some signatures were found at low frequencies. All samples ($n = 13$) had signature 1 mutations, with this being the most prominent signature in most samples. This signature is associated with increasing age and has been identified in all cancer types. Signature 3 ($n = 10$), 15 ($n = 9$), 8 ($n = 8$), 18 ($n = 7$), 12 ($n = 5$) and 25 ($n=4$)) were also common signatures throughout our cohort. With signatures 3, 5 and 18 only identifiable in non-responders, and signature 25 exclusively identified in poor responders. Signature 6 was the most prominent signature identified in the MSI sample MDA-3. This signature is known to be associated with defective DNA mismatch repair and MSI tumours.

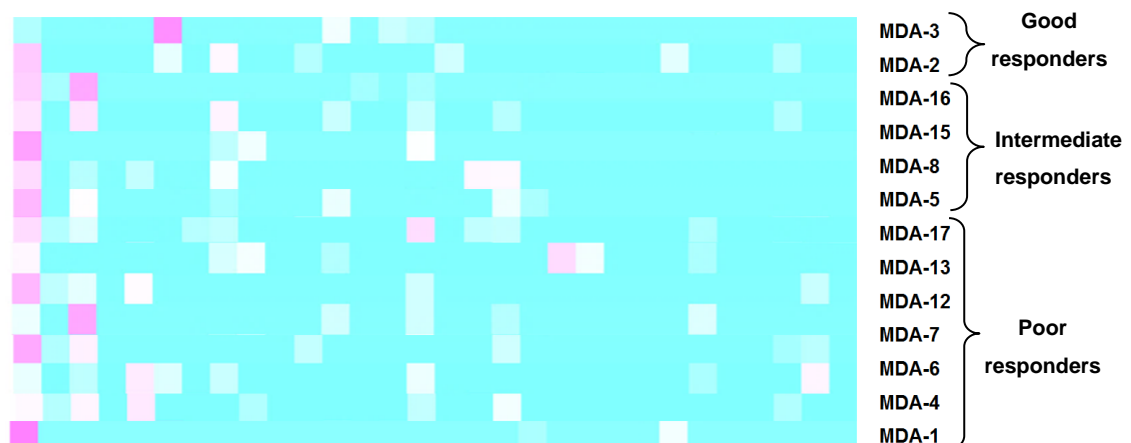


Figure 3.29: Mutational signatures

Whole-exome sequencing was carried out on DNA extracted from tumour biopsies of LARC patients with good ($n = 2$), intermediate ($n = 4$) and poor ($n = 7$) response to NACRT. Data was run through a bioinformatics pipeline described in section 2.1.6 and Fishers exact test was used to identify significantly mutated genes.

3.3.6. Mutations of interest from pre-treatment LARC samples

APC was mutated at a high frequency in both Irish (10 mutations in 7 genes) and American (24 mutations in 14 genes) cohorts. 14 of which were located in the mutational cluster region (MCR) (BH cohort, n = 6; MDACC cohort, n = 8). 59.9% of APC mutations were nonsense, 35.3% were frameshift and 8.8% were splicing mutations. The most common mutations were C>T transition substitutions (38.2%) and G>T transversion substitutions (11.8%), followed by T/- (8.8%), A/- (5.9%), and C/- (5.9%) frameshift deletions and G>A (5.9%) transition substitutions. APC gene substitutions were primarily C>T transitions (59.1%), G>T transversions (18.2%) and G>A transitions (9.1%). A>G transitions and C>A and C>G transversion mutations each accounted for 4.5% substitutions.

54.5% (n=6) of the Irish cohort and 80% (n = 12) of the American cohort contained TP53 mutations. From the 18 TP53 mutations identified in our cohort, the majority of mutations were located in codons 175, 213, 245 and 248. 3 mutations were identified in >1 sample; (R175H (17:7578406_C>T, n = 2), R213* (17:7578212_G>A, n = 2) and R248Q (17:7577538_C>T, n=3)). The most common mutations were C>T (44.4%) and G>A (27.8%) transition substitutions. A and C insertions were identified in 5.6% of samples. TP53 gene substitutions were primarily C>T (50%) and G>A (31.3%) substitution mutations, with A>T, C>A and T>C mutations each accounting for 6.25% substitutions.

KRAS mutations were identified in 36.4% of Irish samples (27.3% synonymous, 9.1% non-synonymous), and 26.7% of American samples (6.7% synonymous, 20% non-synonymous). All non-synonymous KRAS mutations identified in our samples were located within codons 12, 13 and 146 which are frequently mutated in CRCs. G12V mutations were identified in good (BH-643) and intermediate responders, (MDA-10), whilst G13D and A146T mutations were located in poor responders (MDA-12, MDA-13).

BRAF mutations were identified in the pre-treatment biopsy samples of Irish (18.2%, n = 2) and American (6.7%, n = 1) patients, all of whom were non-responders to NACRT treatment. All BRAF mutations identified were localised within exon 15 between codons 594 - 600. D594G (MDA-15) and L597R (BH-607)

mutations identified in intermediate responder biopsy samples, whilst the *V600E* (BH-644) mutation was identified in the pre-treatment biopsy of a poor responder.

PIK3CA gene mutations were identified in 20% of pre-treatment biopsy samples from the American cohort (n=3), all of which were samples from non-responders. All *PIK3CA* mutations identified were missense substitution mutations located within exon 10. Two mutations were found at *E545K* (MDA-1 and MDA-10), and one at *Q546K* (MDA-13).

FBXW7 gene mutations were identified in 26.7% (n = 4) of the American cohort. Two different *FBXW7* mutations were identified, both were G>A substitutions, and were identified in >1 sample. One mutation *R278Q* as a nonsense mutation (G>A) in exon 5, codon 278, and the other was an *R465C* missense mutation (G>A) in exon 9, codon 465).

3.4. Discussion

Currently, patient treatment and prognosis for CRC are based upon TNM staging. However, CRC patients presenting with identical tumour type and grade can have significantly different response rates. Varying mutational aberrations are potential instigators for these differing response rates within CRC patients. Identification of these could result in alternative treatment regimens.

3.4.1. Tumour mutational burden

We found wide variability in tumour mutational burden between samples in our cohort.

Hyper-mutated tumours

Despite the increased numbers in mutations, hyper-mutated samples (tumours in excess of 600 non-synonymous mutations) in both cohorts were isolated within good (MDA-3) and intermediate (BH-601) responders.

From the American cohort, MDA-3 was identified as an MSI tumour, with MMR gene mutations in *Bax*, *MLH3*, *MSH3* and *TGFBR2*. Multiple studies have shown a

more favorable prognosis and stage-adjusted survival rate in CRC patients with MSI tumours compared to MSS tumours (182–185). From the hypermutated sample in the Irish cohort (BH-601 did not contain any MMR pathway mutations, yet it too was hyper-mutated and responded to NACRT to a lesser degree. We believe this response was seen as a result of a *POLE* mutation. *POLE* is involved in DNA repair and replication, and numerous studies have shown that *POLE*^{mut} tumours display a hyper-mutated status in microsatellite stable (MSS) tumours (186,187).

Hypo-mutated tumours

In contrast, non-responders from both cohorts were identified as hypo-mutated tumours (≤ 35 non-synonymous mutations). Due to the low volume of mutations, we believe these select few mutations may be of interest as they potentially determined the patients' poor response to NACRT. Whilst APC and TP53 were commonly mutated in hypo-mutated samples, we also identified ASH1L and HECW1 mutations to be highly expressed in the Irish cohort, whilst CD93 and ELP2 were mutated at a high frequency in hypo-mutators from the American cohort. .

CD93 is involved in intercellular adhesion and clearance on apoptotic cells. It was mutated in poor responders only, with both samples harbouring identical insertion frameshift mutations at codon 121, exon 1 (20_23066468_-/T). These findings coincide with previous studies which show *CD93* is associated with poor response rates in patients (188).

Elongator complex protein 2 (*ELP2*) is a subunit of the RNA polymerase II elongator complex. Due to its role in transcriptional elongation and frequency of mutations in samples with such a low mutation rate, *ELP2* may be of interest. However, to date no link has been established between *ELP2* mutations and cancer; however, it is associated with intellectual disabilities. As a result, it may be of interest to look at *ELP2* in a larger cohort.

HECW1 is a potential tumour suppressor which interacts with p53 for transcription and apoptosis (189). *HECW1* is believed to play a role in the formation of transitional cell carcinoma (190), breast (191), and colorectal cancer (189).

However, none of these studies mentioned about mutational burden in their *HECW1^{mut}* samples.

3.4.2. PI3K/MAPK pathway mutations

Somatic genetic alterations within the PI3K and MAPK signalling pathways have been implicated in tumourigenesis (including rectal cancer), and are associated with resistance to chemotherapy and radiation therapy (93,95). Prof Hennessy's group has previously shown that patients with mutations within these pathways are less likely to achieve pCR, and ultimately achieved worse outcomes and relapse free survival rates (93,192–194). As a result of these findings, we decided to undertake further research in this area to increase LARC patient response rates to NACRT treatment.

KRAS

KRAS is mutated in 35-47% of CRC cases (93,104–107). Our cohort found *KRAS* to be mutated in 36.4% of Irish samples (27.3% synonymous, 9.1% non-synonymous), and 26.7% of American samples (6.7% synonymous, 20% non-synonymous). 100% of our non-synonymous mutations were missense, similar to COSMIC (98.98%). However, we had an increased volume of C>A (50% vs 0.19%) and C>T (50% vs 0.25%) mutations compared to COSMIC which primarily consisted of G>A (60.35%) and G>T (31.29%) substitutions (195). All non-synonymous *KRAS* mutations in our samples were identified in codons 12 (50%), 13 (25%) and 146 (25%). This resembles other studies which have shown 95% of *KRAS* mutations occur within exon 2, codons 12 (80%) and 13 (15%), whilst 5% *KRAS* mutations are located in codons 61 and 146. We found patients with mutations in codons 13 and 146 were poor responders. In line with this observation, multiple studies have shown *KRAS*^{G13D} mutations are associated with resistance to NACRT therapy; and reduced survival rates (disease-free, 5-year and overall survival), and pCR rates (93,109,196–200).

KRAS^{A146} mutations are almost exclusively expressed in CRCs (0.7-4%) (29, 30). Similarly to our findings, numerous studies have found a link between *KRAS*^{A146} mutations and poor response rates. They found *KRAS*^{A146} mutations are associated with MEK dependence, resistance to EGFR therapy, poor recurrence-free survival and overall survival (93,108,109,116,203).

In contrast, patients with *KRAS*^{G12V} mutations displayed improved response rates to NACRT (good and intermediate responders). Currently, *KRAS*^{codon 12} mutations effects on prognosis and overall survival rates are unclear and rather contradictory. Jones et al observed a worse prognosis for *KRAS*^{codon 12} mutated patients (204). As did Li et al, who found higher tumour stage and lymph node metastasis was associated with CRC *KRAS* mutations in codon 12, but not in codon 13 (205). Conversely, Inoue et al showed patients with *KRAS*^{G13D} mutations had the worst 5-year survival rates of a mere 42% compared codon 12 *KRAS* mutations (61.4%), and *KRAS*^{wild-type} (81.4%) (198). This controversy may be due to differing *KRAS*^{codon 12} mutations affecting patients in different ways; therefore results should possibly be assessed according to specific mutation rather per codon.

BRAF

5-12% of all CRC cases harbour mutations within the *BRAF* oncogene (93,104–107). Our study identified *BRAF* mutations in 18.2% (n = 2) of Irish samples and 6.7% (n = 1) of American samples in our cohort . All *BRAF* mutations were localised within exon 15 between codons 594 - 600. In our study, we identified mutations in codons 597 (*L597R*) and 594 (*D594G*) in intermediate responders, whilst the *V600E* mutation was located within a poor responder (exon 15, codon 600).

Mutations within *BRAF*⁵⁹⁴ impairs the normal functioning of kinase (206–208). Our results concur with other studies, which found *BRAF*⁵⁹⁴ is associated with a more favourable prognosis in melanoma (209), and CRC (210). Amaki-Takao et al found patients with *BRAF*^{D594G} mutations had better 2 year survival rates (50%) compared to *BRAF*^{V600E} (8.5%), along with similar prognosis, MSI status and clinicopathological features to *BRAF*^{wild-type} (211).

BRAF^{V600E} as the most prevalent *BRAF* mutation. In line with our findings, numerous studies have identified *BRAF*^{V600E} mutations to be indicative of a poor prognosis, particularly in patients with microsatellite instable CRCs (115).

PIK3CA

PIK3CA mutations were identified in 9% of the Irish cohort (synonymous mutation, n = 1), and 20% of the American cohort (non-synonymous mutations, n = 3). This correlates with other papers, which found *PIK3CA* gene mutations present in 8-20% of CRC cases (89,99,100). 80% of *PIK3CA* mutations occur in two hotspots within exons 9 (codons 542 and 545) and 20 (codon 1047) (212). This is in line with our observations, as all three mutations identified in our American cohort were identified in exon 10 (coding exon 9), in codons 545 (E545K mutation, n=2, MDA-10, MDA-17), and 546 (Q546K mutation, n=1, MDA-13). *PIK3CA* mutations in this exon are associated loss of O-6-methylguanine-DNA methyltransferase (MGMT) expression (required for DNA repair), increased levels of CpG island methylator phenotypes (CIMP) (213), and co-occurrence of *KRAS* mutations (100). 66% of the *PIK3CA* mutated samples in our American cohort also possessed a *KRAS* mutation.

Furthermore, *PIK3CA* mutations were only identified in samples from patients who did not respond to NACRT (poor responders, n=2; intermediate responders, n=1).

PTEN

Our Irish cohort had a similar occurrence of *PTEN* mutations (9.1% , n=1) compared to the COSMIC database. The *PTEN* mutation from our cohort was identified in the MSI tumour sample BH-607. Studies have shown an association between MSI tumours and increased frequency of *PTEN* mutations (101,102). A loss of *PTEN* expression is associated with decreased overall survival (103).

3.4.3. Most commonly mutated genes

Unsurprisingly, gene mutations commonly identified in CRC such as *APC*, *TP53*, *KRAS*, and *PIK3CA* were all identified at a high frequency in our study cohort. However, we also identified a high volume of mutations in novel genes *SYNE1*, *TTN* and *FBXW7* mutations. *KRAS* and *PIK3CA* mutations were previously discussed in the section 'PI3K and MAPK pathway mutations'.

APC

APC is a tumour suppressor gene involved in apoptosis, transcription, cell adhesion and migration. *APC* mutations typically occur within the mutation cluster region (MCR), located in codons 1286-1513. In our studies, we identified a high volume of *APC* mutations in both the Irish (n=10) and American (n=24) cohorts.

14 of which were located in the MCR (BH cohort, n = 6; MDACC cohort, n = 8). *APC* substitution mutations in our cohort consisted primarily of C>T (59.1%) and G>T (18.2%) alterations. COSMIC recorded similar levels with 59.45% and 24.8% respectively (214).

TP53

TP53 is also a tumour suppressor gene which is involved in apoptosis, transcription, cell division and DNA repair. *TP53* is known to be commonly mutated in CRC; therefore it was not surprising that 54.5% of the Irish cohort and 80% of the American cohort displayed non-synonymous *TP53* mutations. Multiple studies have shown the majority of *TP53* mutations in cancer occur as single nucleotide variants (SNVs) or missense mutations, particular in the DNA binding domain at codons 175, 245, 248, 273 and 282. Similarly we found mutations in codons 175, 245 and 248 in both cohorts. However, we also found an increased volume of *TP53* mutations in codon 213 in our Irish cohort (18%).

FBXW7

FBXW7 is a negative regulator of JNK, which is part of the MAPK pathway. Mutations within *FBXW7* have been identified in breast and ovarian cancer cell lines, and are associated with uterine body mixed cancer and hyperlucent lung cancer. We identified a higher frequency of *FBXW7* mutations in our American cohort (26.7%), compared to COSMIC (9.5%). Interestingly, we identified the same two *FBXW7* mutations in numerous samples. All mutations were G>A substitutions. One mutation was a nonsense mutation (exon 5, codon 278), and the other an *R465C* missense mutation (exon 9, codon 465).

3.4.4. Mutations associated with patient response to NACRT

Good responders

1,265 non-synonymous somatic mutations were identified in the pre-treatment LARC biopsy samples of good responders. From which, we identified *MUC16*, *KMT2C* and *TCF20* to be commonly mutated in good responder's samples only. In line with our findings, other studies have shown mutations in *KMT2C*, *MUC16* and *TCF20* have all been identified as good prognostic markers for patients with ependymoma, renal, endometrial or kidney cancers respectively (215–217).

Non-responders 81 mutations were identified in 2 or more samples of non-responders (Irish cohort, n = 58; American cohort, n = 23). BH-601 from the Irish cohort had 4 simultaneous mutations within the tumour suppressor *FAT2* gene and 3 mutations within *WDFY4*.

Genes of particular interest include *ASH1L*, *BRAF*, *ELP2*, *FAT2*, *PIK3CA* and *PTPRB*, for their roles in transcription, cell growth, division, differentiation, adhesion and proliferation. Furthermore, *BRAF*, *PIK3CA* and *PTPRB* are all commonly known oncogenes.

Our findings largely concur with published literature, with mutations in *ASH1L*, *BRAF*, *CSMD1*, *FAT2*, *FBN2*, *MAP4*, *PIK3CA*, *PTPRB* and *TCHH* all identified as poor prognostic markers in various cancer types (223–231). Furthermore, many of these were associated with reduced overall survival (*ASH1L*, *MAP4*, *TCHH*) (223,227–229), angiogenesis (*MAP4*, *PTPRB*) (227,231), metastatic potential (*FAT2*, *MAP4*, *PTPRB*) (226,227,230). In addition, *MAP4* is also associated with angiogenesis, tumour growth and cell migration (227). *BRAF* and *PIK3CA* oncogene mutations were previously discussed in section: PI3K and MAPK pathway mutations.

Poor responders

We identified 9 non-synonymous somatic mutations in a minimum of 2 of poor responder's samples. There was no mutational overlap between the Irish cohort (PCDHA12, TCTE1) and the American cohort (APOB, CD93, IGHV3-11, PZP, RANBP2, TPD52L2, ZIC1). Many of these genes are responsible for features frequently altered within cancer including apoptosis, cell migration, colony formation, transcription, adhesion, proliferation and invasion (232).

Numerous studies have concluded similar findings, suggesting that mutations in *APOB*, *CD93*, *IGHV3-11* and *ZIC1* are associated with poor prognosis in a range of cancer types (188,232–237). Meanwhile, *APOB* is also associated with increased tumour size post-surgery in patients with hepatocellular carcinoma (233).

MDA-4 and MDA-7 had two simultaneous mutations in *ZIC1* and *TPD52L2* respectively. Downregulation of the tumour suppressor gene, *ZIC1* is associated with lymph node metastasis in thyroid cancers. (232,237).

As mentioned previously (see hypo-mutated tumours), identical *CD93* thymine insertion frameshift mutations at exon 1, codon 121 (20_23066468_-/T → E121FS) were identified in samples from two different poor responders. Whilst *IGHV3-11* also had matching ACC inframe deletion mutations in chromosome 14 (14_106573362_ACC/-) in two samples. Mutations within *CD93* are associated with poor response rates (188), whilst *IGHV3-11* mutations are associated with worse overall survival, along with poor prognosis (236). However, the specific mutations identified in these samples have not been identified as potential mutations of interest as of yet.

To date, no studies have shown a link between *PZP*, *RANBP2*, *TCTE1* or *TPD52L2* mutations and poor patient outcome. Nevertheless, we feel that two of these mutations (*RANBP2* and *TPD52L2*) have the potential to affect response rates in CRC. *RANBP2* is a GTP-binding protein from the RAS superfamily. Whilst *TPD52L2* associated with breast cancer and lymphoblastic leukaemia. Due to their roles and the high frequency of their mutations within our cohort, we feel these may be potential gene mutations of interest.

3.4.5. Heterogeneity

Surprisingly, we found a higher volume of tumour mutational clones within good (mean = 3.7 clones) and intermediate (mean = 3.8 clones) responders, compared to poor responders (mean = 1.6 clones). This could be widely due to the low volume of mutations identified within poor responders, compared to good and intermediate responders which included MSI and *POLE* mutated tumours.

Patients in our study who did not respond fully to NACRT had higher MATH scores (intermediate MATH score = 46.04, poor MATH score = 46.19) than that of good responders (MATH score = 39.36). Multiple studies have shown higher MATH scores are associated with poor prognosis, reduced overall survival, risk of metastasis (180,238,239).

Due to intra-tumour heterogeneity, biopsy sampling may target only one subset of mutations. Therefore, the biopsy samples analysed for these patients may not be true representations of the tumour as a whole. Analysis of multiple biopsies may produce a more accurate depiction of the mutations present throughout the tumour; as a result, we carried out mutational analysis for 2 biopsies in 8 samples.

3.4.6. Mutational signatures

Colorectal cancers typically have an average of 3 signatures per sample. Samples in both the Irish and American cohorts had an increased volume of signatures with means of 4.8 and 7.2 respectively, albeit some signatures were found at low frequencies.

COSMIC identified signature 1 in the majority of cancer samples, and found it is associated with age. Therefore it is not surprising to see this signature in 100% of samples in both our cohorts.

We also found a high frequency of samples in both cohorts had signatures 6, 15 and 20, which are all associated with defective DNA mismatch repair. Four samples in our cohorts (BH-601, BH-607, MDA-3 and MDA-4) previously identified with mutations in the MMR pathway were also positive for a minimum of two MMR pathway mutational signatures.

**To determine the impact of neoadjuvant chemoradiotherapy on
circulating tumour DNA and circulating tumour cells as
potential biomarkers of treatment response in LARC patients**

4.1. Introduction

4.1.1. Tumour metastasis as a result of circulating tumour cells

A tumour consists of a mass of incessantly proliferating, mutated cells. As the tumour progresses, it often gains additional mutations. Some of which are passenger mutations, having no real impact on tumour progression. However, some mutations increase a tumours ability to shed cells into and migration throughout the peripheral blood and/or lymphatic systems, ultimately ending in adhesion to, and tumour proliferation in a distant site (metastasis). CRCs typically metastasise to the lymph nodes, liver, lungs, peritoneum and bones (32). Mutations commonly associated with increasing metastatic abilities in CRC include *BRAF*, *KRAS*, *SMAD4*, *FAT2*, *MAP4* and *PTPRB* (205,226,227,230).

4.1.2. Circulating tumour cells

Metastasis was first hypothesised by Recamier in 1829. Despite significant scientific breakthroughs in the world of cancer treatment over the past 190 years, tumour metastasis remains an unsolved problem. 25-50% of LARC patients relapse due to undiagnosed metastasis at the surgical procedure. It is not yet known if these undiagnosed metastases occur naturally at an early stage of tumour progression, or as a result of the cancer treatment procedure itself (33–36).

Detection and destruction of circulating tumour cells have proven to be difficult. This is largely due to the low volume of CTCs circulating throughout the circulatory systems (~one CTC for every $10^6 - 10^8$ haematopoietic cells) (37). Furthermore, current cancer treatment methods are aimed at targeting rapidly growing cells within the body due to cancers rapid proliferative abilities. However, since CTCs do not proliferate whilst travelling throughout the circulatory and lymphatic systems, the vast majority of CTCs are believed to evade current treatment methods. Furthermore, a large percentage of CTCs which survive are often resistant to current treatment regimens (44,45).

4.1.3. Isolation and identification of circulating tumour cells from peripheral blood

Large volumes of CTCs (>5CTCs / 7.5mls blood) are associated with a poor prognosis, reduced recurrence-free and overall survival rates (34,38–43).

Therefore, early identification of CTCs and their mutational composition may aid in early detection and appropriate treatment methods for micrometastases throughout the body. Current methods for identification of CTCs from the blood include immuno-magnetic antigen-dependent techniques which detect membrane proteins e.g. EpCAM; or filtration techniques based on CTCs large size compared to other cellular elements within the blood. These methods enable the ability to identify the presence of CTCs and also allow CTC molecular testing including detecting the presence of *PIK3CA* and *RAS* mutations, thereby facilitating the possibility of a personalised treatment method, possibly ultimately for micrometastases.

4.1.4. Circulating tumour DNA (ctDNA)

Every cell in the body releases cell-free DNA (cfDNA) into the bloodstream. cfDNA released from tumours is known as circulating tumour DNA (ctDNA), which can be extracted from patients' plasma.

Tissue biopsies are currently the gold standard for molecular testing. However, the prospect of liquid biopsies has recently been gaining traction. This is largely due to their relatively non-invasive nature. Since liquid biopsies are carried out on blood samples, they could be most beneficial in detecting tumours where it is difficult to obtain biopsies e.g. lung or brain. In addition, numerous samples can be taken before, during and after cancer treatment to monitor patients' response rates to their designated treatment regimen. This would include the potential to monitor *PIK3CA* and *KRAS* mutations in patients on novel Pi3K and/or MEK inhibitors. Furthermore, tumours are generally heterogeneous in nature; as a result, tissue biopsies are only representative of a fraction of the whole tumour. ctDNA is excreted from cells throughout the entirety of the tumour, and therefore depict a more clinically accurate representation of the tumour as a whole. Finally, the volume of ctDNA is representative of the size of the tumour. This can aid in tumour staging, monitoring patient response to treatment or to see if the patient is in remission.

The objectives of the research described in this chapter were to:

1. To ascertain if TRG status is associated with the type of radiation therapy, gender, or age.
2. To identify if the volume of circulating tumour cells (CTCs) is increased in patients with poor response to treatment, or at various time-points throughout chemoradiation treatment.
3. To detect mutations associated with patient response in LARC patients.
4. To monitor mutational variations in LARC patient tumour tissue and ctDNA samples throughout treatment.

4.2. Results

4.2.1. Clinicopathological characteristics of TRILARC study population

The TRILARC clinical trial was set up to compare two forms of neoadjuvant radiation therapy (RT); 3-D conformal radiotherapy (3-DCRT) and intensity-modulated radiotherapy (IMRT) in LARC patients; and to monitor their response throughout treatment. To date, 66 patients have been enrolled on the TRILARC clinical trial, however this chapter will focus on 35 patients where longitudinal time point data is available. Patients were treated with 5-FU chemotherapy and radiation therapy for 6-8 weeks. Blood samples were collected at 6 time-points throughout the duration of treatment (pre-treatment, week 3 of RT, last week of RT, 4 weeks post-RT, after surgical procedure and 1 year post-surgical procedure), and tested for the presence of circulating tumour cells. One blood sample per patient was analysed at each time-point. The initial tumour site was subsequently removed via total mesorectal excision (TME) and histologically analysed and graded according to the Mandard tumour regression scoring system defined in Table 4.1(240).

Table 4.1: Mandard tumour regression grade (TRG) system (240).

TRG status	Histological analysis of resected tumour
TRG1	Complete regression (fibrosis without detectable tissue of tumour)
TRG2	Fibrosis with scattered tumour cells
TRG3	Fibrosis and tumour cells with a predominance of fibrosis
TRG4	Fibrosis and tumour cells with a predominance of tumour cells
TRG5	Tissue of tumour without changes of regression.

Studies have shown that patients who achieve a pathological complete response (pCR) have better outcomes and survival rates. Currently, we cannot identify which patients will achieve pCR; therefore we aimed to monitor LARC patients' blood samples throughout treatment, in the hope of identifying potential markers to response, since patients who will not achieve pCR will have lower cure rates and more need for novel therapies. Tumour response is widely reported via TRG status, we, therefore, analysed patient samples according to their TRG scores. 35 patients are currently enrolled into the TRILARC clinical trial, have undergone

surgery and were subsequently categorised according to their response to chemoradiation therapy via the Mandard TRG grading system (Table 4.1). pCR (pathological complete response) was achieved in 4/35 patients (11.4 %), whereby no tumour was detected at surgery (TRG1) (Table 4.2). In contrast, 9/35 patients (25.7%) showed minimal (TRG4 = 8/35 (22.9%)) or no (TRG5 = 1/35 (2.9%)) tumour regression post neoadjuvant chemoradiation therapy.

18/35 (51.4%) and 17/35 (48.6%) of patients were enrolled in IMRT and 3-DCRT treatment cohorts respectively. Only patients who were administered IMRT achieved pCR (TRG1), this was seen in 4/18 patients (22.2%) compared to 0/17 patients (0%) on 3-DCRT (Figure 4.1a).

24/35 patients (68.6%) were males, compared to 11/35 females (31.4%) (Table 4.2). Females exhibited a trend to a better response rate than males, with 2/11 females (18.2 %) showing no evidence of residual tumour at surgery (TRG1), compared to 2/24 males (8.3 %).

Patients ranged from 42-84 years, with an average of 63.2 years (Figure 4.1c). There was no significant difference in age between males (mean = 62.6 years) and females (63.5 years) ($p = 0.85$).

All clinical observations are preliminary since the TRILARC clinical trial has not yet been completed.

Table 4.2: Patient demographics of TRILARC study population.

LARC patients (n = 35) were enrolled into the clinical trial, and blood was drawn at 6 time- points before, during and after chemoradiation treatment. 3mls of blood was filtered through a ScreenCell CY device and subsequently stained with haematoxylin and eosin to detect circulating tumour cells. Samples were analysed according to tumour regression grade (TRG), the presence of CTCs and the average volume of CTCs/3mls blood per sample. TRG categories were defined as TRG1 (Complete regression fibrosis without detectable tissue of tumour), TRG2 (Fibrosis with scattered tumour cells), TRG3 (Fibrosis and tumour cells with a predominance of fibrosis), TRG4 (Fibrosis and tumour cells with a predominance of tumour cells) or TRG5 (No tumour regression).

Age (years)		
Average		63.2
Range		42-84
Median		63
Gender (n = 35)		
Male	24	(68.6% %)
Female	11	(31.4% %)
Treatment type (n = 35)		
IMRT	18	(51.4%)
Control 3-DCRT	17	(48.6 %)
TRG grade (n = 35)		
TRG1	4	(11.43%)
TRG2	8	(22.86%)
TRG3	14	(40%)
TRG4	8	(22.86%)
TRG5	1	(2.86%)
Positive for CTCs		
Pre-treatment		22.2%
Week 3 on chemoradiation therapy		50%
Last week on chemoradiation therapy		46.4%
4 weeks after chemoradiation therapy		14.8%
After surgical procedure		21.1%
1 year post-surgical procedure		37.5%

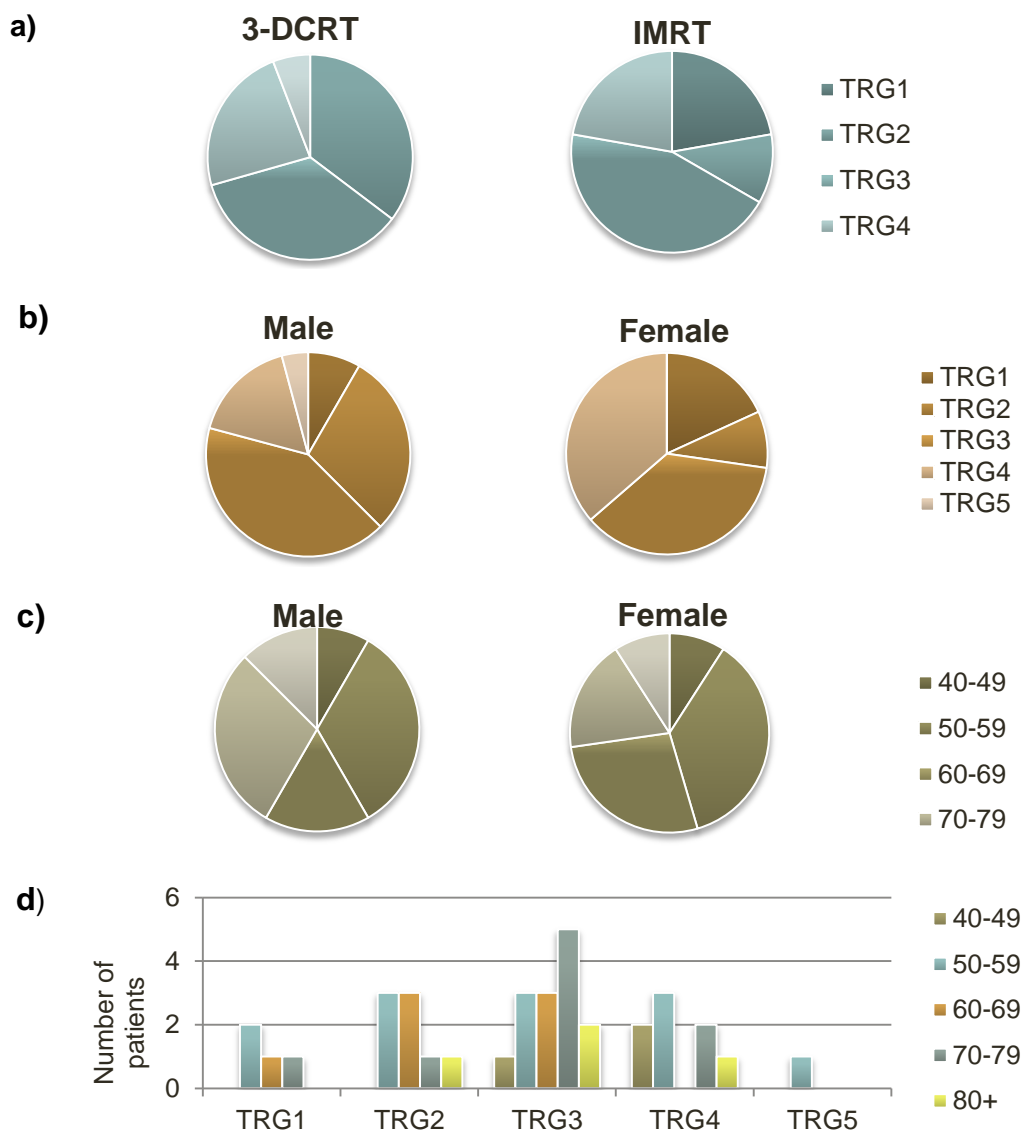


Figure 4.1: Clinicopathological characteristics of TRILARC cohort (a) composition of TRGs according to radiation arm, (b) composition of TRG grades according to gender, (c) comparison of patient age group per gender (d) age group respective of TRG status.

LARC patients ($n = 35$) were enrolled into a clinical trial, and blood was drawn at 6 time-points before, during and after treatment. 3mls of blood was filtered through a ScreenCell CY device and subsequently stained with haematoxylin and eosin to detect circulating tumour cells. Samples were analysed according to tumour regression grade (TRG) and for the presence of CTCs in 3mls blood. TRG categories were defined as TRG1 (Complete regression, fibrosis without detectable tissue of tumour), TRG2 (Fibrosis with scattered tumour cells), TRG3 (Fibrosis and tumour cells with a predominance of fibrosis), TRG4 (Fibrosis and tumour cells with a predominance of tumour cells), or TRG5 (Tissue of tumour without changes of regression).

4.2.2. Increased volumes of circulating rectal tumour cells are shed into the periphery during neoadjuvant chemoradiation therapy.

Circulating tumour cells (CTCs) are cells which detach from the primary tumour and enter the circulatory system. Multiple studies have shown that the presence of more than 5 CTCs/7.5mls blood post-treatment is indicative of a poor response to anti-cancer therapies (34,38–43). However, few studies have analysed the presence of CTCs during treatment, and whether this may predict patient response.

ScreenCell filters were analysed microscopically for the presence of CTCs. The following cytomorphological criteria were used for identification of CTCs, whereby a minimum of 4 of the following was required for positive identification (173–175):

Anisonucleosis (ratio >0.5)

Nucleus size $>16\mu\text{m}$

Irregular nuclei

3-D sheets

High (>2.1) nuclear/cytoplasmic ratio.

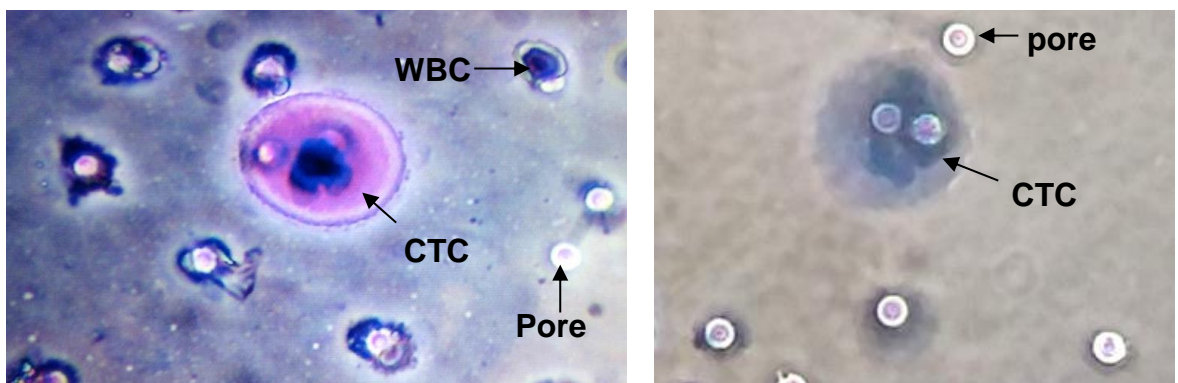


Figure 4.2: Circulating tumour cells (CTCs) isolated from blood samples. White blood cells are scattered throughout samples and primarily trapped in membrane pores.

Our results showed an increase in the percentage of patients with, and a significant increase in the mean number of circulating tumour cells during week 3 of chemoradiation therapy (CRT) (present in 16/32 patients (50%), mean = 2.16 CTCs/3mls blood, $p = 0.0027$), and the last week of CRT (present in 13/28 patients (46.4%), mean = 1.86 CTCs/3mls blood, $p = 0.0137$, compared to pre-treatment (present in 6/27 patients (22.2%), mean = 0.48 CTCs/3mls blood) (Figure 4.3a and b). An increase in the percentage of patients with CTCs was also identified at 1 year follow-up (3/8, 37.5%), however, the numbers of blood samples with one year follow up are still low. The numbers of CTCs significantly decreased post CRT and remained reduced, at 4 weeks post CRT, after surgery and 1 year follow-up (with mean values ranging from 0.26 – 0.38 CTCs/3mls blood) (p -values = 0.0006 – 0.0082). These observations are preliminary since the TRILARC clinical trial has not yet been completed.

CTC positivity post-treatment is indicative of a poor response to anti-cancer therapies. We therefore analysed if mobilisation of CTCs during treatment could be predictive of TRG at surgery in rectal cancer. We found that patients who achieved pCR (TRG1) had a lower level of CTC compared to patients who did not achieve pCR (TRG2-5) (Figure 4.4a). This was particularly evident during week 3 of CRT (pCR = 25 %, non-pCR = 53.6 % positive for CTCs), and last week of CRT (pCR = 25%, non-pCR = 50% positive for CTCs) (Figure 4.4a). Furthermore, patients who achieved pCR (TRG1) had significantly less CTCs/3mls blood during weeks 3 of CRT (mean volume of CTCs/3mls blood, pCR = 0.5, non-pCR = 2.39, $p = 0.024$), and at last week of CRT (mean volume of CTCs/3mls blood, pCR = 0.25, non-pCR = 2.13, $p = 0.005$ compared to patients who did not achieve pCR (TRG2-5) (Figure 4.4b).

3-DCRT and IMRT are two different forms of radiation therapy being tested in our TRILARC clinical trial; IMRT is the novel form which may be less toxic. We are interested in seeing if CTCs in patient blood samples might behave in different ways depending upon the type of radiation therapy administered (Figure 4.5A). Patients in the 3-DCRT arm had significantly higher levels of CTCs identified at week 3 of CRT compared to pre-treatment ($p = 0.0025$), whilst patients in the IMRT arm had significantly more CTCs mobilised during the last week of CRT compared to pre-treatment ($p = 0.034$) (Figure 4.5B). The clinical significance of

these differences will require further follow up. Furthermore, we found that patients who received IMRT had significantly fewer CTCs released into circulation at week 3 of chemoradiation (mean = 1.18 CTCs/3ml blood) compared to patients receiving 3-DCRT (mean = 3.27 CTCs/3mls blood) ($p = 0.036$).

We have previously shown that females in our cohort had better response rates. This agrees with multiple studies which have shown that females with CRC have significantly better long-term survival rates compared to males (241). We found more males were positive for CTCs both pre-treatment (male = 25.7%, female = 14.3%), and after surgery (male = 33.3%, female = 0%, Figure 4.5A). However, there was no difference between the average numbers of CTCs identified in males and females (figure 4.5B). All clinical observations are preliminary since the TRILARC clinical trial has not yet been completed.

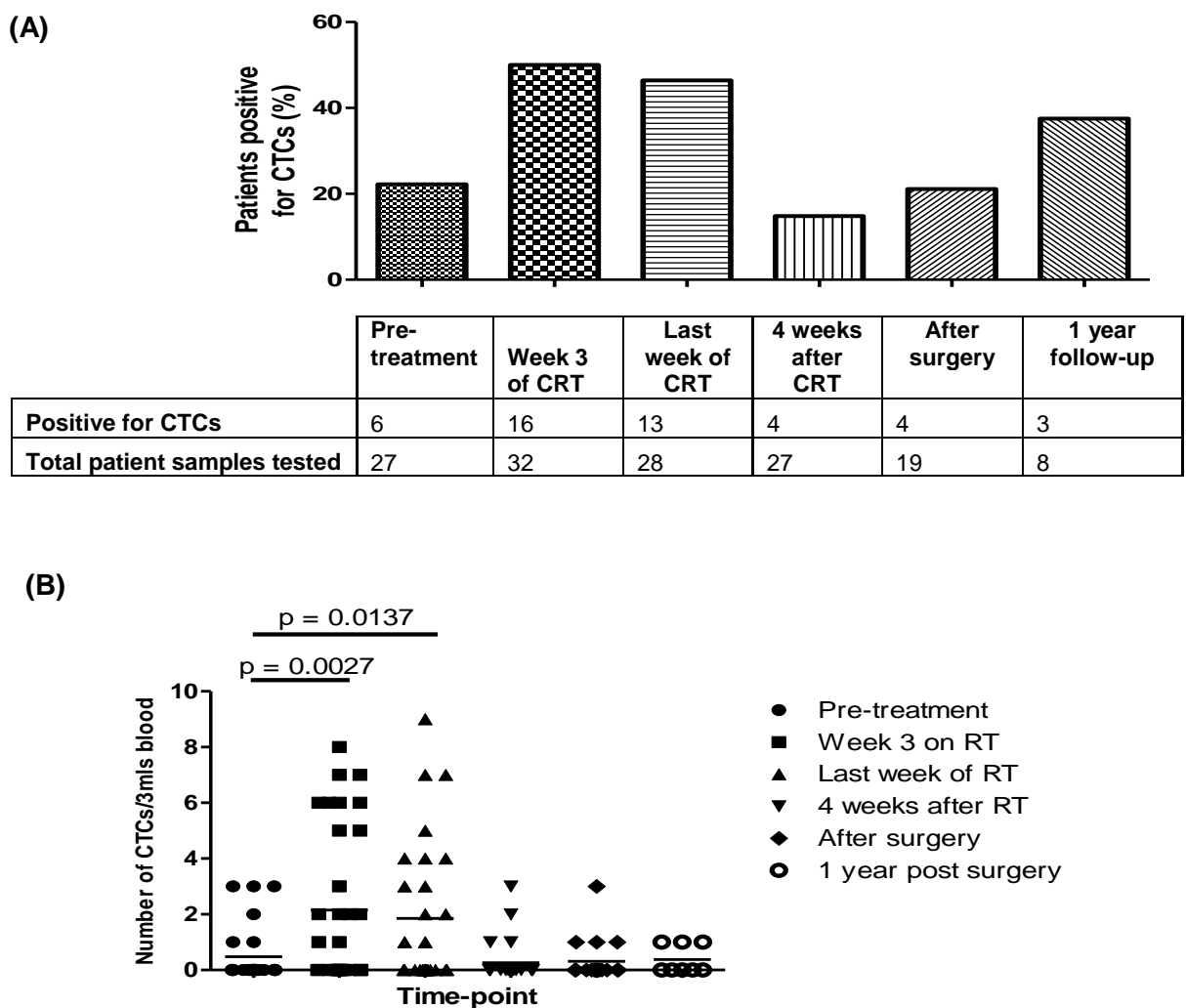


Figure 4.3: (a) Bar chart represents the percentage of patients with blood samples positive for CTCs (b) Scatter plot depicts the number of CTCs identified per patient sample.

LARC patients ($n = 35$) were enrolled into a clinical trial. Blood was drawn at 6 time-points before, during and after chemoradiation therapy (CRT). Blood (3mls) was filtered through a ScreenCell CY device and stained with haematoxylin and eosin to detect and enumerate circulating tumour cells (CTCs). One blood sample per patient was tested at each time-point.

(a) A bar chart represents the percentage of samples which tested positive for CTCs at each of the 6 time-points.

(b) Scatter plot depicts the number of CTCs/3mls blood at each time-point. Each dot is representative of the patient sample. Mean values are represented by a bar. Statistical data analysis was carried out using the Prism software (GraphPad). The unpaired 2-tailed t -test with Welch's correction was used to determine statistical significance for variations between time-points. A confidence interval of 95% was used and p -values ≤ 0.05 were indicative of a result of statistical significance.

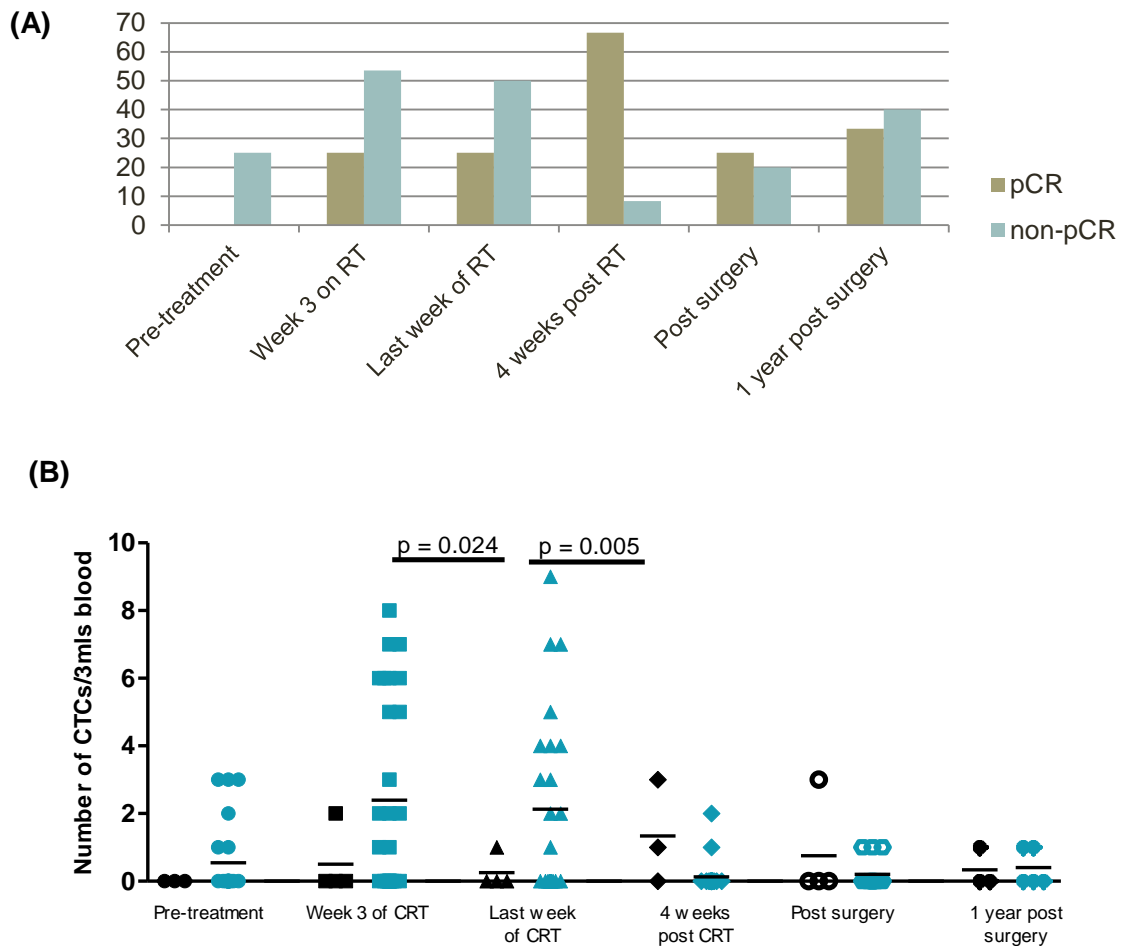


Figure 4.4: The relationship between serial circulating tumour cell (CTC) counts and TRG status (A) Percentage of samples positive for CTCs according to time-point and pCR status. (B) Number of CTCs identified in 3mls blood per sample in patients who achieved pCR (black), and those who did not (TRG2-5) (blue).

LARC patients ($n = 35$) were enrolled into a clinical trial. Blood was drawn at 6 time-points before, during and after chemoradiation therapy (CRT). Blood (3mls) was filtered through a ScreenCell CY device and stained with haematoxylin and eosin to detect CTCs. (A) Bar chart represents the percentage of samples which tested positive for CTCs at each of the 6 time-points in patients subdivided by TRG status. (B) Scatter plots depict the number of CTCs/3mls blood at each time-point. Each dot is representative of a sample. Mean values are represented as a bar. Significant differences ($p < 0.05$) are indicated. Statistical data analysis was carried out using the Prism software (GraphPad). The unpaired 2-tailed t -test with Welch's correction was used to determine statistical significance for variations between time-points. A confidence interval of 95% was used and p -values ≤ 0.05 were indicative of a result of statistical significance.

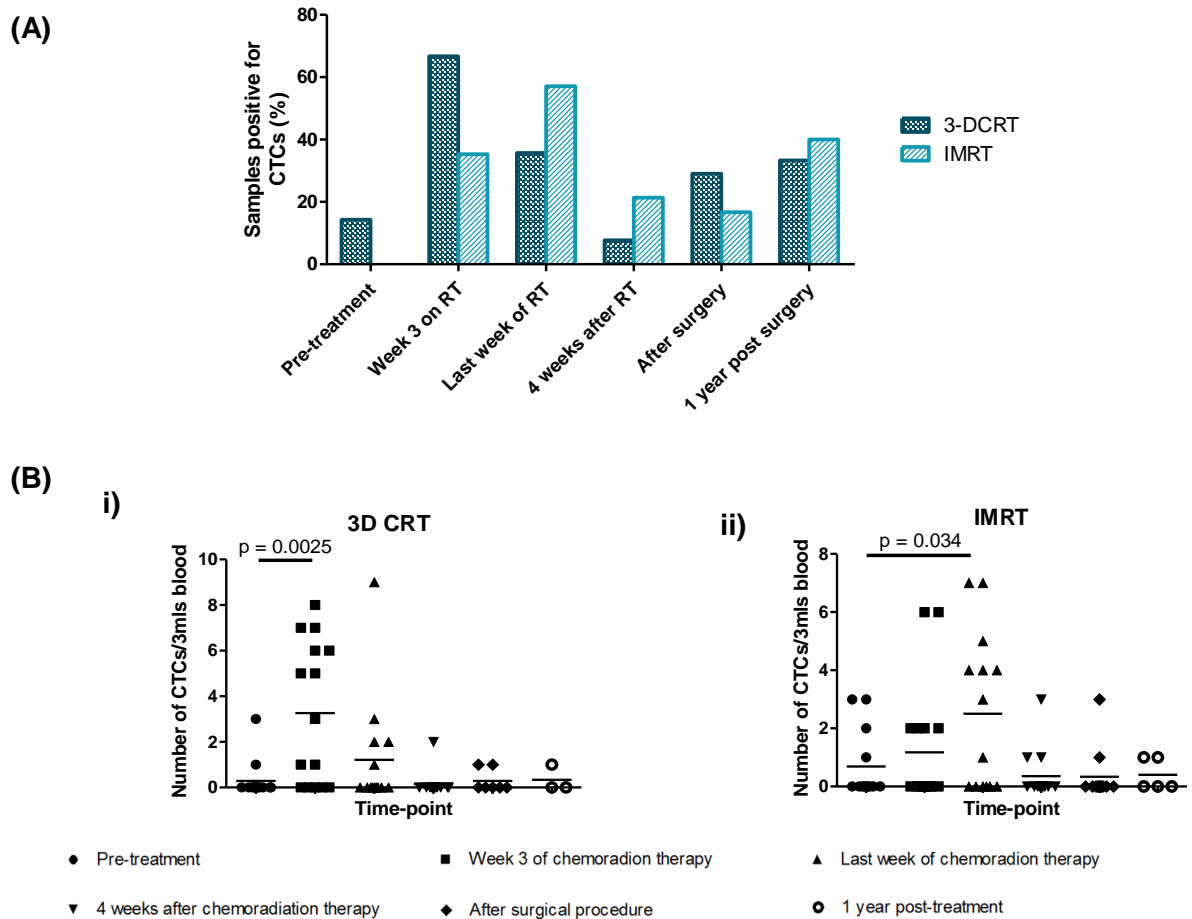
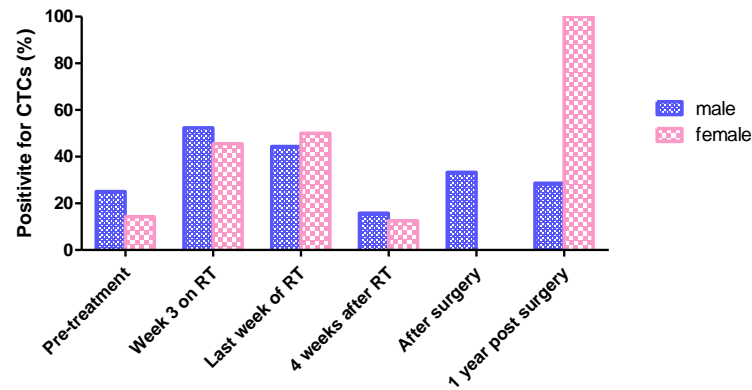


Figure 4.5: The effects of the type of radiation treatment on circulating tumour cells (CTCs) in LARC patients. (A) Percentage of patients with blood samples positive for CTCs according to time-point and the type of radiation therapy, (B) Number of CTCs identified in 3mls blood per patient sample in (i) 3-DCRT and (ii) IMRT arms.

LARC patients ($n = 35$) were enrolled into a clinical trial called TRILARC. Blood was drawn at 6 time-points before, during and after chemoradiation therapy (CRT). Blood (3mls) was filtered through a ScreenCell CY device and stained with haematoxylin and eosin to detect and enumerate CTCs. (A) Bar chart represents the percentage of patients with blood samples which tested positive for CTCs at each of the 6 time-points. (B) Scatter plots depict the number of CTCs/3mls blood at each time-point. Each dot is representative of a patient sample. Mean values are represented as a bar. Significant differences ($p < 0.05$) are indicated. Statistical data analysis was carried out using the Prism software (GraphPad). The unpaired 2-tailed t -test with Welch's correction was used to determine statistical significance for variations between time-points. A confidence interval of 95% was used and p -values ≤ 0.05 were indicative of a result of statistical significance.

(A)



(B)

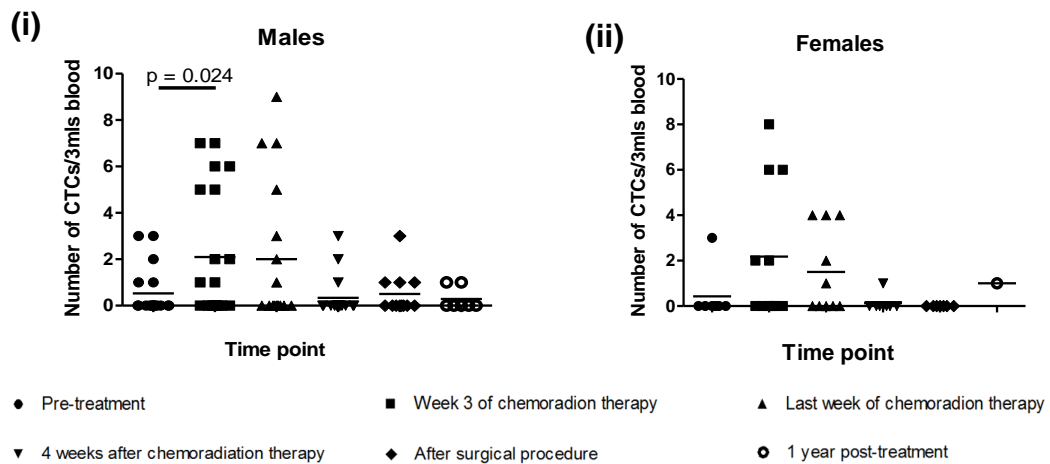


Figure 4.6: The relationship between circulating tumour cells (CTCs) and gender (A) Percentage of patient blood samples positive for CTCs at each time-point by gender. (B) Number of CTCs identified in 3mls blood per sample in (i) males and (ii) females at each time-point.

LARC patients ($n = 35$) were enrolled into a clinical trial called TRILARC. Blood was drawn at 6 time-points before, during and after chemoradiation therapy (CRT). Blood (3mls) was filtered through a ScreenCell CY device and stained with haematoxylin and eosin to detect and enumerate CTCs. (A) Bar chart represents the percentage of patients with blood samples which tested positive for CTCs at each of the 6 time-points. (B) Scatter plots depict the number of CTCs/3mls blood at each time-point. Each dot is representative of a patient sample. Mean values are represented as a bar. Significant differences ($p < 0.05$) are indicated.

Statistical data analysis was carried out using the Prism software (GraphPad). The unpaired 2-tailed t -test with Welch's correction was used to determine statistical significance for variations between time-points. A confidence interval of 95% was used and p -values ≤ 0.05 were indicative of a result of statistical significance.

4.2.3. Mutations in rectal tumours and matched ctDNA

We monitored tumour mutational profiles from 35 patients at 6 time-points prior to, during and post CRT treatment (pre-treatment, week 3 of CRT, last week of CRT, 4 weeks post CRT, post-surgical procedure and 1 year post-surgical procedure) in ctDNA, with tumour tissue collection from the diagnostic biopsy, surgery and tumour biopsy samples at the time of recurrence. We compared the mutational profiles of both ctDNA and tumour tissue.

Tumour mutations were predominantly identified in *KRAS* (represented as blue in Figure 4.7), with *KRAS* mutations attributing to a minimum of 60.3% of overall mutations (identified at week 3 of CRT), and up to a maximum of 100% of overall mutations (identified at tumour recurrence tissue). *KRAS* mutations consisted primarily of *KRAS*^{G12D} (mean overall occurrence = 34.88%, range = 24.7 - 75%), *KRAS*^{G13S} (mean overall occurrence = 11.12%, range 7.35-25%), and *KRAS*^{G12S} (mean overall occurrence = 7.54%, range = 0-12.1%).

Increased frequency of *NRAS* mutations (represented as red in figure 4.9) was seen in ctDNA samples (mean frequency = 23.7%), compared to tumour tissue samples (mean frequency = 5.8%). *G13D*, *G12S* and *G12D* mutations comprised 40.2%, 29.3% and 9.7% of *NRAS* mutations in ctDNA respectively.

BRAF and *EGFR* mutations were identified at low frequency (mean overall frequency = 0.5 and 0.75% respectively), whilst *PIK3CA* mutations accounted for an average of 8.25% of total mutations (*PIK3CA*^{E542K} = 6%, *PIK3CA*^{E545K} = 2.25%). 17.24% of pre-treatment tumour tissue samples and 32.4% of surgical resection tissue samples were wildtype for *KRAS*, *NRAS*, *BRAF*, *EGFR* and *PIK3CA*. None of these patients have progressed into metastatic disease, as of yet.

KRAS^{G12D} was the most frequent mutation, with 62.86 % (22/35) of patients presenting with a *KRAS*^{G12D} mutation prior to NACRT treatment, either in their ctDNA or biopsy tissue samples or both. *KRAS*^{G12D} mutations were identified in ctDNA and/or tumour of 33/35 (94.3%) of patients at some stage before, during or after treatment (figure 4.10).

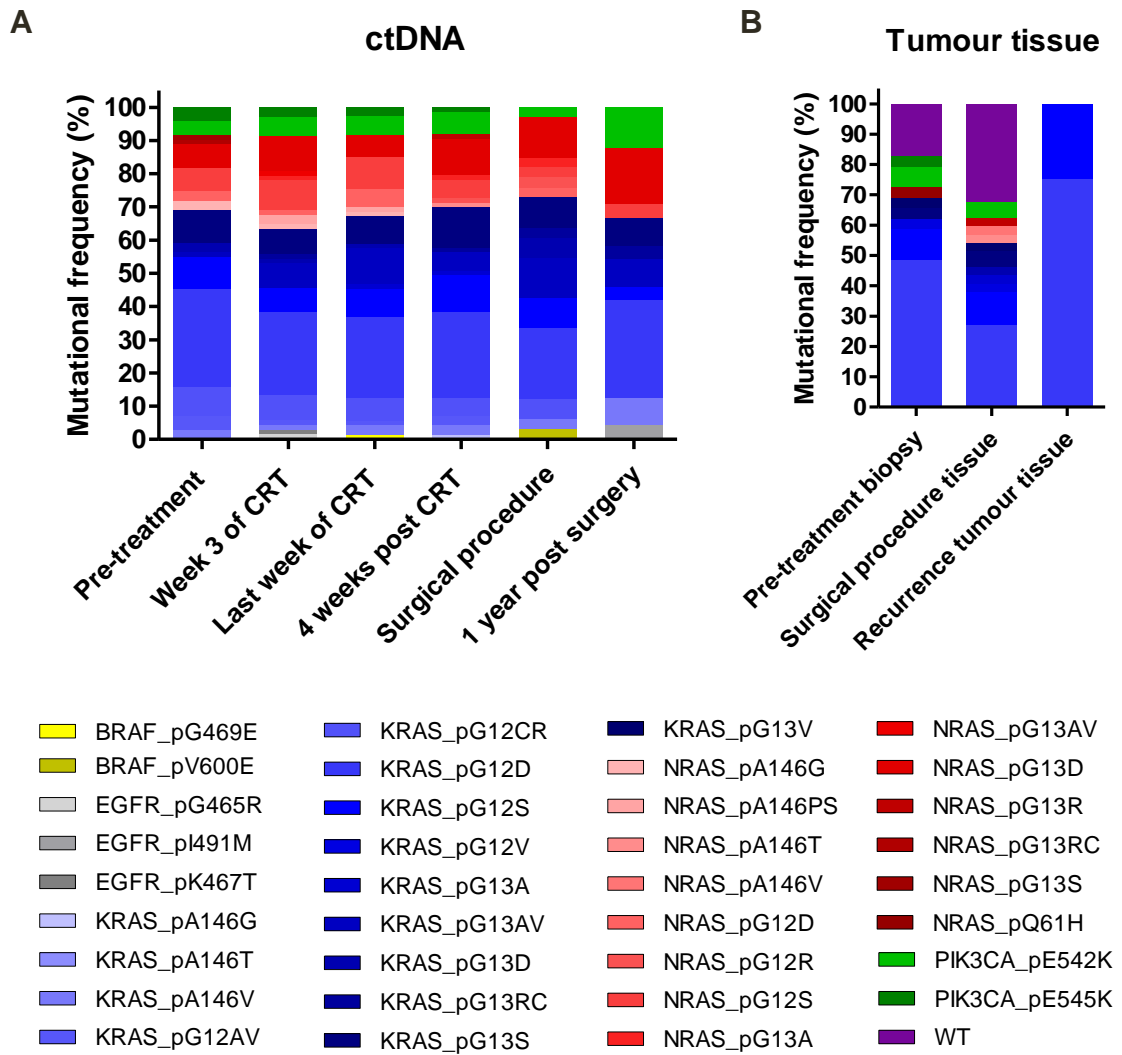


Figure 4.7: Mutational profiles obtained from (A) ctDNA and (B) tumour tissue samples from LARC patients participating in the TRILARC clinical trial, before during and after NACRT treatment.

DNA was extracted and mutational analysis carried out on ctDNA and tumour tissue samples collected from 35 LARC patients at various time-points before, during and after neoadjuvant chemoradiation therapy (NACRT) treatment from (ctDNA = pre-treatment, week 3 of chemoradiation therapy (CRT), last week of CRT, 4 weeks post CRT, post-surgical procedure and 1 year post-surgical procedure tumour tissue = pre-treatment, week 3 of CRT, surgical procedure, recurrence) samples.

Mutational frequency results were divided up according to the time-point, source (ctDNA or tumour tissue) and gene (BRAF (yellow), EGFR (grey), KRAS (blue), NRAS (red) and PIK3CA (green)).

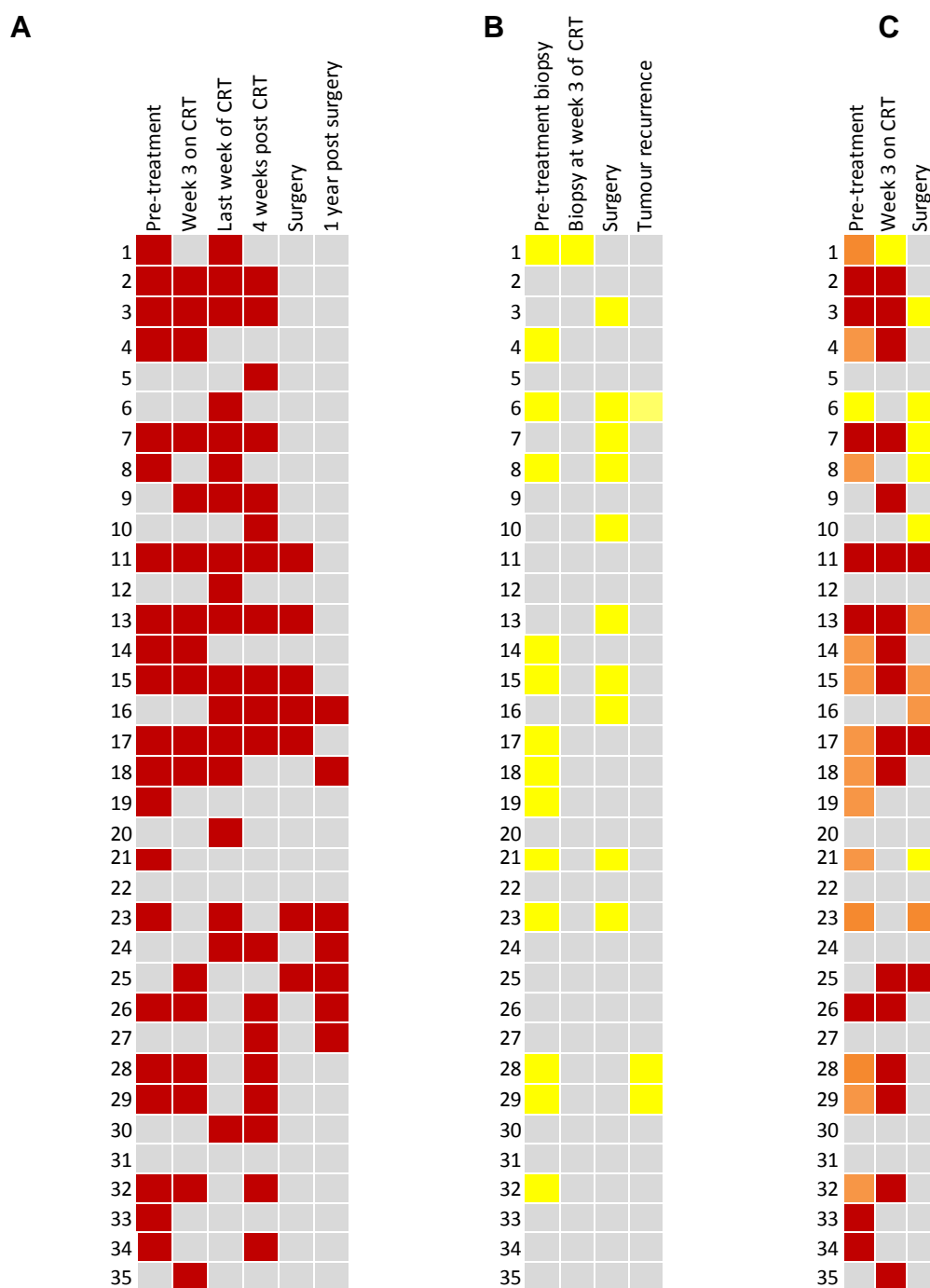


Figure 4.8: KRAS^{G12D} mutations

DNA was extracted and mutational analysis carried out on ctDNA and tumour tissue samples collected from 35 LARC patients at various time-points before, during and after NACRT treatment from (ctDNA = pre-treatment, week 3 of CRT, last week of CRT, 4 weeks post CRT, post-surgical procedure and 1 year post-surgical procedure tumour tissue = pre-treatment, week 3 of CRT, surgical procedure, recurrence) samples. KRAS^{G12D} was the most common mutation identified within samples. Mutations are represented in red (ctDNA only), yellow (tissue only), orange (ctDNA and tissue) and grey (WT).

4.2.4. Mutational variations between pre-treatment and post-chemoradiation therapy surgical specimens isolated from ctDNA and tumour tissue samples from LARC patients.

Variations were identified between mutational profiles in ctDNA and tissue samples within our cohort. In total, 101 individual mutations were identified at 25 mutational loci in the pre-treatment and surgical procedure ctDNA and tumour tissue samples. This consisted of 66 pre-treatment, 53 post-treatment, with 18 mutations co-occurring both pre-treatment and surgical procedure.

Mutations identified only within ctDNA

ctDNA mutational profiles may be representative of the whole tumour rather than a selected region as with tissue sampling. This was perhaps evident in our cohort, with 68.8% (53/77) of mutations in pre-treatment (represented in red in Figure 4.9) and 52.8% (28/53) of mutations in surgical samples identified solely in ctDNA (represented in red in Figure 4.10). Mutations in $KRAS^{G12CR}$, $KRAS^{G13AV}$, $NRAS^{G12D}$, $NRAS^{G12S}$ and $NRAS^{G13D}$ were identified exclusively in ctDNA samples both pre-treatment and at the surgical procedure.

Mutations identified only within tumour tissue samples

9.1% (7/77) of pre-treatment mutations (represented as yellow in Figure 4.9) and 39.6% (21/53) of post-treatment mutations (represented as yellow in Figure 4.10) were found within surgical resection samples and not identified in ctDNA. Mutations in $KRAS^{G12V}$ and $KRAS^{G13V}$ were detected in tissue samples alone, and not identified in ctDNA from pre- or post-treatment samples.

Co-occurring mutations

The mutations co-occurring in ctDNA and tissue samples collected pre-treatment were $KRAS^{G12D}$ (75%, n=12), $KRAS^{G12S}$ (12.5%, n=2), $KRAS^{G13S}$ (6.25%, n=1) and $PIK3CA^{E542K}$ (6.25%, n=1). $KRAS^{G12D}$ mutations were the only mutations identified in both tissue and ctDNA samples obtained at the time of surgical resection.

TRG status

In regards to TRG status, mutations in $KRAS^{G13D}$, $NRAS^{G12S}$, $NRAS^{G13D}$ and

PIK3CA^{E545K} in pre- and post-treatment samples were detected solely in patients who did not respond fully to NACRT (TRG ≥ 2). Meanwhile, *BRAF*^{V600E} and *NRAS*^{Q61H} mutations were identified exclusively in patients who did achieve pCR (TRG1). Furthermore, *KRAS*^{G12CR} mutations were lost in patients with TRG grades of 4 or 5, but were retained tumour in a TRG of 3 or less.

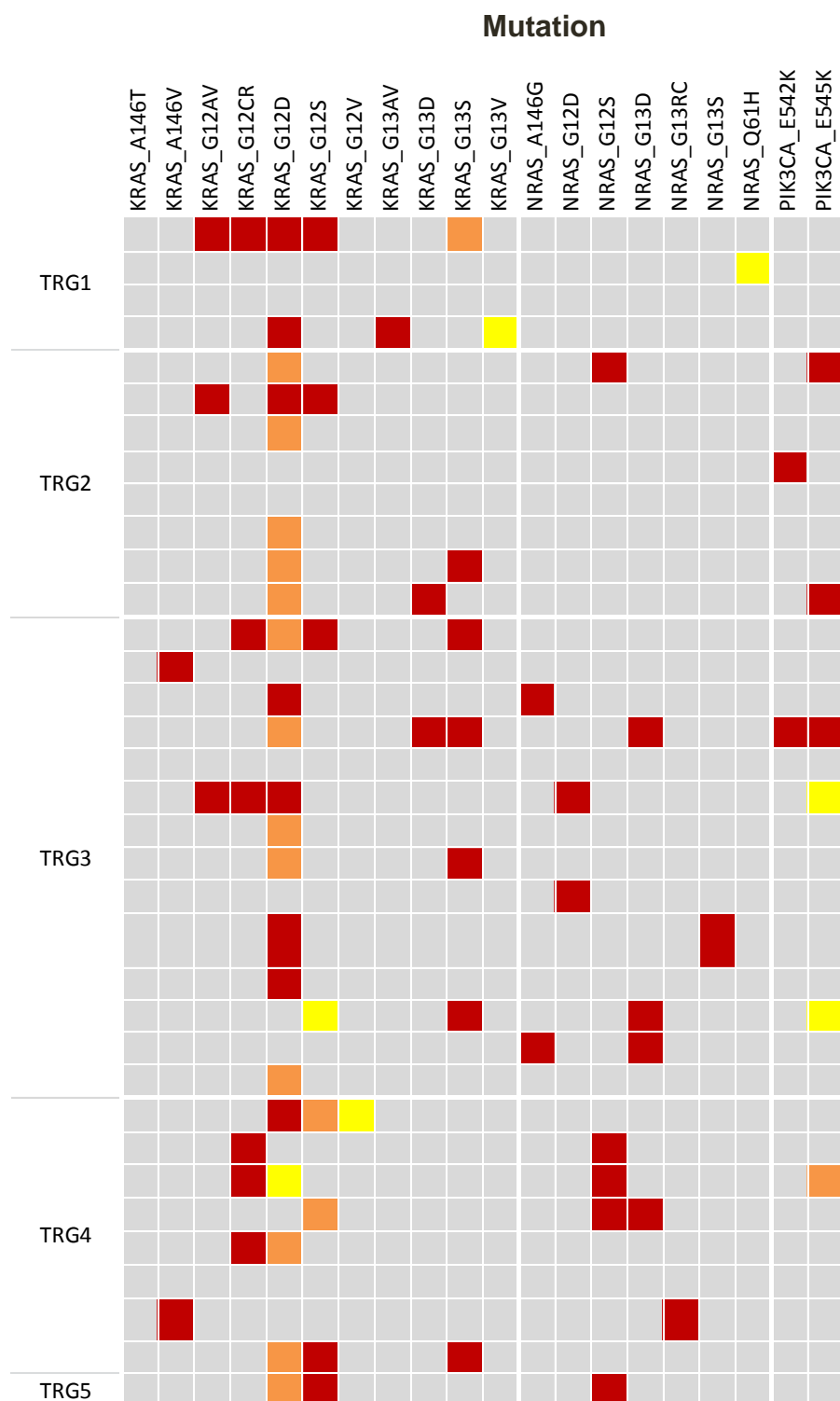


Figure 4.9: Mutations identified in pre-treatment tumour tissue and ctDNA samples from LARC patients enrolled in the TRILARC clinical trial, and divided according to TRG status.

DNA was extracted and mutational analysis carried out on ctDNA and tumour tissue samples collected from 35 LARC patients prior to NACRT treatment. Mutations are represented in yellow (present in pre-treatment biopsy sample only), red (present in pre-treatment ctDNA sample alone) or orange (present in both pre treatment biopsy and ctDNA samples), whilst WT is represented as grey

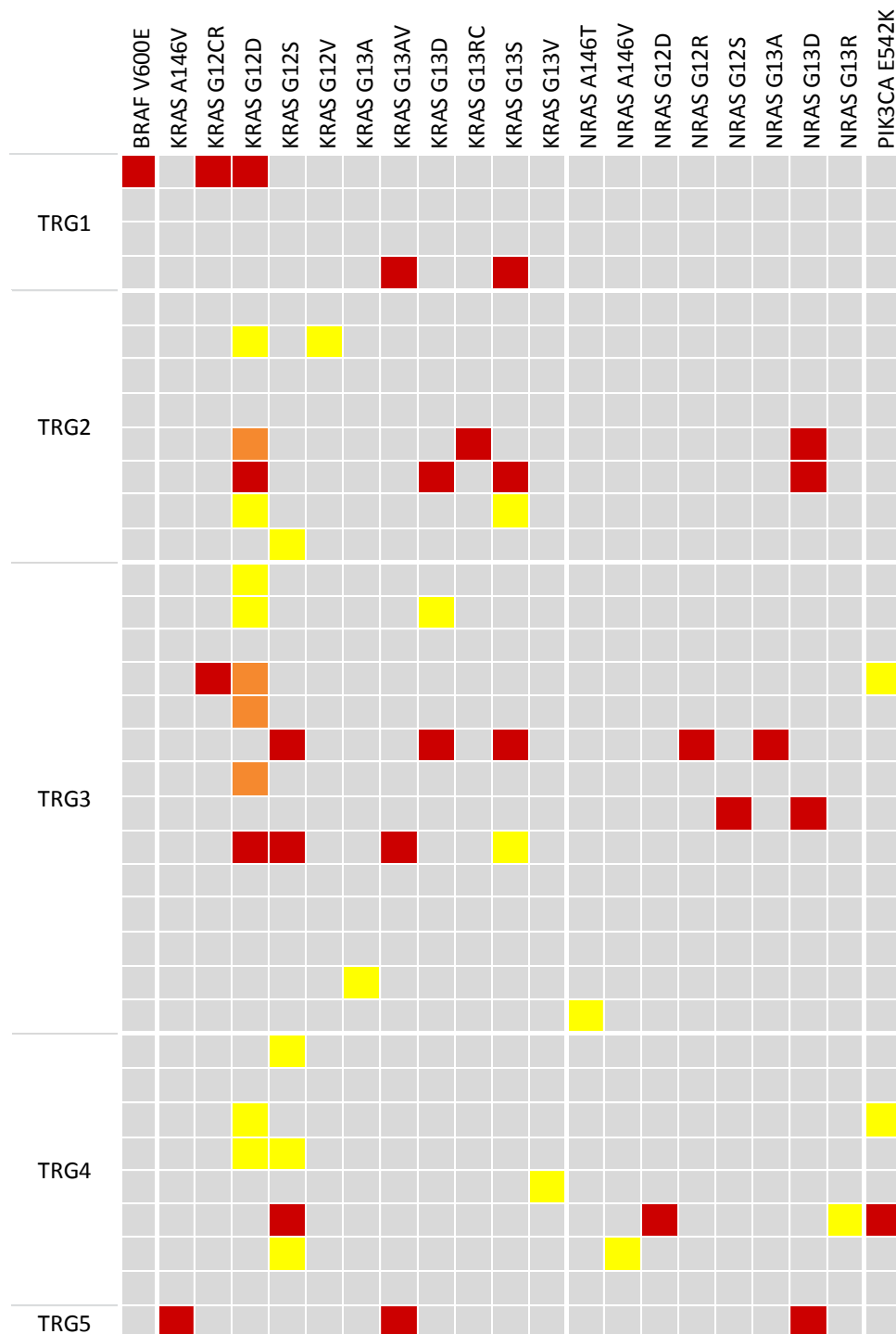


Figure 4.10: Mutations identified in surgical resection tumour tissue and ctDNA samples from LARC patients enrolled into the TRILARC clinical trial. DNA was extracted and mutational analysis carried out on ctDNA and tumour tissue samples collected from 35 LARC patients post-surgical procedure. Mutations are represented in yellow (present in surgically resected tissue sample only), red (present only in ctDNA sample taken at the time of surgical resection alone) or orange (present in both surgical resection tissue and ctDNA samples), whilst WT is represented as grey.

4.2.5. Intra-tumour mutational alterations as a result of NACRT treatment

Of the 77 mutations identified in the pre-treatment ctDNA and/or biopsy samples, only 19.4% of mutations remained throughout treatment. Meanwhile, 72.7% of ctDNA and/or biopsy mutations were lost prior to surgical resection (Figure 4.11). These included all mutations in *KRAS*^{G12AV}, *NRAS*^{G13S}, *NRAS*^{Q61H} and *PIK3CA*^{E545K}. However, an additional 36 mutations were gained over the course of NACRT treatment. Mutations gained during treatment included mutations in *BRAF* (V600E), *KRAS* (G13A, G13RC) and *NRAS* (A146V, G12R, G13A, G13R, A146T).

We found that patients who retained their E545K mutations progressed into metastatic tumours. Furthermore, metastatic patients lost mutations in *KRAS*^{G12AV} (n = 1), *KRAS*^{G13S} (n = 1), *NRAS*^{G12S} (n = 4) and *NRAS*^{G13D} (n = 1). Meanwhile, one patient gained an *NRAS*^{A146V} mutation.

In addition, patient 19 is the only patient who was graded as TRG5 at surgery. Upon surgical resection, this patient displayed a different array of mutations than previously identified. They lost all their previous mutations (*KRAS*^{G12D}, *KRAS*^{G12S}, *NRAS*^{G12S}), but gained a whole new group of mutations (*KRAS*^{146V}, *KRAS*^{G13AV}, *NRAS*^{G13D}).

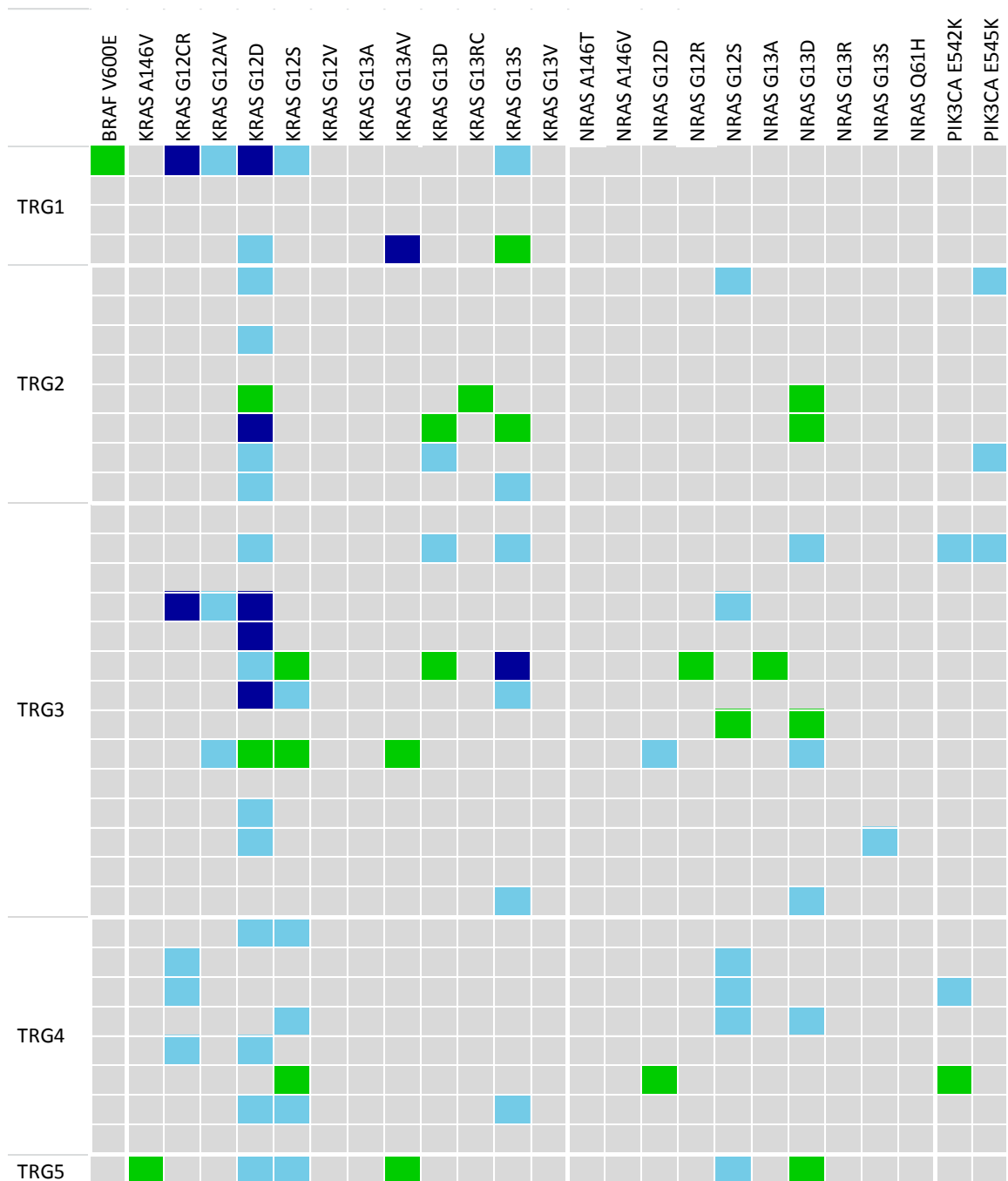


Figure 4.11: Overview of mutational status before and post-NACRT treatment.

DNA was extracted and mutational analysis carried out on ctDNA samples collected from 35 LARC patients prior to NACRT, and post-surgical procedure. This graph represents if ctDNA mutations were lost (light blue), gained (green) or retained (dark blue) throughout NACRT treatment. WT is represented as grey.

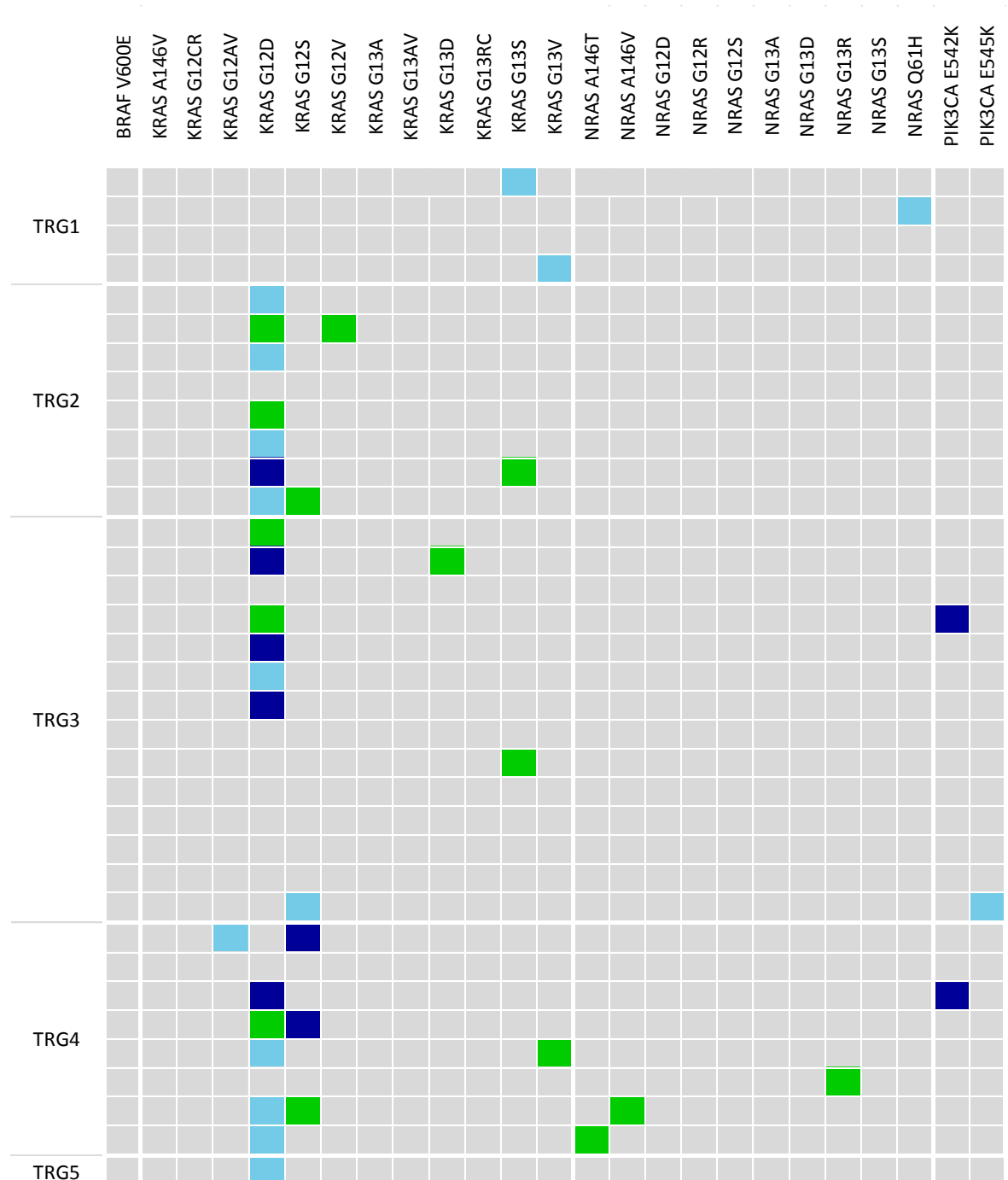


Figure 4.12: Overview of mutational status identified in tumour tissue samples before and post-NACRT treatment.

DNA was extracted and mutational analysis carried out on tumour tissue samples collected from 35 LARC patients prior to NACRT and post-surgical procedure. This graph represents if tumour tissue mutations were lost (light blue), gained (green) or retained (dark blue) throughout NACRT treatment. WT is represented as grey.

4.2.6. Mutational characteristics identified in metastatic LARC patients.

To date, 8 patients have been identified with metastasis, four of whom have died. Metastases occurred in the liver (75%, n = 6), lungs (62.5%, n = 5), bone (25%, n = 2), brain (25%, n = 2) and peritoneum (12.5%, n = 1). Patient demographics are represented in Table 4.3.

17 mutations were identified in the *KRAS* (n = 10), *NRAS* (n = 5) and *PIK3CA* (n = 2) genes. 78.2% of mutations were identified in ctDNA samples only, compared to 15.1% in tissue samples and 6.7% of mutations identified in both tissue and corresponding ctDNA (Figure 4.13). The lower frequency of mutations identified in tumour tissue samples is partly as a result of fewer tissue samples (n = 3), than ctDNA (n = 6) collected throughout the course of the study.

7/8 (87.5%) of TRILARC patients who progressed onto metastatic disease possessed a *PIK3CA* mutation.

Table 4.3: Patient demographics of TRILARC study population who progressed onto metastatic disease.

LARC patients (n = 8) were enrolled into the TRILARC clinical trial and treated with neoadjuvant chemoradiation therapy (NACRT). Patients were assessed according to their response to treatment according to the TRG scoring system. TRG categories were defined as TRG1 - TRG5. DNA was extracted and mutational analysis carried out on ctDNA and tumour tissue samples collected from 8 LARC patients at various time-points before, during and after NACRT treatment (ctDNA = pre-treatment, week 3 of CRT, last week of CRT, 4 weeks post CRT, post-surgical procedure and 1 year post-surgical procedure; tumour tissue = pre-treatment, week 3 of CRT, surgical procedure, recurrence).

Age (years)					
Average					65.6
Range					42-80
Median					68.5
Gender (n = 8)					
Male	6				(75%)
Female	2				(25%)
Treatment type (n = 8)					
IMRT	5				(62.5%)
Control 3-DCRT	3				(37.5%)
TRG grade (n = 8)					
TRG1 - Complete regression, no detectable tumour	0				(0%)
TRG2 - Fibrosis with scattered tumour cells	2				(25%)
TRG3 – Fibrosis containing tumour cells	2				(25%)
TRG4 – Tumour containing fibrosis	4				(50%)
TRG5 - No tumour regression	0				(0%)
Metastatic sites (n = 8)					
Liver	6				(75%)
Lungs	5				(62.5%)
Bone	2				(25%)
Brain	2				(25%)
Peritoneum	1				(12.5%)
Total number of ctDNA mutations					
	BRAF	EGFR	KRAS	NRAS	PIK3CA
Pre-treatment	-	-	16	4	1
Week 3 of chemoradiation	-	-	17	5	2
Last week of chemoradiation	-	-	16	8	3
4 weeks post chemoradiation	-	-	19	3	4
Surgical procedure	-	-	3	-	-
1 year post surgery	-	-	-	-	-
Total number of biopsy mutations					
	BRAF	EGFR	KRAS	NRAS	PIK3CA
Pre-treatment	-	-	7	-	2
Week 3 of CRT	-	-	-	-	-
Surgical procedure	-	-	10	1	2
Recurrence	-	-	4	-	-

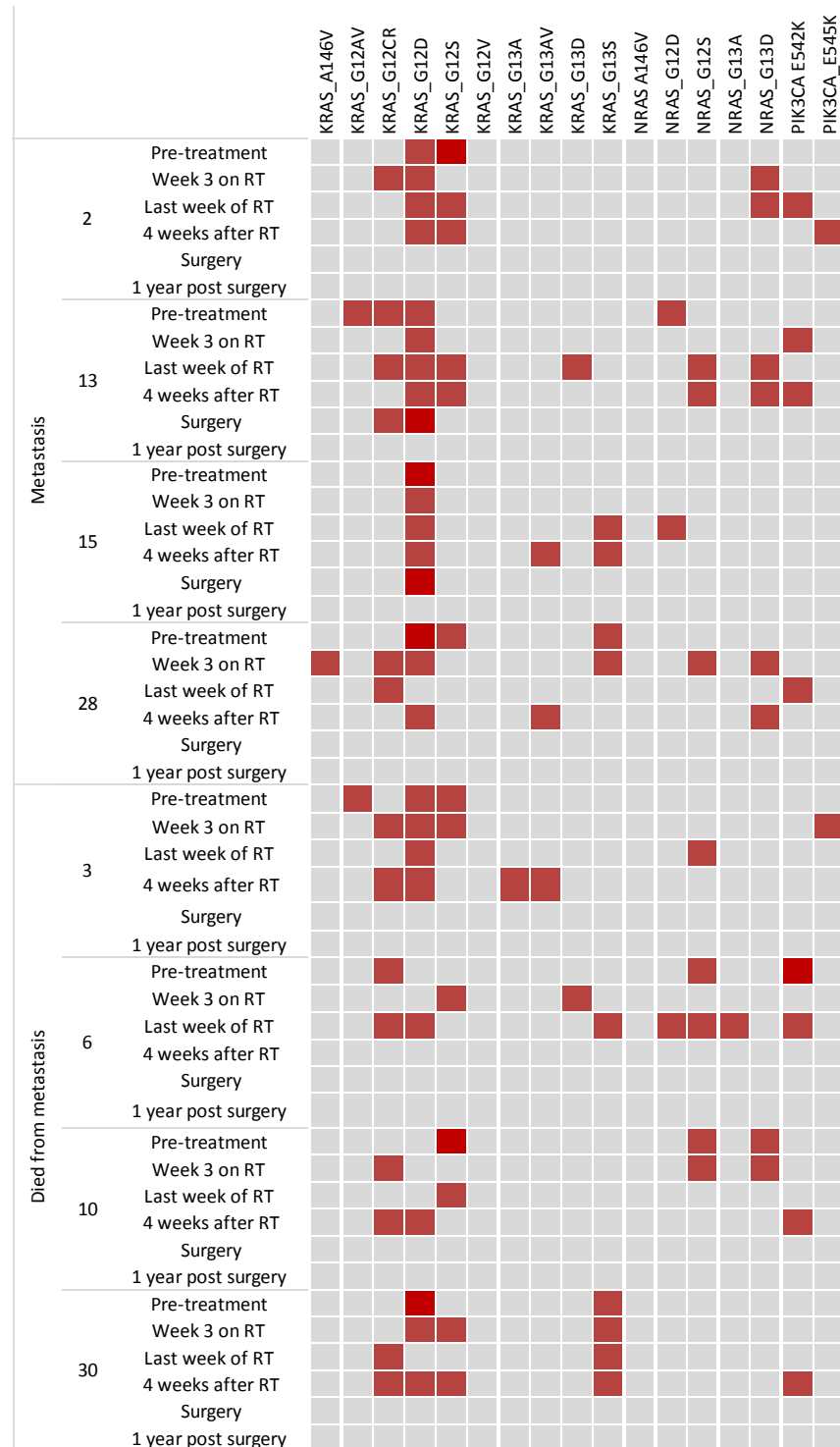


Figure 4.13: Mutations identified in ctDNA of eight LARC patients who developed recurrent rectal cancer.

DNA was extracted and mutational analysis carried out on ctDNA samples collected from 8 LARC patients at various time-points before, during and after NACRT treatment from (pre-treatment, week 3 of CRT, last week of CRT, 4 weeks post CRT, post-surgical procedure and 1 year post-surgical procedure) samples. Mutations are represented in red (ctDNA) or grey (WT).

			KRAS_A146V	KRAS_G12AV	KRAS_G12CR	KRAS_G12D	KRAS_G12S	KRAS_G12V	KRAS_G13A	KRAS_G13AV	KRAS_G13D	KRAS_G13S	NRAS_A146V	NRAS_G12D	NRAS_G12S	NRAS_G13A	NRAS_G13D	PIK3CA_E542K	PIK3CA_E545K
Metastasis	2	Pre-treatment																	
		Week 3 on RT																	
		Surgery																	
	13	Recurrence																	
		Pre-treatment																	
		Week 3 on RT																	
		Surgery																	
	15	Recurrence																	
		Pre-treatment																	
		Week 3 on RT																	
		Surgery																	
	28	Recurrence																	
Died from metastasis	3	Pre-treatment																	
		Week 3 on RT																	
		Surgery																	
	6	Recurrence																	
		Pre-treatment																	
		Week 3 on RT																	
		Surgery																	
	10	Recurrence																	
		Pre-treatment																	
		Week 3 on RT																	
		Surgery																	
	30	Recurrence																	
		Pre-treatment																	
		Week 3 on RT																	
		Surgery																	
		Recurrence																	

Figure 4.14: Mutations identified in tumour tissue of eight LARC patients who developed recurrent rectal cancer.

DNA was extracted and mutational analysis carried out on tumour tissue samples collected from 8 LARC patients pre-treatment, week 3 of chemoradiation (CRT), surgical procedure and recurrence samples. Mutations are represented in yellow (tissue), or grey (WT).

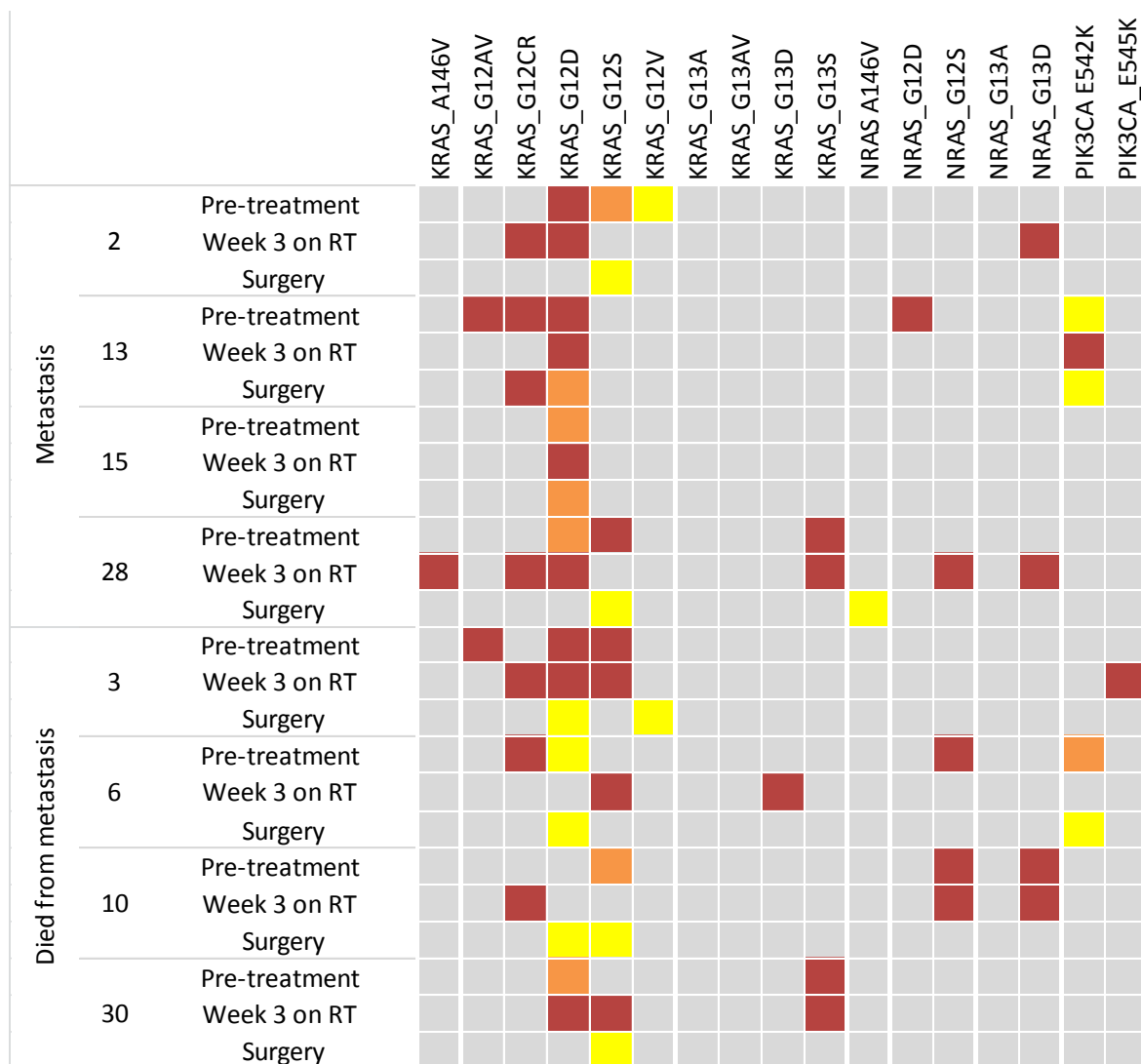


Figure 4.15: Mutations identified in ctDNA of eight LARC patients who developed recurrent rectal cancer.

DNA was extracted and mutational analysis carried out on ctDNA and tumour tissue samples collected from 8 LARC patients at various time-points before, during and after NACRT treatment from (ctDNA = pre-treatment, week 3 of chemoradiation (CRT), last week of CRT, 4 weeks post CRT, post-surgical procedure and 1 year post-surgical procedure; tumour tissue = pre-treatment, week 3 of CRT, surgical procedure, recurrence) samples. Mutations are represented in red (ctDNA only), yellow (tissue only) orange (ctDNA and tissue) or grey (WT).

4.3. Discussion

Treatment for CRC is currently based upon TNM stage, with all LARC patients being treated uniformly with NACRT (chemoradiation therapy for approximately 6 weeks followed by surgical resection of the tumour). Although patients present with the same tissue, histological subtype and stage disease; the response to treatment is far from uniform, with 15-27% of patients achieving pathological complete response (pCR). A further 25-50% of LARC patients will relapse as a result of metastasis. In the hope of further understanding the mechanisms behind tumours response, or lack thereof to current treatment regimens and of identifying novel biomarkers of treatment response, we monitored LARC patients before, during and after NACRT treatment.

11.4% of patients in our cohort achieved pathologic complete response (pCR), whereby no tumour was remaining at tumour resection post chemoradiation therapy. This is slightly lower than current findings as previously stated, which show 15-27% of LARC patients achieve pCR (15).

Variability between radiation therapies

Patients in the TRILARC clinical trial were treated with 3-DCRT or the novel IMRT. Studies have shown that IMRT has improved target coverage and dose uniformity, whilst also minimising toxicity levels to normal surrounding tissue, compared to 3-DCRT (243). Although preliminary, we also found that only patients who received IMRT (22%) achieved pCR, compared to none from the 3D-CRT cohort.. Li et al did not find any difference in complete remission rates in patients with extra nodal natural killer / T-cell lymphomas when treated with IMRT or 3-DCRT. However, they did report that IMRT patients displayed increased local recurrence-free survival, progression-free survival and overall survival than that of the 3-DCRT cohort (244). Furthermore, Xu et al reported increased overall survival rates in patients with oesophageal cancer treated with IMRT compared to 3-DCRT(245). Our findings need further follow up and completion of the TRILARC clinical trial to verify.

Gender variances

CRC is more common in males than females; in our study 68.6% of our cohort was male. However, we found females participating in the study were more likely to achieve pCR (18.2%) compared to males (8.3%). This correlates with Abdalmassih et al, who also found that female RC patients have better survival rates post-NACRT than males (241). However, again, our results are preliminary and require further follow up and completion of the TRILARC trial to verify.

Metastatic sites

Sites of tumour metastasis from patients included in our cohort included the liver (75%, n = 6), lungs (62.5%, n = 5), bone (25%, n = 2), brain (25%, n = 2) and peritoneum (12.5%, n = 1). RC usually metastasises to the liver, lungs, bones, peritoneum, locoregional or distant lymph nodes (32), however brain metastases are a rare occurrence for RC. Brain metastasis are reported to occur in 0.6 – 3.2% of rectal cancer cases (246). Currently, we are reporting brain metastasis in 3.03% of our total cohort. However the clinical trial is still ongoing with many patients still undergoing the process of NACRT for their primary tumours, therefore these percentages are likely to rise further.

Circulating tumour cells

Our study found more than a two-fold increase in the detection frequency and number of CTCs during week 3 (50% patients positive for CTCs) and last week of radiation therapy (46.4%) compared to pre-treatment (22.2%). This is in agreement with numerous studies which have also found an increase in CTCs during chemoradiation therapy (247,248). However, we noted that this increase in CTC positivity and volume identified was limited to patients who did not achieve pCR (TRG2-5), whilst patients who did achieve pCR were unaffected by chemoradiation therapy.

Furthermore, Martin et al, also identified an increase in circulating tumour microemboli (CTMs) released into the periphery during radiation therapy (248). This correlates with our findings that CTMs were released during the early stages of CRT (week 3 of CRT). However, we did not identify any CTMs during the last week of CRT.

ctDNA vs tissue

Our cohort displayed mutational variability between ctDNA and tissue samples. This could be down to several reasons. Tumours are commonly formed from numerous clones as a result of intra-tumour heterogeneity. Tissue samples are typically only representative of a small fraction of the tumour and its corresponding mutations, whereas ctDNA is released from all tumour cells. Furthermore, both sample types were run on two different mutational analytical panels. Whilst both panels detect mutations in *BRAF*, *EGFR*, *KRAS*, *NRAS* and *PIK3CA*, the volume of variants differs between the panels. DNA extracted from tissue was run on the iPLEX HS Colon Panel which detects 86 mutational variants, whereas ctDNA was run on the UltraSEEK Colon Panel which detects 107 mutational variants.

Due to mutational variabilities between tissue and ctDNA samples, we feel the patient mutational profile perhaps should be compiled from both methods. This will potentially give a mutational profile which is more representative of the tumour as a whole without the need for multiple biopsies, whilst potentially simultaneously representing the mutational profile of micrometastases throughout the body. Similar findings and conclusion were found by Toor et al in respect to lung and gastrointestinal cancers (249).

Mutations

KRAS mutations are reported in 35-47% of CRCs (93,104–107). However we identified *KRAS* mutations in 100% of ctDNA and 70% of tissue specimens from our TRILARC cohort. *KRAS*^{G12D} mutations were identified in 94.7% of patients at some point during their time in the TRILARC clinical trial. This is most likely due to the ultra-sensitive detection methods used herein. The UltraSEEK and iPLEX HS colon panels can detect mutational variants in samples with mutational allele frequencies as low as 0.1% and 1%, respectively. Chen et al reported *KRAS* mutations in 93.7% of their cohort when analysing ctDNA, and too found *KRAS*^{G12D} to be the most common mutation (250).

PIK3CA gene mutations are reported to occur in 8-20% of CRC cases (89,99,100). However our study identified *PIK3CA* mutations in 50% of patients from our TRILARC clinical trial; with *PIK3CA* mutations identified in 7.9% of tissue samples (iPLEX) compared to 47.4% of ctDNA samples (UltraSEEK). Both techniques

identify the same four *PIK3CA* mutations, therefore variations between both samples are possibly a result at least in part of intra-tumour heterogeneity.

19 patients in the TRILARC clinical trial (50%) were *PIK3CA*-*KRAS*^{co-mut}. Of which, 7 patients have since progressed onto metastatic disease. All 7 patients had *KRAS* mutations in G12CR, G12D and G12S, whilst 85.7% of these patients also harboured *PIK3CA*^{E542K} mutations in their tumours.

Furthermore, 83.3% (n = 5) of TRILARC patients with *PIK3CA* mutations at both E542K and E545K also harboured G13S mutations.

Importance of ctDNA analysis

ctDNA identified 63.6% of pre-treatment and 52.8% of surgical mutations which were not identified in tissue samples at either time-point. In addition, *NRAS* mutations were most commonly identified in ctDNA (n = 87), compared to tissue (n = 4). This is a result of intra-tumour heterogeneity, along with the UltraSEEK Colon Panel including an additional 10 mutational variants than that of the iPLEX HS Colon Panel.

Furthermore, mutations in *KRAS* (*G12AV*, *G12DR*, *G13AV*, and *G13D*); *NRAS* (*G12D*, *G12S*, *G13D*, and *G13S*) and *PIK3CA* (*E545K*) were only identified in ctDNA samples. Since the variants are present in both panels, this could be due in part to tumour heterogeneity. Tissue biopsies only sample tissue from one location of the tumour. As seen previously in chapter 3, tumours are vastly heterogeneous, therefore biopsy sampling limits the volume of mutations which can be identified. ctDNA is released from all cancerous cells, and therefore may allow identification of more mutations and produce a more reliable depiction of the tumours mutational status as a whole.

Determination in-vitro if inhibition of the PI3K and MAPK signalling pathways augments rectal cancer chemoradiotherapy sensitivity.

5.1. Introduction

The phosphatidylinositol-3-kinase (PI3K) and mitogen-activated protein kinase (MAPK) pathways are two signalling cascades involved in the activation and regulation of vital cellular functions such as proliferation, differentiation, apoptosis, transcription and intracellular trafficking. Somatic genetic alterations which activate the pro-oncogenic PI3K and MAPK signalling pathways have been linked to multiple forms of cancers, including CRC (91–93).

5.1.1. Current treatment of colorectal cancer

The standard treatment of locally advanced rectal cancer (LARC) is neoadjuvant chemoradiation therapy (NACRT), consisting of 5-fluorouracil (5-FU) or Capecitabine combined chemoradiotherapy for approximately 6 weeks, followed by surgical resection of the tumour. Currently, 73-85% of LARC patients fail to achieve a pathological complete response (pCR). These patients have remaining cancerous cells, ranging from scattered cells to large islands of resistant tumour in their resected tissue post-chemoradiation therapy (15). As a result, these patients have subsequent high relapse and death rates (16).

5.1.2. Chemoradiotherapy resistance within colorectal cancer patients

We, and others have shown that PI3K and MAPK pathway mutations are associated with resistance to chemotherapy and radiation therapy, and poor patient outcomes (93,192–194). Therefore, we hypothesise that inhibition of the PI3K and MAPK signalling pathways may have the potential to augment rectal cancer chemoradiotherapy sensitivity, thereby increasing treatment effectiveness in LARC.

5.1.3. PI3K pathway mutations associated with colorectal cancer

The majority of PI3K pathway mutations in rectal cancer patients occur within the *PIK3CA* oncogene, and the *PTEN* tumour suppressor gene. Somatic missense mutations, deletions and amplifications in *PIK3CA* have been linked to multiple forms of cancer, including CRC (92,95,100,251). *PIK3CA* mutations have been reported in 8-20% of all CRC cases (99,100), with 80% of these mutations occurring in three hotspots; codons 542, 545 (exon 10) and codon 1047 (exon 21) (92). All three hotspot mutations are known to be oncogenic and increase PI3K

activity (92,252–254). In general, patients with *PIK3CA* mutations are less likely to achieve pCR (93) and have a higher risk of local recurrence with a more rapid onset than patients who are wild-type for *PIK3CA* (99).

PTEN is mutated in 5-14% of all CRC cases, with the higher frequency found in MSI tumours (101,102). Loss of *PTEN* expression is associated with decreased overall survival (103).

5.1.4. PI3K inhibitor, Copanlisib

There are currently multiple PI3K pathway inhibitors in clinical development, which target various elements within the PI3K pathway; however our study will focus on the Bayer PI3K inhibitor, Copanlisib. Copanlisib is a potent, highly selective, small-molecule PI3K inhibitor which preferentially inhibits the PI3K Class I catalytic isoforms p110 α and p110 δ ; although it also has the ability to inhibit the p110 β and p110 γ isoforms to a lesser degree (122). Copanlisib has been shown to have pro-apoptotic and anti-tumorigenic properties both in vivo and in vitro (122,124–126). It is currently involved in several clinical trials for cancers including HER2 positive breast cancer (phase 1/2), Endometrial endometrioid adenocarcinoma (phase 2) and Non-Hodgkin's lymphoma (phase 3).

5.1.5. MAPK pathway mutations associated with colorectal cancer

The most common mutations in CRC within the MAPK pathway are located in the *KRAS* (35-47%)(93,104), and *BRAF* (5-10%) oncogenes (93,105,107). 95% of *KRAS* mutations occur in codons 12 (80%) and 13 (15%) of exon 2. Approximately 5% of all CRC *KRAS* mutations occur within exon 3 (codon 61) and exon 4 (codon 146). These hotspot mutations have been linked with resistance to anti-EGFR therapies (108), poor recurrence-free survival and overall survival (93,109,116). *RAS* plays an important role in both the PI3K and MAPK signalling pathways; therefore a mutation within *RAS* can affect both pathways. 80% of all *BRAF* mutations in CRC patients occur at *V600E* (91). This mutation is indicative of a poor prognosis, particularly in microsatellite stable CRCs (115).

5.1.6. MEK inhibitor, Refametinib

Refametinib, also known as RDEA119, or BAY86-9766; is a highly selective, allosteric, small-molecule MEK 1/2 inhibitor. Iverson et al previously demonstrated that it has increased sensitivity to MEK1 over MEK2 in vitro (IC_{50} 19nM vs 47nM) (255). Refametinib has been involved in 10 phase 1/2 clinical trials worldwide. These clinical trials involved a range of solid tumours, particularly hepatocellular, pancreatic and advanced-stage tumours; and in some, refametinib was combined with drugs such as Sorafenib, Gemcitabine, Regorafenib and Copanlisib (256–258). However, BAYER has now decided to not to pursue refametinib for additional preclinical or clinical oncology research at this time, due to toxicity concerns.

5.1.7. Copanlisib and Refametinib targeting the PI3K and MAPK pathways.

Copanlisib and refametinib target the PI3K ($p110\alpha$, δ) and MAPK (MEK1/2) pathways respectively. Prior knowledge of the signalling pathways and drug targets has led to 5 theoretical scenarios which we predict to occur within *PI3K/MAPK* mutated cell lines. These are outlined in Figure 5.1 – 5.3.

Wild-type: Since *WT* cell lines do not harbour mutations within either pathway, we predict that they will be non-responsive to either inhibitor.

PIK3CA mutant: *PIK3CA* mutations only affect the PI3K pathway; therefore we envisage these cell lines will be sensitive to the PI3K inhibitor copanlisib, and non-responsive to refametinib.

KRAS mutant: *KRAS* is involved in both the PI3K and MAPK pathways, therefore it is expected that *KRAS* mutated cell lines will be sensitive to either drug alone, with heightened sensitivity for the two inhibitors used in combination.

BRAF mutant: *BRAF* is only present in the MAPK pathway, and should therefore be primarily targeted by the MEK inhibitor, refametinib. Copanlisib does have a weak inhibitory effect on mTOR, which may slightly inhibit the MAPK pathway, but to a far lesser degree than that of refametinib.

PIK3CA-KRAS mutant: Similar to *KRAS* mutated, these cell lines are involved in both the PI3K and MAPK pathways, therefore we predict these tumours would respond to either drug alone, but a combination of both drugs would be necessary for optimal inhibition.

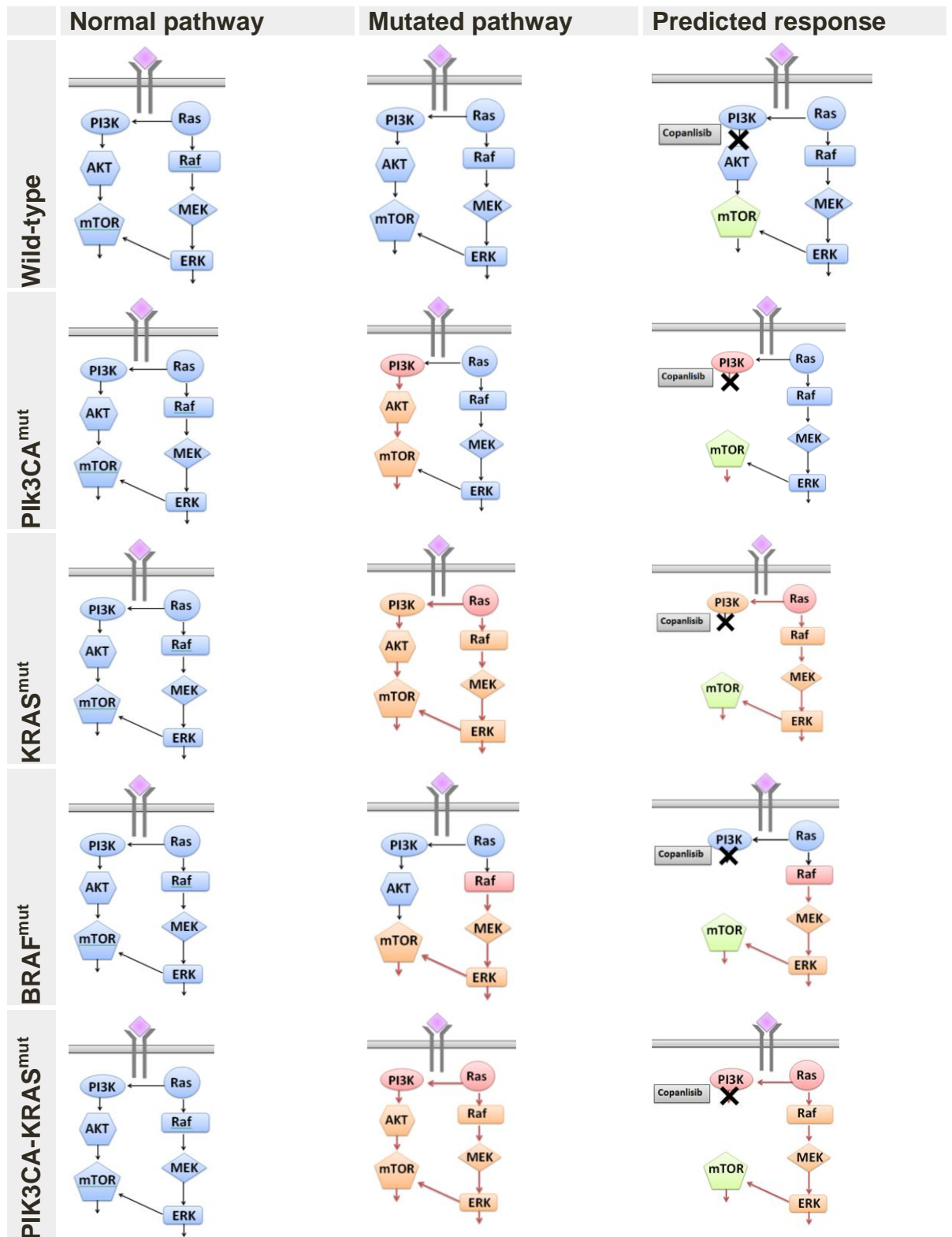


Figure 5.1: Representation of the effects of PIK3CA, RAS, RAF and PIK3CA/RAS mutations within the cells, and how PI3K inhibitors alter the signalling pathways.

The chart represents normal functioning proteins (blue), mutated proteins (red), proteins affected as a result of the mutation (orange), proteins which have been partially inhibited (green), and the inhibitors target (X).

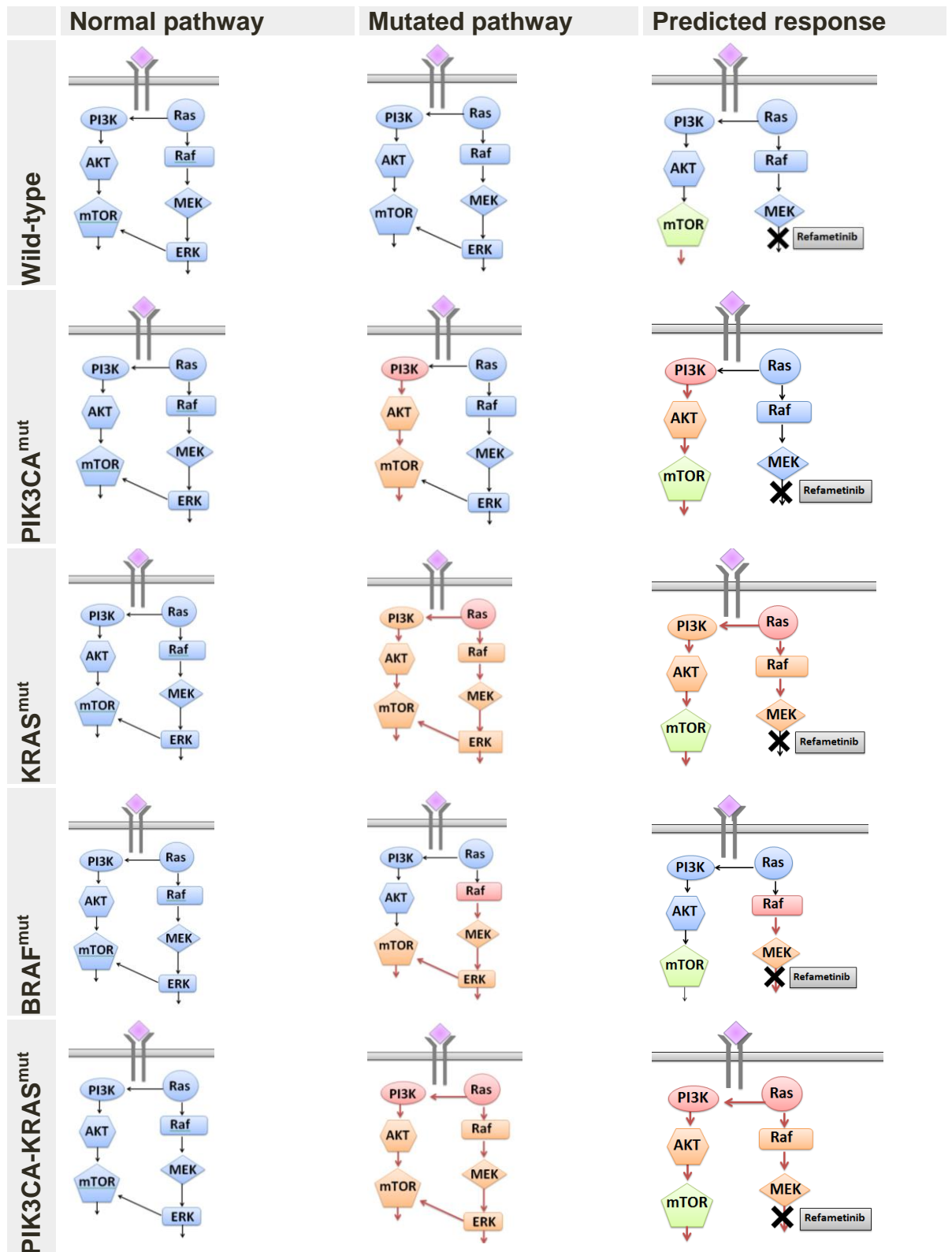


Figure 5.2: Representation of the effects of PIK3CA, Ras, Raf and PIK3CA/Ras mutations within the cells, and how MEK inhibitors alter the signalling pathways.

The chart represents normal functioning proteins (blue), mutated proteins (red), proteins affected as a result of the mutation (orange), proteins which have been partially inhibited (green), and the inhibitors target (X).

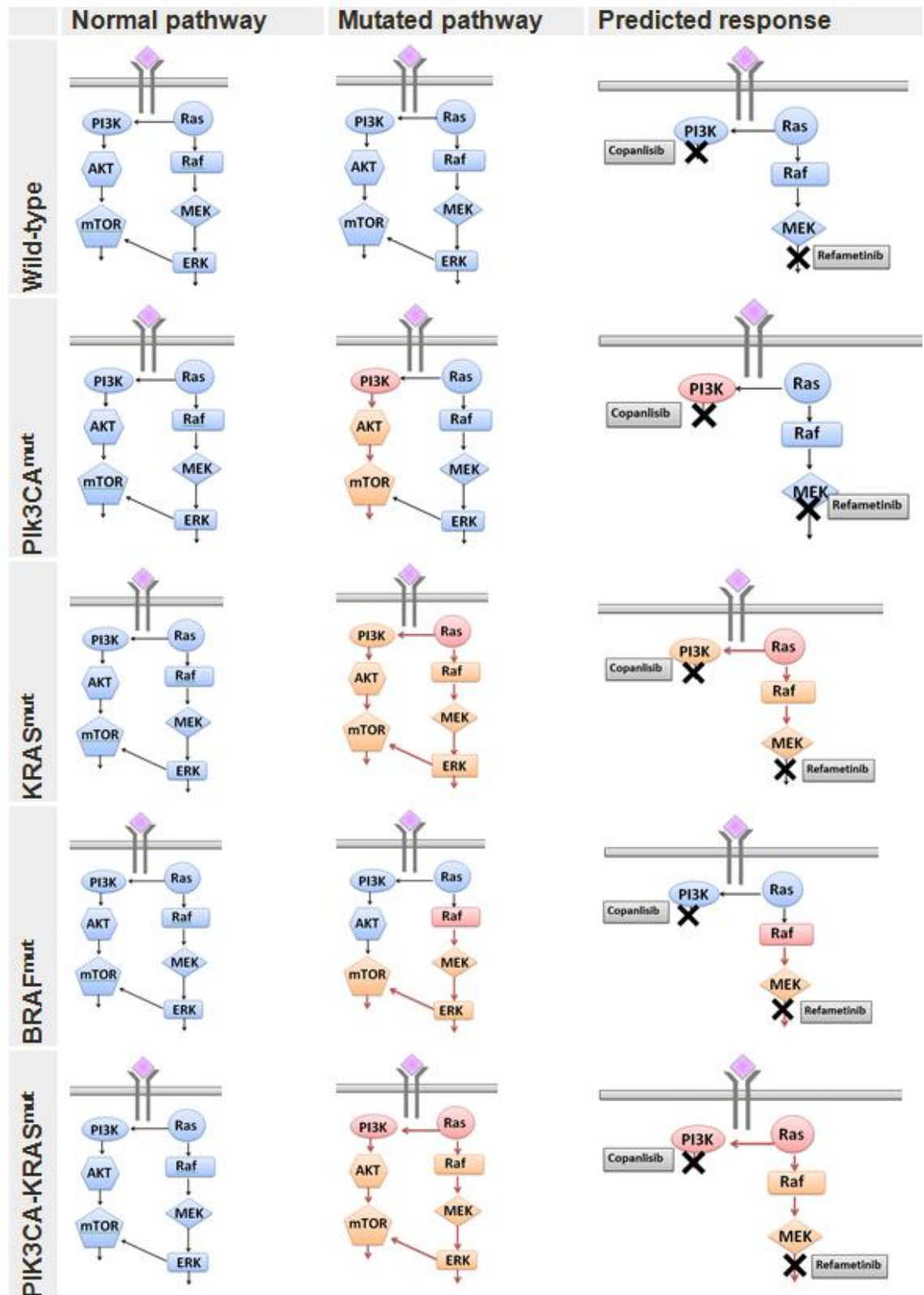


Figure 5.3 Representation of the effects of PIK3CA, Ras, Raf and PIK3CA/Ras mutations within the cells, and how a combination of PI3K and MEK inhibitors alter the signalling pathways.

The chart represents normal functioning proteins (blue), mutated proteins (red), proteins affected as a result of the mutation (orange), proteins which have been partially inhibited (green), and the inhibitors target (X).

The objectives of the research described in this chapter were to:

1. Investigate whether copanlisib and refametinib inhibit proliferation in a panel of CRC cell lines exhibiting a range of PI3K and MAPK pathway mutations.
2. To ascertain whether PI3K and MAPK pathway mutations alter CRC cells proliferative abilities to form whole colonies from single cells, post copanlisib, refametinib or chemotherapy treatment.
3. To determine if copanlisib and refametinib enhance chemoradiotherapy sensitivity in CRC cancer cell lines with or without mutations within the PI3K and/or MAPK pathways.

5.2. CRC cell line anti-proliferative response to copanlisib and/or refametinib in vitro is dependent on their PI3K and MAPK pathway mutational status.

As discussed in section 5.1.1, mutations within the PI3K and MAPK signalling pathways have been linked not only to the formation of multiple forms of cancers, including CRC, but also to their resistance to chemotherapy and radiation therapy. The novel Bayer PI3K α inhibitor copanlisib, and MEK 1/2 inhibitor refametinib have been shown to cause anti-proliferative and pro-apoptotic effects in various forms of cancer cells, including breast, endometrial, gastric and lung (122,259). However little work has been carried out on the anti-proliferative effects of copanlisib and refametinib (as single and dual agents) in PI3K and MAPK mutated CRC cell lines.

5.2.1 Identification of a panel of colorectal cancer cell lines with varying PI3K/MAPK pathway mutations

We acquired a panel of 10 CRC cell lines of varying PI3K and / MAPK pathway mutations. Mutational status was analysed using data from the cancer cell line encyclopedia and COSMIC databases (90,176). All cell lines were validated via STR powerplex assay (Source BioScience, LifeSciences), and mutations were confirmed in our cell lines using Agena MassArray analysis.

Cell lines were divided into 5 different groups depending on mutational status: wild type (WT) (C2BBE1, Caco-2, CL-14), *BRAF* mutated (LS-411N, Colo-205), *PIK3CA* mutated (SNU-C4), *KRAS* mutated (LS-513, LS-1034) and *PIK3CA-KRAS* co-mutated (DLD-1, LS-174T). The details of the cell lines and their mutational status are described in Table 5.1.

Table 5.1: Mutation status of the colorectal cancer cell lines included in the study.

A panel of 10 CRC cell lines harbouring varying PI3K and / MAPK pathway mutation status was acquired. Mutational status was analysed using data from the cancer cell line encyclopedia and COSMIC databases. All cell lines were validated via an STR powerplex assay and mutations were confirmed in our cell lines using Agena MassArray analysis. Cell lines were divided into 5 different groups depending on mutational status: wild type (C2BBe1, Caco-2, CL-14), BRAF^{mut} (LS-411N, Colo-205), PIK3CA^{mut} (SNU-C4), KRAS^{mut} (LS-513, LS-1034) and PIK3CA-KRAS^{co-mut} (DLD-1, LS-174T).

Cell line	Tissue type of origin	PIK3CA mutation	KRAS mutation	BRAF mutation
C2BBe1 (ATCC CRL-2102)	Colonic enterocyte, colorectal carcinoma	WT	WT	WT
Caco-2 (ATCC HTB-37)	Colorectal adenocarcinoma	WT	WT	WT
CL-14 (ACC 504)	Colon, carcinoma	WT	WT	WT
LS-411N (ATCC CRL-2159)	Cecum, Dukes type B, colorectal carcinoma	WT	WT	V600E
Colo-205 (ATCC CCL-222)	Colon, Dukes type D, Colorectal adenocarcinoma.	WT	WT	V600E
SNU-C4 (KCLB 0000C4)	Colon, Colorectal adenocarcinoma	E545G	WT	WT
LS-513 (ATCC CRL-2134)	Dukes type C, colorectal adenocarcinoma	WT	G12D	WT
LS-1034 (ATCC CRL-2158)	Dukes type C, colorectal carcinoma	WT	A146P	WT
DLD-1 (ATCC CCL-221)	Colon, Dukes type C, colorectal adenocarcinoma	D549N, E545K, R741R	G13D	WT
LS-174T (ATCC CL-188)	Colon, Dukes type B, colorectal adenocarcinoma	H1047R	G12D	WT

5.2.2. Determination of copanlisib and refametinib sensitivity in a panel of colorectal cancer cell lines via MTS proliferation assays.

Proliferation assays were carried out on ten colorectal cancer (CRC) cell lines with varying PI3K / MAPK pathway mutational statuses as described in Table 5.1. Each cell line was plated in 96 well plates (10^3 cells/100ul/well), and treated with varying concentrations of copanlisib (maximum concentration = 200nm), refametinib (maximum concentration = 2000nm), or copanlisib and refametinib (maximum concentration = 200nm and 1000nm respectively). Plates were incubated at 37°C with 5% CO₂ for 5 days. Proliferation was measured via a colourimetric MTS assay whereby the colour intensity is directly proportional to cell viability within the well.

CRC cell lines harbouring PI3K pathway mutations (*PIK3CA* and/or *KRAS*) were sensitive to the PI3K inhibitor copanlisib (Figure 5.4, Table 5.2). The *PIK3CA*^{mut} *KRAS*^{WT} *BRAF*^{WT} cell line (SNU-C4) was the cell line most sensitive to copanlisib (mean IC₅₀ = 28 ± 6nM), with lower IC₅₀ values than either *PIK3CA*^{WT} *KRAS*^{mut} (LS-1034 IC₅₀ = 153 ± 25nM, LS-513 IC₅₀ = 74 ± 16nM), or *PIK3CA*-*KRAS*^{mut} (DLD-1 IC₅₀ = 84 ± 30nM, LS-174 IC₅₀ = 134 ± 29nM) cell lines. Neither the WT (C2BBE1, Caco-2, and CL-14) nor *BRAF*^{V600E} *PIK3CA*^{WT} *KRAS*^{WT} (LS-411N, Colo-205) cell lines achieved IC₅₀s when treated with copanlisib up to a maximum concentration of 200nm.

All mutated cell lines achieved IC₅₀s when treated with the MEK inhibitor refametinib (Figure 5.5, Table 5.2). The *KRAS*^{mut} *PIK3CA*^{WT} cell lines were most sensitive to refametinib (LS-1034 IC₅₀ = 44 ± 3nM, LS-513 IC₅₀ = 28 ± 8nM); followed by *BRAF*^{V600E} (LS-411N IC₅₀ = 190 ± 83nM, Colo-205 IC₅₀ = 478 ± 199nM); *PIK3CA*^{mut} (SNU-C4 IC₅₀ = 326 ± 144nM) and *PIK3CA*-*KRAS*^{co-mut} (DLD-1 IC₅₀ = 745 ± 245nM, LS-174T IC₅₀ = 560 ± 164nM) cell lines. The WT cell lines (CL-14, Caco-2 and C2BBE1) were resistant to the MEK inhibitor, and failed to achieve IC₅₀s even at the maximum concentration of 2000nm.

The combination of copanlisib and refametinib achieved IC₅₀'s for all mutated cell lines and the wild-type cell line C2BBE1 (Figure 5.6, Figure 5.7, Table 5.2).

Furthermore, the combination enhanced growth inhibition relative to testing either inhibitor alone in WT (C2BBe1), *PIK3CA*^{mut} (SNU-C4), *BRAF*^{V600E} (LS-411N, Colo-205) and *PIK3CA-KRAS*^{co-mut} (DLD-1, LS-174T) cell lines (figure 5.8). The *KRAS*^{mut} cell lines LS-1034 and LS-513 responded better to refametinib alone compared to the copanlisib: refametinib combination (LS-1034 IC₅₀ = 44nM vs 21:105nM; LS-513 IC₅₀ = 28nM vs 7:35nM). Wild-type cell lines CL-14 and Caco-2 failed to achieve an IC₅₀ with either drug alone or in combination.

The copanlisib-refametinib combination had a synergistic response in the majority of cell lines, apart from *KRAS*^{mut} LS-1034 and Wild type Caco-2, which had additive and nearly additive responses (LS-1034 CI @ ED₇₅ = 1.03 ± 0.64, Caco-2 CI @ ED₇₅ = 0.91 ± 0.69) (figure 5.7, table 5.2). The combination was most beneficial in two of the wild-type (CL-14, C2BBe1) and *PIK3CA-KRAS*^{co-mut} (DLD-1, LS-174T) cell lines. CL-14 showed very strong synergism (CI @ ED₇₅ = 0.02 ± 0.03), however it remained incapable of achieving an IC₅₀. DLD-1 (CI @ ED₇₅ = 0.20 ± 0.02), LS-174T (CI @ ED₇₅ = 0.25 ± 0.12), and C2BBe1 (CI @ ED₇₅ = 0.28 ± 0.15), all displayed strong synergism.

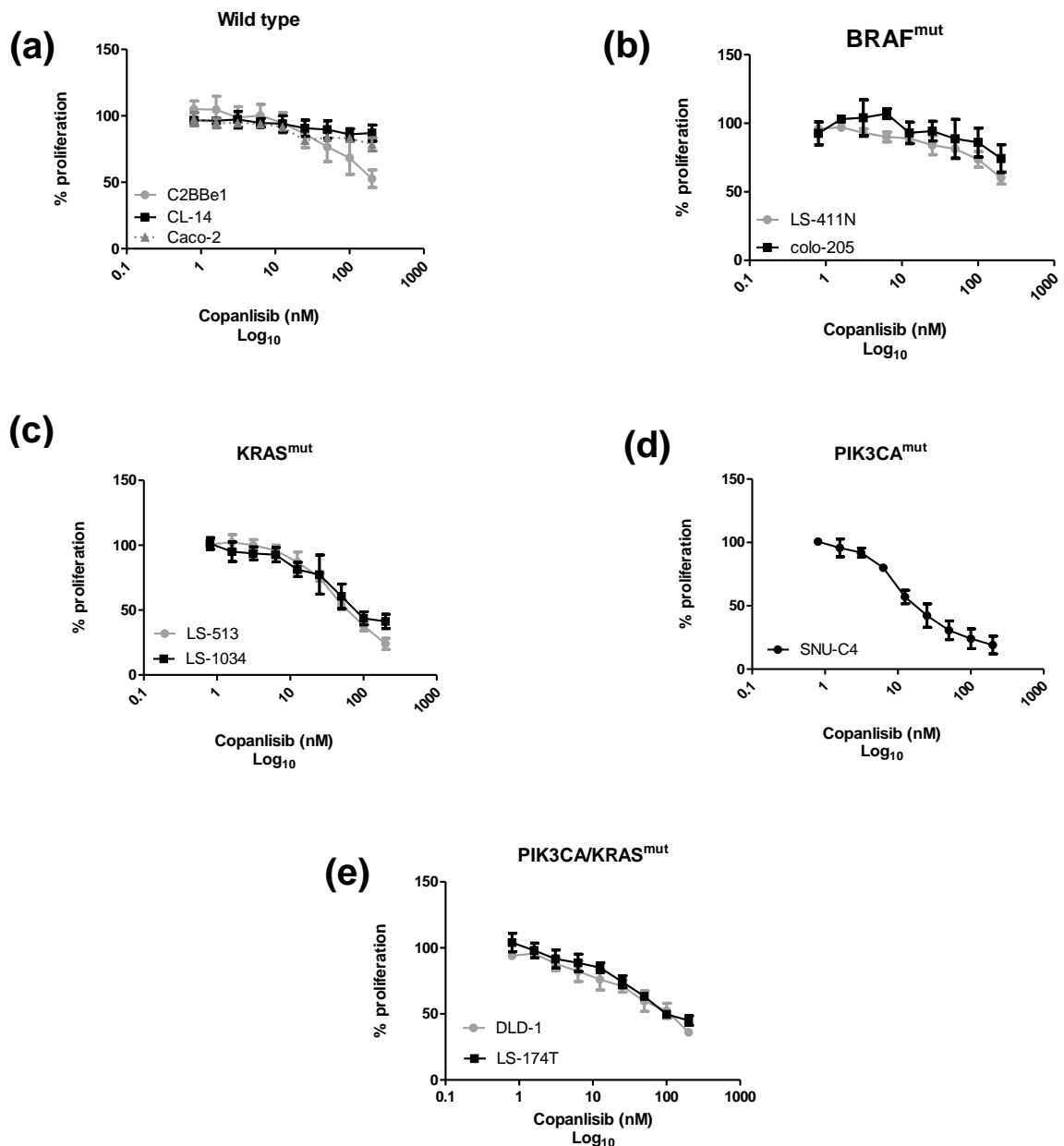


Figure 5.4: Efficacy of copanlisib in a panel of CRC cell lines with varying PI3K and MAPK pathway mutations, consisting of (a) Wild-type, (b) BRAF^{mut}, (c) KRAS^{mut}, (d) PIK3CA^{mut}, (e) PIK3CA-KRAS^{co-mut}.

Colorectal cancer lines were plated in triplicate at 1×10^4 cells/ml in 96 well plates (100ul per well). Cells were treated with serial 1:2 dilutions of the PI3K inhibitor copanlisib (200nm – 0.78nm) or DMSO/TFA control. Cells were incubated at 37°C with 5% CO₂ for 5 days. Proliferation was measured via a colourimetric MTS assay whereby the colour intensity is directly proportional to cell viability within the well. Absorbance was read at 490nm using a 96-well plate reader. Dose-response curves to copanlisib were generated. Data are representative of the mean and standard deviation of 3 independent experiments. Drug concentrations are represented as a Log₁₀.

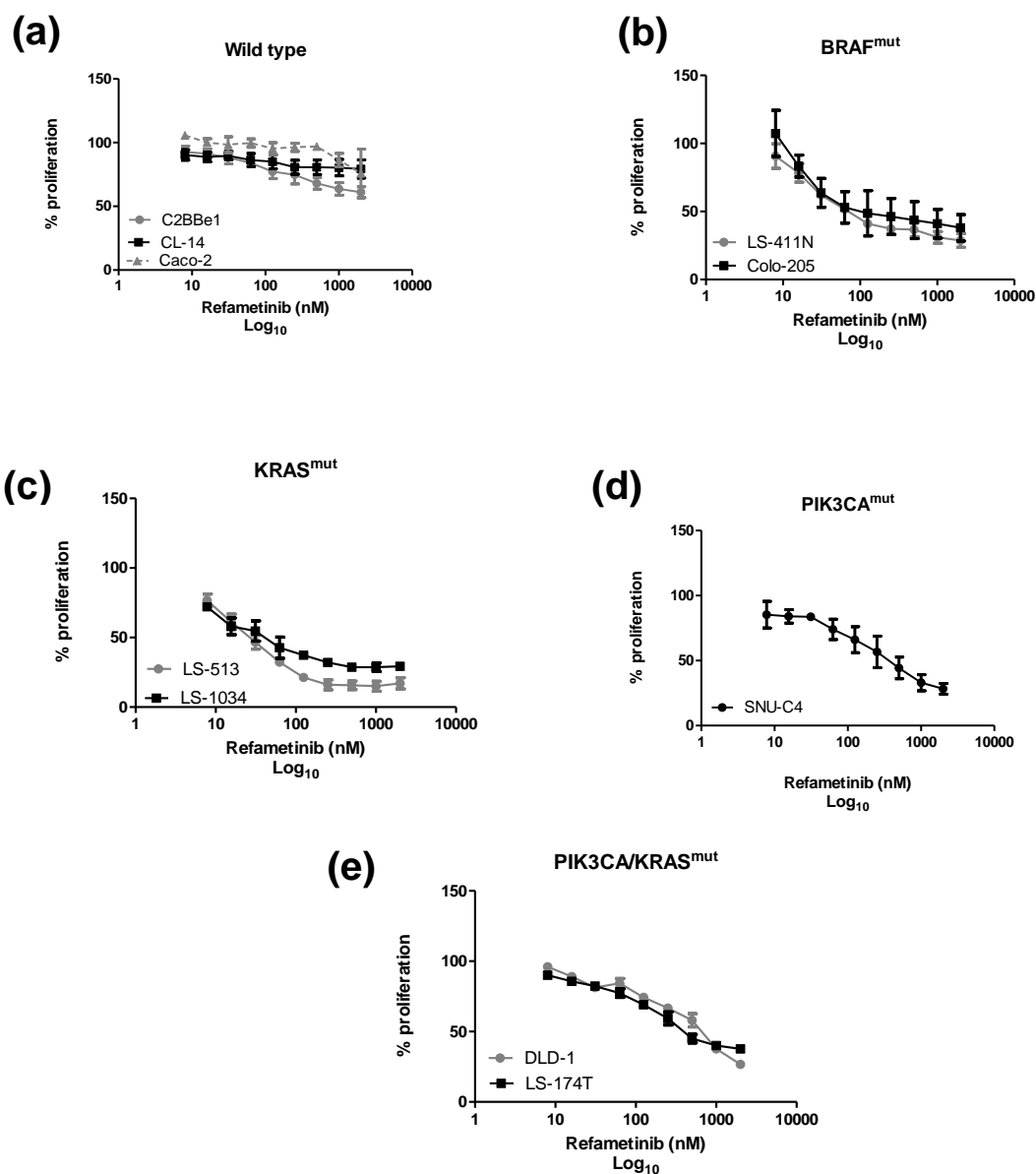


Figure 5.5: Efficacy of refametinib in a panel of CRC cell lines with varying PI3K and MAPK pathway mutations, consisting of (a) Wild-type, (b) $BRAF^{mut}$, (c) $KRAS^{mut}$, (d) $PIK3CA^{mut}$, (e) $PIK3CA$ - $KRAS^{co-mut}$.

Colorectal cancer lines were plated in triplicate at 1×10^4 cells/ml in 96 well plates (100ul per well). Cells were treated with serial 1:2 dilutions of the MEK inhibitor refametinib (2mM-7.8nM) or DMSO control. Cells were incubated at 37°C with 5% CO_2 for 5 days. Proliferation was measured via a colourimetric MTS assay whereby the colour intensity is directly proportional to cell viability within the well. Absorbance was read at 490nm using a 96-well plate reader. Dose-response curves to refametinib were generated. Data are representative of the mean and standard deviation of 3 independent experiments. Drug concentrations are represented as a Log_{10} .

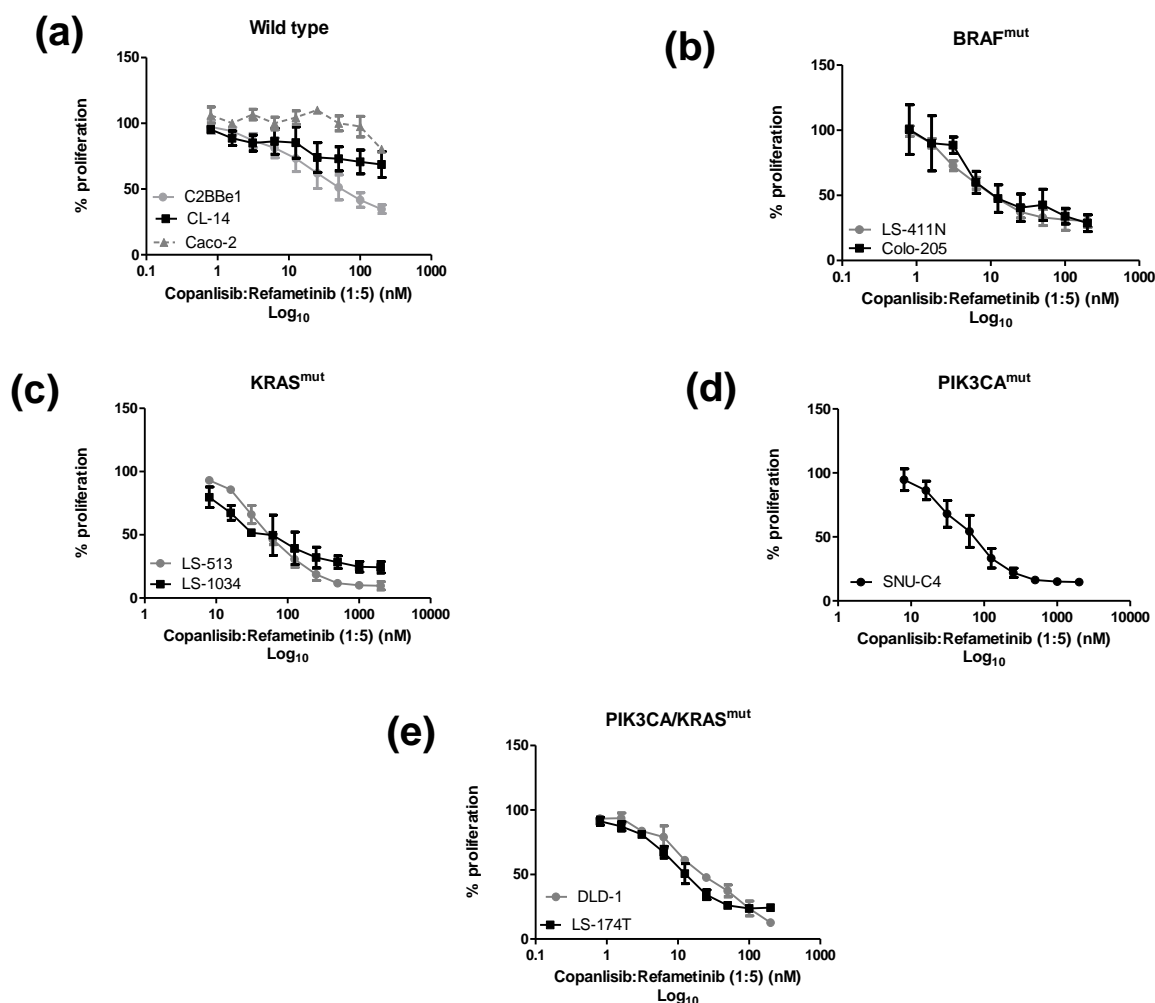


Figure 5.6: Efficacy of the combination of copanlisib and refametinib in a panel of CRC cell lines with varying PI3K and MAPK pathway mutations, consisting of (a) Wild-type, (b) $BRAF^{mut}$, (c) $KRAS^{mut}$, (d) $PIK3CA^{mut}$, (e) $PIK3CA-KRAS^{co-mut}$.

Colorectal cancer lines were plated in triplicate at 1×10^4 cells/ml in 96 well plates (100ul per well). Cells were treated with serial 1:2 dilutions of the MEK inhibitor Refametinib (1mM-3.9nM) or DMSO control, and the PI3K inhibitor Copanlisib (200nM – 0.78nM) or DMSO/TFA control. Cells were incubated at 37°C with 5% CO₂ for 5 days. Proliferation was measured via a colourimetric MTS assay whereby the colour intensity is directly proportional to cell viability within the well. Absorbance was read at 490nm using a 96-well plate reader. Dose-response curves to each drug alone and in combination were generated with CalcuSyn (Biosoft), which is based on the Chou-Talalay synergy quantification method. The ratio of copanlisib: refametinib in this assay is fixed at 1:5, with the maximum concentrations for serial dilution set at 200nM and 1000nM respectively. Data are representative of the mean and standard deviation of 3 independent experiments. Drug concentrations are represented as a Log₁₀.

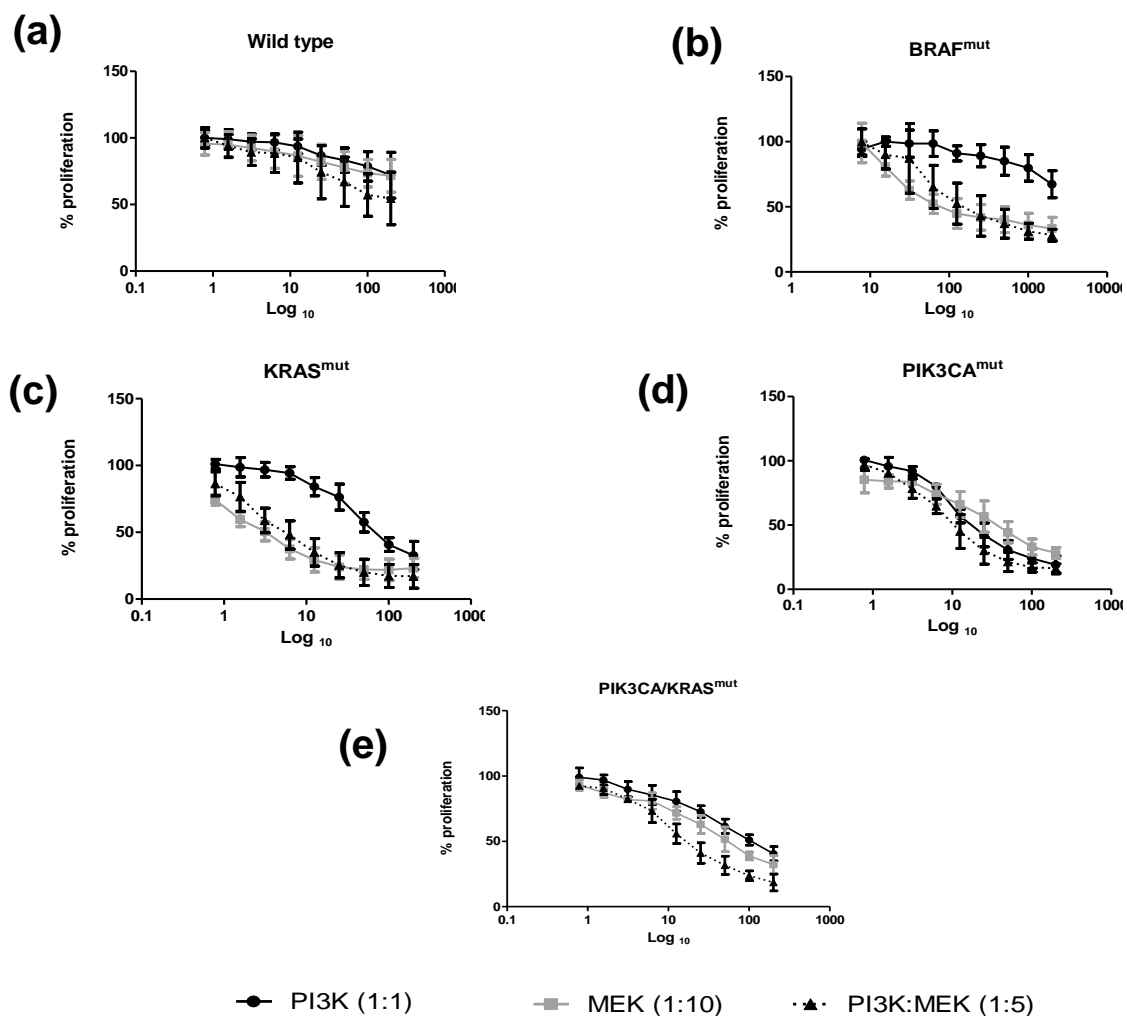


Figure 5.7: Efficacy of Copanlisib (●), Refametinib (■), and a combination of copanlisib and refametinib (▲), in a panel of CRC cell lines, with the mean values for (a) Wild-type, (b) BRAF^{mut}, (c) KRAS^{mut}, (d) PIK3CA^{mut}, (e) PIK3CA-KRAS^{co-mut}.

Colorectal cancer lines were plated in triplicate at 1×10^4 cells/ml in 96 well plates (100ul per well). Cells were treated with serial 1:2 dilutions of the MEK inhibitor Refametinib (1mM-3.9nM) or DMSO control, and/or the PI3K inhibitor Copanlisib (200nm – 0.78nm) or DMSO/TFA control. Cells were incubated at 37°C with 5% CO₂ for 5 days. Proliferation was measured via a colourimetric MTS assay whereby the colour intensity is directly proportional to cell viability within the well. Absorbance was read at 490nm using a 96-well plate reader. Dose-response curves to each drug alone and in combination were generated with CalcuSyn (Biosoft), which is based on the Chou-Talalay synergy quantification method. The ratio of copanlisib: refametinib in this assay is fixed at 1:5, with the maximum concentrations for serial dilution set at 200nM and 1000nM respectively. Data is representative of the mean and standard deviation of 3 independent experiments. Drug concentrations are represented as a Log₁₀.

Table 5.2: The IC₅₀s of copanlisib and refametinib inhibitors in combination compared to the IC₅₀ of each drug as a single agent, and combination index (CI) values at ED₅₀, ED₇₅ and ED₉₀ for the combination of copanlisib and refametinib.

Colorectal cancer lines were plated in triplicate at 1×10^4 cells/ml in 96 well plates (100ul per well). Cells were treated with serial 1:2 dilutions of the MEK inhibitor Refametinib (2mM-7.8nM) or DMSO control, and / or the PI3K inhibitor Copanlisib (200nm – 0.78nm) or DMSO/TFA control. Cells were incubated at 37°C with 5% CO₂ for 5 days. Proliferation was measured via a colourimetric MTS assay whereby the colour intensity is directly proportional to cell viability within the well. Absorbance was read at 490nm using a 96-well plate reader. Dose-response curves to each drug alone and in combination were generated with CalcuSyn (Biosoft), which is based on the Chou-Talalay synergy quantification method. The ratio of copanlisib: refametinib in this assay is fixed at 1:5, with the maximum concentrations for serial dilution set at 200nM and 1000nM respectively. Data is representative of the mean and standard deviation of 3 independent experiments. Combination Index (CI) values at ED₅₀, ED₇₅ and ED₉₀ were calculated using the Chou-Talalay equation using the CalcuSyn software, whereby the CI values can be synergistic (CI<0.9), additive (CI=0.9-1.1), or antagonistic (CI>1.1).

Standard deviations are representative of three independent experiments.

	Cell line	IC ₅₀ (nM)			ED values		
		Copanlisib	Refametinib	Copanlisib : refametinib	ED ₅₀	ED ₇₅	ED ₉₀
WT	C2BBE1	>200	>2000	63 ± 25	315 ± 125	0.30 ± 0.08	0.28 ± 0.15
	CL-14	>200	>2000	>200	>1000	0.03 ± 0.03	0.02 ± 0.03
	Caco-2	>200	>2000	>200	>1000	0.82 ± .061	0.91 ± 0.69
BRAF ^{V600E}	Colo-205	>200	478 ± 199	38 ± 32	190 ± 160	0.39 ± .23	0.12 ± .14
	LS-411n	>200	190 ± 83	23 ± 7	115 ± 35	0.74 ± 0.45	0.33 ± 0.26
KRAS ^{mut}	LS-1034	153 ± 25	44 ± 3	21 ± 9	105 ± 45	0.84 ± 0.47	0.54 ± 0.11
	LS-513	74 ± 16	28 ± 8	7 ± 2	35 ± 10	1.4 ± 0.51	0.73 ± 0.31
PIK3CA ^{mut}	SNU-C4	28 ± 6	326 ± 144	16 ± 6	80 ± 30	0.82 ± 0.10	0.68 ± 0.07
PIK3CA/	DLD-1	84 ± 30	745 ± 245	16 ± 3	80 ± 15	0.31 ± 0.05	0.20 ± 0.02
KRAS ^{mut}	LS-174T	134 ± 29	560 ± 164	19 ± 3	95 ± 15	0.32 ± 0.06	0.25 ± 0.12

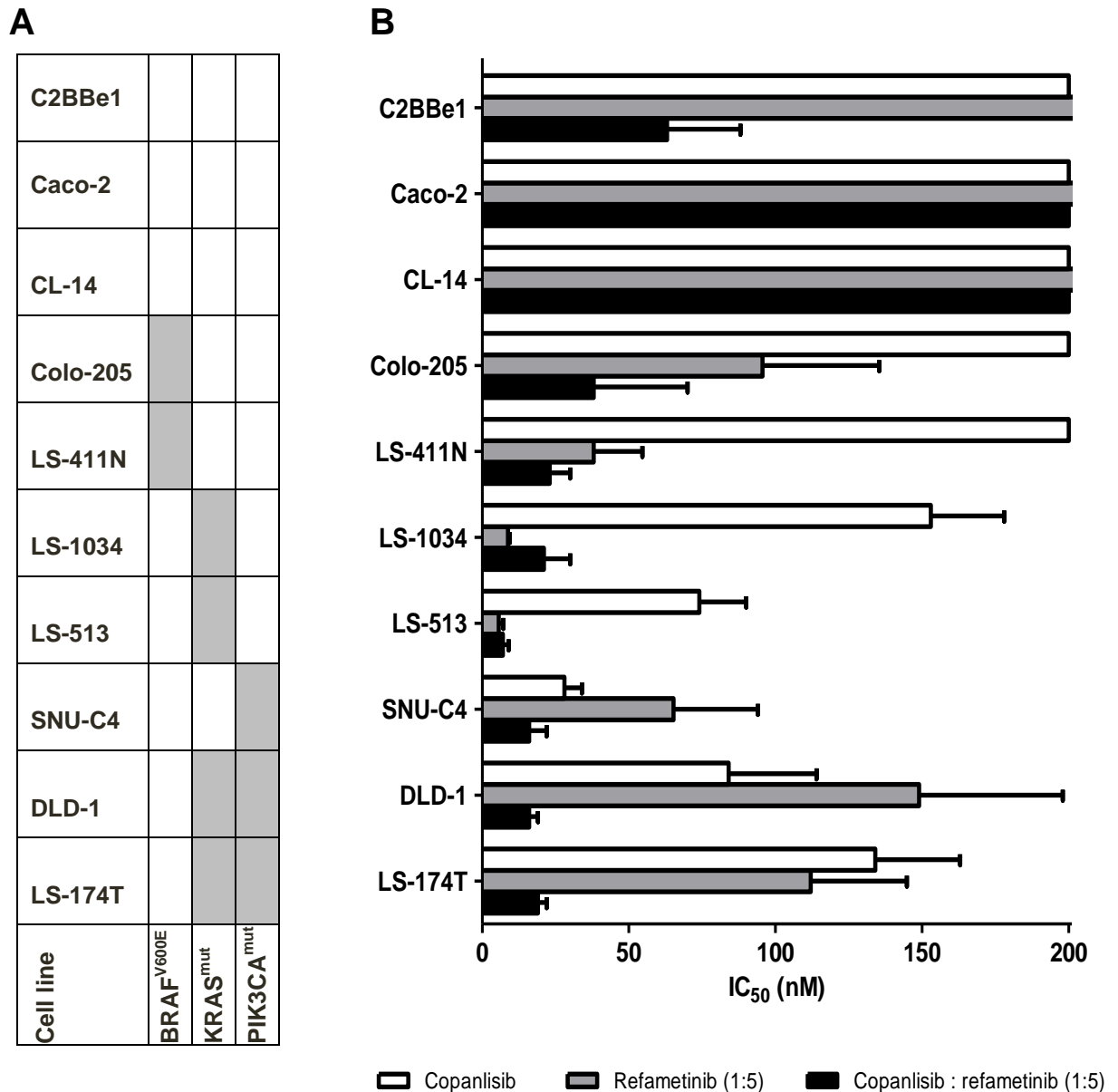


Figure 5: IC₅₀ values for copanlisib and refametinib and the combination of copanlisib and refametinib in CRC cell lines with varying mutational status. (A) Mutational status of cell lines. (B) IC₅₀ values for the 10 CRC cell lines treated with copanlisib with a maximum concentration of 200nM; refametinib with a maximum concentration of 2000nM (represented as a 1:5 dilution); and copanlisib and refametinib with a maximum concentration of 200nM and 1000nM respectively (represented as a 1:5 dilution). Results are a mean of 3 independent experiments.

5.2.3 PI3K and MAPK pathway mutations determine the anti-proliferative abilities of copanlisib, refametinib and 5-FU chemotherapy in CRC cell lines in clonogenic assays.

The proliferation assays carried out in 5.2.2 demonstrated that copanlisib and refametinib have anti-proliferative effects in a range of CRC cell lines when used as single or dual agents. As a result, we expanded our study to determine whether copanlisib and refametinib could increase chemoradiotherapy sensitivity in PI3K and MAPK pathway mutated CRC cell lines. Previous proliferation assays were carried out in a confluent environment, which may facilitate tumour growth; therefore we first established if solitary CRC cells possess the ability to proliferate whilst undergoing treatment with copanlisib, refametinib or 5-fluorouracil (5-FU) chemotherapy as single agents. This was achieved through clonogenic assays.

Wild-type (Caco-2), *KRAS*^{mut} (LS-1034), *BRAF*^{mut} (LS-411N), *PIK3CA*^{mut} (SNU-C4) and *PIK3CA-KRAS*^{mut} (DLD-1) cell lines were plated in 6 well plates, and treated with serial 1:2 dilutions of copanlisib (maximum concentration = 200nm), refametinib (maximum concentration 2000nm) and 5-FU chemotherapy (maximum concentration = 250um), and incubated for 2 weeks, until colony formation. IC₇₅ values were subsequently determined for each cell line (Table 5.3).

PIK3CA^{mut} cell lines (SNU-C4, IC₇₅ = 3.1nM), Wild-type cell lines (Caco-2, IC₇₅ = 6.1nM) and *KRAS*^{mut} cell lines (LS-1034, IC₇₅ = 8.6nM) were most sensitive to copanlisib (Figure 5.8). This reflected the results of the 2D toxicity assays for *PIK3CA* and *KRAS* mutated cell lines shown (Figure 5.4). However, wild-type cell lines were more sensitive to the copanlisib when the cells were plated at a lower confluency and treated for a longer incubation period than that of the proliferation assays.

Inhibition of colony formation was most marked in *PIK3CA*^{mut} (SNU-C4, IC₇₅ = 4.4nM), *BRAF*^{mut} (LS-411N, IC₇₅ = 4.6nM), and *KRAS*^{mut} (LS-1034, IC₇₅ = 33.25nM) cell lines when treated with refametinib (Figure 5.9). *PIK3CA-KRAS*^{mut} (DLD-1, IC₇₅ = 500nM) and wild-type (Caco-2, IC₇₅ = 250nM) cell lines were most resistant to treatment with refametinib, in line with the 2D toxicity assay results, shown in Figure 5.5.

Treatment with 5-FU chemotherapy was most responsive in *PIK3CA*^{mut} (SNU-C4, IC₇₅ = 0.056uM) and *KRAS*^{mut} (LS-1034, IC₇₅ = 0.06uM) mutated cell lines. In contrast, the *PIK3CA-KRAS*^{mut} cell line (DLD-1) was the least responsive (IC₇₅ = 0.73uM) (Figure 5.10).

Table 5.3: IC₇₅ values of cell lines treated in clonogenic assays with Copanlisib, Refametinib and 5-fluorouracil (5-FU) chemotherapy.

BRAF^{mut} (LS-411N, n=5,000 cells), *PIK3CA-KRAS*^{mut} (DLD-1, n = 1,000 cells), *PIK3CA*^{mut} (SNU-C4, n = 2,000 cells), *KRAS*^{mut} (LS-1034, n = 3,000 cells) and Wild-type (Caco-2, n = 50,000 cells) CRC cells were seeded in T25 flasks (Corning). Cells were incubated at 37°C, with 5% CO₂ for 24 hours, and treated with serial dilutions of copanlisib (200nm-0.025nm), refametinib (2000nm-25nm) and 5-FU chemotherapy (250µm - 31nm). Cells were incubated for 2 weeks, until colony formation. Cells were fixed and stained with 0.1% crystal violet. Wells were rinsed with 1ml acetic acid to remove crystal violet, which was subsequently diluted (1:5), and the staining intensity was read on a plate reader at 595nm. IC₇₅ values were calculated via an automated median-effect plot (Chou plot) using the CalcuSyn (Biosoft) software.

	IC ₇₅				
	LS-411N	DLD-1	SNU-C4	LS-1034	Caco-2
Copanlisib (nM)	100	50	3.1	8.6	6.1
Refametinib (nM)	4.6	500	4.4	33.25	250
5-FU chemotherapy (uM)	0.29	0.73	0.056	0.06	0.13

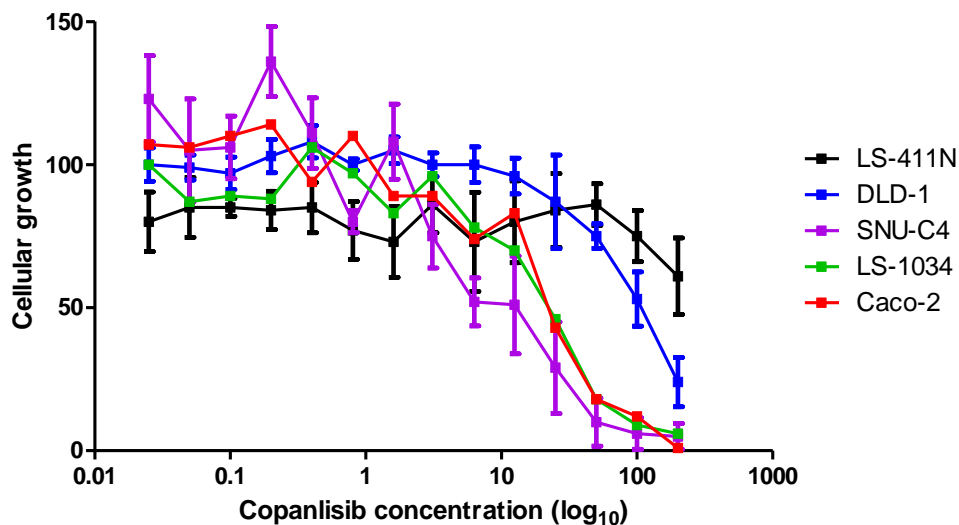


Figure 5.8: Clonogenic assays for BRAF^{mut} (LS-411N = ■), PIK3CA-KRAS^{mut} (DLD-1 = ■), PIK3CA^{mut} (SNU-C4 = ■), KRAS^{mut} (LS-1034 = ■) and wild-type (Caco-2 = ■) colorectal cancer (CRC) cell lines treated with the PI3K inhibitor copanlisib.

Cells (LS-411N = 1,000 cells; DLD-1 = 200 cells; SNU-C4 = 400 cells; LS-1034 = 3,000 cells and Caco-2 = 10,000 cells) were plated in 6 well plates (2mls per well) and incubated at 37°C, with 5% CO₂ for 24 hours. Cells were treated with serial 1:2 dilutions of the PI3K inhibitor Copanlisib (200nm - 0.025nm), and a DMSO/TFA control (200nm). Cells were incubated for a further 2 weeks, until colony formation. Cells were fixed and stained with 0.1% crystal violet. Wells were rinsed with 1ml acetic acid to remove crystal violet, which was subsequently diluted (1:5), and the staining intensity was read on a plate reader at 595nm. CalcuSyn software (Biosoft) was used to calculate IC₇₅ values required for drug concentrations for the clonogenic study via an automated median-effect plot (Chou plot). Error bars represent the standard deviation, with experiments run in triplicate.

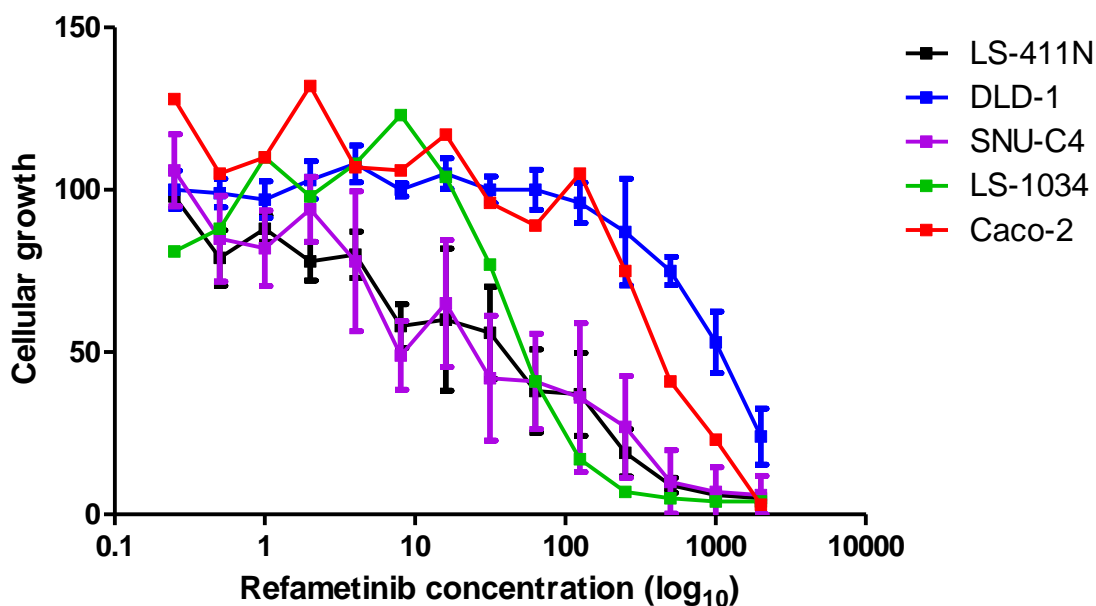


Figure 5.9: Clonogenic assays for BRAF^{mut} (LS-411N = ■), PIK3CA-KRAS^{mut} (DLD-1 = ■), PIK3CA^{mut} (SNU-C4 = ■), KRAS^{mut} (LS-1034 = ■) and wild-type (Caco-2 = ■) colorectal cancer (CRC) cell lines treated with the MEK inhibitor refametinib.

Cells (LS-411N = 1,000 cells; DLD-1 = 200 cells; SNU-C4 = 400 cells; LS-1034 = 3,000 cells and Caco-2 = 10,000 cells) were plated in 6 well plates (2mls per well) and incubated at 37°C, with 5% CO₂ for 24 hours. Cells were treated with serial 1:2 dilutions of the MEK inhibitor Refametinib (2000nm - 0.25nm), and a DMSO control (2000nm). Cells were incubated for a further 2 weeks, until colony formation. Cells were fixed and stained with 0.1% crystal violet. Wells were rinsed with 1ml acetic acid to remove crystal violet, which was subsequently diluted (1:5), and the staining intensity was read on a plate reader at 595nm. CalcuSyn software (Biosoft) was used to calculate IC₇₅ values required for drug concentrations for the clonogenic study via an automated median-effect plot (Chou plot). Error bars represent the standard deviation, with experiments run in triplicate.

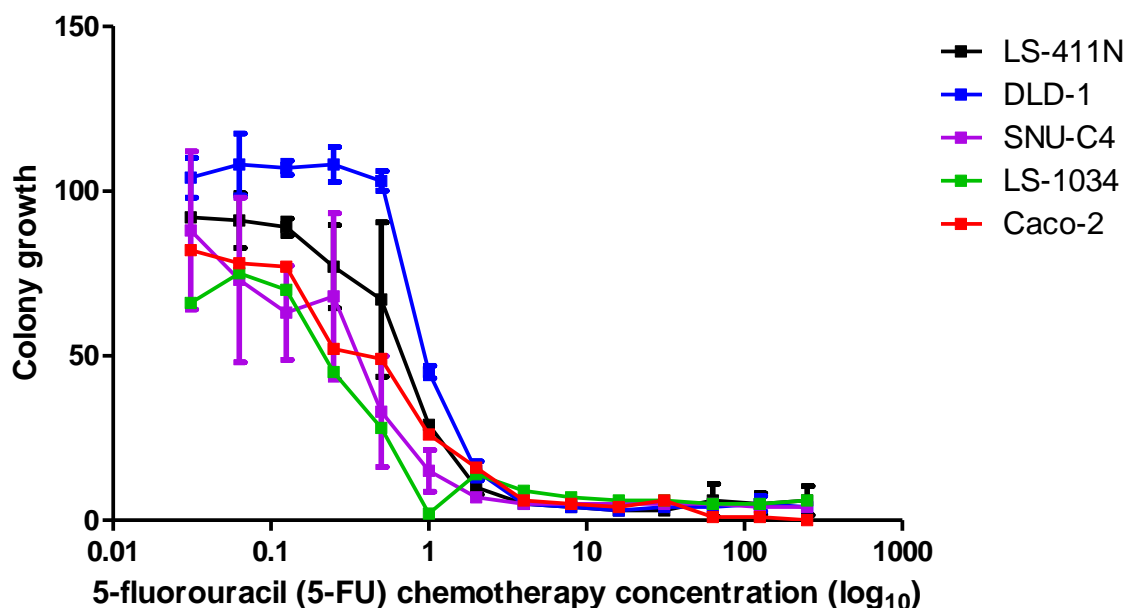


Figure 5.10: Clonogenic assays for BRAF^{mut} (LS-411N = ■), PIK3CA-KRAS^{mut} (DLD-1 = ■), PIK3CA^{mut} (SNU-C4 = ■), KRAS^{mut} (LS-1034 = ■) and wild-type (Caco-2 = ■) colorectal cancer (CRC) cell lines treated with 5-fluorouracil (5-FU) chemotherapy.

Cells (LS-411N = 1,000 cells; DLD-1 = 200 cells; SNU-C4 = 400 cells; LS-1034 = 3,000 cells and Caco-2 = 10,000 cells) were plated in 6 well plates (2mls per well) and incubated at 37°C, with 5% CO₂ for 24 hours. Cells were treated with serial 1:2 dilutions of the 5-FU chemotherapy (250µm - 31nm), and a DMSO control (250µm). Cells were incubated for a further 2 weeks until colony formation. Cells were fixed and stained with 0.1% crystal violet. Wells were rinsed with 1ml acetic acid to remove crystal violet, which was subsequently diluted (1:5), and the staining intensity was read on a plate reader at 595nm. CalcuSyn software (Biosoft) was used to calculate IC₇₅ values required for drug concentrations for the clonogenic study via an automated median-effect plot (Chou plot). Error bars represent the standard deviation, with experiments run in triplicate.

5.2.4. Copanlisib and refametinib used together as a standard of care for locally advanced rectal cancer increase the chemoradiation sensitivity of colorectal cancer (CRC) cell lines with PI3K and MAPK pathway mutations in clonogenic assays.

Following on from the promising results in our proliferation and clonogenic assays, we wished to determine if copanlisib and refametinib could enhance the effect of 5-FU chemoradiation therapy in CRC cell lines. Due to the varying sensitivities of each cell line towards copanlisib and refametinib, we used IC75 values calculated from our previous clonogenic experiments (Table 5.3) alongside a standard radiation dose of 2Gy. Clonogenic assays were performed in T25 flasks to facilitate radiation of CRC cells. A range of treatment combinations was set up to determine variances between treatment groups (supplementary figures 2-6).

Cellular growth was decreased by an average of 42.8% post-5-FU chemotherapy plus radiation (5R) therapy compared to vehicle-treated control cells (Table 4.4, figures 4.7 - 4.11). The wild-type cell line (Caco-2) was least sensitive to 5R therapy, with only an 18% reduction in cellular growth compared to the vehicle control. In contrast, all mutated cell lines had cellular growth reductions ranging between 48 and 51% of their corresponding vehicle controls. However, cellular proliferation was significantly reduced in all cell lines regardless of mutational background (p-values ranging from 0.003 – 0.046).

Growth inhibition was further enhanced with the addition of copanlisib to 5-FU chemoradiation therapy (P5R) compared to 5R therapy alone in all five cell lines (mean percentage growth inhibition = 72.8%) (Table 5.4). There was a significant reduction in cellular proliferation in all CRC cell lines in the P5R arm compared to the vehicle-treated controls. However, growth inhibition was most marked in the *KRAS^{mut}* cell line LS-1034 (mean percentage growth inhibition = $80 \pm 8\%$ vs $48 \pm 4.9\%$, $p = 0.011$) and the wild-type cell line Caco-2 (mean percentage growth inhibition = $56 \pm 7.9\%$ vs $18 \pm 6.8\%$, $p = 0.045$) which displayed a significant reduction in cellular growth when treated with P5R compared to 5R treatment alone (Table 5.4).

Similar growth-inhibitory effects were observed with the addition of refametinib alongside 5-FU chemotherapy and radiation (M5R), which had a mean percentage growth inhibition of 70.4%. Similar to P5R treatment, all cell lines in the M5R arm displayed a significant reduction in cellular growth compared to the vehicle-treated controls. Whilst cellular growth was significantly decreased in *KRAS^{mut}* cell line, LS-1034 (mean percentage growth inhibition = $76 \pm 8.4\%$ vs $48 \pm 4.9\%$, $p = 0.02$), and the wild type cell line, Caco-2 (mean percentage growth inhibition = $57 \pm 6\%$, vs $18 \pm 6.8\%$, $p = 0.0001$) in the M5R arm compared to 5R treated cells. In the other 3 cell lines, as with P5R treatment, there was growth inhibition associated with M5R treatment but which did not quite reach statistical significance (Table 5.4).

Growth inhibition was most marked with the addition of both copanlisib and refametinib to 5-FU chemotherapy and radiation (PM5R), which had a mean percentage growth of only 15.2%. All cell lines showed a significant reduction in cellular growth compared to the vehicle-treated control. However *PIK3CA-KRAS^{mut}* DLD-1 (mean percentage growth inhibition = 91 ± 2.1 vs $51 \pm 14.8\%$, $p=0.033$), *KRAS^{mut}* LS-1034 (mean percentage growth inhibition = 85 ± 6 vs $48 \pm 4.9\%$, $p=0.033$), *BRAF^{mut}* LS-411N (mean percentage growth inhibition = $90 \pm 0.7\%$ vs $48 \pm 11.2\%$, $p = 0.024$) and wild-type, Caco-2 (mean percentage growth inhibition = $76 \pm 4.6\%$ vs $18 \pm 6.8\%$, $p=0.002$) cell lines also responded significantly better to PM5R therapy than 5R therapy alone. Furthermore, cellular growth was significantly reduced in both *BRAF^{mut}* (P5R, $p = 0.047$; M5R, $p = 0.04$) and WT (P5R, $p = 0.021$; M5R, $p = 0.013$) cell lines in PM5R treated cells compared to P5R or M5R arms (Table 5.4).

Table 5.4: Survival fraction and p-values of clonogenic assays

PIK3CA-KRAS^{mut} (DLD-1 = 1,000 cells), PIK3CA^{mut} (SNU-C4 = 2000 cells), KRAS^{mut} (LS-1034 = 3,000 cells), BRAF^{mut} (LS-411N = 5,000 cells) and wild-type (WT) (Caco-2 = 50,000 cells) colorectal cancer (CRC) cells were plated in T25 flasks (20mls per flask) and incubated for 24 hours. Cells were treated with their IC₇₅ concentration of copanlisib, refametinib and 5-fluorouracil (5-FU) chemotherapy alongside radiation (2Gy). Cells were incubated until colony formation (2 weeks). Cells were fixed and stained with 0.1% crystal violet. Flasks were rinsed with 3mls asceic acid (30%) to remove crystal violet, which was subsequently diluted (1:5), and the stain intensity was read on a plate reader at 595nm.

Clonogenic assay results are displayed as a percentage of surviving cells using the matched untreated control group as a baseline.

Each cell line is grouped by treatment as follows: Control (C); 5-FU chemoradiotherapy treatment (5R); Copanlisib and 5-FU

chemoradiotherapy treatment (P5R); Refametinib and 5-FU chemoradiotherapy treatment (M5R); Copanlisib, Refametinib and 5-FU

chemoradiotherapy treatment (PM5R).

P-values were determined for treatments compared to both untreated control (C) and concurrent 5-FU chemoradiotherapy treatment (5R) groups using the unpaired 2-tailed t-test with Welch's correction was used with a confidence interval of 95%. Data are representative of the mean and standard deviation of 3 independent experiments.

	survival fraction					p-value						
	C	5R	P5R	M5R	PM5R	C:5R	C:P5R	C:M5R	C:PM5R	5R:P5R	5R:M5R	5R:PM5R
DLD	100	49 (± 14.8)	21 (± 13.8)	20 (± 7.8)	9 (± 2.1)	0.027	0.005	0.043	0.000	0.062	0.165	0.033
SNU	100	51 (± 18.9)	27 (± 6.4)	33 (± 17)	18 (± 10)	0.046	0.003	0.021	0.005	0.178	0.081	0.076
1034	100	52 (± 4.9)	20 (± 8)	23 (± 8.4)	15 (± 6)	0.003	0.003	0.004	0.002	0.011	0.020	0.001
411N	100	52 (± 11.2)	24 (± 5.2)	29 (± 6.8)	10 (± 0.7)	0.018	0.002	0.003	0.000	0.087	0.160	0.024
Caco	100	82 (± 6.8)	44 (± 7.9)	43 (± 6)	24 (± 4.6)	0.046	0.007	0.004	0.001	0.045	0.000	0.002

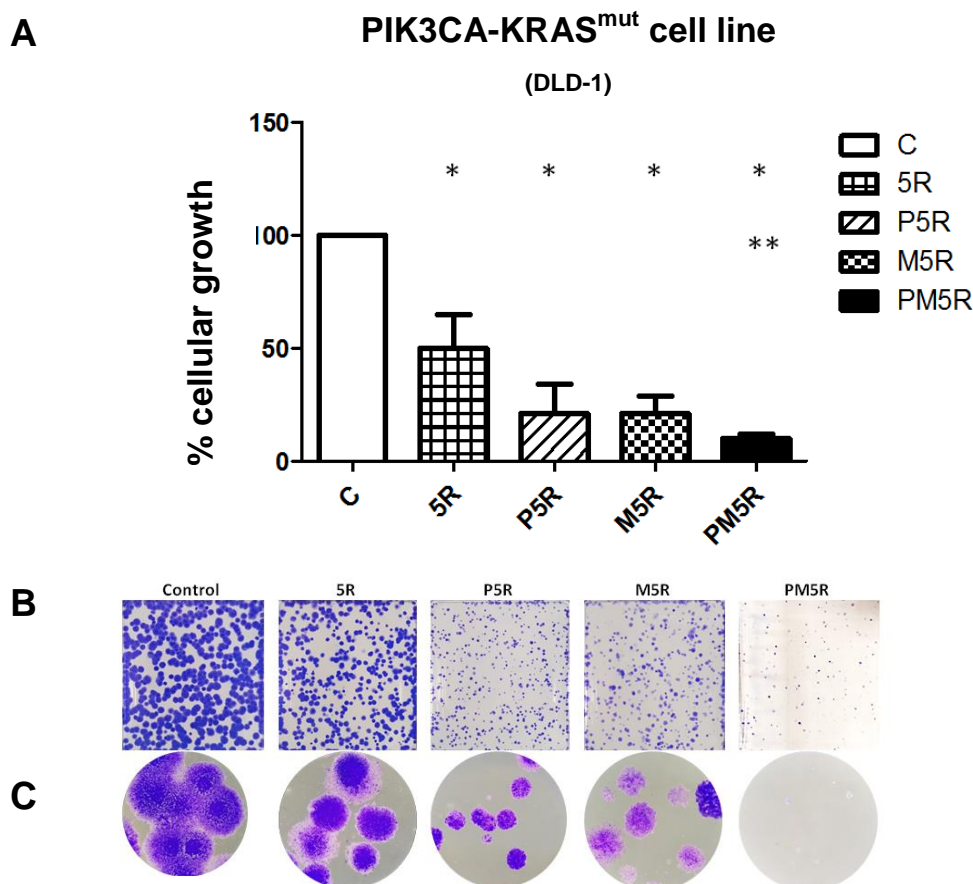


Figure 5.11: Cellular growth of PIK3CA-KRAS^{mut} DLD-1 cells treated with DMSO/DMSO-TFA vehicle control (C), 5-FU chemoradiotherapy (5R), copanlisib and chemoradiotherapy (P5R), refametinib and chemoradiotherapy (M5R) and copanlisib, refametinib and chemoradiotherapy (PM5R) in clonogenic assays.

1,000 PIK3CA-KRAS^{mut} CRC cells (DLD-1) were plated in T25 flasks (20mls per flask) and incubated for 24 hours. Cells were treated with copanlisib (50nm), refametinib (500nm), 5-FU chemotherapy (730nm) and radiation (2Gy). Cells were incubated until colony formation (2 weeks). Cells were fixed and stained with 0.1% crystal violet. Wells were rinsed with 1ml acetic acid to remove crystal violet, which was subsequently diluted (1:5), and the staining intensity was read on a plate reader at 595nm. Prism software (GraphPad) was used to for the generation of graphs and to calculate the statistical significance between various treatment cohorts. The unpaired 2-tailed t-test with Welch's correction was used with a confidence interval of 95%. Error bars represent the standard deviation, with experiments run in triplicate. Data are representative of the mean and standard deviation of 3 independent experiments. * $p < 0.05$ compared to control, ** $P < 0.05$ compared to 5-fu chemoradiotherapy (5R). Representative clonogenic assays are shown in panel B (4x magnification) and C (macroscopic view of the flask).

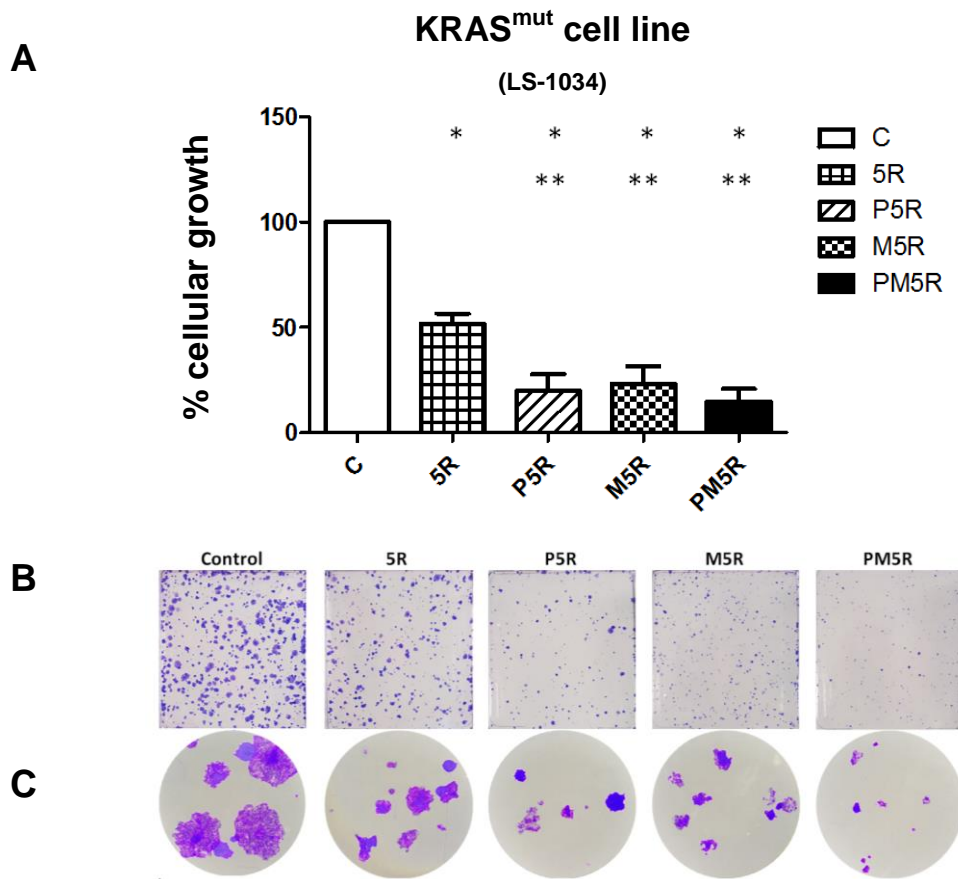


Figure 5.12 Cellular growth of KRAS^{mut} LS-1034 treated with DMSO/DMSO-TFA vehicle control (C), 5-FU chemoradiotherapy (5R), copanlisib and chemoradiotherapy (P5R), refametinib and chemoradiotherapy (M5R) and copanlisib, refametinib and chemoradiotherapy (PM5R) in clonogenic assays.

3,000 KRAS^{mut} CRC cells (LS-1034) were plated in T25 flasks (20mls per flask) and incubated for 24 hours. Cells were treated with copanlisib (8.6nm), refametinib (33nm), 5-FU chemotherapy (60nm) and radiation (2Gy). Cells were incubated until colony formation (2 weeks). Cells were fixed and stained with 0.1% crystal violet. Wells were rinsed with 1ml acetic acid to remove crystal violet, which was subsequently diluted (1:5), and the staining intensity was read on a plate reader at 595nm. Prism software (GraphPad) was used to for the generation of graphs and to calculate the statistical significance between various treatment cohorts. The unpaired 2-tailed *t*-test with Welch's correction was used with a confidence interval of 95%. Error bars represent the standard deviation, with experiments run in triplicate. Data are representative of the mean and standard deviation of 3 independent experiments. **p*<0.05 compared to control, ***P*<0.05 compared to 5-fu chemoradiotherapy (5R). Representative clonogenic assays are shown in panel B (4x magnification) and C (macroscopic view of the flask).

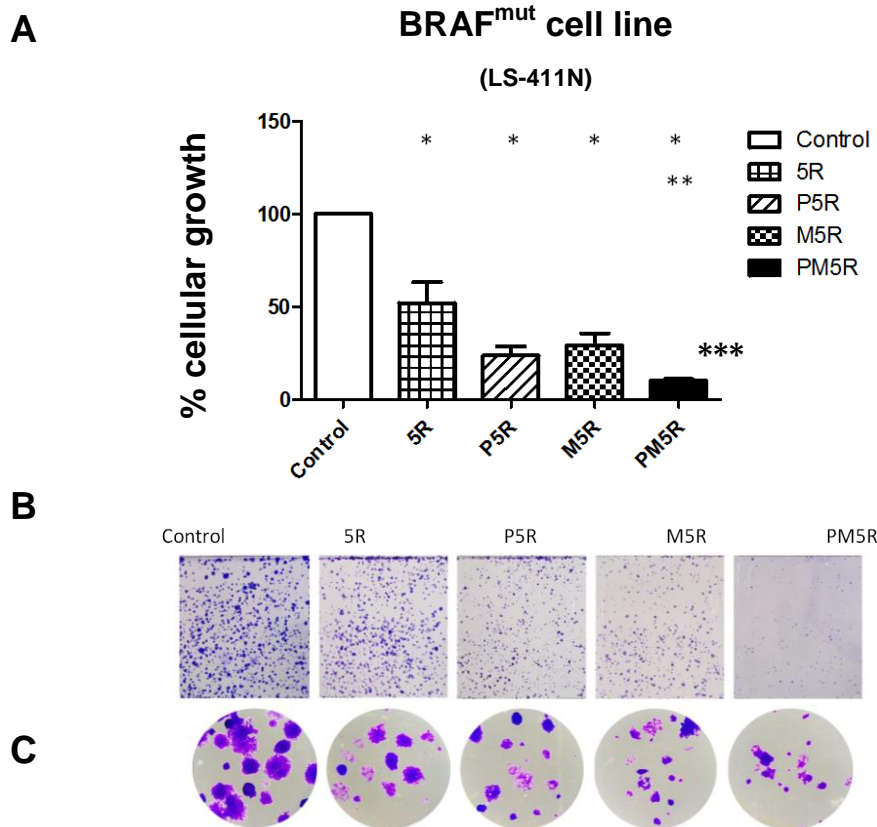


Figure 5.13: Cellular growth of BRAF^{mut} LS-411N treated with DMSO/DMSO-TFA vehicle control (C), 5-FU chemoradiotherapy (5R), copanlisib and chemoradiotherapy (P5R), refametinib and chemoradiotherapy (M5R) and copanlisib, refametinib and chemoradiotherapy (PM5R) in clonogenic assays.

5,000 BRAF^{mut} CRC cells (LS-411N) were plated in T25 flasks (20mls per flask) and incubated for 24 hours. Cells were treated with copanlisib (100nm), refametinib (4.6nm), 5-FU chemotherapy (290nm) and radiation (2Gy). Cells were incubated until colony formation (2 weeks). Cells were fixed and stained with 0.1% crystal violet. Wells were rinsed with 1ml acetic acid to remove crystal violet, which was subsequently diluted (1:5), and the staining intensity was read on a plate reader at 595nm. Prism software (GraphPad) was used to for the generation of graphs and to calculate the statistical significance between various treatment cohorts. The unpaired 2-tailed t-test with Welch's correction was used with a confidence interval of 95%. Error bars represent the standard deviation, with experiments run in triplicate. Data are representative of the mean and standard deviation of 3 independent experiments. * $p < 0.05$ compared to control, ** $p < 0.05$ compared to 5-fu chemoradiotherapy (5R). *** $p < 0.05$ compared to P5R or M5R. Representative clonogenic assays are shown in panel B (4x magnification) and C (macroscopic view of the flask).

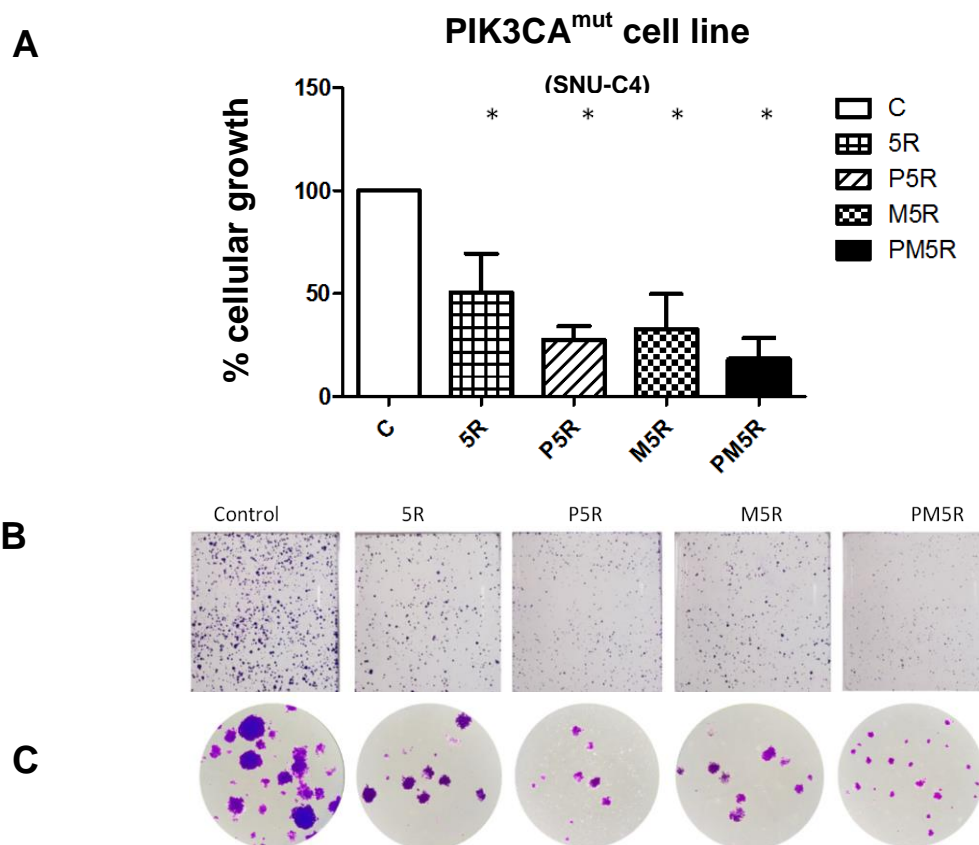


Figure 5.14: Cellular growth of PIK3CA^{mut} SNU-C4 treated with DMSO/DMSO-TFA vehicle control (C), 5-FU chemoradiotherapy (5R), copanlisib and chemoradiotherapy (P5R), refametinib and chemoradiotherapy (M5R) and copanlisib, refametinib and chemoradiotherapy (PM5R) in clonogenic assays.

2,000 PIK3CA^{mut} CRC cells (SNU-C4) were plated in T25 flasks (20mls per flask) and incubated for 24 hours. Cells were treated with copanlisib (3.1nm), refametinib (4.4nm), 5-FU chemotherapy (130nm) and radiation (2Gy). Cells were incubated until colony formation (2 weeks). Cells were fixed and stained with 0.1% crystal violet. Wells were rinsed with 1ml acetic acid to remove crystal violet, which was subsequently diluted (1:5), and the staining intensity was read on a plate reader at 595nm. Error bars represent the standard deviation, with experiments run in triplicate. Data are representative of the mean and standard deviation of 3 independent experiments. * $p < 0.05$ compared to control, ** $P < 0.05$ compared to 5-fu chemoradiotherapy (5R). Representative clonogenic assays are shown in panel B (4x magnification) and C (macroscopic view of the flask).

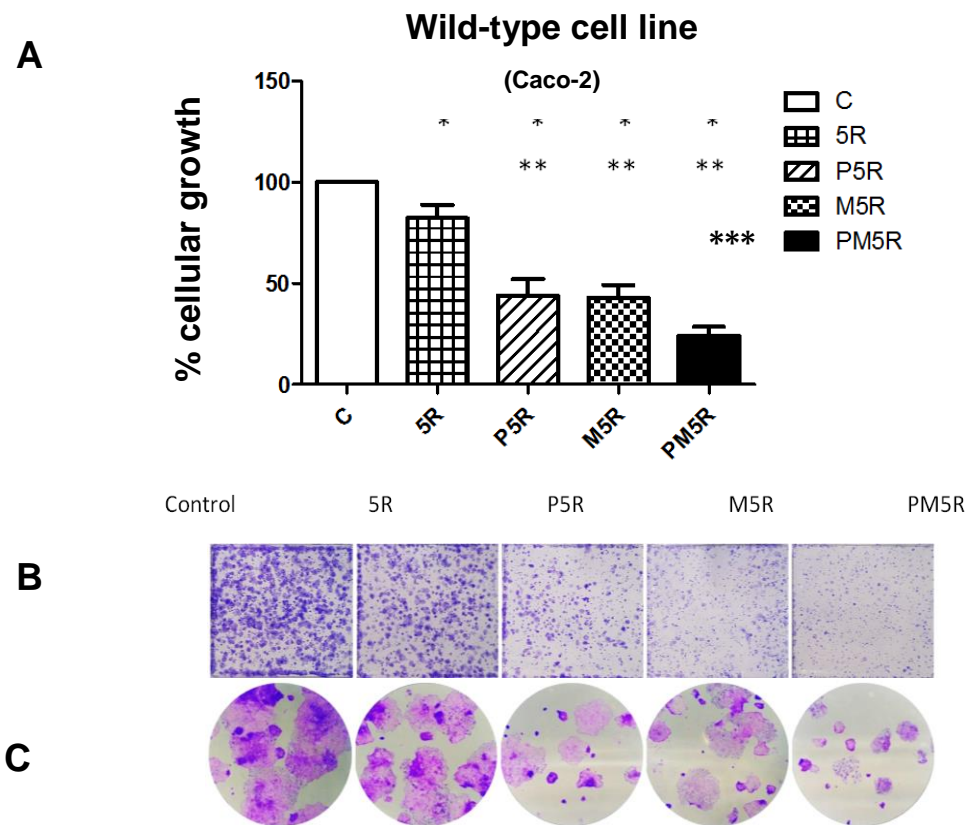


Figure 5.15: Cellular growth of wild-type Caco-2 CRC cell lines treated with DMSO/DMSO-TFA vehicle control (C), 5-FU chemoradiotherapy (5R), copanlisib and chemoradiotherapy (P5R), refametinib and chemoradiotherapy (M5R) and copanlisib, refametinib and chemoradiotherapy (PM5R) in clonogenic assays.

50,000 wild-type CRC cells (Caco-2) were plated in T25 flasks (20mls per flask) and incubated for 24 hours. Cells were treated with copanlisib (6.1nm), refametinib (250nm), 5-FU chemotherapy (130nm) and radiation (2Gy). Cells were incubated until colony formation (2 weeks). Cells were fixed and stained with 0.1% crystal violet. Wells were rinsed with 1ml acetic acid to remove crystal violet, which was subsequently diluted (1:5), and the staining intensity was read on a plate reader at 595nm. Prism software (GraphPad) was used to for the generation of graphs and to calculate the statistical significance between various treatment cohorts. The unpaired 2-tailed *t*-test with Welch's correction was used with a confidence interval of 95%. Error bars represent the standard deviation, with experiments run in triplicate. Data are representative of the mean and standard deviation of 3 independent experiments. **p* < 0.05 compared to control, ***P* < 0.05 compared to 5-fu chemoradiotherapy (5R) ****p* < 0.05 compared to P5R or M5R. Representative clonogenic assays are shown in panel B (4x magnification) and C (macroscopic view of the flask).

5.3. Discussion

Advances are constantly being made in cancer research, with personalised therapy gaining increasing attention. Many cancer types have driver mutations which are known to affect patient response to various anti-tumour therapies e.g. HER-2 in breast cancer, KRAS mutations in lung cancer etc. Mutations within the PI3K and MAPK signalling pathways are common in CRC (91–93), and are associated with resistance to chemotherapy and radiation therapy, and poor patient outcomes (93,192–194). However, efforts to find a suitable target within these pathways have to date, been largely in vain, as many drugs cause high levels of toxicity or their efficacy is limited by drug resistance. We targeted the driver mutations within the PI3K and MAPK signalling pathways in the hope of reducing cellular proliferation and increasing tumour cell death in response to standard chemoradiotherapy.

The PI3K inhibitor copanlisib has been shown to induce apoptosis, whilst simultaneously inhibiting cellular proliferation, migration, differentiation and survival in a range of cancer cell lines, including prostate, breast, colon and pancreatic cancer cell lines (122). To date, limited work has been carried out on copanlisib effects in CRC. We therefore decided to exploit this, and focus our study on a panel of 10 CRC cell lines of varying PI3K/MAPK mutations, and investigate how they respond to copanlisib treatment alone, and in combination with refametinib, and current standard rectal cancer chemoradiation therapy.

PIK3CA mutated cell lines were the most sensitive to copanlisib in both the 2D toxicity assays and 3-D clonogenic assays. This is largely attributable to SNU-C4s interaction solely within the PI3K pathway. Our results concur with those of Liu et al., who have previously demonstrated that copanlisib has increased anti-tumourigenic activity (>40 fold) in breast cancer cell lines with *PIK3CA*^{mut} compared to *PIK3CA*^{wild-type} (122). *KRAS* mutated cell lines were sensitive to copanlisib, albeit at higher IC₅₀ concentrations than the *PIK3CA* mutated cell line (mean IC₅₀ = 113.5nM vs 28 nM). *RAS* is involved in both the PI3K and MAPK pathways; perhaps explaining why targeting the PI3K pathway alone cannot yield the same sensitivity as *PIK3CA* mutated cell lines which are probably more singularly dependent on the PI3K pathway. Our results concur with those of Clarke et al, who demonstrated that *PIK3CA* mutated cell lines are significantly more

sensitive to the PI3K inhibitor pictilisib than *KRAS* mutant cell lines (260). *PIK3CA*-*KRAS* dual mutated cell lines responded to copanlisib similarly to *KRAS* mutated cell lines, possibly, at least in part for the same reason. Knockdowns and knockouts of p110 α (PI3K catalytic subunit) in *PIK3CA*-*KRAS* dual mutated CRC cell lines (DLD-1 and HCT-116) also resulted in inhibition of cellular growth and downstream PI3K signalling (261,262).

Furthermore specific genetic mutations altered cell line sensitivity to copanlisib. Despite LS-513 and LS-1034s identical cancer type (colorectal carcinoma), stage (Dukes type C), and mutation status (*KRAS* mutant), LS-513 required less than half the copanlisib dosage needed for LS-1034 to achieve an IC₅₀ (LS-513 = 74 \pm 16nm, LS-1034 = 153 \pm 25nm). The main identifiable difference between the two cell lines is the specific *KRAS* mutation, with LS-513 harbouring a *G12D* mutation compared to LS-1034's *A146P* mutation. LS-513 was found to be more sensitive to copanlisib than LS-1034 (259). Furthermore, DLD-1 (IC₅₀ = 84 \pm 30nm) was more sensitive than LS-174T (134 \pm 29nm). DLD-1 has 3 *PIK3CA* mutations (*D549N*, *E545K* and *R741R*) and a *G13D* *KRAS* mutation, compared to LS-174T with has a *PIK3CA*^{H1047R} mutation and *KRAS*^{G12D} mutation. In contrast, both *BRAF*^{mut} and WT cell lines were copanlisib resistant. Liu et al, also reported copanlisib resistance within *BRAF*^{mut} and WT CRC cell lines (259).

MEK is one of the main components of the MAPK (RAS/RAF/MEK/ERK) pathway, which is involved in the control of cellular proliferation, growth, migration, differentiation, and apoptosis. Mutations within this pathway can result in uncontrolled proliferation and ultimately tumour growth. Several elements within the MAPK pathway have been targeted; however, to date, no inhibitor has been validated for use in CRC patients. *PIK3CA* mutated CRC cells were sensitive to refametinib. This may be in part, a result of mTOR inhibition through ERK in the MAPK pathway. WT CRC cell lines were resistant to Refametinib alone, as previously seen by Liu (259). *KRAS* and *BRAF* mutated CRC cell lines were sensitive to refametinib due to their MAPK pathway mutations. Multiple other studies have also shown *KRAS* and *BRAF* mutated cell line sensitivity towards MEK 1/2 inhibitors both in vitro and in vivo (260,263–265). However, variations in drug sensitivity did occur between *BRAF* mutated cell lines, with LS-411N displaying heightened sensitivity (IC₅₀ = 190 \pm 83nm) towards refametinib

compared to Colo-205 ($IC_{50} = 478 \pm 199\text{nm}$). Both cell lines harbour *V600E* mutations, however, Colo-205 is a semi-adherent cell line cultured from Dukes stage D tumour (i.e. tumour which has metastasised), compared to LS-411N which was an adherent cell line cultured from Dukes stage B (i.e. tumour has grown through the muscularis propria, but no lymph node involvement). *PIK3CA-KRAS* dual mutated CRC cell lines were the least sensitive to refametinib. This coincides with a study carried out by Jing et al. also showed that *PIK3CA-KRAS* dual mutated tumours were less sensitive to MEK inhibitors than their *RAS* or *RAF* mutated counterparts, resulting in a cytostatic rather than cytotoxic response (263).

Simultaneous treatment with copanlisib and refametinib resulted in a synergistic anti-proliferative response in 2D toxicity assays in most of the cell lines, with the exception of *KRAS^{mut}* LS-1034 and Wild type Caco-2, which had additive and nearly additive responses. The combination was most beneficial in two of the wild-type (CL-14, C2BBE1) and *PIK3CA-KRAS^{mut}* (DLD-1, LS-174T) cell lines. *KRAS* and *PIK3CA-KRAS* dual mutated cell lines use both the PI3K and MAPK pathways, therefore dual inhibition targets two of the main driving forces within the tumour, resulting in a synergistic response. Also probably underlying this synergy, several studies have also shown that inhibition of one signalling pathway (e.g. PI3K) may result in upregulation of another signalling pathway (e.g. MAPK) (266). Our findings correlate with those of Clarke et al, who treated 47 CRC cell lines with the PI3K inhibitor (cobimetinib) and MEK inhibitor (pictilisib). They found *KRAS* (\pm *PIK3CA*) mutations were strong predictors of synergism. Furthermore, both of our studies showed synergism in *KRAS* mutated cell lines (LS-1034 and LS-513), whilst strong synergism was demonstrated in *PIK3CA-KRAS* dual mutated cell lines (DLD-1 and LS-174T) (260).

In 3-D clonogenic assays, 5-FU chemoradiotherapy significantly reduced tumour cellular growth compared to (untreated and vehicle) controls in all groups. In wild-type and *KRAS* CRC mutated cell lines, the addition of either copanlisib and/or refametinib to 5-FU CRT significantly inhibited cell growth compared to 5-FU chemoradiotherapy alone. Since Caco-2 is wild-type for mutations within the PI3K or MAPK pathway, we did not expect such a promising response. However, this

suggests that the addition of inhibitors, either copanlisib or refametinib, may enhance chemoradiotherapy response regardless of their mutational status. *BRAF* and *PIK3CA-KRAS* dual-mutated CRC cell lines only showed a significant reduction in cellular growth when copanlisib and refametinib were used in conjunction with 5-FU chemoradiotherapy versus CRT alone. This correlates with the toxicity assays for *PIK3CA-KRAS*^{mut} and *BRAF*^{mut} cell lines, which showed varying levels of synergism when copanlisib and refametinib were combined. Furthermore, cellular growth was significantly reduced in both *BRAF* mutated and WT cell lines in PM5R treated cells compared to P5R or M5R arms. However, it should be noted that our study involved colonic cancer cell lines which are not typically treated with radiation therapy. Therefore further studies involving rectal cancer cell lines may be more clinically significant.

Furthermore this study focused primarily on proliferation rates of the cancer cells. While proliferation is a vital step in cancer cell growth, other cellular functions could be further analysed for a more rounded view of the affected pathways within the cells. Proteomic studies could be carried out using reverse phase protein arrays (RPPA) or western blots to measure alterations within protein expression levels as a result of treatment with copanlisib, refametinib and / or chemoradiation. This could include measuring apoptosis (AKT, BAK, BAX, BCL2, caspases, PARP), DNA repair (CHK1, MGMT, AGT, PARP), signal transduction (PI3K, RAF, RAS, JNK, PTEN) or cellular stress (CHK1, p53) and transcription (AKT, mTOR, MDM2).

Cancer cell motility can be tested using Boyden chamber or scratch assays for cell migration; whilst cell invasion assays can be used to measure cellular ability to move through an extracellular matrix. Apoptosis could be measured via the Annexin V-FITC or TUNEL assays, whilst DNA damage can be analysed with a comet assay, FISH, ELISA or PCR and agarose gel.

Nevertheless, our findings suggest that copanlisib and/or refametinib may have the ability to enhance the effectiveness of standard chemoradiation therapy in colorectal cancer patients. Further in vivo analysis was carried out to prove that copanlisib or refametinib could have potential in colorectal cancer therapy, which is summarised in chapter 6

**Inhibition of the PI3K signalling pathway increases
chemoradiotherapy sensitivity of genetically defined colorectal
cancer mouse models.**

6.1. Introduction

6.1.1. Overview

PI3K pathway aberrations can result from overexpression of receptor tyrosine kinases, somatic *PIK3CA* mutations or amplifications, and/or loss of *PTEN* function. Mutations within the PI3K pathway (e.g. *PIK3CA*, *KRAS*) have been linked to resistance to chemotherapy and radiation therapy. Therefore personalised therapies which target these mutations may enhance chemoradiation sensitivity.

6.1.2. PI3K inhibitor, Copanlisib

Copanlisib is a potent, highly selective, small-molecule pan class I PI3K α/δ inhibitor. It also targets PI3K β and γ isoforms to a lesser degree, and has a mild inhibitory effect on mTOR. Copanlisib was the first intravenous PI3K α -delta inhibitor to be approved by the U.S. Food and Drug Administration (FDA), under the name of Aliqopa. It received early FDA approval due to the overall response rates seen in the Phase II CHRONOS-1 (NCT01660451) clinical trial which was carried out in 104 patients with relapsed follicular lymphoma who failed to respond to a minimum of two prior systemic therapies.

6.1.3. Our preliminary in vitro study (chapter 5)

Copanlisib has been studied to investigate its pro-apoptotic and anti-tumorigenic properties both in vitro and in vivo. Preliminary in vitro analysis carried out in chapter 5 included proliferation assays using the novel BAYER PI3K inhibitor (copanlisib), and MEK inhibitor (refametinib), in 10 colorectal cancer cell (CRC) lines with varying PI3K and MAPK pathway mutations. In vitro, we have shown that CRC cell lines with mutations in *PIK3CA* and / *KRAS* are sensitive to copanlisib in 2D toxicity assays. We found the *PIK3CA* mutated cell line was most sensitive to the PI3K inhibitor alone, the *KRAS* mutated cell lines were most sensitive to the MEK inhibitor alone, and the *PIK3CA-KRAS* dual-mutated cell lines displayed the most synergistic response to the PI3K:MEK inhibitor combination; whilst the *PIK3CA-KRAS/BRAF*^{wild-type} cell lines were largely resistant to both drugs. Following on from these findings, we used clonogenic assays to determine if the PI3K and MEK inhibitors can augment the effect of

chemoradiation therapy in vitro (see chapter 5). The addition of the PI3K inhibitor copanlisib to chemoradiation resulted in reduced proliferation in all CRC cell lines, compared to chemoradiotherapy treatment alone, with a significant reduction identified in *KRAS* mutated and wild-type CRC cell lines.

6.1.4. Previous in vivo studies of copanlisib.

Liu et al demonstrated complete tumour regression in *PIK3CA^{mut}* HER-2 amplified, breast cancer rat models when treated with copanlisib every second day (122). Furthermore, Okabe et al used a combination of copanlisib and ponatinib (ABL tyrosine kinase inhibitor) therapy to increase survival rates and reduce tumour growth in leukaemia derived allograft mouse models (267). Dewaert et al reported anti-tumour activity in multiple myeloma xenograft models when treated with copanlisib (268).

6.1.5. Clinical trials involving copanlisib

Copanlisib is currently involved in several clinical trials including phase 1 (advanced cancers), phase 2 (mature T-cell + NK cell neoplasm, endometrial endometrioid adenocarcinoma, breast cancer (PANTHER trial)) and phase 3 (non-Hodgkin's lymphoma (CHRONOS trial)).

In vitro, we have demonstrated copanlisib's ability to enhance chemoradiation therapy sensitivity in CRC cell lines (chapter 5). As a result of these promising findings, we wished to further validate these findings in vivo, with the ultimate objective of justifying a clinical trial to determine the efficacy of copanlisib-chemoradiotherapy in LARC. Therefore, our main objectives in this chapter were to:

1. Create xenograft models via subcutaneous implantation of four colorectal cancer cell lines harbouring various PI3K pathway mutations (wild-type, *PIK3CA^{mut}*, *KRAS^{mut}*, and *PIK3CA-KRAS^{mut}*).
2. Treat mice xenograft models bearing these mutations in control, chemoradiotherapy and copanlisib-chemoradiotherapy cohorts.
3. Establish whether a combination of copanlisib, standard chemotherapy and radiation therapy can be tolerated in vivo by mice.
4. Determine the impact of treatment in each cohort on tumour growth, mean survival and overall survival.
5. Determine if copanlisib enhances chemoradiotherapy sensitivity in wild-type, *PIK3CA^{mut}*, *KRAS^{mut}* and *PIK3CA-KRAS^{mut}* xenograft models of CRC.

6.2. Results

6.2.1 Colorectal cancer response to treatment in vivo is dependent on the mutational status of the tumour.

6-8 week old SCID mice were implanted subcutaneously with cancer cell lines (wild-type Caco-2 (3.5×10^6 cells/100ul PBS); *KRAS*^{mut} LS-1034; *PIK3CA*^{mut} SNU-C4 and *PIK3CA-KRAS*^{mut} DLD-1 (2.5×10^6 cells/100ul PBS)). When tumours reached 100mm³, mice were separated into control; vehicle; copanlisib; chemoradiotherapy or copanlisib-chemoradiotherapy treatment regimens. Copanlisib (7mg/kg) was administered intravenously twice a day on days one and two. 5-fluorouracil (5-FU) chemotherapy (20mg/kg) was administered intraperitoneally, and mice were subsequently radiated in a Faxitron CP 160 x-ray generator at 1.8Gy on days 1, 3 and 5. Mice were sacrificed when tumours reached 400mm³.

We found treatment responsiveness depended on the mutational status of the tumour. Wild type xenografts (Caco-2) did not display any response to chemoradiotherapy (5R) compared to control (C) until all 3 rounds of treatment were administered, after which a significant reduction in tumour growth was seen on days 14 ($p = 0.035$) and 15 ($p = 0.031$) (Figure 6.1, supplementary figure 7). In contrast, copanlisib-chemoradiotherapy (P5R) significantly reduced tumour growth, compared to controls (C), in the wild-type xenografts within 24 hours of their first treatment ($p = 0.03$) (Figure 6.2, table 6.1). P5R treatment continued to be associated with a significant reduction in tumour growth on days 3, 6, 7, 13-18 and 25, compared to the control arms.

PIK3CA^{mut} xenografts (SNU-C4 cells) showed a significant reduction in tumour growth on days 16-18 when treated with chemoradiation alone (5R), compared to controls (Figure 6.1). *PIK3CA*^{mut} tumours were the most responsive to initial treatment with copanlisib-chemoradiotherapy. These tumours demonstrated a significant reduction in tumour growth 24 hours after the first round of copanlisib-chemoradiation treatment compared to both control ($p = 0.01$) and chemoradiation alone (5R) ($p = 0.001$) (Figure 6.2, table 6.1, supplementary figure 7) treated xenografts. The copanlisib-chemoradiation therapy (P5R) treated cohort had significantly reduced tumour growth compared to control mice on days 2-9,

14, 15, 19, 20, compared to the 5R treated mouse cohort from days 2-9 and 14-23.

Tumour growth was significantly decreased in the *KRAS*^{mut} xenograft (LS-1034) mice 24 hours after the first round of treatment with copanlisib-chemoradiation (P5R) compared to untreated controls (C) ($p = 0.019$), and remained significantly reduced, up to day 15. In comparison, it took 5 days and 3 rounds of chemoradiotherapy before a significant reduction was achieved in the chemoradiation (5R) treated cohort compared to the untreated controls (C) ($p = 0.031$) (Figure 6.2, table 6.1, supplementary figure 7). Tumour size in the *KRAS*^{mut} xenografts treated with chemoradiation (5R) remained significantly smaller than in untreated control (C) mice from days 6-15 (Figure 6.1).

Copanlisib did not enhance overall sensitivity to chemoradiotherapy in the mice bearing *PIK3CA-KRAS*^{mut} tumours (DLD-1). Tumour growth was similar in both the 5R and P5R treated cohorts, with a reduction in tumour growth observed within 48 hours of treatment initiation, although this did not reach significance. Both 5R and P5R treated xenografts displayed a significant reduction in tumour growth from control mice only on day 22 (p values = 0.044 and 0.017 respectively) (Figure 6.1, Figure 6.2, supplementary figure 7).

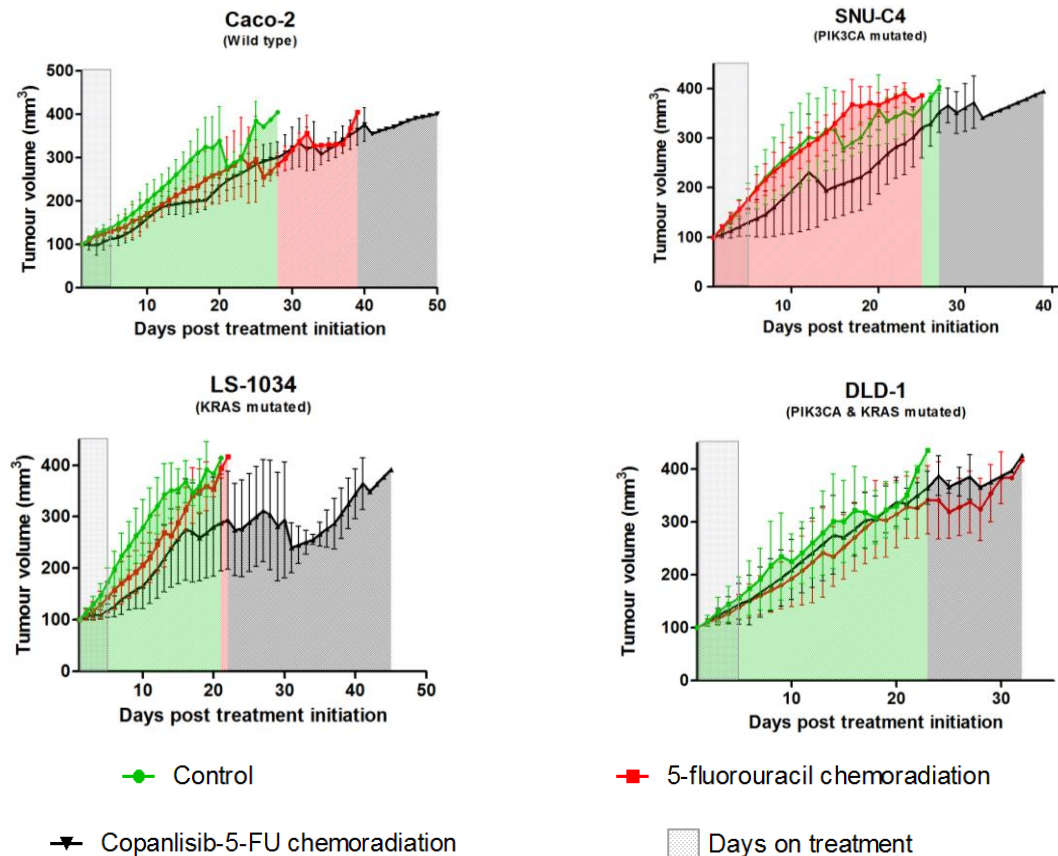


Figure 6.1: Mean tumour growth in wild-type (Caco-2), PIK3CA (SNU-C4), KRAS (LS-1034) and PIK3CA-KRAS (DLD-1) xenograft models.

Colorectal cancer cells ($PIK3CA^{mut}$ (SNU-C4), $n = 2.5 \times 10^6$ cells/100ul; $KRAS^{mut}$ (LS-1034), $n = 2.5 \times 10^6$ cells/100ul; $PIK3CA-KRAS^{mut}$ (DLD-1), $n = 2.5 \times 10^6$ cells/100ul; wild-type (Caco-2), $n = 3.5 \times 10^6$ cells/100ul) were implanted in the right flank of 6-8 week old BALB/C SCID mice. When tumours reached 100mm^3 , mice were randomised into untreated control (C) (●), 5-fluorouracil (5-FU) chemoradiotherapy (5R) (■) and copanlisib plus chemoradiotherapy (P5R) (▼) treatment arms. Copanlisib (7mg/kg) was administered intravenously twice a day on days 1 and 2. 5-FU chemotherapy (20mg/kg) was administered intraperitoneally, and mice were subsequently radiated in a Faxitron CP 160 x-ray generator at 1.8Gy on days 1, 3 and 5. Tumour measurements were taken every third day until tumours reached 400mm^3 , when mice were sacrificed. The grey box indicates the 5 days whilst treatment was ongoing. Prism software (GraphPad) was used for generation of graphs and statistical analysis. Variations in tumour growth between various treatment cohorts was analysed using the one way ANOVA Kruskal-Wallis test (did not assume Gaussian distributions), and the Dunns test, using a confidence interval of 95%. Error bars are representative of standard deviations in each treatment group. Mice whose survival rates were above or below the mean $\pm 2 \times \text{s.d.}$ were removed from the analysis.

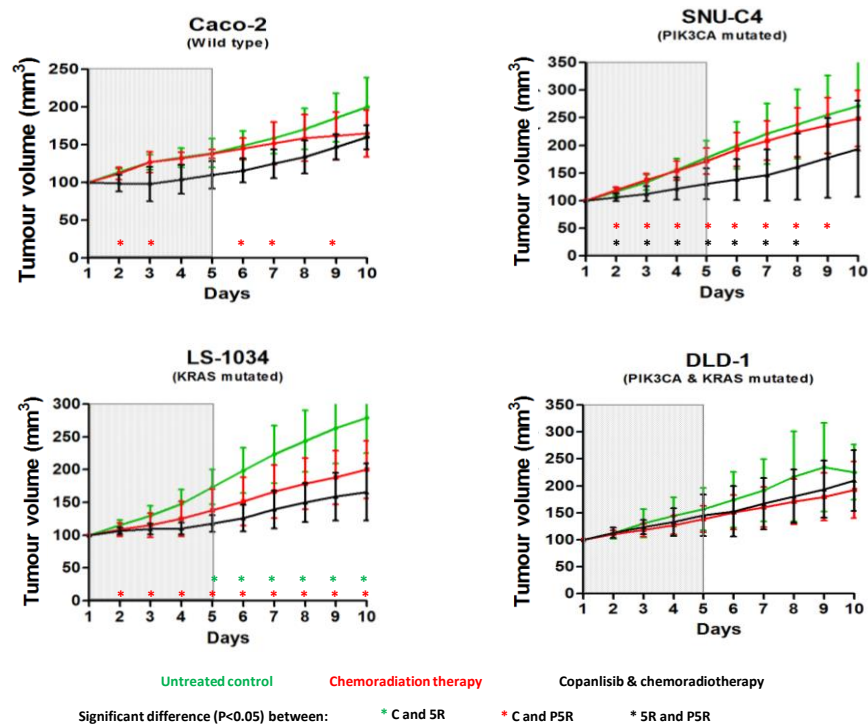


Figure 6.2: Mean tumour growth in wild-type (Caco-2), PIK3CA (SNU-C4), KRAS (LS-1034) and PIK3CA-KRAS (DLD-1) xenograft models during days 1-10 of treatment.

Colorectal cancer cells ($PIK3CA^{mut}$ (SNU-C4), $n = 2.5 \times 10^6$ cells/100ul; $KRAS^{mut}$ (LS-1034), $n = 2.5 \times 10^6$ cells/100ul; $PIK3CA-KRAS^{mut}$ (DLD-1), $n = 2.5 \times 10^6$ cells/100ul; wild-type (Caco-2), $n = 3.5 \times 10^6$ cells/100ul) were implanted in the right flank of 6-8 week old BALB/C SCID mice. When tumours reached 100mm^3 , mice were randomised into untreated control (C) (●), 5-fluorouracil (5-FU) chemoradiotherapy (5R) (■) and copanlisib plus chemoradiotherapy (P5R) (▼) treatment arms.

Copanlisib (7mg/kg) was administered intravenously twice a day on days 1 and 2. 5-FU chemotherapy (20mg/kg) was administered intraperitoneally, and mice were subsequently radiated in a Faxitron CP 160 x-ray generator at 1.8Gy on days 1, 3 and 5. Tumour measurements were taken every third day until tumours reached 400mm^3 , when mice were sacrificed. The grey box indicates the 5 days whilst treatment was ongoing. Prism software (GraphPad) was used for generation of graphs and statistical analysis. Variations in tumour growth between various treatment cohorts was analysed using the one way ANOVA Kruskal-Wallis test (did not assume Gaussian distributions), and the Dunns test, using a confidence interval of 95%. Error bars are representative of standard deviations in each treatment group. * Significant difference ($p < 0.05$) between C and 5R, ** significant difference ($p < 0.05$) between 5R and P5R. F-tests for two sample variances were carried out to calculate F and F-critical values, which determine if the 2 tailed t-test should be of equal or unequal variance.

Table 6.1: P-values for tumour growth (days 2-10) for wild type, PIK3CA, KRAS and PIK3CA-KRAS xenografts.

CRC cells (*PIK3CA^{mut}* (SNU-C4), $n = 2.5 \times 10^6$ cells/100ul; *KRAS^{mut}* (LS-1034), $n = 2.5 \times 10^6$ cells/100ul; *PIK3CA-KRAS^{mut}* (DLD-1), $n = 2.5 \times 10^6$ cells/100ul; wild-type (Caco-2), $n = 3.5 \times 10^6$ cells/100ul) were implanted in the right flank of 6-8 week old BALB/C SCID mice. When tumours reached 100mm³, mice were randomised into untreated control (C), 5-FU chemoradiotherapy (5R) and copanlisib-5-FU chemoradiotherapy (P5R) treatment regimens. Copanlisib (7mg/kg) was administered intravenously twice a day on days 1 and 2. 5-FU chemotherapy (20mg/kg) was administered intraperitoneally, and mice were subsequently radiated in a Faxitron CP 160 x-ray generator at 1.8Gy on days 1, 3 and 5. Tumour measurements were taken every third day until tumours reached 400mm³, when mice were sacrificed. *P*-values represent growth variations between chemoradiation vs copanlisib chemoradiation (5R:P5R), control vs copanlisib chemoradiation (C:P5R), and control vs chemoradiation (C:5R) treated mice. *F*-tests for two sample variances were carried out to calculate *F* and *F*-critical values, which determine if the 2 tailed *t*-test should be of equal or unequal variance. Significant values ($P < 0.05$) are represented in bold.

	Wild-type (Caco-2)			PIK3CA ^{mut} (SNU-C4)			KRAS ^{mut} (LS-1034)			PIK3CA-KRAS ^{co-mut} (DLD-1)		
	5R:P5R	C:P5R	C:5R	5R:P5R	C:P5R	C:5R	5R:P5R	C:P5R	C:5R	5R:P5R	C:P5R	C:5R
Day 2	0.107	0.035	0.648	0.001	0.010	0.434	0.696	0.019	0.136	0.505	0.915	0.607
Day 3	0.132	0.050	0.505	0.002	0.009	0.519	0.453	0.004	0.092	0.399	0.526	0.260
Day 4	0.142	0.053	0.330	0.004	0.003	0.821	0.185	0.001	0.083	0.571	0.469	0.212
Day 5	0.098	0.069	0.384	0.006	0.005	0.669	0.138	0.0003	0.031	0.675	0.572	0.285
Day 6	0.105	0.027	0.324	0.007	0.008	0.701	0.103	0.0001	0.019	0.925	0.392	0.288
Day 7	0.320	0.033	0.323	0.009	0.011	0.587	0.140	0.0005	0.018	0.762	0.369	0.221
Day 8	0.375	0.051	0.419	0.033	0.025	0.596	0.118	0.0003	0.010	0.678	0.300	0.187
Day 9	0.552	0.065	0.338	0.080	0.048	0.544	0.154	0.0004	0.007	0.577	0.259	0.120
Day 10	0.554	0.097	0.280	0.142	0.085	0.518	0.140	0.0004	0.006	0.534	0.583	0.239

6.2.2. Effects of treatment on survival in xenograft models

Tumour growth was reduced in all tumour models when treated with chemoradiation alone (5R) and copanlisib-chemoradiation (P5R), resulting in increased overall survival rates. Chemoradiotherapy (5R) alone did not significantly increase mean overall survival times in any of the genetically defined colorectal cancer mouse models compared to untreated control mice (Figure 6.3). However, mice bearing wild-type tumours displayed a 69% increase in overall survival when treated with chemoradiation alone (mean 5R = 37.2 days) compared to untreated controls (mean C = 22 days). In contrast, mice bearing PI3K pathway mutations did not respond as well to chemoradiation alone (5R), with increased overall survival times of 18.7% (*PIK3CA^{mut}*; mean 5R = 22.2 days, mean C = 18.7 days), 27.6% (*KRAS^{mut}*; mean 5R = 19.9 days, mean C = 15.6 days) and 33.7% (*PIK3CA-KRAS^{mut}*; mean 5R = 23 days, mean C = 17.2 days) compared to untreated controls (Table 6.2, Table 6.4).

Mice bearing wild-type and single gene mutated xenografts (*PIK3CA^{mut}* and *KRAS^{mut}*) generally responded best when treated with copanlisib-chemoradiotherapy (P5R); compared to untreated controls (C) or chemoradiation alone (5R). This was particularly evident in mice bearing *KRAS^{mut}* xenografts who had an increased overall survival of 81% (mean P5R = 28.3 days) compared to untreated controls (mean C = 15.6 days). Mean overall survival times were significantly increased with copanlisib-chemoradiation therapy (P5R) in mice bearing both wild-type (mean = 38.6 ± 8.4 days, p = 0.0057) and *KRAS^{mut}* (mean = 28.3 ± 11.1 days, p = 0.014) xenograft tumours compared to untreated controls (C) (Table 6.2, Table 6.3). Copanlisib did not significantly increase the mean survival of mice bearing *PIK3CA-KRAS^{co-mut}* xenografts when added to chemoradiation therapy.

Chemoradiotherapy increased median overall survival in all xenograft models compared to control-treated mice (WT = 60%; *PIK3CA^{mut}* = 22%; *KRAS^{mut}* = 23.4%; *PIK3CA-KRAS^{mut}* = 27% increase) (Figure 6.4, Table 6.4). However the median overall survival was further increased in the copanlisib-chemoradiotherapy (P5R) treated xenografts (WT = 82.5%; *PIK3CA^{mut}* = 67.3%; *KRAS^{mut}* = 77.3%; *PIK3CA-KRAS^{mut}* = 30.3% increase compared to the untreated control mice). The results were most marked in mice bearing the *PIK3CA^{mut}* and *KRAS^{mut}* xenografts,

whose median overall survival was 37.1% and 43.7% higher with copanlisib-5-FU chemoradiotherapy treatment respectively than with 5-FU chemoradiotherapy treatment. However, the addition of copanlisib to chemoradiation (P5R) did not have any effect on median overall survival in the PIK3CA-KRAS^{mut} xenograft mouse models compared to chemoradiation alone (5R). Overall survival was significantly increased in mice bearing wild-type (P = 0.0046) and KRAS^{mut} (P = 0.0012) xenografts with copanlisib-chemoradiotherapy treatment compared to untreated controls (Figure 6.4,

Table 6.6).

Table 6.2: Mean number of days for xenografted tumours to reach 400mm³.

CRC cells (PIK3CA (SNU-C4), $n = 2.5 \times 10^6$ cells/100ul; KRAS (LS-1034), $n = 2.5 \times 10^6$ cells/100ul; PIK3CA-KRAS (DLD-1), $n = 2.5 \times 10^6$ cells/100ul; wild-type (Caco-2), $n = 3.5 \times 10^6$ cells/100ul) were implanted in the right flank of 6-8 week old BALB/C SCID mice. When tumours reached 100mm³, mice were randomised to untreated control (C), 5-FU chemoradiotherapy (5R) and copanlisib-chemoradiotherapy (P5R) treatment regimens. Copanlisib (7mg/kg) was administered intravenously twice a day on days 1 and 2. 5-FU chemotherapy (20mg/kg) was administered intraperitoneally, and subsequently mice treated radiated in a Faxitron CP 160 x-ray generator at 1.8Gy on days 1, 3 and 5. Tumour measurements were taken every third day until tumours reached 400mm³, when mice were sacrificed.

	C	5R	P5R
Wild-type (Caco-2)	22 ± 4.1	37.2 ± 17.7	38.6 ± 8.4
PIK3CA^{mut} (SNU-C4)	18.7 ± 6.5	22.2 ± 6.8	25.6 ± 9.6
KRAS^{mut} (LS-1034)	15.6 ± 2.7	19.9 ± 5.6	28.3 ± 11.1
PIK3CA-KRAS^{mut} (DLD-1)	17.2 ± 5	23 ± 6.2	22.3 ± 5.5

Table 6.3: Overall survival. F value, F-crit and p-values for the mean number of days it took for tumours to reach 400mm³, comparing control vs. chemoradiotherapy (C: 5R); control vs. copanlisib-chemoradiotherapy (C: P5R); and chemoradiotherapy vs. copanlisib-chemoradiotherapy (P5R) treatment regimens in wild-type, PIK3CA^{mut}, KRAS^{mut} and PIK3CA-KRAS^{mut} xenograft models.

CRC cells (PIK3CA^{mut} (SNU-C4), $n = 2.5 \times 10^6$ cells/100ul; KRAS^{mut} (LS-1034), $n = 2.5 \times 10^6$ cells/100ul; PIK3CA-KRAS^{mut} (DLD-1), $n = 2.5 \times 10^6$ cells/100ul; wild-type (Caco-2), $n = 3.5 \times 10^6$ cells/100ul) were implanted in the right flank of 6-8 week old BALB/C SCID mice. When tumours reached 100mm³, mice were randomised to untreated control (C), chemoradiotherapy (5R) and copanlisib-chemoradiotherapy (P5R) treatment regimens. Copanlisib (7mg/kg) was administered intravenously twice a day on days 1 and 2. 5-FU chemotherapy (20mg/kg) was administered intraperitoneally, and subsequently mice were radiated in a Faxitron CP 160 x-ray generator at 1.8Gy on days 1, 3 and 5. Tumour measurements were taken every third day until tumours reached 400mm³, when mice were sacrificed. F-tests for two sample variances were carried out to calculate F and F-critical values, which determine if the 2 tailed t-test should be of equal or unequal variance. Significant values ($p < 0.05$) are represented in bold.

Mutation status	Value	C:5R	C:P5R	5R:P5R
Wild-type	F-value	17.279	4.191	4.123
	F-Crit	6.388	6.591	9.117
	P-value	0.134	0.006	0.855
PIK3CA	F-value	1.093	2.163	1.980
	F-Crit	3.787	3.787	3.787
	P-value	0.322	0.117	0.426
KRAS	F-value	4.344	17.183	3.956
	F-Crit	3.787	3.787	3.787
	P-value	0.076	0.014	0.084
PIK3CA-KRAS	F-value	1.547	1.235	1.253
	F-Crit	3.787	3.787	3.787
	P-value	0.058	0.077	0.796

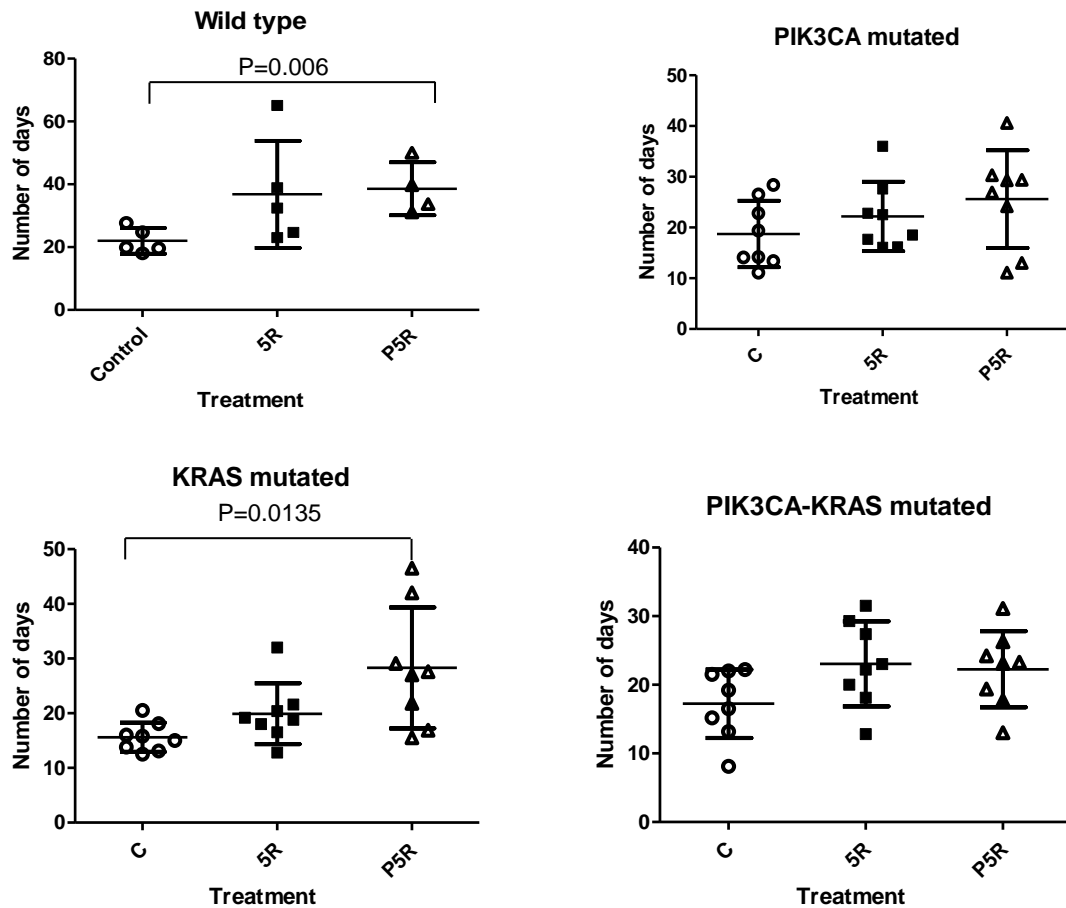


Figure 6.3: Scatter plot depicting the mean number of days per xenograft tumour to reach 400mm³. Tumours were divided into wild-type (Caco-2), PIK3CA^{mut} (SNU-C4), KRAS^{mut} (LS-1034) and PIK3CA-KRAS^{co-mut} (DLD-1) mutations.

CRC cells (PIK3CA (SNU-C4), $n = 2.5 \times 10^6$ cells/100ul; KRAS (LS-1034), $n = 2.5 \times 10^6$ cells/100ul; PIK3CA-KRAS (DLD-1), $n = 2.5 \times 10^6$ cells/100ul; wild-type (Caco-2), $n = 3.5 \times 10^6$ cells/100ul) were implanted in the right flank of 6-8 week old BALB/C SCID mice. When tumours reached 100mm³, mice were randomised into untreated control (C = ○), 5-FU chemoradiotherapy (5R = ■) and copanlisib- 5-FU chemoradiotherapy (P5R = △) treatment regimens. Copanlisib (7mg/kg) was administered intravenously twice a day on days 1 and 2. 5-FU chemotherapy (20mg/kg) was administered intraperitoneally, and mice were subsequently radiated in a Faxitron CP 160 x-ray generator at 1.8Gy on days 1, 3 and 5. Tumour measurements were taken every third day until tumours reached 400mm³, when mice were sacrificed. Significant differences ($p < 0.05$) are indicated. Prism software (GraphPad) was used for generation of graphs and statistical analysis. Tumour growth was analysed using the unpaired 2-tailed *t*-test with Welch's correction and a confidence interval of 95%. Error bars are representative of the mean and standard deviations per treatment group.

Table 6.4: Mean, median, range and standard deviation values for survival times in mice bearing wild-type, PIK3CA, KRAS and PIK3CA-KRAS mutant xenografts by treatment cohort (untreated control (C), chemoradiotherapy (5R) and copanlisib chemoradiotherapy (P5R)).

CRC cells (PIK3CA (SNU-C4), $n = 2.5 \times 10^6$ cells/100ul; KRAS (LS-1034), $n = 2.5 \times 10^6$ cells/100ul; PIK3CA-KRAS (DLD-1), $n = 2.5 \times 10^6$ cells/100ul; wild-type (Caco-2), $n = 3.5 \times 10^6$ cells/100ul) were implanted in the right flank of 6-8 week old BALB/C SCID mice. When tumours reached 100mm³, mice were randomised to untreated control (C), chemoradiotherapy (5R) and copanlisib-chemoradiotherapy (P5R) treatment regimens. Copanlisib (7mg/kg) was administered intravenously twice a day on days 1 and 2. 5-FU chemotherapy (20mg/kg) was administered intraperitoneally, and mice were subsequently radiated in a Faxitron CP 160 x-ray generator at 1.8Gy on days 1, 3 and 5. Tumour measurements were taken every third day until tumours reached 400mm³, when mice were sacrificed.

		Wild-type (%)	PIK3CA ^{mut} (%)	KRAS ^{mut} (%)	PIK3CA-KRAS ^{mut} (%)
Mean	C	22 ± 4.1	18.7 ± 6.5	15.6 ± 2.7	17.2 ± 5
	5R	37.2 ± 17.7	22.2 ± 6.8	19.9 ± 5.6	23 ± 6.2
	P5R	38.6 ± 8.4	25.6 ± 9.6	28.3 ± 11.1	22.3 ± 5.5
Median	C	20	16.8	15.4	17.8
	5R	32	20.5	19	22.6
	P5R	36.5	28.1	27.3	23.2
Range	C	18 - 27.7	11.1 - 28.4	12.5 - 20.5	8.1 - 22.2
	5R	23 - 65.1	16.1 - 36	12.8 - 32	12.8 - 31.5
	P5R	31 - 50	11 - 40.6	15.5 - 46.5	13 - 31.1

Further survival analysis demonstrated that of the untreated control mice, only 13% of those bearing *KRAS*^{mut} xenograft survived up to day 20, compared to mice bearing WT (40%), *PIK3CA*^{mut} (38%) or *PIK3CA-KRAS*^{mut} (38%) xenografts (Table 6.5). Similarly, *KRAS*^{mut} xenograft models were the least responsive to chemoradiotherapy (5R) (38% survival on day 20), compared to WT (100%), *PIK3CA*^{mut} (50%), or *PIK3CA-KRAS*^{co-mut} (75%) xenograft models. However, 75% of *KRAS*^{mut} xenograft mice remained alive at 20 days when treated with copanlisib-chemoradiotherapy (P5R). Mice bearing WT tumours treated with chemoradiotherapy, either with (P5R) or without copanlisib (5R), 100% were alive at day 20 compared to 40% in the matched untreated control cohort.

No mice in any of the four control groups were alive at 30 days. Survival rates were also analysed in the 5R and P5R treated mice at 30 days. The addition of copanlisib to chemoradiation did not increase survival in mice bearing *PIK3CA-KRAS*^{co-mut} xenografts (5R and P5R = 13% survival). Both *PIK3CA*^{mut} and *KRAS*^{mut} xenograft mice had a 13% survival rate when treated with 5R, compared to a 25% survival rate with P5R. Mice bearing wild-type xenografts had the best survival rates at 30 days in both 5R and P5R treated cohorts (60% and 100% respectively).

Survival rates were also analysed in the 5R and P5R treated mice at 40 days. In the *KRAS*^{mut} and *PIK3CA*^{mut} xenograft models, only mice who received copanlisib in addition to chemoradiation survived to 40 days (25% and 13% respectively). In the WT xenograft model, 20% of mice who were treated with chemoradiation survived to 40 days, while the addition of copanlisib to chemoradiation increased the survival rate to 25% (Table 6.5).

		Wild-type (%)			PIK3CA (%)			KRAS (%)			PIK3CA-KRAS (%)		
		C	5R	P5R	C	5R	P5R	C	5R	P5R	C	5R	P5R
% Survival	10 days	100	100	100	100	100	100	100	100	100	88	100	100
	20 days	40	100	100	38	50	75	13	38	75	38	75	63
	30 days	0	60	100	0	13	25	0	13	25	0	13	13
	40 days	0	20	25	0	0	13	0	0	25	0	0	0

Table 6.5: Survival fractions at 10, 20, 30 and 40 days post commencement of treatment.

CRC cells (PIK3CA (SNU-C4), $n = 2.5 \times 10^6$ cells/100ul; KRAS (LS-1034), $n = 2.5 \times 10^6$ cells/100ul; PIK3CA-KRAS (DLD-1), $n = 2.5 \times 10^6$ cells/100ul; wild-type (Caco-2), $n = 3.5 \times 10^6$ cells/100ul) were implanted in the right flank of 6-8 week old BALB/C SCID mice. When tumours reached 100mm^3 , mice were randomised to untreated control (C), chemoradiotherapy (5R) and copanlisib-chemoradiotherapy (P5R) treatment regimens. Copanlisib (7mg/kg) was administered intravenously twice a day on days 1 and 2. 5-FU chemotherapy (20mg/kg) was administered intraperitoneally, and mice were subsequently radiated in a Faxitron CP 160 x-ray generator at 1.8Gy on days 1, 3 and 5. Tumour measurements were taken every third day until tumours reached 400mm^3 , when mice were sacrificed.

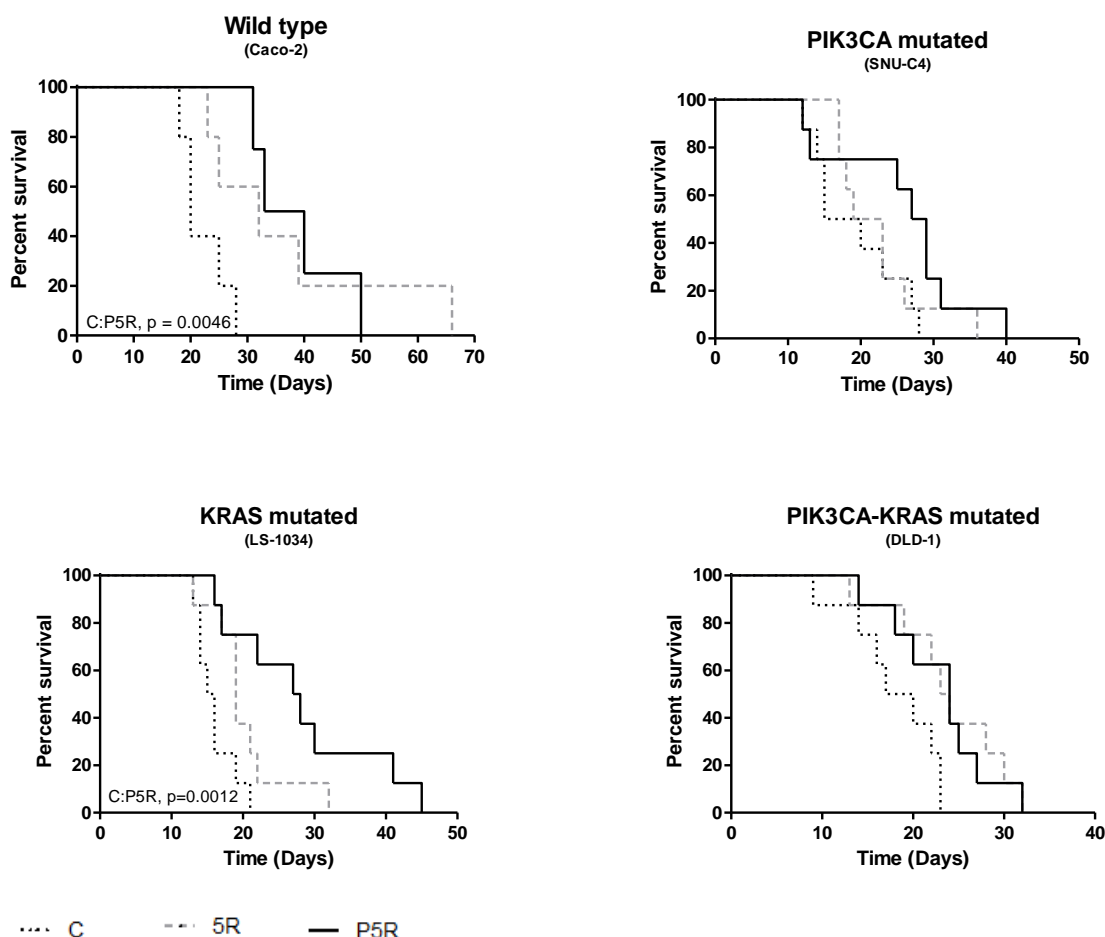


Figure 6.4: Kaplan-Meier survival curves for mice implanted with wild-type (Caco-2), PIK3CA^{mut} (SNU-C4), KRAS^{mut} (LS-1034) and PIK3CA-KRAS^{mut} (DLD-1) tumours

CRC cells (PIK3CA (SNU-C4), $n = 2.5 \times 10^6$ cells/100ul; KRAS (LS-1034), $n = 2.5 \times 10^6$ cells/100ul; PIK3CA-KRAS (DLD-1), $n = 2.5 \times 10^6$ cells/100ul; wild-type (Caco-2), $n = 3.5 \times 10^6$ cells/100ul) were implanted in the right flank of 6-8 week old BALB/C SCID mice. When tumours reached 100mm³, mice were randomised to untreated control (C), 5-FU chemoradiotherapy (5R) and copanlisib-chemoradiotherapy (P5R) treatment regimens. Copanlisib (7mg/kg) was administered intravenously twice a day on days 1 and 2. 5-FU chemotherapy (20mg/kg) was administered intraperitoneally, and mice were subsequently radiated in a Faxitron CP 160 x-ray generator at 1.8Gy on days 1, 3 and 5. Tumour measurements were taken every third day until tumours reached 400mm³, when mice were sacrificed. Prism software (GraphPad) was used for generation of graphs and statistical analysis. Survival was calculated using Kaplan-Meier survival curves, and p-values were calculated using the log-rank (Mantel-Cox) test. The Bonferroni method was used to calculate the statistical significance for the p-value, assuming a significant value of 0.05.

Table 6.6: Log-rank (Mantel-Cox) test used to determine significant differences in survival curves

CRC cells (PIK3CA (SNU-C4), $n = 2.5 \times 10^6$ cells/100ul; KRAS (LS-1034), $n = 2.5 \times 10^6$ cells/100ul; PIK3CA-KRAS (DLD-1), $n = 2.5 \times 10^6$ cells/100ul; wild-type (Caco-2), $n = 3.5 \times 10^6$ cells/100ul) were implanted in the right flank of 6-8 week old BALB/C SCID mice. When tumours reached 100mm^3 , mice were randomised into untreated control (C), chemoradiotherapy (5R) and copanlisib-chemoradiotherapy (P5R) treatment regimens. Copanlisib (7mg/kg) was administered intravenously twice a day on days 1 and 2. 5-FU chemotherapy (20mg/kg) was administered intraperitoneally, and subsequently radiated in a Faxitron CP 160 x-ray generator at 1.8Gy on days 1, 3 and 5. Tumour measurements were taken every third day until tumours reached 400mm^3 , when mice were sacrificed. Kaplan-Meier curves were used to plot survival curves. P-values were subsequently determined from the Log-rank (Mantel-cox) test, and significant values of $p < 0.0167$ were calculated from the Bonferroni method (assuming a significant value of 0.05, and number of possible tests (K) = 3).

	Wild-type	PIK3CA	KRAS	PIK3CA-KRAS
C:5R	0.0439	0.5047	0.0448	0.0335
C:P5R	0.0046	0.0454	0.0012	0.0219
5R:P5R	0.8398	0.227	0.1019	0.8228

6.2.3. Tolerability of copanlisib chemoradiotherapy in vivo.

Clinical trial data has reported manageable side effects of copanlisib including hypertension, hyperglycaemia, infections (particularly pneumonia), embryo-foetal toxicity, leukopenia, neutropenia, thrombocytopenia, diarrhoea, nausea and cutaneous reactions.

A preliminary pilot study was carried out in 10 mice to determine optimal drug scheduling and to ensure mice had sufficient time to recover between treatments. Copanlisib was given twice daily on days 1 and 2, and mice were left to recover for 1-2 hours between copanlisib IV injections. Chemotherapy and radiation were separated by 1-2 hours, and given on days 1, 3 and 5, to allow for mice to recover in between. To minimise weight loss as a result of possible diarrhoea or nausea, mice were given high fat DietGel, alongside dry food for a week during treatment. Mice were weighed every 2-3 days, monitored more often if their weight dropped by 10% and culled if it dropped by 20% since the start of treatment.

Overall, the dosages of copanlisib (7mg/kg x 4), chemotherapy (20mg/kg x 3) and radiation (1.8Gy x 3) were all well tolerated by the mice. Mice demonstrated little or no weight loss during treatments in all cohorts (Figure 6.5).

Splenomegaly was evident in mice bearing wild-type (n=1) and *PIK3CA-KRAS^{mut}* (n=2) xenografts in the P5R treatment cohorts (Figure 6.6, supplementary figure 9). Spleens were significantly larger in mice with *KRAS^{mut}* 5R treated xenografts compared with control (p = 0.0002) or P5R-treated mice (0.038). Similarly, mice with *PIK3CA^{mut}* xenografts had significantly smaller spleens when treated with P5R than 5R (p = 0.047). In contrast, mice with *PIK3CA-KRAS^{mut}* xenografts displayed significant splenomegaly after P5R treatment compared with control (p = 0.048) or 5R treatment (p = 0.043). No significant difference was identified in wild-type tumours (Figure 6.6).

Liver mass was significantly increased in mice with *PIK3CA-KRAS^{mut}* xenografts when treated with P5R compared to control or 5R (

Figure 6.8, supplementary figure 11). Conversely, mice with wild type xenografts had significantly smaller livers in the P5R cohort compared to control ($p = 0.03$) or 5R ($p = 0.003$) treated cohorts.

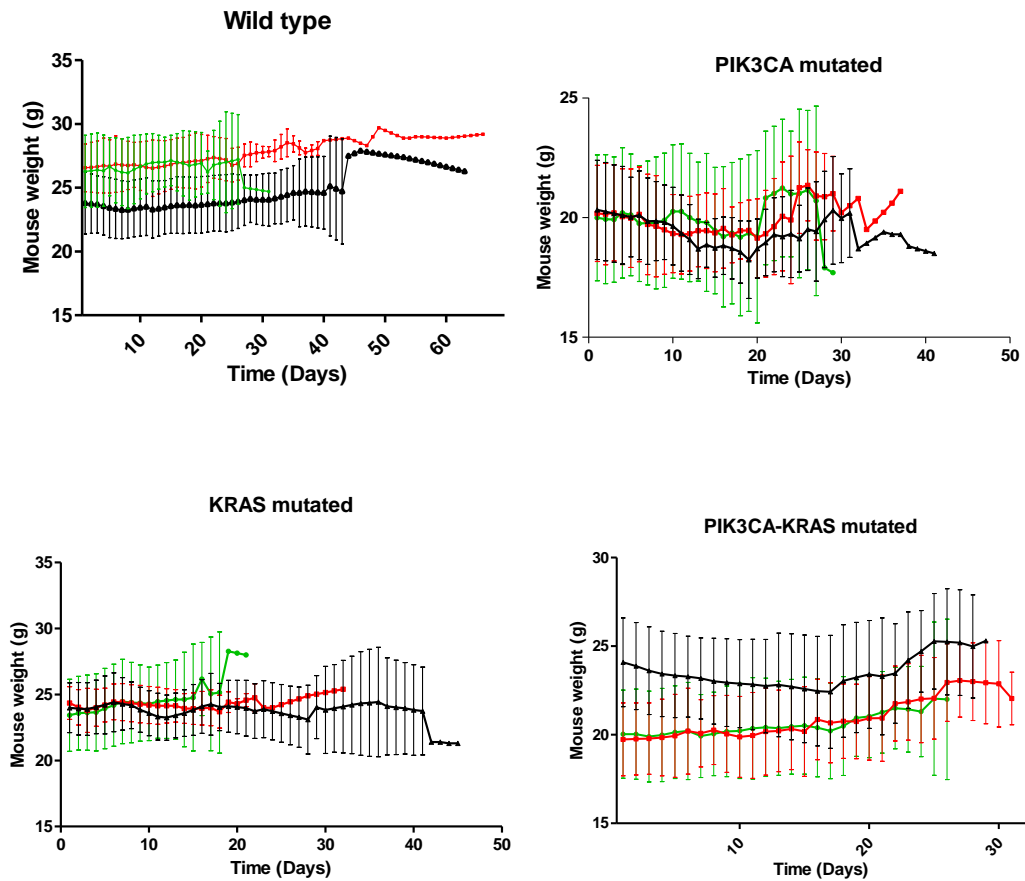
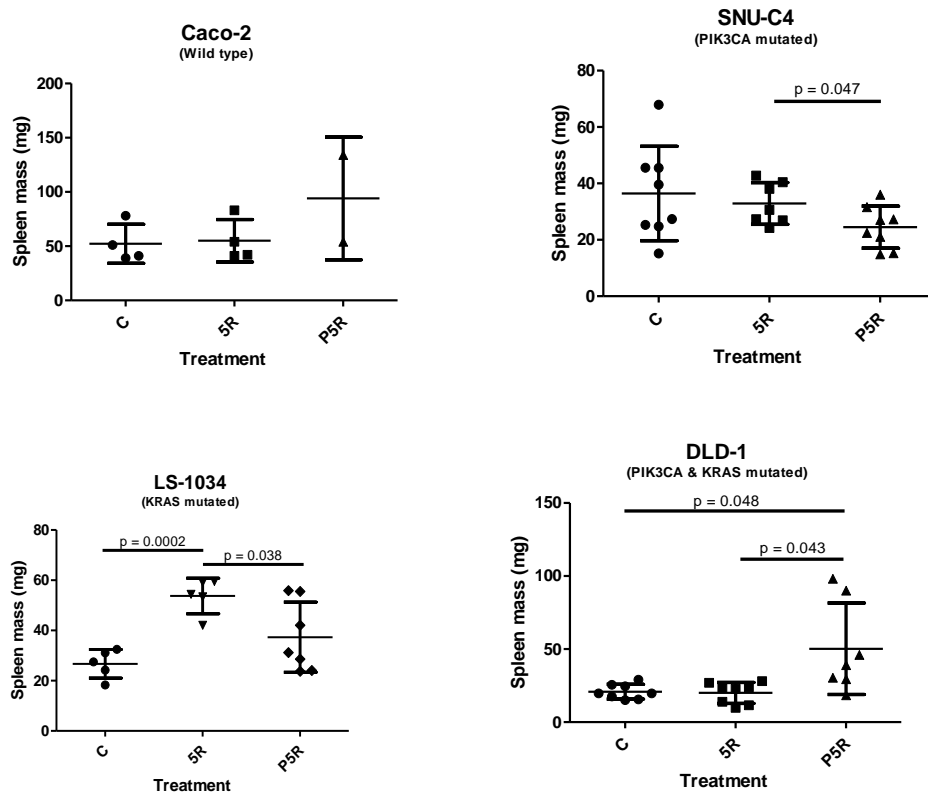


Figure 6.5: Mean body weight alterations over the course of the study.

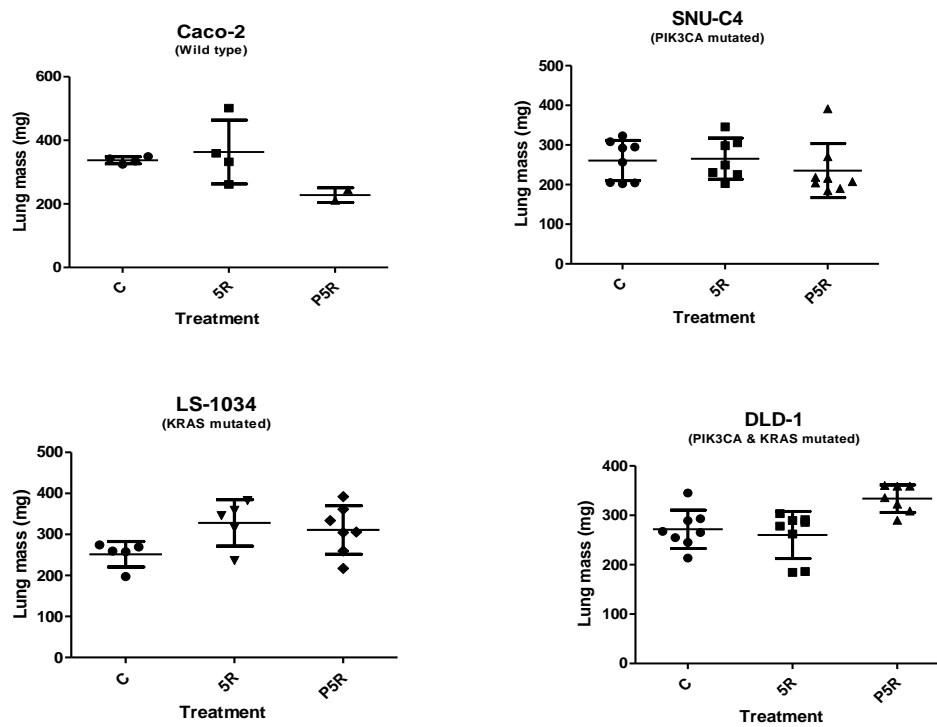
CRC cells (PIK3CA (SNU-C4), $n = 2.5 \times 10^6$ cells/100ul; KRAS (LS-1034), $n = 2.5 \times 10^6$ cells/100ul; PIK3CA-KRAS (DLD-1), $n = 2.5 \times 10^6$ cells/100ul; wild-type (Caco-2), $n = 3.5 \times 10^6$ cells/100ul) were implanted in the right flank of 6-8 week old BALB/C SCID mice. When tumours reached 100mm^3 , mice were randomised to untreated control (C) (●), chemoradiotherapy (5R) (■) and copanlisib-chemoradiotherapy (P5R) (▼) treatment regimens. Copanlisib (7mg/kg) was administered intravenously twice a day on days 1 and 2. 5-FU chemotherapy (20mg/kg) was administered intraperitoneally, and subsequently mice were radiated in a Faxitron CP 160 x-ray generator at 1.8Gy on days 1, 3 and 5. Tumour measurements were taken every third day until tumours reached 400mm^3 , when mice were sacrificed. Measurements show mean body weight alterations starting from day 1 of treatment, until the study endpoint. Error bars are representative of the mean and standard deviations per treatment group.



	C (mg)	5R (mg)	P5R (mg)
Wild type	52 ± 18	55 ± 20	94 ± 57
KRAS	27 ± 6	54 ± 7	39 ± 15
PIK3CA	36 ± 17	33 ± 7	25 ± 8
PIK3CA-KRAS	21 ± 5	20 ± 7	50 ± 31

Figure 6.6: Spleen mass in wild-type (Caco-2 = ▲), KRAS^{mut} (LS-1034 = ○), PIK3CA^{mut} (SNU-C4 = ■) and PIK3CA-KRAS^{mut} (DLD-1 = ◇) xenograft mice at the time of sacrifice.

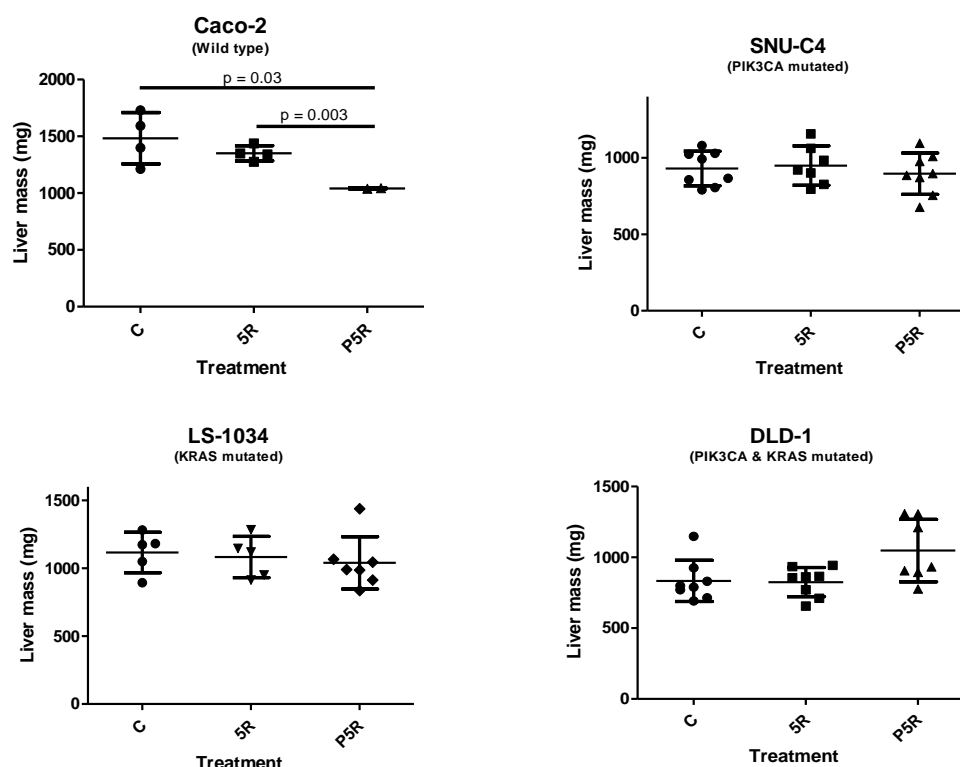
CRC cells (PIK3CA (SNU-C4), $n = 2.5 \times 10^6$ cells/100ul; KRAS (LS-1034), $n = 2.5 \times 10^6$ cells/100ul; PIK3CA-KRAS (DLD-1), $n = 2.5 \times 10^6$ cells/100ul; wild-type (Caco-2), $n = 3.5 \times 10^6$ cells/100ul) were implanted in the right flank of 6-8 week old BALB/C SCID mice. When tumours reached 100mm³, mice were randomised to untreated control (C), chemoradiotherapy (5R) and copanlisib-chemoradiotherapy (P5R) treatments. Copanlisib (7mg/kg) was administered intravenously twice a day on days 1 and 2. 5-FU chemotherapy (20mg/kg) was administered intraperitoneally, and subsequently radiated in a Faxitron CP 160 x-ray generator at 1.8Gy on days 1, 3 and 5. Tumour measurements were taken every third day until tumours reached 400mm³, when mice were sacrificed. Error bars are representative of the mean and standard deviations per treatment group.



	C	5R	P5R
Wild type	337 ± 11	363 ± 101	228 ± 24
KRAS	246 ± 33	328 ± 57	312 ± 65
PIK3CA	261 ± 51	265 ± 52	235 ± 68
PIK3CA-KRAS	272 ± 39	260 ± 48	334 ± 28

Figure 6.7: Scatter plot depicting lung mass (mg) excised from wild-type (Caco-2 = ▲), KRAS^{mut} (LS-1034 = ○), PIK3CA^{mut} (SNU-C4 = ■) and PIK3CA-KRAS^{mut} (DLD-1 = ◇) xenograft models.

CRC cells (PIK3CA (SNU-C4), $n = 2.5 \times 10^6$ cells/100ul; KRAS (LS-1034), $n = 2.5 \times 10^6$ cells/100ul; PIK3CA-KRAS (DLD-1), $n = 2.5 \times 10^6$ cells/100ul; wild-type (Caco-2), $n = 3.5 \times 10^6$ cells/100ul) were implanted in the right flank of 6-8 week old BALB/C SCID mice. When tumours reached 100mm³, mice were randomised to untreated control (C), chemoradiotherapy (5R) and copanlisib-chemoradiotherapy (P5R) treatments. Copanlisib (7mg/kg) was administered intravenously twice a day on days 1 and 2. 5-FU chemotherapy (20mg/kg) was administered intraperitoneally, and subsequently radiated in a Faxitron CP 160 x-ray generator at 1.8Gy on days 1, 3 and 5. Tumour measurements were taken every third day until tumours reached 400mm³, when mice were sacrificed and tumour, liver, lungs and spleen were excised. Prism software (GraphPad) was used for generation of graphs and statistical analysis was carried out using the unpaired 2-tailed t-test with Welch's correction and a confidence interval of 95%. Error bars are representative of the mean and standard deviations per treatment group



	C	5R	P5R
Wild type	1483 ± 226	1351 ± 67	1041 ± 3
KRAS	208 ± 455	1716 ± 535	1822.2 ± 453
PIK3CA	931 ± 113	950 ± 129	896 ± 135
PIK3CA-KRAS	834 ± 146	825 ± 103	1048 ± 220

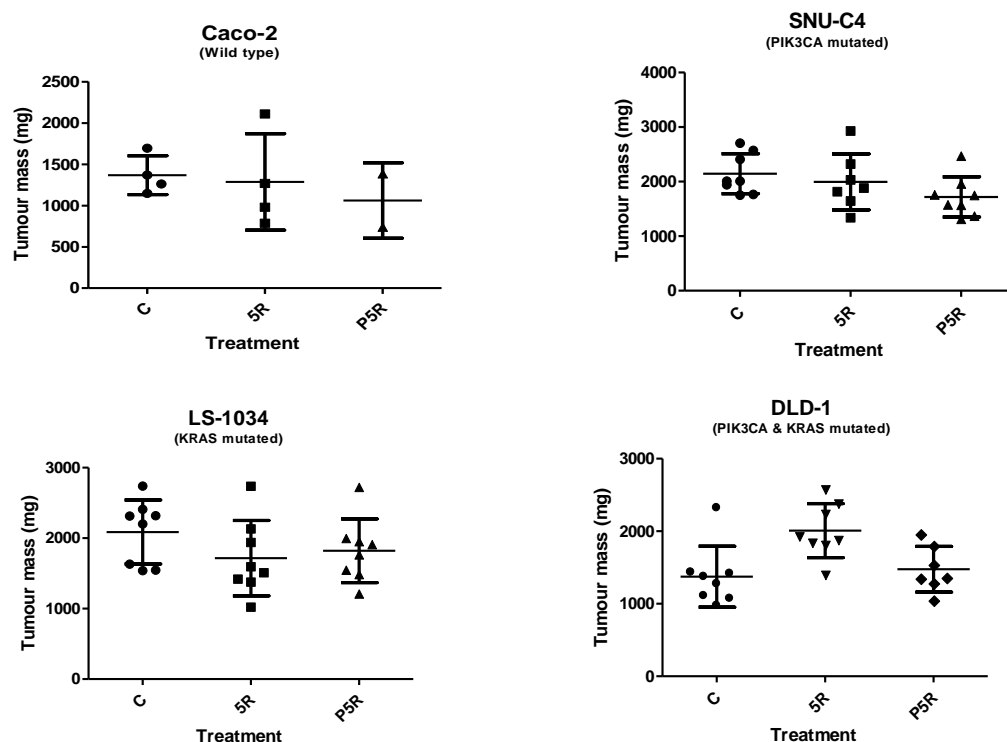
Figure 6.8: Scatter plot depicting liver mass (mg) excised from wild-type (Caco-2 = ▲), KRAS^{mut} (LS-1034 = ○), PIK3CA^{mut} (SNU-C4 = ■) and PIK3CA-KRAS^{mut} (DLD-1 = ◇) xenograft models.

CRC cells (PIK3CA (SNU-C4), $n = 2.5 \times 10^6$ cells/100ul; KRAS (LS-1034), $n = 2.5 \times 10^6$ cells/100ul; PIK3CA-KRAS (DLD-1), $n = 2.5 \times 10^6$ cells/100ul; wild-type (Caco-2), $n = 3.5 \times 10^6$ cells/100ul) were implanted in the right flank of 6-8 week old BALB/C SCID mice. When tumours reached 100mm³, mice were randomised to untreated control (C), chemoradiotherapy (5R) and copanlisib-chemoradiotherapy (P5R) treatments. Copanlisib (7mg/kg) was administered intravenously twice a day on days 1 and 2. 5-FU chemotherapy (20mg/kg) was administered intraperitoneally, and subsequently radiated in a Faxitron CP 160 x-ray generator at 1.8Gy on days 1, 3 and 5. Tumour measurements were taken every third day until tumours reached 400mm³, when mice were sacrificed and tumour, liver, lungs and spleen were excised. Prism software (GraphPad) was used for generation of graphs and statistical analysis was carried out using the unpaired 2-tailed t-test with Welch's correction and a confidence interval of 95%. Error bars are representative of the mean and standard deviations per treatment group

6.2.4. Macroscopic variability between tumours based on their mutational status and treatment regimens.

Tumours were weighed at the time of sacrifice, as soon as they were removed from the mice. Tumour mass was generally consistent, irrespective of treatment regimens (Table 6.7, Figure 6.9, supplementary figure 8). However, some minor differences emerged. *PIK3CA-KRAS^{mut}* tumours from the control cohort weighed significantly less than tumours treated with chemoradiation ($p = 0.006$), whilst *PIK3CA^{mut}* tumours weighed significantly more in the control group than their P5R treatment counterparts ($p = 0.036$).

Macroscopic analysis showed tumours in the *PIK3CA^{mut}* control cohort displayed increased bleeding within the tumour tissue compared to the 5R or P5R treatment groups (Figure 6.11). Oedema and bruising occurred in *KRAS^{mut}* (Figure 6.12), and to a lesser extent wild-type tumours (Figure 6.10); irrespective of the treatment group. No difference could be noted macroscopically in *PIK3CA-KRAS^{mut}* tumours across the 3 treatment cohorts (Figure 6.13).



	C (mg)	5R (mg)	P5R (mg)
Wild type	1368 ± 236	1286 ± 583	1062 ± 456
KRAS	2152 ± 449	1684 ± 570	1831 ± 488
PIK3CA	2145 ± 367	1994 ± 513	1719 ± 369
PIK3CA-KRAS	1374 ± 420	2009 ± 373	1476 ± 315

Figure 6.9: Scatter plot depicting primary tumour mass (mg) excised from wild-type (Caco-2 = ▲), KRAS^{mut} (LS-1034 = ○), PIK3CA^{mut} (SNU-C4 = ■) and PIK3CA-KRAS^{mut} (DLD-1 = ◇) xenograft models.

CRC cells (PIK3CA (SNU-C4), $n = 2.5 \times 10^6$ cells/100ul; KRAS (LS-1034), $n = 2.5 \times 10^6$ cells/100ul; PIK3CA-KRAS (DLD-1), $n = 2.5 \times 10^6$ cells/100ul; wild-type (Caco-2), $n = 3.5 \times 10^6$ cells/100ul) were implanted in the right flank of 6-8 week old BALB/C SCID mice. When tumours reached 100mm³, mice were randomised to untreated control (C), chemoradiotherapy (5R) and copanlisib-chemoradiotherapy (P5R) treatments. Copanlisib (7mg/kg) was administered intravenously twice a day on days 1 and 2. 5-FU chemotherapy (20mg/kg) was administered intraperitoneally, and subsequently mice were radiated in a Faxitron CP 160 x-ray generator at 1.8Gy on days 1, 3 and 5. Tumour measurements were taken every third day until tumours reached 400mm³, when mice were sacrificed and tumour, liver, lungs and spleen were excised. Prism software (GraphPad) was used for generation of graphs and statistical analysis was carried out using the unpaired 2-tailed t-test with Welch's correction and a confidence interval of 95%. Error bars are representative of the mean and standard deviations per treatment group

	C:5R	C:P5R	5R:P5R
WT	0.802	0.312	0.665
KRAS	0.156	0.262	0.673
PIK3CA	0.519	0.036	0.251
PIK3CA-KRAS	0.006	0.606	0.011

Table 6.7: P-values for variation in tumour mass for wild type, KRAS, PIK3CA and PIK3CA-KRAS tumours, depending on the treatment regimen. CRC cells (PIK3CA (SNU-C4), $n = 2.5 \times 10^6$ cells/100ul; KRAS (LS-1034), $n = 2.5 \times 10^6$ cells/100ul; PIK3CA-KRAS (DLD-1), $n = 2.5 \times 10^6$ cells/100ul; wild-type (Caco-2), $n = 3.5 \times 10^6$ cells/100ul) were implanted in the right flank of 6-8 week old BALB/C SCID mice. When tumours reached 100mm³, mice were randomised to untreated control (C), chemoradiotherapy (5R) and copanlisib-chemoradiotherapy (P5R) treatment regimens. Copanlisib (7mg/kg) was administered intravenously twice a day on days 1 and 2. 5-FU chemotherapy (20mg/kg) was administered intraperitoneally, and mice were subsequently radiated in a Faxitron CP 160 x-ray generator at 1.8Gy on days 1, 3 and 5. Tumour measurements were taken every third day until tumours reached 400mm³, when mice were sacrificed and tumour, liver, lungs and spleen were excised. Prism software (GraphPad) was used for generation of graphs and statistical analysis was carried out using the unpaired 2-tailed t-test with Welch's correction and a confidence interval of 95%.

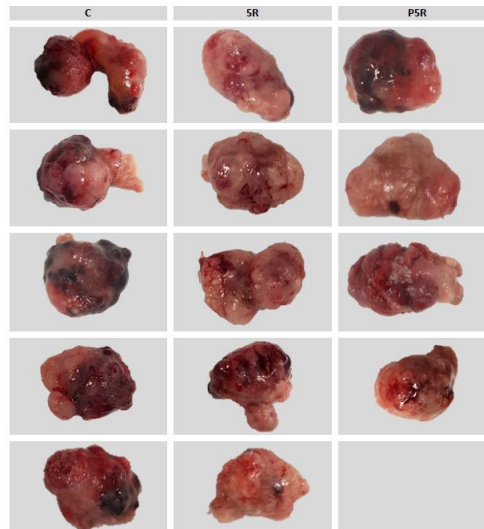


Figure 6.10: Macroscopic view of wild-type tumours from mice after sacrifice CRC cells (PIK3CA (SNU-C4), $n = 2.5 \times 10^6$ cells/100ul; KRAS (LS-1034), $n = 2.5 \times 10^6$ cells/100ul; PIK3CA-KRAS (DLD-1), $n = 2.5 \times 10^6$ cells/100ul; wild-type (Caco-2), $n = 3.5 \times 10^6$ cells/100ul) were implanted in the right flank of 6-8 week old BALB/C SCID mice. When tumours reached 100mm^3 , mice were randomised to untreated control (C), chemoradiotherapy (5R) and copanlisib-chemoradiotherapy (P5R) treatment regimens. Copanlisib (7mg/kg) was administered intravenously twice a day on days 1 and 2. 5-FU chemotherapy (20mg/kg) was administered intraperitoneally, and mice were subsequently radiated in a Faxitron CP 160 x-ray generator at 1.8Gy on days 1, 3 and 5. Tumour measurements were taken every third day until tumours reached 400mm^3 , when mice were sacrificed and tumour, liver, lungs and spleen were excised.



Figure 6.11: Macroscopic view of PIK3CA^{mut} tumours from mice after sacrifice.

CRC cells (PIK3CA (SNU-C4), $n = 2.5 \times 10^6$ cells/100ul; KRAS (LS-1034), $n = 2.5 \times 10^6$ cells/100ul; PIK3CA-KRAS (DLD-1), $n = 2.5 \times 10^6$ cells/100ul; wild-type (Caco-2), $n = 3.5 \times 10^6$ cells/100ul) were implanted in the right flank of 6-8 week old BALB/C SCID mice. When tumours reached 100mm³, mice were randomised to untreated control (C), chemoradiotherapy (5R) and copanlisib-chemoradiotherapy (P5R) treatment regimens. Copanlisib (7mg/kg) was administered intravenously twice a day on days 1 and 2. 5-FU chemotherapy (20mg/kg) was administered intraperitoneally, and mice were subsequently radiated in a Faxitron CP 160 x-ray generator at 1.8Gy on days 1, 3 and 5. Tumour measurements were taken every third day until tumours reached 400mm³, when mice were sacrificed and tumour, liver, lungs and spleen were excised.



Figure 6.12: Macroscopic view of KRAS^{mut} tumours from mice after sacrifice. CRC cells (PIK3CA (SNU-C4), $n = 2.5 \times 10^6$ cells/100ul; KRAS (LS-1034), $n = 2.5 \times 10^6$ cells/100ul; PIK3CA-KRAS (DLD-1), $n = 2.5 \times 10^6$ cells/100ul; wild-type (Caco-2), $n = 3.5 \times 10^6$ cells/100ul) were implanted in the right flank of 6-8 week old BALB/C SCID mice. When tumours reached 100mm³, mice were randomised to untreated control (C), chemoradiotherapy (5R) and copanlisib-chemoradiotherapy (P5R) treatment regimens. Copanlisib (7mg/kg) was administered intravenously twice a day on days 1 and 2. 5-FU chemotherapy (20mg/kg) was administered intraperitoneally, and mice were subsequently radiated in a Faxitron CP 160 x-ray generator at 1.8Gy on days 1, 3 and 5. Tumour measurements were taken every third day until tumours reached 400mm³, when mice were sacrificed and tumour, liver, lungs and spleen were excised.



Figure 6.13: Macroscopic view of PIK3CA-KRAS^{mut} tumours from mice after sacrifice.

CRC cells (PIK3CA (SNU-C4), $n = 2.5 \times 10^6$ cells/100ul; KRAS (LS-1034), $n = 2.5 \times 10^6$ cells/100ul; PIK3CA-KRAS (DLD-1), $n = 2.5 \times 10^6$ cells/100ul; wild-type (Caco-2), $n = 3.5 \times 10^6$ cells/100ul) were implanted in the right flank of 6-8 week old BALB/C SCID mice. When tumours reached 100mm^3 , mice were randomised to untreated control (C), chemoradiotherapy (5R) and copanlisib-chemoradiotherapy (P5R) treatment regimens. Copanlisib (7mg/kg) was administered intravenously twice a day on days 1 and 2. 5-FU chemotherapy (20mg/kg) was administered intraperitoneally, and mice were subsequently radiated in a Faxitron CP 160 x-ray generator at 1.8Gy on days 1, 3 and 5. Tumour measurements were taken every third day until tumours reached 400mm^3 , when mice were sacrificed and tumour, liver, lungs and spleen were excised.

6.2.5. Microscopic variability between tumours based on their mutational status and treatment regimens.

Caco-2

Caco-2 (WT) tumours consisted of highly proliferative (Ki67 positive), well-differentiated, glandular epithelium encasing large necrotic cores (Figure 6.14A-D). Mass inflammatory cell infiltration was identified within the necrotic tissue (Figure 6.14A, B). Ki67 positive cells were scattered throughout the spleen in all treatment groups (control = 3/5, chemoradiation (5R) = 5/5, copanlisib-chemoradiation (P5R) = 2/4 xenografts), and in the liver and lungs of 1/5 (20%) Caco-2 xenografts treated with chemoradiation therapy.

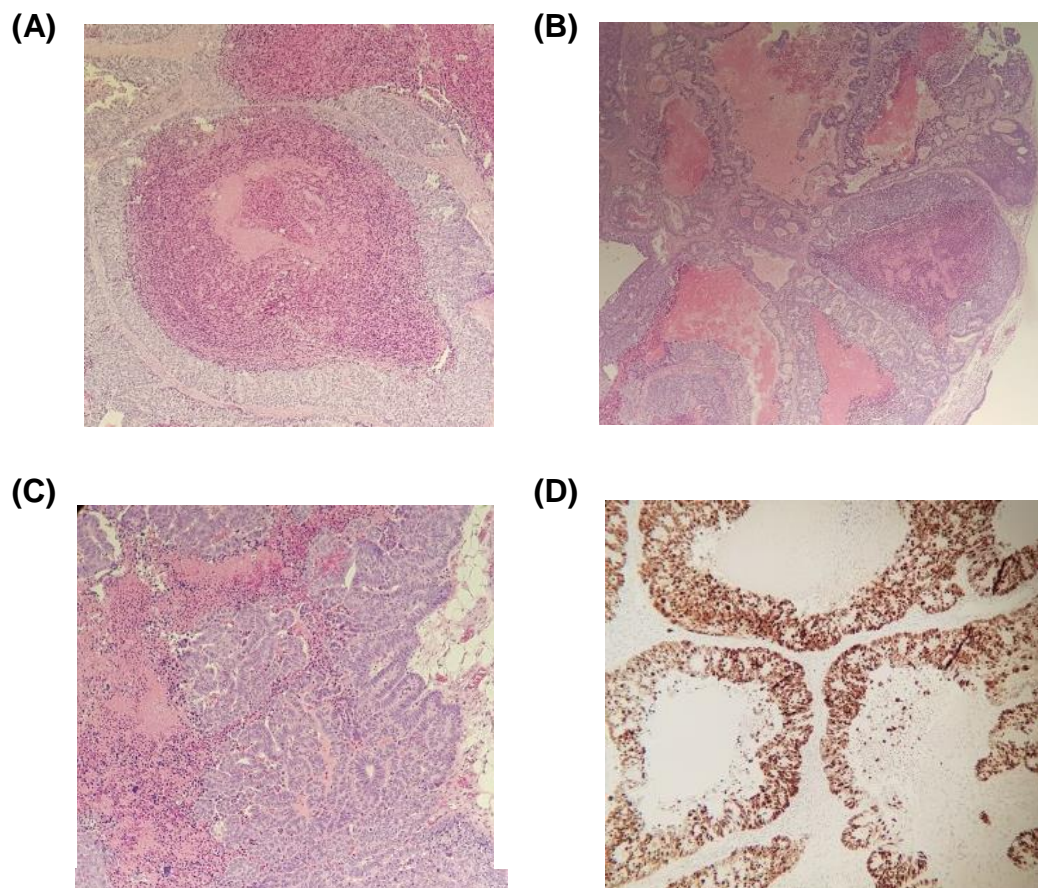


Figure 6.14: Microscopic view of Caco-2 (WT) primary tumours. (A) H&E of a necrotic core with mass inflammatory cell infiltration (x20). (B) H&E of numerous necrotic cores (pink) surrounded by tumour tissue (purple) (4x), (C) H&E of a well-differentiated tumour (10x). (D) Ki67 staining of proliferative glandular tumour epithelium surrounding necrotic cores (20x).

DLD-1

DLD-1 (PIK3CA-KRAS^{mut}) tumours were composed of highly proliferative (Ki67 positive), poorly differentiated epithelium which surrounded a necrotic core. Islands of proliferative tissue were scattered amongst necrotic tissue (Figure 6.15A, B). A large metastatic tumour was identified in the lung of a DLD-1 xenograft that was treated with chemoradiation therapy (5R) (Figure 6.15C, D). Ki67 positive cells were identified scattered amongst lung samples in 2/8 xenografts treated with 5R, and in clusters in 3/8 untreated control xenografts (Figure 6.15E). Ki67 staining was positive in spleens from xenografts in the control (5/8), chemoradiation (7/8) and copanlisib-chemoradiation (5/8) treatment arms (Figure 6.15F).

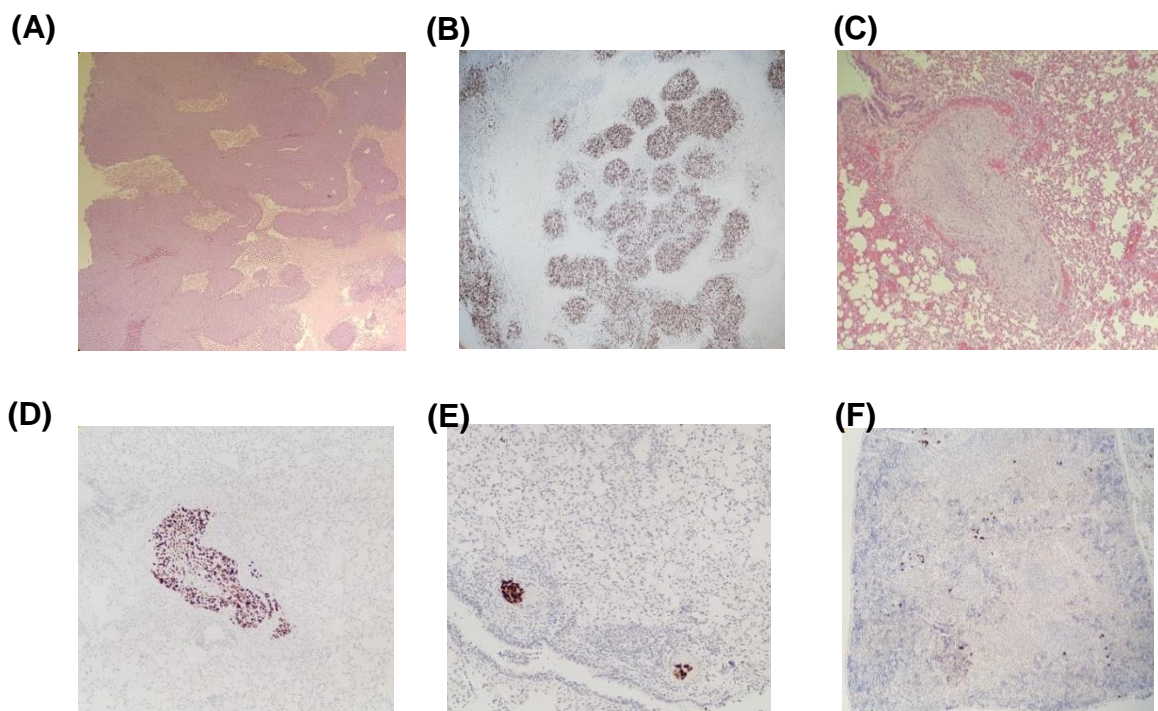


Figure 6.15: Microscopic view of DLD-1 (PIK3CA-KRAS^{mut}) xenograft tissues (A) H&E of primary tumour (10x), (B) Ki67 stain of proliferative tumour islands amongst necrotic tissue (10x), (C) H&E of large secondary lung metastasis (20x), (D) Ki67 stain of large secondary lung metastasis (20x), (E) Ki67 positive cluster in lung tissue (10x) (F) Ki67 positive scattered cells in spleen (4x).

LS-1034:

LS-1034 (KRAS^{mut}) tumours consisted of nodules of well-differentiated glandular epithelium, each encasing necrotic cores held together by connective tissue (Figure 6.16A-D). Large islands of inflammatory infiltration were identified within necrotic cores (Figure 6.16B). A secondary tumour was identified in the lung of a xenograft treated with chemoradiation (5R) (Figure 6.16E). Ki67 was negative in liver specimens for all treatment groups whilst 1/8 chemoradiation treated lung specimen was positive for Ki67. However Ki67 was positive in 4/8 control, 5/8 chemoradiation (5R) and 6/8 copanlisib-chemoradiation (P5R) splenic samples. From which, 1/8 samples from each of the 5R and P5R treatments contained large clusters of Ki67 positive cells (Figure 6.16F).

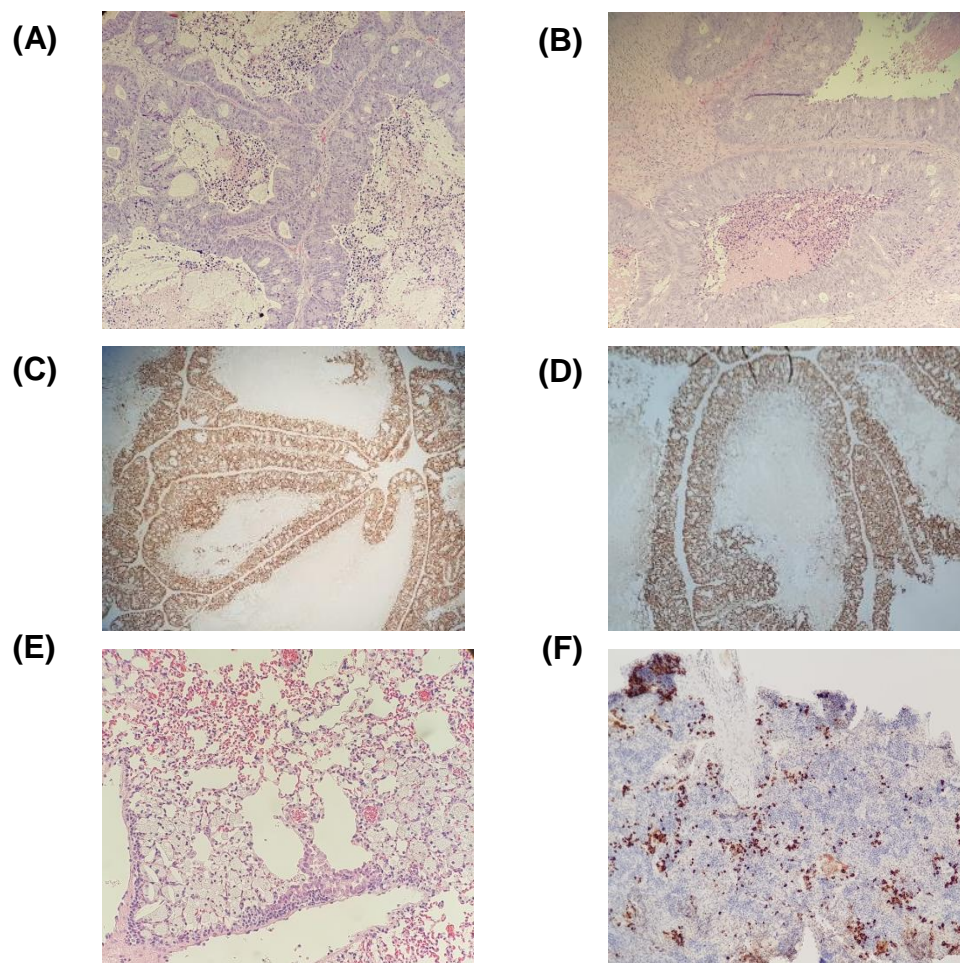


Figure 6.16: Microscopic view of LS-1034 (KRAS^{mut}) xenograft tissues. (A) H&E of primary tumour tissue with necrotic cores (20x), (B) H&E of primary tumour tissue with inflammatory cell infiltration into necrotic core (20x), (C) Ki67 staining of primary tumour (x20), (D) Ki67 staining of primary tumour (x20), (E) H&E of secondary tumour metastasis in lung (x10), (F) Ki67 staining of proliferative clusters in spleen (x10).

SNU-C4:

SNU-C4 (PIK3CA^{mut}) tumours were composed of poorly differentiated glandular epithelium with a necrotic core containing large islands of tumourigenic epithelium (Figure 6.17A-B). Secondary lung metastases were identified in control (1/8) and copanlisib-CRT (P5R) (1/8) treated xenografts (Figure 6.17C-D). 1/8 liver samples from each of the treatment arms contained positive Ki67 cells scattered throughout. Furthermore, single Ki67 positive cells were scattered throughout splenic tissue in control (1/8), CRT (5R) (2/8) and copanlisib-CRT (P5R) (5/8) treated xenografts. Ki67 positive cells were also identified scattered throughout the lungs of 1/8 control, 2/8 CRT, and 2/8 copanlisib-CRT xenograft mice.

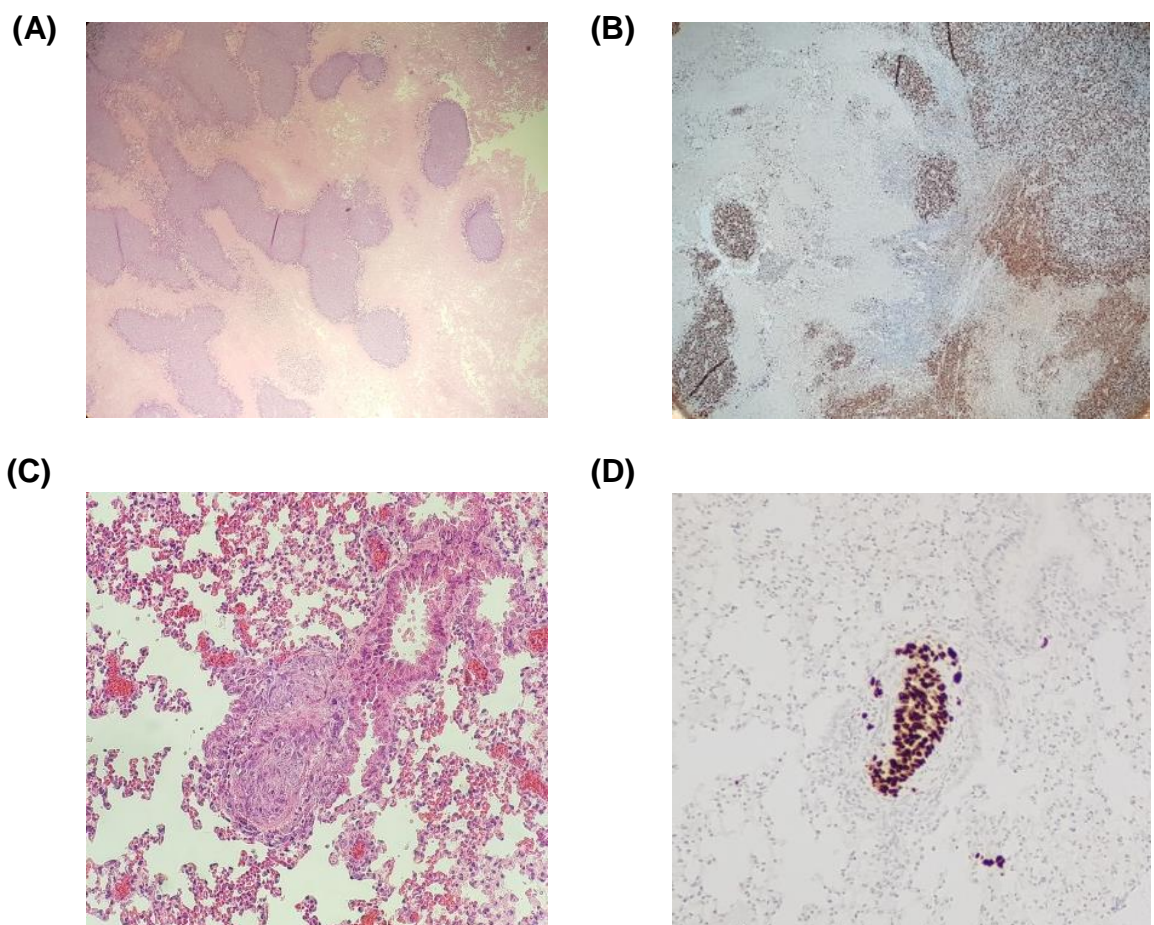


Figure 6.17: Microscopic view of SNU-C4 (PIK3CA^{mut}) xenograft tissues. (A) H&E of primary tumour, with islands of glandular epithelium amongst necrotic tissue (x10), (B) Ki67 staining of proliferative islands of cellular growth (x10), (C) H&E stain of secondary metastatic tumour in lung (20x), (D) Ki67 stain of secondary metastatic tumour in lung (20x).

6.2.6. Ki67 quantitative data

Tumours were divided into four, with one quarter undergoing histochemical (H&E) and immunohistochemical (Ki67) analysis. Tumours and organs were analysed and divided into the following grading system:

Score	Appearance
0	Negative
1	<20 positive cells, individually dispersed throughout tissue
2	>20 positive cells, individually dispersed throughout tissue
3	Small clusters of positive cells
4	Large islands of positive tissue
5	>50% of tissue positive

Table 6.8: Ki67 quantification in tumour samples.

CRC cells (PIK3CA (SNU-C4); KRAS (LS-1034); PIK3CA-KRAS (DLD-1); wild-type (Caco-2) were implanted in the right flank of 6-8 week old BALB/C SCID mice. When tumours reached 100mm³, mice were randomised to untreated control (C), chemoradiotherapy (5R) and copanlisib-chemoradiotherapy (P5R) treatment regimens. Copanlisib (7mg/kg) was administered intravenously twice a day on days 1 and 2. 5-FU chemotherapy (20mg/kg) was administered intraperitoneally, and mice were subsequently radiated in a Faxitron CP 160 x-ray generator at 1.8Gy on days 1, 3 and 5. Tumour measurements were taken every third day until tumours reached 400mm³, when mice were sacrificed and tumour, liver, lungs and spleen were excised. Organs were formalin fixed paraffin embedded and stained with a Ki67 antibody. Ki67 positivity was scored upon a 6 point grading system (0 = negative, 1 = <20 positive cells, individually dispersed throughout tissue, 2 = >20 positive cells, individually dispersed throughout tissue, 3 = small clusters of positive cells, 4 = large islands of positive tissue, 5 = >50% of tissue positive). Charts are colour coded from lowest (green) to highest (red) frequency positivity.

	Grade	DLD-1	SNU-C4	Caco-2	LS-1034
Contol	0	0	0	0	0
	1	0	0	0	0
	2	0	0	0	0
	3	0	0	0	0
	4	0	0	0	0
	5	8	8	5	8
5R	0	0	0	0	0
	1	0	0	0	0
	2	0	0	0	0
	3	0	0	0	0
	4	0	0	0	0
	5	8	8	5	8
P5R	0	0	0	0	0
	1	0	0	0	0
	2	0	0	0	0
	3	0	0	0	0
	4	0	0	0	0
	5	8	8	4	8

Table 6.9: Ki67 quantification in spleen samples

CRC cells (PIK3CA (SNU-C4); KRAS (LS-1034); PIK3CA-KRAS (DLD-1); wild-type (Caco-2) were implanted in the right flank of 6-8 week old BALB/C SCID mice. When tumours reached 100mm³, mice were randomised to untreated control (C), chemoradiotherapy (5R) and copanlisib-chemoradiotherapy (P5R) treatment regimens. Copanlisib (7mg/kg) was administered intravenously twice a day on days 1 and 2. 5-FU chemotherapy (20mg/kg) was administered intraperitoneally, and mice were subsequently radiated in a Faxitron CP 160 x-ray generator at 1.8Gy on days 1, 3 and 5. Tumour measurements were taken every third day until tumours reached 400mm³, when mice were sacrificed and tumour, liver, lungs and spleen were excised. Organs were formalin fixed paraffin embedded and stained with a Ki67 antibody. Ki67 positivity was scored upon a 6 point grading system (0 = negative, 1 = <20 positive cells, individually dispersed throughout tissue, 2 = >20 positive cells, individually dispersed throughout tissue, 3 = small clusters of positive cells, 4 = large islands of positive tissue, 5 = >50% of tissue positive). Charts are colour coded from lowest (green) to highest (red) frequency positivity.

	Grade	DLD-1	SNU-C4	Caco-2	LS-1034
Control	0	2	7	2	4
	1	4	1	2	4
	2	1	0	1	0
	3	1	0	0	0
	4	0	0	0	0
	5	0	0	0	0
5R	0	2	5	0	4
	1	5	3	4	3
	2	0	0	0	0
	3	1	0	0	0
	4	0	0	1	1
	5	0	0	0	0
P5R	0	4	2	2	2
	1	3	5	2	4
	2	1	1	0	1
	3	0	0	0	1
	4	0	0	0	0
	5	0	0	0	0

Table 6.10: Ki67 quantification in liver samples

CRC cells (PIK3CA (SNU-C4); KRAS (LS-1034); PIK3CA-KRAS (DLD-1); wild-type (Caco-2) were implanted in the right flank of 6-8 week old BALB/C SCID mice. When tumours reached 100mm³, mice were randomised to untreated control (C), chemoradiotherapy (5R) and copanlisib-chemoradiotherapy (P5R) treatment regimens. Copanlisib (7mg/kg) was administered intravenously twice a day on days 1 and 2. 5-FU chemotherapy (20mg/kg) was administered intraperitoneally, and mice were subsequently radiated in a Faxitron CP 160 x-ray generator at 1.8Gy on days 1, 3 and 5. Tumour measurements were taken every third day until tumours reached 400mm³, when mice were sacrificed and tumour, liver, lungs and spleen were excised. Organs were formalin fixed paraffin embedded and stained with a Ki67 antibody. Ki67 positivity was scored upon a 6 point grading system (0 = negative, 1 = <20 positive cells, individually dispersed throughout tissue, 2 = >20 positive cells, individually dispersed throughout tissue, 3 = small clusters of positive cells, 4 = large islands of positive tissue, 5 = >50% of tissue positive). Charts are colour coded from lowest (green) to highest (red) frequency positivity.

	Grade	DLD-1	snu-c4	Caco	LS-1034
Contol	0	7	8	5	8
	1	0	0	0	0
	2	0	0	0	0
	3	1	0	0	0
	4	0	0	0	0
	5	0	0	0	0
5R	0	8	7	5	8
	1	0	1	0	0
	2	0	0	0	0
	3	0	0	0	0
	4	0	0	0	0
	5	0	0	0	0
P5R	0	8	7	4	7
	1	0	1	0	0
	2	0	0	0	0
	3	0	0	0	1
	4	0	0	0	0
	5	0	0	0	0

Table 6.11: Ki67 quantification of *lung samples*

CRC cells (PIK3CA (SNU-C4); KRAS (LS-1034); PIK3CA-KRAS (DLD-1); wild-type (Caco-2) were implanted in the right flank of 6-8 week old BALB/C SCID mice. When tumours reached 100mm³, mice were randomised to untreated control (C), chemoradiotherapy (5R) and copanlisib-chemoradiotherapy (P5R) treatment regimens. Copanlisib (7mg/kg) was administered intravenously twice a day on days 1 and 2. 5-FU chemotherapy (20mg/kg) was administered intraperitoneally, and mice were subsequently radiated in a Faxitron CP 160 x-ray generator at 1.8Gy on days 1, 3 and 5. Tumour measurements were taken every third day until tumours reached 400mm³, when mice were sacrificed and tumour, liver, lungs and spleen were excised. Organs were formalin fixed paraffin embedded and stained with a Ki67 antibody. Ki67 positivity was scored upon a 6 point grading system (0 = negative, 1 = <20 positive cells, individually dispersed throughout tissue, 2 = >20 positive cells, individually dispersed throughout tissue, 3 = small clusters of positive cells, 4 = large islands of positive tissue, 5 = >50% of tissue positive). Charts are colour coded from lowest (green) to highest (red) frequency positivity.

	Grade	DLD-1	SNU-C4	Caco-2	LS-1034
Control	0	5	8	5	8
	1	0	0	0	0
	2	0	0	0	0
	3	2	0	0	0
	4	1	0	0	0
	5	0	0	0	0
5R	0	5	6	5	7
	1	2	1	0	0
	2	0	0	0	0
	3	0	1	0	1
	4	1	0	0	0
	5	0	0	0	0
P5R	0	8	5	4	8
	1	0	2	0	0
	2	0	0	0	0
	3	0	1	0	0
	4	0	0	0	0
	5	0	0	0	0

6.3. Discussion

KRAS^{mut}, PIK3CA^{WT}

In our in vivo study, we found *KRAS^{mut}* tumours grew more rapidly than any other mutation group in both the untreated controls (C) and 5-FU chemoradiation (5R) cohorts. Furthermore, no significant difference was found in mean overall survival between 5-FU chemoradiation (5R) and our untreated control xenografts, suggesting *KRAS* mutations may indeed result in resistance to chemoradiotherapy. This theory coincides with multiple studies which demonstrated *RAS* mutations resulted in radiation resistance (142). However, the association between *KRAS* mutations and resistance towards chemotherapy and/or radiation therapy is a highly controversial topic, with conclusions varying widely between studies.

To further strengthen our findings, we found tumour growth was significantly reduced in *KRAS^{mut}* xenografts when copanlisib was given alongside chemoradiation therapy (P5R), thereby inactivating the PI3K pathway and the *KRAS* mutation. We found these mice had the slowest tumour growth out of all mutated tumour xenograft models. Furthermore, they displayed significantly increased the mean overall survival rates compared to untreated controls, and increased survival rates on days 20, 30 and 40; with only P5R xenografts remaining up to day 40. In addition, our study showed the use of copanlisib with chemoradiation triggered an accelerated tumour response to treatment, compared to chemoradiation alone. *KRAS* tumour growth was significantly reduced within 24 hours of the first round of copanlisib-chemotherapy (P5R) treatment, and remained significantly reduced 2 weeks post-treatment initiation in the P5R cohort compared to untreated controls. However, *KRAS* tumours required 3 rounds of CRT before any significant difference could be found in tumour size in the 5R group compared to untreated controls. Therefore, our data suggests that inactivation of the PI3K pathway sensitises *KRAS^{mut}* tumour to chemoradiation therapy, and accelerates tumour response to treatment. These findings are in line with Gupta et al, who demonstrated a synergistic improvement in *RAS^{mut}* bladder cancer cells when treated with the PI3K inhibitor LY294002 alongside radiation, compared to radiation alone (271,272).

PIK3CA^{WT}, KRAS^{WT}

In vivo, copanlisib enhanced chemoradiotherapy response in WT xenograft models, resulting in significantly reduced tumour growth and increased the mean overall survival rates compared to untreated controls, which was otherwise insignificant in chemoradiation therapy treated models. Tumour growth was significantly reduced within 24 hours in the P5R arm, compared to 5 days and 3 rounds of treatment in the 5R arm. Median overall survival was increased in 5R and P5R treated xenograft models by 60% and 82.5% respectively, compared to untreated controls. This data suggests that copanlisib has the potential to enhance chemoradiotherapy sensitivity in CRCs which are wild-type for *PIK3CA* or *RAS*. This correlates with Patnaik et al, who treated non-Hodgkin's lymphoma patients with copanlisib, and found all seven patients who responded to copanlisib were wild-type for *PIK3CA* mutations.

PIK3CA^{mut}, KRAS^{WT}

Our in vivo study showed *PIK3CA^{mut}* tumours were the most responsive cell line to initial treatment with copanlisib-chemoradiotherapy. Similarly, Liu et al reported around a 40 fold increase in copanlisib sensitivity in *PIK3CA^{mut}* cell lines compared to *PIK3CA^{WT}* (122). We found *PIK3CA* mutated tumours were the only xenograft model to show a significant reduction in tumour growth when treated with P5R compared to 5R alone; a significant reduction which was observed for 18 days (81.1% of the mean lifespan of 5R treated mice). Furthermore, the median overall survival in *PIK3CA* mutated xenografts was increased by 37.1% when treated with P5R compared to 5R treated mice, and 67.3% compared to untreated controls. Multiple studies have shown anti-tumourigenic properties of copanlisib in *PIK3CA^{mut}* cell lines (122,124,126). Of particular interest was Gupta et al, who showed that the PI3K pathway is the primary pathway associated with chemoradiation resistance, rather than the MAPK/ERK pathways (273). Furthermore, Wang et al reported that *PIK3CA^{mut}* CRCs demonstrated poorer response rates to first-line chemotherapy than that of their *PIK3CA^{WT}* counterparts, both in vitro and in vivo (192). Therefore, targeting the PI3K pathway should increase chemoradiotherapy sensitivity, as was the case with our study.

In vivo, the addition of copanlisib did not significantly improve tumour growth or overall survival compared to chemoradiotherapy alone. These findings are similar to our in vitro study, which showed that copanlisib alone did not enhance chemoradiotherapy sensitivity in *PIK3CA-KRAS^{co-mut}* cancer cells. Rather, they required both a PI3K and MAPK inhibitor alongside chemoradiotherapy to significantly reduce tumour cell growth. Numerous studies have shown that inhibition of one signalling pathway may result in upregulation of another signalling pathway, as may be the case in our experiments (266). Furthermore, Wee et al demonstrated that *PIK3CA-KRAS* mutated CRC xenograft models required a combination of both PI3K and MEK inhibitors to halt tumour progression (274). Our in vivo study was carried out on colonic cancer cell lines which are not usually treated with radiation, therefore in future it may be of interest to extend this study to rectal cancer xenografts as they may have a more radioresistant phenotype. Further immunohistochemical staining of cellular responses of interest could include markers for apoptosis (caspase 3, apoptosis-inducing factor (AIF), PARP), necrosis (TNF α), DNA repair (PARP1, XRCC3, RAD51), oxidative stress (SOD1), macrophages (CD68) and / or angiogenesis (CD31, VEGF).

6.4. Overview of results chapters

Whole exome sequencing of CRC samples

Mutations within the PI3K and MAPK pathways are commonly mutated in CRC (PIK3CA, KRAS) and associated with lymph node positivity (PIK3C, BRAF).

Mutations in MUC16, KMT2C and TCF20 were associated with good response in CRC to NACRT.

Mutations in PCDHA12, TCTE1, APOB, CD93 and TPD52L2 were associated with poor NACRT response, whilst RANBP2 and ZIC1 were also associated with lymph node positivity

Signatures associated with age and defective DNA mismatch repair were common in CRC samples.

Clinical trial of LARC patient response to NACRT

22.2% of patients administered IMRT achieved pCR, vs 0% of the 3-DCRT cohort. Patients who did not achieve pCR had a significant increase in the mean number of CTCs during CRT (week 3 and last week) compared to pre-treatment.

PI3K and MAPK pathway mutations were identified in all CRC samples, with KRAS, NRAS and PIK3CA mutations being the most prevalent.

87.5% of patients who progressed onto metastatic disease possessed a PIK3CA mutation.

Inhibition of PI3K and MAPK pathways in CRC cell lines

PIK3CA+/KRAS mutated cell lines are sensitive to the PI3K inhibitor copanlisib, whilst BRAF mutated cell lines are also sensitive to the MEK inhibitor refametinib. A combination of both drugs is most beneficial in PIK3CA/KRAS^{co-mut} and wild-type cell lines.

The addition of copanlisib or refametinib significantly reduces tumour cell growth in KRAS^{mut} or wild-type cell lines. Whilst both inhibitors are required with chemoradiation to significantly reduce tumour cell growth in BRAF^{mut} and PIK3CA/KRAS^{co-mut} cell lines.

Inhibition of the PI3K pathway in CRC xenografts

Copanlisib-chemoradiotherapy (P5R) resulted in a significant reduction in tumour growth and a significant increase in overall survival in wild-type and KRAS^{mut} xenografts compared to untreated controls.

PIK3CA^{mut} xenografts were the most responsive xenografts to initial P5R treatment.

The addition of copanlisib to chemoradiation did not show any additional benefit to PIK3CA/KRAS^{co-mut} xenografts, and therefore may require the addition of a MAPK inhibitor.

Potential future work in respect to genomic analysis to determine functionality of CRC

Genomic analysis could be carried out to determine the effects of NACRT, copanlisib and refametinib within the body. This could be carried out through reverse phase protein arrays, which detects alterations within protein levels of a sample. This could be carried out on samples from all four studies, with particular interest in alterations within the PI3K and MAPK pathways throughout treatment.

Discussion

Colorectal cancer is the second most common cancer in Ireland, with the second highest mortality rate. Over the past couple of decades, our knowledge, understanding and treatment of cancer have developed dramatically. We now understand that specific mutational aberrations within tumours i.e. in the PI3K and MAPK pathways are responsible for tumour progression, metastasis and resistance to cancer therapies (93,192–194). However, many cancers, including CRC are still treated based on tumour location, histological subtype and tumour grade. Personalised therapy is the ultimate goal. However, in order to achieve this goal, we must first identify the specific mutational aberrations responsible, locate drugable targets, create therapies which do not succumb to cancer resistance and identify markers to predict and measure patient response to therapy. This PhD project sought to target most of these obstacles which are currently plaguing the field of oncology.

In chapters three and four, we worked to identify mutational aberrations within LARC samples which may be driving tumour progression or predict patient response to NACRT. In chapter three, we carried out whole-exome sequencing on DNA extracted from 26 LARC patient pre-treatment tumour biopsies. The cohort consisted of good (n = 5), intermediate (n = 11) and poor (n = 10) responders to NACRT. We assessed mutational profiles in respect to mutational load, type, response to NACRT, heterogeneity and mutational signatures. Whole-exome sequencing data showed tumours can become hyper-mutated if they are MSI tumours containing mutations within the MMR pathway (e.g. *MSH3*, *MLH3*, *Bax*), or MSS tumours containing *POLE* mutations (responsible for DNA repair). MSI tumours are widely known to be indicative of a good prognosis (275). However, *POLE* mutations are rapidly evolving as potential markers for favourable prognosis and reduced probability of recurrence (276). Similarly in our study, patients harbouring these mutations had good or intermediate responses to NACRT, thereby suggesting specific mutations rather than mutational burden is responsible for patient response. This was further supported by the low volume of mutations (≤ 35 non-synonymous mutations) identified in one-third of non-responder. This concurred with Innocenti et al also found low tumour mutational burden to be indicative of a poor prognosis in CRC (277). Furthermore, poor responders had reduced intra-tumour heterogeneity compared to good or intermediate responders.

In chapter four, we enlisted 35 LARC patients into the TRILARC clinical trial. During which, patients were treated with NACRT, with the radiation therapy consisting of either 3-DCRT or the novel IMRT. We monitored the circulating tumour cells (CTCs), circulating tumour DNA (ctDNA) mutations and cancerous tissue mutations before, during and after therapy. Only patients receiving IMRT in the TRILARC clinical trial achieved pCR. IMRT is known to target the tumour more directly, and at a higher intensity than 3-DCRT. Therefore this may explain why patients receiving IMRT may be responding better. The TRILARC clinical trial, along with other studies have shown CRT results in an increased volume of CTCs being shed into the circulation (247,248).

Finally, in chapters five and six, we utilised the information gathered from our previous work, and that of others; that PI3K and MAPK pathway mutations are common in CRC (91–93), and are associated with poor patient outcomes and chemotherapy and radiation therapy resistance (93,192–194). We targeted the PI3K and/or MAPK pathways with the novel BAYER PI3K inhibitor copanlisib, and MEK inhibitor refametinib in the hope of enhancing chemoradiation therapy sensitivity in the PI3K/MAPK mutated CRC cells, both in vitro and in vivo. CRC cell lines (n = 10) were treated with copanlisib (PI3K inhibitor) and refametinib (MEK inhibitor); both as single and dual agents in 2D proliferation assays. One cell line from each mutation group (n = 5) were subsequently treated with 5-FU chemoradiation therapy in conjunction with one or both inhibitors. Finally, PI3K pathway mutated cell lines (n = 3) and a wild-type cell line (n = 1) were implanted into BALB-C xenografts, and divided into untreated control, 5-FU chemoradiation therapy alone or 5-FU chemoradiotherapy combined with the PI3K inhibitor copanlisib.

Since our study is primarily based on the PI3K and MAPK pathways and their effects on NACRT effectiveness in LARC patients, I will now delve a little deeper into these aspects of my project.

BRAF

BRAF is reportedly mutated in 5-12% of CRCs (93,104–107). 11.5% of patients in our whole-exome sequencing (WES) study, and 5.3% of patients from the TRILARC clinical trial (ctDNA only) displayed *BRAF* mutations.

However, *BRAF* mutational effects on prognosis were rather contradictory. *BRAF* mutations in the WES study were indicative of a negative prognosis with all *BRAF*^{mut} patients failing to achieve pCR (intermediate = *BRAF*^{D594G}, *BRAFL597R*; poor = *BRAF*^{V600E}). In contrast, *BRAF*^{mut} patients in the TRILARC study achieved pCR (*BRAF*^{V600E}) or TRG2 (*BRAF*^{G469E}). However, the *BRAF*^{V600E} mutation was only identified at the surgical procedure, and not in any of the other 4 samples taken previously. As a result, this mutation was most likely not a driving mutation in this tumour at this stage, and may therefore not have played a large role in its prognosis. *BRAF*^{V600E} tumours are associated with a negative prognosis (115,278,279).

In vitro, *BRAF*^{V600E} cell lines are sensitive to refametinib and resistant to copanlisib in 2D proliferation and 3D clonogenic assays. However, when the drugs are combined, they resulted in a synergistic reduction in cellular growth in 2D proliferation assays. These findings were further solidified when *BRAF*^{V600E} cells required both copanlisib and refametinib alongside chemoradiation to significantly reduce cellular growth in 3D clonogenic assays compared to chemoradiation therapy alone, or combined with either drug alone.

PIK3CA

PIK3CA mutations are present in 8-20% of CRCs (89,99,100), with 80% of *PIK3CA* mutations occurring within hotspots in codons 542, 545 and 1047 (92). Our whole-exome sequencing study yielding 11.5% of LARC patients containing *PIK3CA* mutations occurring within codons 545 (*PIK3CA*^{E545K} = 7.7%) and 546 (*PIK3CA*^{Q546K} = 3.8%). Meanwhile, *PIK3CA* mutations were identified in 50% of patients from our TRILARC clinical trial; with *PIK3CA* mutations identified in 7.9% of tissue samples (MassARRAY; *PIK3CA*^{E542K} = 6.3%, *PIK3CA*^{E545K} = 1.6%), compared to 47.4% of ctDNA samples (UltraSEEK; *PIK3CA*^{E542K} = 28.9%, *PIK3CA*^{E545K} = 2.6%, *PIK3CA*^{E542K}/*PIK3CA*^{E545K} = 15.8%).

Our project revealed *PIK3CA* mutations were associated with failure to achieve pCR with NACRT, with 100% of *PIK3CA*^{mut} patients in the whole-exome sequencing study and 94.1% of *PIK3CA*^{mut} TRILARC patients retaining cancerous cells after chemoradiation therapy. Multiple studies have shown *PIK3CA* mutations

are associated with poor prognosis (280,281), metastasis and higher grade tumours (282). This is also in agreement with our study where 87.5% of TRILARC patients who progressed onto metastatic disease possessed a *PIK3CA* mutation. Likewise, Shen et al found a significant association between *PIK3CA*^{E545K} mutations and tumour recurrence (281).

In vitro analysis proved the *PIK3CA*^{E545G} cell line was the most sensitive cell line to the PI3K inhibitor copanlisib in both the 2D proliferation assays and 3D clonogenic assays. The *PIK3CA*^{E545G} cell line was also sensitive to the MEK inhibitor refametinib, and displayed a synergistic response to copanlisib-refametinib treatment in 2D proliferation assays. This was further reinforced in 3D clonogenic assays which showed copanlisib and refametinib combined with chemoradiotherapy was more effective than chemoradiotherapy combined with either inhibitor alone. Other studies have shown *PIK3CA* mutated cell lines are sensitive to copanlisib (122), however its sensitivity to refametinib could be due to cross-talk between the PI3K and MAPK pathways through ERK.

In vivo, the addition of copanlisib enhanced the median overall survival compared to chemoradiation therapy treated mice alone. Furthermore, *PIK3CA*^{E545G} tumours were most responsive to initial treatment with copanlisib-chemoradiotherapy. *PIK3CA*^{E545G} xenografts were the only model who displayed a significant reduction in tumour growth when copanlisib was used in conjunction with 5-FU chemoradiation therapy, compared to chemoradiation therapy alone. Furthermore, this significant reduction remained for 81.1% of the mean lifespan of 5R treated mice. Copanlisib has been shown to inhibit tumour growth and have anti-tumour activity both in xenograft models and in human clinical trials (122,124).

KRAS

KRAS is typically mutated in 35-47% CRCs (93,104,105), with the majority of *KRAS* mutations identified in codons 12, 13, 61 and 146. *KRAS* mutations were identified in 30.8% of our whole-exome sequencing study, with non-synonymous mutations occurring within codons 12, 13 and 146. Whereas in the TRILARC clinical trial, 100% of patients had *KRAS* mutations in their ctDNA, and 65.8% of

patients containing *KRAS* mutations in their tissue samples at some stage during the clinical trial.

In vitro, *KRAS* mutated cell lines were sensitive to copanlisib and were the most sensitive cell lines to refametinib in 2D proliferation assays. However, *KRAS*^{A146P} (LS-1034) was less sensitive to copanlisib treatment alone or combined with refametinib compared to the *KRAS*^{G12D} (LS-513) cell line. This could be a result of alternate *KRAS* mutations. *KRAS*^{A146} mutations are known to be common in CRC, but to a lesser degree than codon 12 or 13 mutations; therefore little research has been carried out on these mutations. However, they have been associated with MEK dependence, poor overall survival and recurrence-free survival. (93,108,109,116,203). Our studies also suggest that mutations in this codon are indicative of a worse response to NACRT. In our whole-exome sequencing study, the patient with a *KRAS*^{A146} mutation was a poor responder to NACRT. Furthermore, ten patients in our TRILARC clinical trial (26%) possessed *KRAS*^{A146} mutations. Of which, 89% were non-responders (TRG2+), the only TRG5 patient possessed a *KRAS*^{A146V} mutation at surgery, and one patient has since progressed onto a metastatic tumour. Chemoradiation significantly reduced *KRAS*^{mut} tumour growth both in 3D clonogenic assays and during initial treatments in vivo compared to the untreated controls. Despite this, *KRAS*^{A146P} mutated tumours were the least responsive cell line to CRT, and ultimately resulted in no significant difference in mean overall survival between 5R and untreated controls, despite the fact DLD-1 xenografts exhibits both a *KRAS*^{G13D} and *PIK3CA*^{E545K} mutation. Therefore, this suggests that *KRAS*^{A146} mutations are indicative of a worse prognosis, whether a *KRAS* mutation in another codon is present or not.

However, a significant improvement was identified in vitro and in vivo when treated with copanlisib combined with chemoradiotherapy. In vitro, treatment with P5R, M5R or PM5R all significantly reduced tumour growth compared to 5R alone. Whilst in vivo, tumour growth was significantly reduced within 24 hours after treatment with copanlisib-chemoradiation therapy (P5R), and lasting for a further 2 weeks, compared to untreated controls. Treatment with P5R also significantly increased the mean overall survival compared to untreated controls. PI3K inhibitors have been previously reported to increase radiation sensitivity in Ras mutated cancer cells (271,272).

Since there was no difference in vitro between P5R, M5R or PM5R therapy, this suggests the addition of either inhibitor alone may be beneficial for KRAS mutated tumours. Furthermore, the positive results from the in vivo study further support this theory.

PIK3CA-KRAS^{co-mut}

Co-mutations in *PIK3CA* and *KRAS* are associated with metastasis and advanced tumour stages (282). *PIK3CA* mutations in exon 10 (codons 514-555) are associated with co-occurrence with *KRAS* mutations (100). Whole-exome sequencing identified *PIK3CA* mutations in 11.5% (n = 3) of samples, all of which were located within exon 10. Patient MDA-10 (*PIK3CA*^{E545K}, *KRAS*^{G12V}) was an intermediate responder despite its dual mutational status, compared to MDA-13 (*PIK3CA*^{Q546K}, *KRAS*^{G13D}) and MDA-1 (*PIK3CA*^{E545K}, *KRAS*^{WT}) who were both poor responders. Patients in the WES study displaying *KRAS*^{G12V} mutations had good (*PIK3CA*^{WT}, *KRAS*^{mut}) or intermediate (*PIK3CA*^{mut}, *KRAS*^{mut}) response to NACRT, therefore this suggests *KRAS*^{G12V} mutations may act as a good prognostic marker. Contrary to this, patients in our TRILARC cohort possessing *KRAS*^{G12V} mutations all progressed onto metastatic cancer. Furthermore, numerous papers find *KRAS*^{G12V} mutations to be a poor prognostic marker, exhibiting worse progression-free survival, worse overall survival, risk of tumour progression and increased mortality (111,283–286). Therefore, this suggests that either patients with *KRAS*^{G12V} mutations in the WES study contained other mutations which took precedence over this mutation rendering its effects null, or the patients may have lost the *KRAS*^{G12V} mutation during treatment. Further analysis of post-treatment samples from the WES cohort will be necessary to clearly understand this anomaly.

50% of patients in the TRILARC clinical trial were *PIK3CA-KRAS^{co-mut}*. Patients with *PIK3CA* mutations (particularly *PIK3CA*^{E542K}) and co-occurring *KRAS* mutations in G12CR, G12D and G12S were associated with progression onto metastatic disease. *KRAS*^{G12D} is associated with metastatic CRC and liver cancer (287), whilst *KRAS*^{G12S} is associated with worse overall survival and tumour recurrence (114).

In addition, *KRAS*^{G13S} mutations potentially resulted in an improved response in dual *PIK3CA* (E542K and E545K) mutated LARC patients, resulting in TRGs of 1-3, compared to metastatic disease in the lung, liver and bone without the G13S mutation.

In vitro, *PIK3CA-KRAS*^{co-mut} cells were sensitive to high doses of copanlisib and refametinib, with DLD-1 (*PIK3CA*^{E545K}, *KRAS*^{G13D}) being more sensitive to copanlisib than LS-174T (*PIK3CA*^{H1047R}, *KRAS*^{G12D}) in 2D proliferation assays. In 3D clonogenic assays, the *PIK3CA-KRAS*^{co-mut} cell line (DLD-1) was the most resistant cell line to refametinib and 5-FU chemotherapy when used as single agents. Studies have shown *PIK3CA-KRAS*^{co-mut} tumours are more resistant to MEK inhibitors than Ras or Raf mutated tumours, resulting in a cytostatic response rather than cytotoxic (263).

Neither copanlisib nor refametinib alone significantly enhanced chemoradiotherapy response in 3D clonogenic assays. This was further proven in our in vivo study, whereby the addition of copanlisib did not significantly improve tumour growth or overall survival compared to chemoradiotherapy alone. However, when copanlisib and refametinib were used in combination in 2D proliferation assays, this resulted in strong synergism. Similarly, Clarke et al found CRC cell lines harbouring *KRAS* mutations responded synergistically towards dual PI3K and MEK inhibition, however, *PIK3CA-KRAS*^{co-mut} cell lines were strongly synergistic (260).

Likewise, in the 3D clonogenic assays, both drugs were necessary in conjunction with chemoradiotherapy to result in a significant decrease in cellular growth compared to chemoradiotherapy alone. Therefore, our study suggests that *PIK3CA-KRAS*^{co-mut} cell lines require inhibition of both the PI3K and MAPK pathways in conjunction with chemoradiotherapy to enhance patient response to NACRT. Numerous studies have shown that inhibition of one signalling pathway may result in upregulation of another signalling pathway (266). Furthermore, Wee et al demonstrated that *PIK3CA-KRAS*^{co-mut} CRC xenograft models required a combination of both PI3K and MEK inhibitors to halt tumour progression (274).

WT

In the whole-exome sequencing study, patients were wild-type for *PIK3CA*, *KRAS* and *BRAF* in good (80%), intermediate (72.7%) and poor (60%) responders. In respect to the TRILARC clinical trial cohort, patients were wild-type for all three mutations in tissue (pre-treatment samples = 23.1%, surgical resections = 26.7%, recurrences = 0%); and ctDNA (mean prior to surgical procedure = 19.7%, surgical procedure = 71%, 1 year follow up = 76.3%).

In vitro, WT cell lines were resistant to the PI3K and MEK inhibitors alone or in combination in 2D proliferation assays. This concurs with other studies previously published (122). However, when they were combined with 5-FU chemoradiation in 3D clonogenic assays, cellular growth was significantly reduced. This finding was further supported with our in vivo study which too found that copanlisib enhanced chemoradiation therapy sensitivity in WT xenograft models. Whereby tumour growth was significantly reduced and mean overall survival was increased compared to untreated controls, a result which was not achieved in the chemoradiation therapy (5R) treated cohort. Furthermore, we found the addition of copanlisib enhanced tumour response time to treatment, reducing tumour growth within 24 hours compared to 4 days and 3 rounds of chemoradiation therapy without the use to copanlisib.

We also found the effects of copanlisib and refametinib were most marked when used in combination, in both 3D clonogenic assays and 2D proliferation. In the latter, the combination resulted in a nearly additive effect in Caco-2, and strong synergy in CL-14 and C2BBE1. Whilst in 3D clonogenic assays, the addition of both inhibitors alongside chemoradiation was significantly reduced compared to either drug used alone with chemoradiation therapy. Therefore, the addition of a MEK inhibitor may further enhance the benefits previously displayed in our CRC models treated with copanlisib-chemoradiation therapy.

Conclusion

In conclusion, tumour mutational status affects patient response to NACRT; therefore identification of mutations can suggest appropriate personalised

treatment regimens. However, due to intra-tumour heterogeneity and the continuous mutational progression and alterations occurring within tumours, numerous samples before, during and after treatment will provide the best representation of the tumour and its response to treatment. Tumour biopsies are invasive and expensive, therefore liquid biopsies in the form of ctDNA could be an ideal alternative.

In vitro, *PIK3CA* + / *KRAS*^{mut} cell lines are sensitive to copanlisib; *BRAF*^{mut}, *KRAS*^{mut} and *PIK3CA*^{mut} cell lines are sensitive to refametinib, however all cell lines including wild-type respond best to a combination of the two drugs.

In vivo, chemoradiation therapy did not significantly improve overall survival in any of the xenograft models in comparison to untreated controls. However, copanlisib-chemoradiation therapy significantly reduced tumour growth in WT, *PIK3CA*^{mut} and *KRAS*^{mut} xenografts, whilst overall survival is significantly increased in WT and *KRAS*^{mut} xenografts. However, *PIK3CA-KRAS*^{co-mut} xenografts did not benefit from the combination. Therefore, *PIK3CA*^{mut}, *KRAS*^{mut}, and WT tumours may benefit from copanlisib-chemoradiation therapy. However *BRAF*^{mut} and *PIK3CA-KRAS*^{co-mut} tumours may require the addition of a MEK inhibitor for optimal tumour inhibition.

Future directions

Due to the potentially clinically significant findings from this project further investigation will be carried out by Prof. Bryan Hennessy and his team.

Whole-exome sequencing

Due to the interesting results and mutational variation identified before and after treatment in the TRILARC clinical trial cohort, Prof. Bryan Hennessy, Dr. Simon Furney and Dr. Sinead Toomey intend to extend the whole-exome sequencing study, to include post-treatment samples. These results will be subjected to a similar analysis as I have carried out in the pre-treatment cohort.

Furthermore, from the exome sequencing results, the team will select around 100 genes of interest and will sequence these genes in a new cohort of samples to validate our findings from the current study. The genes of interest will include many of which have been identified in this project, including genes associated with good, poor or non-responders, commonly mutated genes and mutations within the MMR, DNA repair, PI3K and MAPK pathways. The tumour samples collected from patients enrolled in the TRI-LARC trial will be used to confirm and validate the results from the whole exome sequencing study. Using the correlation between different datasets they will summarise the data at a functional and pathway level. This will further allow us to determine which pathways are implicated in treatment-resistant disease and preliminarily determine how chemoradiation treatment impacts molecular evolution in tumours of differential responsiveness at a functional level. Alterations that are enriched in residual tumour cells will thereby be categorised into several key pathways, with an emphasis on targetable pathways.

TRILARC

The TRILARC clinical trial is currently ongoing and aims to enrol 240 patients altogether over the next 4 years. The tumour samples collected from patients enrolled in the TRI-LARC trial will be used to confirm and validate the results from the whole-exome sequencing study. The oncology and bio-banking team will continue to collect CTCs, ctDNA from patient plasma and corresponding tissue

samples throughout the trial, in the hope of further cementing the findings identified in this project.

In vitro and in vivo studies

We are now aiming to convert the work carried out in the in vitro and in vivo studies into a phase I clinical trial. This will be carried out similar to the PANTHER trial, whereby LARC patients will be enrolled into the clinical trial, and given copanlisib in conjunction with chemotherapy and radiation therapy. Copanlisib will be given via a lyophilised 6ml (60mg) intravenous infusion over one hour on days 1, 8 and 15 of each 28-day cycle. Patients will also receive a continuous intravenous infusion of 5-FU chemotherapy (225mg/m²) daily and 28 fractions of external-beam pelvic radiation therapy (50.4 Gy) over 6-8 weeks. Radiation will be administered using a LINAC with ≥6MV energy and an Image-Guided Radiation Therapy (IGRT) capacity for improved accuracy and precision. Acute toxicities will be assessed weekly during radiotherapy and at 2 and 4 weeks post-treatment. Late toxicities will be assessed at 3, 6, 9, 12, 18 and 24 months post-treatment and annually up to 10 years.

Similar to the TRILARC clinical trial, bloods will be collected from patients before, during and after treatment to monitor mutational alterations in the ctDNA. Primary outcomes will include identification of the maximum tolerated dose of copanlisib in conjunction with chemotherapy and radiation therapy, and to monitor clinical benefit of the drug combination which will be calculated based on pCR rates. Secondary outcomes will include monitoring of tumour response to treatment, disease-free survival, overall survival, adverse effects and toxicities associated with the combination.

References

1. Young, Barbara; Lowe, James S.; Stevens A. Wheater's functional histology. 5th ed. Churchill Livingstone; 2006.
2. Martini, Frederick H.; Bartholomew EF. Essentials of Anatomy and Physiology. Fourth edi. Berriman, Leslie; George-O'Brien, Nicole; Titcha, Alan; Robbins, Blythe; Duke, Jon; Shaw R et al, editor. Pearson Benjamin Cummings; 2007. 537-543 p.
3. Gunawardene, Ashok R; Corfe, Bernard M; Staton CA. Classification and functions of enteroendocrine cells of the lower gastrointestinal tract. *Int J Exp Pathol*. 2011;92(4):219–31.
4. Pabst, Oliver; Pires Da Cunha, Andre; Weiner HL. Mucosal Immunology. Fourth edi. mestECKy, Jiri; Strober, Warren; Russel, Michael; Cheroutre, Hilde; Lambrecht, Bart N; Kelsall B, editor. Academic Press; 2015. 831-848 p.
5. National Cancer Registry Ireland (NCRI). Incidence: 2015-2017 estimated averages and mortality: 2012-2014 averages. 2018.
6. Clarke, Nicholas; Mcdevitt, Joseph; Kearney, Patricia M; Sharp L. Increasing late stage colorectal cancer and rectal cancer mortality demonstrates the need for screening : a population based study in Ireland , 1994-2010. *BMC Gastroenterol*. 2014;14(92):1–10.
7. National Cancer Registry Ireland (NCRI). All Ireland cancer atlas 1995-2007. Colorectal cancer. 2008.
8. National Cancer Registry Ireland (NCRI). Cancer Trends, no 9: cancers of colon, rectosigmoid junction and rectum. 2019;(9).
9. Norton, Jefferey, A.; Barie, Philip S.; Bollinger, R. Randal; Chang AE, editor. Surgery. Basic Science and Clinical Evidence. Second edi. Springer; 2008. chapter 51, pg 1057.
10. Laposata M. Laboratory Medicine, the diagnosis of disease in the clinical laboratory. McGraw Hill; 2010.
11. National Institutes of Health. Advances in Colorectal Cancer Research [Internet]. 2015 [cited 2018 Mar 20]. Available from: <https://www.nih.gov/research-training/advances-colorectal-cancer-research>
12. National Cancer Registry Ireland (NCRI). Colorectal Cancer in Ireland: 1994-2010.

13. Sauer, Rolf; Becker, Heinz; Hohenberger, Werner; Rodel C. Preoperative versus Postoperative Chemoradiotherapy for Rectal Cancer. *N Engl J Med*. 2004;351(17):1731–40.
14. Sauer, Rolf; Liersch, Torsten; Merkel, Susanne; Fietkau, Rainer; Hohenberger, Werner; Hess C. Preoperative Versus Postoperative Chemoradiotherapy for Locally Advanced Rectal Cancer : Results of the German CAO / ARO / AIO-94 Randomized Phase III Trial After a Median Follow-Up of 11 Years. *J Clin Oncol*. 2012;30(16):1926–33.
15. Janjan, Nora A; Khoo VSAJ. Tumour down-staging and sphincter preservation with preoperative chemoradiation in locally advanced rectal cancer: the M. D. Anderson Cancer Center experience. *Int J Radiat Oncol Biol physics*. 1999;44(5):1027–38.
16. Pucciarelli, S; Toppan, P; Friso, ML; Russo V. Complete pathologic response following preoperative chemoradiation therapy for middle to lower rectal cancer is not a prognostic factor for a better outcome. *Dis Colon Rectum*. 2004;47(11):1798–807.
17. Bernier, Jacques; Hall, Eric J.; Giaccia A. Radiation oncology: a century of achievements. *Nat Rev Cancer*. 2004;4(9):737–47.
18. Werb Z. ECM and cell surface proteolysis: Regulating cellular ecology. *Cell*. 1997;91(4):439–42.
19. Yadav P, Shankar BS. Radio resistance in breast cancer cells is mediated through TGF- β signalling, hybrid epithelial-mesenchymal phenotype and cancer stem cells. *Biomed Pharmacother [Internet]*. 2019;111(December 2018):119–30. Available from: <https://doi.org/10.1016/j.biopha.2018.12.055>
20. Lee JM, Bernstein A. p53 mutations increase resistance to ionizing radiation (y radiation/DNA damage/transgenic mice/carcinogenesis). *Genetics*. 1993;90(June):5742–6.
21. Kumar A, Chandna S. Evidence for a radiation-responsive “p53 gateway” contributing significantly to the radioresistance of lepidopteran insect cells. *Sci Rep [Internet]*. 2018;8(1):1–14. Available from: <http://dx.doi.org/10.1038/s41598-017-18521-5>
22. Kim, NW; Piatyszek, MA; Prowse, KR; Harley, CB; West MHP. Specific association of human telomerase activity with immortal cells and cancer. *Science (80-)*. 1994;266(5193):2011–5.
23. Hanrahan, Douglas; Weinberg RA. The Hallmarks of Cancer. *Cell*.

2000;100:57–70.

24. Hanahan D, Weinberg RA. Hallmarks of Cancer : The Next Generation. *Cell* [Internet]. 2011;144(5):646–74. Available from: <http://dx.doi.org/10.1016/j.cell.2011.02.013>
25. Hyeon Joo Ab, Oh; Hande, Prakash; Lansdorp, P.M; Natarajan A. Induction of telomerase activity and chromosome aberrations in human tumour cell lines following X-irradiation. *Mutat Res / Fundamental Mol Mech Mutagen*. 1998;401(1–2):121–31.
26. Fannon P, Silver ARJ, Bouffler SD. Upregulation of telomerase activity by X-irradiation in mouse leukaemia cells is independent of Tert, Terc, Tnks and Myc transcription. *Carcinogenesis*. 2000;21(4):573–8.
27. Shen C, Houghton PJ. The mTOR pathway negatively controls ATM by up-regulating miRNAs. *Proc Natl Acad Sci U S A*. 2013;110(29):11869–74.
28. Jang NY, Kim DH, Cho BJ, Choi EJ, Lee JS, Wu HG, et al. Radiosensitization with combined use of olaparib and PI-103 in triple-negative breast cancer. *BMC Cancer*. 2015;15(1):1–9.
29. De Sousa MML, Bjørås KØ, Hanssen-Bauer A, Solvang-Garten K, Otterlei M. P38 MAPK signaling and phosphorylations in the BRCT1 domain regulate XRCC1 recruitment to sites of DNA damage. *Sci Rep*. 2017;7(1):1–12.
30. Xu J, Escamilla J, Mok S, David J, Priceman S, West B, et al. CSF1R signaling blockade stanches tumor-infiltrating myeloid cells and improves the efficacy of radiotherapy in prostate cancer. *Cancer Res*. 2013;73(9):2782–94.
31. Shiao, Stephen L; Ruffell, Brian, DeNardo, David G; Faddegon, Bruce A; Park, Catherine C; Coussens LM. Th2-polarized CD4+ T cells and macrophages limit efficacy of radiation therapy Stephen. *Cancer Immunol Researcg*. 2015;3(5):518–25.
32. Patanaphan, V; Salazar O. Colorectal cancer: metastatic patterns and prognosis. *South Med J*. 1993;86(1):38–41.
33. Petschow BW., Burnett B, Shaw AL., Weaver EM., Klein GL. Serum-derived bovine immunoglobulin/ protein isolate: Postulated mechanism of action for management of enteropathy. *Clin Exp Gastroenterol*. 2014;7(1):181–90.
34. Hardingham JE, Kotasek D, Sage RE, Eaton MC, Pascoe VH, Dobrovic A. Detection of circulating tumor cells in colorectal cancer by immunobead-

- PCR is a sensitive prognostic marker for relapse of disease. *Mol Med.* 1995;1(7):789–94.
35. Tsavellas, G.; Patel, H.; Allen-Mersh TG. Detection and clinical significance of occult tumour cells in colorectal cancer. *Br J Surg.* 2001;88(10):1307–20.
 36. Scheele, J; Stang, R; Altendorf-Hofmann, A; Paul M. Resection of colorectal liver metastases. *World J Surg.* 1995;19(1):59–71.
 37. Taenzer, Aline; Alix-Panabières, Catherine; Wikman, Harriet; Pantel K. Circulating tumor-derived biomarkers in lung cancer. *J Thorac Dis.* 2012;4(5):448–9.
 38. Peach, G.; Kim, C.; Zacharakis, E.; Purkayastha, S.; Ziprin P. Prognostic significance of circulating tumour cells following surgical resection of colorectal cancers: A systematic review. *Br J Cancer.* 2010;102(9):1327–34.
 39. Rahbari, Nuh N.; Aigner, Maximilian; Thorlund, Kristian; Mollberg, Nathan; Motschall, Edith; Jensen K et al. Meta-analysis Shows That Detection of Circulating Tumor Cells Indicates Poor Prognosis in Patients With Colorectal Cancer. *Gastroenterology.* 2010;138(5):1714–1726.e13.
 40. Thorsteinsson, M.; Jess P. The clinical significance of circulating tumor cells in non-metastatic colorectal cancer - A review. *Eur J Surg Oncol.* 2011;37(6):459–65.
 41. Chang, M.-C; Chang, Y.-T; Chen, J.-Y; Jeng, Y.-M; Yang, C.-Y; Tien Y-W. et al. Clinical Significance of Circulating Tumor Microemboli as a Prognostic Marker in Patients with Pancreatic Ductal Adenocarcinoma. *Clin Chem.* 2016;62(3):505–13.
 42. Liberko, Marian; Kolostova, Katarina; Bobek V. Essentials of circulating tumor cells for clinical research and practice. *Crit Rev Oncol / Hematol.* 2013;88(2):338–56.
 43. Lu, Yan-jun; Wang, Peng; Peng, Jing; Wang, Xiong; Zhu, Yao-wu; Shen N. Meta-analysis reveals the prognostic value of circulating tumour cells detected in the peripheral blood in patients with non-metastatic colorectal cancer. *Sci Rep.* 2017;7(905):1–9.
 44. Hiraiwa, Kunihiro; Takeuchi, Hiroya; Hasegawa, Hirotooshi; Saikawa, Yoshiro; Suda K. Clinical Significance of Circulating Tumor Cells in Blood from Patients with Gastrointestinal Cancers. *Ann Surg Oncol.* 2008;15(11):3092–100.
 45. Cohen, Steven J; Alpaugh, R Katherine; Gross, Steve; Hara, Shawn M O;

- Smirnov, Denis A; Terstappen LWMM et al. Isolation and Characterization of Circulating Tumor Cells in Patients with Metastatic Colorectal Cancer. *Clin Colorectal Cancer*. 2006;6(2):125–32.
46. Winslow T. DNA structure [Internet]. Terese Winslow LLC, Medical and Scientific Illustration. 2015. p. 10. Available from: <https://www.teresewinslow.com/cellular-scientific/kk32f0cqnc2ia3ufdhw838fy2rsi9f>
 47. Winslow T. Transcription and translation [Internet]. Terese Winslow LLC, Medical and Scientific Illustration. p. 17. Available from: <https://www.teresewinslow.com/cellular-scientific/p09q5stxxeczawdc9auefwynyb3nrzs>
 48. Gartner, Jared J; Parker, Stephen C J; Prickett, Todd D; Dutton-Regester, Ken; Stitzel, Michael L; Lin JC et al. Whole-genome sequencing identifies a recurrent functional synonymous mutation in melanoma. *Proc Natl Acad Sci U S A*. 2013;110:13481–6.
 49. Supek, Fran; Miñana, Belén; Valcárcel, Juan; Gabaldón, Toni; Lehner B. Synonymous mutations frequently act as driver mutations in human cancers. *Cell*. 2014;156:1324–35.
 50. Fearon, Eric R.; Vogelstein B. A genetic model for colorectal tumourigenesis. *Cell*. 1990;61(5):759–67.
 51. Loeb, Lawrence A; Loeb, Keith R; Anderson JP. Multiple mutations and cancer. *Proc Natl Acad Sci U S A*. 2003;100(3):776–81.
 52. Pino, Maria S; Chung DC. The Chromosomal Instability Pathway in Colon Cancer. *Gastroenterology*. 2010;138(6):2059–72.
 53. Palombo F, Iaccarino I, Nakajima E, Ikejima M, Shimada T, Jiricny J. hMutS β , a heterodimer of hMSH2 and hMSH3, binds to insertion / deletion loops in DNA. *Curr Biol*. 1996;6(9):1181–4.
 54. Habraken, Yvette; Sung, Patrick; Prakash, Louise; Prakash S. Enhancement of MSH2 – MSH3-mediated mismatch recognition by the yeast MLH1 – PMS1 complex. *Curr Biol*. 1997;7(10):790–3.
 55. Alani E. The *Saccharomyces cerevisiae* Msh2 and Msh6 Proteins Form a Complex That Specifically Binds to Duplex Oligonucleotides Containing Mismatched DNA Base Pairs. *Mol Cell Biol*. 1996;16(10):5604–15.
 56. Genschel, Jochen; Littman, Susan J; Drummond, James T; Modrich, Paul; Natl, Proc; Sci A. Isolation of MutS β from Human Cells and Comparison

- of the Mismatch Repair Specificities of MutS β and MutS α . *J Biol Chem.* 1998;273(31):19895–901.
57. Kolodner R. Biochemistry and genetics of eukaryotic mismatch repair. *Genes Dev.* 1996;10(12):1433–42.
 58. Greene, Christopher N; Jinks-Robertson S. Frameshift Intermediates in Homopolymer Runs Are Removed Efficiently by Yeast Mismatch Repair Proteins. *Mol Cell Biol.* 1997;17(5):2844–50.
 59. Sia, Elaine Ayres; Kokoska, Robert J; Dominska, Margaret; Greenwell, Patricia; Petes, Thomas D; Hill C et al. Microsatellite Instability in Yeast : Dependence on Repeat Unit Size and DNA Mismatch Repair Genes. *Mol Cell Biol.* 1997;17(5):2851–8.
 60. Drotschmann, Karin; Aronshtam, Alexander; Fritz, Hans-joachim; Marinus, M G; Genetik M. The Escherichia coli MutL protein stimulates binding of Vsr and MutS to heteroduplex DNA. *Nucleic Acids Res.* 1998;26(4):948–53.
 61. Flores-Rozas, H; Kolodner R. The Saccharomyces cerevisiae MLH 3 gene functions in MSH3-dependent suppression of frameshift mutations. *Proc Natl Acad Sci U S A.* 1998;95(21):12404–9.
 62. Syngal, S; Fox, EA; Li C. Interpretation of genetic test results for hereditary nonpolyposis colorectal cancer: implications for clinical predisposition testing. *JAMA.* 1999;282(3):247–53.
 63. Bhattacharyya, N P; Skandalis, A; Ganesh, A; Groden, J; Meuth M. Mutator phenotypes in human colorectal carcinoma cell lines. *Proc Natl Acad Sci U S A.* 1994;91(July):6319–23.
 64. Parsons, Ramon; Li, Guo-Min; Longley MJ. Hypermutability and mismatch repair deficiency in RER+ tumor cells. *Cell.* 1993;75(6):1227–36.
 65. Woerner, Stefan M.; Benner, Axel; Sutter, Christian; Schiller, Marian; Yuan, Yan P.; Keller G et al. Pathogenesis of DNA repair-deficient cancers: A statistical meta-analysis of putative Real Common Target genes. *Oncogene.* 2003;22(15):2226–35.
 66. Knudson AG. Mutation and Cancer : Statistical Study of Retinoblastoma. *Proc Natl Acad Sci U S A.* 1971;68(4):820–3.
 67. Toyota, Minoru; Ahuja, Nita; Ohe-Toyota, Mutsumi; Herman, James G.; Baylin, Stephen B.; Issa J-PJ. CpG island methylator phenotype in colorectal cancer. *Proc Natl Acad Sci U S A.* 1999;96(July):8681–6.
 68. Ogino, Shuji; Kawasaki, Takako; Kirkner, Gregory J; Loda, Massimo; Fuchs

- CS. CpG Island Methylator Phenotype-Low (CIMP-Low) in Colorectal Cancer : Possible Associations with Male Sex and KRAS Mutations. *J Mol Diagnostics*. 2006;8(5):582–8.
69. Winawer, Sidney; Fletcher, Robert; Rex, Douglas; Bond, John; Burt, Randall; Ferrucci J et al. Colorectal Cancer Screening and Surveillance : Clinical Guidelines and Rationale - Update Based on New Evidence. *Am Gastroenterol Assoc*. 2003;124(2):544–60.
 70. Lindahl T. Instability and decay of the primary structure of DNA. *Nature*. 1993;362(6422):709–15.
 71. Fang, Jun; Seki, Takahiro; Maeda H. Therapeutic strategies by modulating oxygen stress in cancer and inflammation. *Adv Drug Deliv Rev*. 2009;61(4):290–302.
 72. Oberreuther-Moschner, Daniela, L; Rechkemmer, Gerhard; Pool-Zobel BL. Basal colon crypt cells are more sensitive than surface cells toward hydrogen peroxide, a factor of oxidative stress. *Toxicol Lett*. 2005;159(3):212–8.
 73. Foksinki, Marek; Rozalski, Rafal; Guz, Jolanta; Ruszkowska, Barbara; Sztukowska, Paulina; Piwowarski M. Urinary excretion of dna repair products correlates with metabolic rates as well as with maximum life spans of different mammalian species. *Free Radic Biol Med*. 2004;37(9):1449–54.
 74. Hussain, S. Perwez; Hofseth, Lorne J; Harris CC. Radical causes of cancer. *Nat Rev Cancer*. 2003;3(4):276–85.
 75. Coussens LM, Werb Z. Inflammation and cancer. *Nature* [Internet]. 2002;420(6917):860–7. Available from:
<http://www.scopus.com/record/display.url?eid=2-s2.0-0037180757&origin=inward&txGid=nrzriWhg2oR6fypyvyqK169:76>
 76. Rutter, Matthew D; Saunders, Brian P; Wilkinson, K A Y H; Rumbles, Steve; Schofield, Gillian; Kamm MA et al. Clinical alimentary tract - Thirty-Year Analysis of a Colonoscopic Surveillance Program for Neoplasia in Ulcerative Colitis. *Gastroenterology* [Internet]. 2006;130(4):1030–8. Available from:
[https://www.gastrojournal.org/article/S0016-5085\(05\)02562-X/pdf](https://www.gastrojournal.org/article/S0016-5085(05)02562-X/pdf)
 77. Munkholm P. Review article: the incidence and prevalence of colorectal cancer in inflammatory bowel disease. *Aliment Pharmacology Ther* [Internet]. 2003;18(Suppl. 2):1–5. Available from:
<https://onlinelibrary.wiley.com/doi/pdf/10.1046/j.1365-2036.18.s2.2.x>

78. Flossmann, Enrico; Rothwell PM. Effect of aspirin on long-term risk of colorectal cancer: consistent evidence from randomised and observational studies. *Lancet*. 2007;369(9573):1603–13.
79. Cole BF, Logan RF, Halabi S, Benamouzig R, Sandler RS, Grainge MJ, et al. Aspirin for the chemoprevention of colorectal adenomas: Meta-analysis of the randomized trials. *J Natl Cancer Inst*. 2009;101(4):256–66.
80. Baron JA. Epidemiology of Non-Steroidal Anti-Inflammatory Drugs and Cancer. *Prog Exp tumour Res*. 2003;37:1–24.
81. Labayle D, Fischer D, Vielh P, Drouhin F, Pariente A, Bories C, et al. Sulindac causes regression of rectal polyps in familial adenomatous polyposis. *Gastroenterology*. 1991;101(3):635–9.
82. National Cancer Registry Ireland (NCRI). Colorectal cancer incidence, mortality, treatment and survival in Ireland 1994-2010. [Internet]. Cork; Available from:
<https://www.ncri.ie/sites/ncri/files/pubs/ColorectalCancerIncidenceMortalityTreatmentandSurvivalinIreland1994-2010.pdf>
83. Ning, Y; Wang, L; Giovannucci E. A quantitative analysis of body mass index and colorectal cancer: findings from 56 observational studies. *Obes Rev*. 2010;11(1):19–30.
84. Angeli JPF, Garcia CCM, Sena F, Freitas FP, Miyamoto S, Medeiros MHG, et al. Lipid hydroperoxide-induced and hemoglobin-enhanced oxidative damage to colon cancer cells. *Free Radic Biol Med* [Internet]. 2011;51(2):503–15. Available from:
<http://dx.doi.org/10.1016/j.freeradbiomed.2011.04.015>
85. Helleday, Thomas; Eshtad, Saeed; Nik-zainal S. Mechanisms underlying mutational. *Nat Publ Gr*. 2014;15(9):585–98.
86. Nik-Zainal, Serena; Alexandrov, Ludmil B.; Wedge, David C.; Van Loo, Peter; Greenman, Christopher D.; Raine K et al. Mutational processes molding the genomes of 21 breast cancers. *Cell*. 2012;149(5):979–93.
87. Alexandrov LB, Stratton MR. Mutational signatures : the patterns of somatic mutations hidden in cancer genomes. *Curr Opin Genet Dev*. 2014;24:52–60.
88. Alexandrov, Ludmil B; Nik-zainal, Serena; Wedge, David C; Aparicio SAJR. Signatures of mutational processes in human cancer. *Nature*. 2013;500(7463):415–21.
89. Alexandrov, Ludmil B.; Nik-Zainal, Serena; Wedge, David C.; Campbell,

- Peter J.; Stratton MR. Deciphering Signatures of Mutational Processes Operative in Human Cancer. *Cell Rep.* 2013;3(1):246–59.
90. COSMIC - Catalogue of somatic mutations in cancer [Internet]. [cited 2014 Oct 9]. Available from: <https://cancer.sanger.ac.uk/cosmic>
 91. Davies, Helen; Bignell, Graham R; Cox, Charles; Stephens P. Mutations of the BRAF gene in human cancer. *Nature.* 2002;417(6892):949–54.
 92. Samuels, Yarden; Wang ZBA. High frequency of mutations of the PIK3CA gene in human cancers. *Science* (80-). 2004;304(5670):554.
 93. Abdul-jalil, Khairun I; Sheehan, Katherine M; Toomey, Sinead; Schmid, Jasmin; Prehn, Jochen; Grady AO et al. The Frequencies and Clinical Implications of Mutations in 33 Kinase-Related Genes in Locally Advanced Rectal Cancer : A Pilot Study. *Ann Surg Oncol.* 2014;21:2642–9.
 94. Castellano, Esther; Downward J. Ras interaction with PI3K: More than just another effector pathway. *Genes and Cancer.* 2011;2(3):261–74.
 95. Steelman, Linda S.; Chappell, William H.; Abrams, Stephen L.; Kempf, C. Ruth; Long, Jacquelyn; Laidler P et al. Roles of the Raf/MEK/ERK and PI3K/PTEN/Akt/mTOR pathways in controlling growth and sensitivity to therapy-implications for cancer and aging. *Aging (Albany NY).* 2011;3(3):192–222.
 96. Krasilnikov MA. Phosphatidylinositol-3 kinase dependent pathways: the role in control of cell growth, survival, and malignant transformation. *Biochemistry.* 2000;65(1):59–67.
 97. Utermark, Tamara; Rao, Trisha; Cheng, Hailing; Wang, Qi; Lee, Sang Hyun; Wang ZC et al. The p110 α and p110 β isoforms of PI3K play divergent roles in mammary gland development and tumorigenesis. *Genes Dev.* 2012;26(14):1573–86.
 98. Lawrence, Michael S; Stojanov, Petar; Mermel, Craig H; Garraway, Levi A; Todd, R; Meyerson M et al. Discovery and saturation analysis of cancer genes across 21 tumour types. *Nature.* 2014;505(7484):495–501.
 99. He, Youji; Van't Veer, Laura J.; Mikolajewska-Handlich, Izabela; Van Velthuysen, Marie Louise F.; Zeestraten, Eliane C.M.; Nagtegaal ID. et al. PIK3CA mutations predict local recurrences in rectal cancer patients. *Clin Cancer Res.* 2009;15(22):6956–62.
 100. Rosty, Christophe; Young, Joanne P.; Walsh, Michael D.; Clendenning, Mark; Sanderson, Kristy; Walters RJ. et al. PIK3CA Activating Mutation in

Colorectal Carcinoma: Associations with Molecular Features and Survival. PLoS One. 2013;8(6):1–9.

101. Goel, Ajay; Arnold, Christian N; Niedzwiecki, Donna; Carethers, John M; Dowell, Jeannette M; Wasserman L et al. Frequent Inactivation of PTEN by Promoter Hypermethylation in Microsatellite Instability-High Sporadic Colorectal Cancers Frequent Inactivation of PTEN by Promoter Hypermethylation in Microsatellite Instability-High Sporadic Colorectal Cancers. *Cancer Res.* 2004;64(214):3014–21.
102. Berg, Marianne; Danielsen, Stine A.; Ahlquist, Terje; Merok, Marianne A.; Ågesen TH., Vatn MH. et al. DNA Sequence Profiles of the Colorectal Cancer Critical Gene Set KRAS-BRAF-PIK3CA-PTEN-TP53 Related to Age at Disease Onset. *PLoS One.* 2010;5(11):e13978.
103. Atreya, Chloe E.; Sangale, Zaina; Xu, Nafei; Matli, Mary R.; Tikishvili, Eliso; Welbourn W et al. PTEN expression is consistent in colorectal cancer primaries and metastases and associates with patient survival. *Cancer Med.* 2013;2(4):496–506.
104. Tan, Cong; Du X. KRAS mutation testing in metastatic colorectal cancer. *World J Gastroenterol.* 2012;18(37):5171–80.
105. Zenonos K. RAS signaling pathways, mutations and their role in colorectal cancer. *World J Gastrointest Oncol.* 2013;5(5):97.
106. Helwick C. BRAF Mutations in Colorectal Cancer: The Next Frontier [Internet]. *The Asco Post.* 2013 [cited 2017 Jan 23]. Available from: <https://www.ascopost.com/issues/april-15-2013/braf-mutations-in-colorectal-cancer-the-next-frontier/>
107. Markman M. Colorectal Cancer and KRAS/BRAF [Internet]. *Medscape.* 2017 [cited 2018 Mar 28]. Available from: <https://emedicine.medscape.com/article/1690010-overview>
108. Mao, Chen; Wu, Xin Yin; Yang, Zu Yao; Threapleton, Diane Erin; Yuan, Jin Qiu; Yu, Yuan Yuan; Tang JL. Concordant analysis of KRAS, BRAF, PIK3CA mutations, and PTEN expression between primary colorectal cancer and matched metastases. *Sci Rep.* 2015;5:8065.
109. Phipps, A. I.; Buchanan, D. D.; Makar, K. W.; Win, A. K.; Baron, J. A.; Lindor, N. M.; Potter, J. D.; Newcomb PA. KRAS-mutation status in relation to colorectal cancer survival: The joint impact of correlated tumour markers. *Br J Cancer.* 2013;108(8):1757–64.

110. Andreyev, H J N; Norman, A R; Cunningham, D; Oates, J; Dix, B R; Iacopetta BJ et al. Kirsten ras mutations in patients with colorectal cancer : the “ RASCAL II ” study. *Br J Cancer*. 2001;85(5):692–6.
111. Imamura, Yu; Morikawa, Teppel; Liao X. Specific Mutations in KRAS Codons 12 and 13, and Patient Prognosis in 1075 BRAF-wild-type Colorectal Cancers. *Clin cancer Res*. 2013;18(17):617–32.
112. Yan, Zhongfa; Deng, Xiaobing; Chen, Mingxing; Xu, Ying; Ahram, Mamoun; Sloane, Bonnie F; Friedman E. Oncogenic c-Ki- ras but Not Oncogenic c-Ha- ras Up-regulates CEA Expression and Disrupts Basolateral Polarity in Colon Epithelial Cells. *J Biol Chem*. 1997;272(44):27902–7.
113. Kalady, Matthew; DeJulius, Kathryn; Sanchez J. BRAF Mutations in Colorectal Cancer Are Associated With Distinct Clinical Characteristics and Worse Prognosis. *Dis Colon Rectum*. 2012;55(2):128–33.
114. Antonios Margonis, Georgios; Buettner, Stefan; Andreatos, Nikolaos; Kim Y. Association of BRAF Mutations With Survival and Recurrence in Surgically Treated Patients With Metastatic Colorectal Liver Cancer. *JAMA Surg*. 2018;153(7).
115. Popovici, Vlad; Budinska, Eva; Bosman, Fred T.; Tejpar, Sabine; Roth, Arnaud D.; Delorenzi M. Context-dependent interpretation of the prognostic value of BRAF and KRAS mutations in colorectal cancer. *BMC Cancer*. 2013;13(439).
116. Loupakis, F; Ruzzo, A; Cremolini, C; Vincenzi, B; Salvatore, L; Santini D et al. KRAS codon 61 , 146 and BRAF mutations predict resistance to cetuximab plus irinotecan in KRAS codon 12 and 13 wild-type metastatic colorectal cancer. *Br J Cancer*. 2009;101(4):715–21.
117. Prahallad, Anirudh; sun, Chong; Huang, Sidong; Di Nicolantonio, Frederica; Salazar R. Unresponsiveness of colon cancer to BRAF(V600E) inhibition through feedback activation of EGFR. *Nature*. 2012;483:100–3.
118. Corcoran, Ryan B; Ebi, Hiromichi; Turke, Alexa B; Coffee, Erin M; Cogdill, Alexandria P; Brown RD et al. EGFR-mediated re-activation of MAPK signalling contributes to insensitivity of BRAF mutant colorectal cancers to RAF inhibition with vemurafenib. *Cancer Discov*. 2012;2(3):227–35.
119. Wagner, Erwin; Nebreda AnR. Signal integration by JNK and p38 MAPK pathways in cancer development. *Nat Rev Cancer*. 2009;9:537–49.
120. Sobolewski, Cyril; Cerella, Claudia; Dicato, Mario; Ghibelli, Lina; Diederich

- M. The Role of Cyclooxygenase-2 in Cell Proliferation and Cell Death in Human Malignancies. *Int J Cell Biol*. 2010;2010(article ID 215158).
121. Liu, Bing; Qu, Liyan; Yan S. Cyclooxygenase -2 promotes tumor growth and suppresses tumor immunity. *Cancer Cell Int*. 2015;106:2–7.
 122. Liu N, Rowley BR, Bull CO, Schneider C, Haegebarth A, Schatz CA, et al. BAY 80-6946 Is a Highly Selective Intravenous PI3K Inhibitor with Potent p110 α and p110 δ Activities in Tumor Cell Lines and Xenograft Models. *Mol Cancer Ther*. 2013;11:2319–30.
 123. Bayer. Aliquopa (copanlisib) [Internet]. 2018 [cited 2018 Sep 27]. Available from: <https://www.hcp.aliqopa-us.com/>
 124. Patnaik, A; Appleman, L J; Tolcher, A W; Papadopoulos, K P; Beeram, M; Rasco DW et al. First-in-human phase I study of copanlisib (BAY 80-6946), an intravenous pan-class I phosphatidylinositol 3-kinase inhibitor , in patients with advanced solid tumors and. *Ann Nutr Metab*. 2016;27(10):557–60.
 125. Larson, Sarah M; Peng, Mao Yu; Mead, Monica; Vandross A. Inhibition of PI3K Alpha and PI3K Delta with Copanlisib Shows Preclinical Activity As a Single Agent and in Combination in Multiple Myeloma. *Blood*. 2017;130(Suppl1):3084.
 126. Paul, Juliane; Soujon, Maurice; Wengner, Antje M; Lim ST. Simultaneous Inhibition of PI3K δ and PI3K α Induces ABC-DLBCL Regression by Blocking BCR- Dependent and -Independent Activation of NF- κ B and AKT Article Simultaneous Inhibition of PI3K δ and PI3K α Induces ABC-DLBCL Regression by Blocking BCR-Dependent. *Cancer Cell*. 2017;31:64–78.
 127. ClinicalTrial.gov. Copanlisib Chinese PK Study [Internet]. Bayer. 2019. p. ClinicalTrials.gov Identifier: NCT03498430. Available from: <https://clinicaltrials.gov/ct2/show/NCT03498430?term=Copanlisib&draw=2&rank=1>
 128. ClinicalTrial.gov. Copanlisib Pharmacodynamic Study [Internet]. Bayer. 2017. p. ClinicalTrials.gov Identifier: NCT02155582. Available from: <https://clinicaltrials.gov/ct2/show/NCT02155582?term=Copanlisib&draw=2>
 129. ClinicalTrial.gov. COPANLISIB (BAY80-6946) Drug-drug Interaction and Cardiovascular Safety Study in Advanced Solid Tumor and Non-Hodgkin's Lymphoma Patients [Internet]. Bayer. 2019. p. ClinicalTrials.gov Identifier: NCT02253420. Available from:

- <https://clinicaltrials.gov/ct2/show/NCT02253420?term=Copanlisib&draw=2>
130. ClinicalTrial.gov. Copanlisib and Nivolumab in Treating Patients With Metastatic Solid Tumors or Lymphoma [Internet]. 2019. p. ClinicalTrials.gov Identifier: NCT03502733. Available from:
<https://clinicaltrials.gov/ct2/show/NCT03502733?term=Copanlisib&draw=2>
131. ClinicalTrial.gov. Phase 1 Study of PI3 (Phosphatidylinositol-3)-Kinase Inhibitor Copanlisib With Gemcitabine or Cisplatin Plus Gemcitabine in Patients With Advanced Cancer [Internet]. Bayer. 2017. p. ClinicalTrials.gov Identifier: NCT01460537. Available from:
<https://clinicaltrials.gov/ct2/show/NCT01460537?term=Copanlisib&draw=2>
132. ClinicalTrial.gov. Phase Ib Study of PI3(Phosphoinositol 3)-Kinase Inhibitor Copanlisib With MEK (Mitogen-activated Protein Kinase) Inhibitor Refametinib (BAY86-9766) in Patients With Advanced Cancer [Internet]. Bayer. 2015. p. ClinicalTrials.gov Identifier: NCT01392521. Available from:
<https://clinicaltrials.gov/ct2/show/NCT01392521?term=Copanlisib&draw=2>
133. ClinicalTrial.gov. BAY80-6946 Open Label, Phase I Study in Patients With Advanced Cancer [Internet]. Bayer. 2017. p. ClinicalTrials.gov Identifier: NCT00962611. Available from:
<https://clinicaltrials.gov/ct2/show/NCT00962611?term=Copanlisib&draw=2>
134. ClinicalTrial.gov. Phase I Study of PI3(Phosphoinositol 3)-Kinase Inhibitor BAY80-6946 With Paclitaxel in Patients With Advanced Cancer [Internet]. Bayer. 2017. p. ClinicalTrials.gov Identifier: NCT01411410. Available from:
<https://clinicaltrials.gov/ct2/show/NCT01411410?term=Copanlisib&draw=2>
135. ClinicalTrial.gov. Effect of Copanlisib on Metformin PK and PD [Internet]. Bayer. 2019. p. ClinicalTrials.gov Identifier: NCT03655301. Available from:
<https://clinicaltrials.gov/ct2/show/NCT03655301?term=Copanlisib&draw=2>
136. ClinicalTrial.gov. Copanlisib Mass Balance Study [Internet]. Bayer. 2014. p. ClinicalTrials.gov Identifier: NCT02119221. Available from:
<https://clinicaltrials.gov/ct2/show/NCT02119221?term=Copanlisib&draw=2>
137. ClinicalTrial.gov. Niraparib and Copanlisib in Treating Patients With Recurrent Endometrial, Ovarian, Primary Peritoneal, or Fallopian Tube Cancer. Bayer. 2019. p. ClinicalTrials.gov Identifier: NCT03586661.
138. ClinicalTrial.gov. Study of Copanlisib in Hepatic or Renal Impairment [Internet]. Bayer. 2019. p. ClinicalTrials.gov Identifier: NCT03172884. Available from:

- <https://clinicaltrials.gov/ct2/show/NCT03172884?term=Copanlisib&draw=2>
139. ClinicalTrial.gov. Phase 1 Study of the Combination of Rogaratinib With Copanlisib in Patients With Fibroblast Growth Factor Receptor (FGFR)-Positive, Locally Advanced or Metastatic Solid Tumors (ROCOCO) [Internet]. Bayer. 2019. p. ClinicalTrials.gov Identifier: NCT03517956. Available from:
<https://clinicaltrials.gov/ct2/show/NCT03517956?term=Copanlisib&draw=2>
 140. ClinicalTrial.gov. Copanlisib With Ibrutinib for Patients With Recurrent/Refractory Primary Central Nervous System Lymphoma (PCNSL) [Internet]. Bayer. 2019. p. ClinicalTrials.gov Identifier: NCT03581942. Available from:
<https://clinicaltrials.gov/ct2/show/NCT03581942?term=Copanlisib&draw=2>
 141. ClinicalTrial.gov. Japanese Phase Ib/II Copanlisib in Relapsed, Indolent B-cell NHL [Internet]. Bayer. 2019. p. ClinicalTrials.gov Identifier: NCT02342665. Available from:
<https://clinicaltrials.gov/ct2/show/NCT02342665?term=Copanlisib&draw=2>
 142. ClinicalTrial.gov. Copanlisib, Letrozole, and Palbociclib in Treating Patients With Hormone Receptor Positive HER2 Negative Stage I-IV Breast Cancer [Internet]. 2019. p. ClinicalTrials.gov Identifier: NCT03128619. Available from:
<https://clinicaltrials.gov/ct2/show/NCT03128619?term=Copanlisib&draw=2>
 143. ClinicalTrial.gov. Phase Ib/II Trial of coPANlisib in Combination With Trastuzumab in HER2-positive Breast Cancer. (Panther Study) (Panther) [Internet]. 2019. p. ClinicalTrials.gov Identifier: NCT02705859. Available from:
<https://clinicaltrials.gov/ct2/show/NCT02705859?term=Copanlisib&draw=2>
 144. ClinicalTrial.gov. Copanlisib in Association With Cetuximab in Patients With Recurrent and/or Metastatic Head and Neck Squamous Cell Carcinomas Harboring a PI3KCA Mutation/Amplification and/or a PTEN Loss (COPAN-ORL06) [Internet]. Bayer. 2019. p. ClinicalTrials.gov Identifier: NCT02822482. Available from:
<https://clinicaltrials.gov/ct2/show/NCT02822482?term=Copanlisib&draw=2&rank=2>
 145. ClinicalTrial.gov. Copanlisib and Gemcitabine in Relapsed/Refractory PTCL [Internet]. Bayer. 2018. p. ClinicalTrials.gov Identifier: NCT03052933. Available from:

- <https://clinicaltrials.gov/ct2/show/NCT03052933?term=Copanlisib&draw=2>
146. ClinicalTrial.gov. Study of PI3Kinase Inhibition (Copanlisib) and Anti-PD-1 Antibody Nivolumab in Relapsed/Refractory Solid Tumors With Expansions in Mismatch-repair Proficient (MSS) Colorectal Cancer [Internet]. Bayer. 2019. p. ClinicalTrials.gov Identifier: NCT03711058. Available from: <https://clinicaltrials.gov/ct2/show/NCT03711058?term=Copanlisib&draw=2>
147. ClinicalTrial.gov. An Study to Evaluate the Safety and Efficacy of Copanlisib in Combination With Nivolumab in Patients With Advanced Solid Tumors [Internet]. Bayer. 2019. p. ClinicalTrials.gov Identifier: NCT03735628. Available from: <https://clinicaltrials.gov/ct2/show/NCT03735628?term=Copanlisib&draw=2>
148. ClinicalTrial.gov. Safety, Tolerability, Efficacy and Pharmacokinetics of Copanlisib in Pediatric Patients [Internet]. Bayer. 2019. p. ClinicalTrials.gov Identifier: NCT03458728. Available from: <https://clinicaltrials.gov/ct2/show/NCT03458728?term=Copanlisib&draw=2>
149. ClinicalTrial.gov. Open-label, Uncontrolled Phase II Trial of Intravenous PI3K Inhibitor BAY80-6946 in Patients With Relapsed, Indolent or Aggressive Non-Hodgkin's Lymphomas [Internet]. Bayer. 2019. p. ClinicalTrials.gov Identifier: NCT01660451. Available from: <https://clinicaltrials.gov/ct2/show/NCT01660451?term=Copanlisib&draw=2>
150. ClinicalTrial.gov. Phase II Copanlisib in Relapsed/Refractory Diffuse Large B-cell Lymphoma (DLBCL) [Internet]. Bayer. 2019. p. NCT02391116. Available from: <https://clinicaltrials.gov/ct2/show/NCT02391116?term=Copanlisib&draw=2>
151. ClinicalTrial.gov. Copanlisib and Rituximab in Marginal Zone Lymphoma Patients [Internet]. 2019. p. ClinicalTrials.gov Identifier: NCT03474744. Available from: <https://clinicaltrials.gov/ct2/show/NCT03474744?term=Copanlisib&draw=2>
152. ClinicalTrial.gov. Response-Adapted Therapy With Copanlisib and Rituximab in Untreated Follicular Lymphoma [Internet]. 2019. p. ClinicalTrials.gov Identifier: NCT03789240. Available from: <https://clinicaltrials.gov/ct2/show/NCT03789240?term=Copanlisib&draw=2>
153. ClinicalTrial.gov. Copanlisib Hydrochloride and Nivolumab in Treating Patients With Recurrent or Refractory Diffuse Large B-cell Lymphoma or Primary Mediastinal Large B-cell Lymphoma [Internet]. 2019. p.

- ClinicalTrials.gov Identifier: NCT03484819. Available from:
<https://clinicaltrials.gov/ct2/show/NCT03484819?term=Copanlisib&draw=2>
154. ClinicalTrial.gov. Phase IIa Study of Copanlisib in Relapsed or Refractory Mantle Cell Lymphoma (MCL) [Internet]. Bayer. 2017. p. ClinicalTrials.gov Identifier: NCT02455297. Available from:
<https://clinicaltrials.gov/ct2/show/NCT02455297?term=Copanlisib&draw=2>
155. ClinicalTrial.gov. Copanlisib in Treating Patients With Persistent or Recurrent Endometrial Cancer [Internet]. 2019. p. ClinicalTrials.gov Identifier: NCT02728258. Available from:
<https://clinicaltrials.gov/ct2/show/NCT02728258?term=Copanlisib&draw=2>
156. ClinicalTrial.gov. Copanlisib (BAY 80-6946) in Combination With Gemcitabine and Cisplatin in Advanced Cholangiocarcinoma [Internet]. Bayer. 2019. p. ClinicalTrials.gov Identifier: NCT02631590. Available from:
<https://clinicaltrials.gov/ct2/show/NCT02631590?term=Copanlisib&draw=2>
157. ClinicalTrial.gov. Fulvestrant and Palbociclib With or Without Copanlisib in Treating Patients With Hormone Receptor Positive, HER2 Negative, Stage IV Breast Cancer [Internet]. Bayer. 2018. p. ClinicalTrials.gov Identifier: NCT03377101. Available from:
<https://clinicaltrials.gov/ct2/show/NCT03377101?term=Copanlisib&draw=2>
158. ClinicalTrial.gov. Copanlisib and Rituximab in Relapsed Indolent B-cell Non-Hodgkin's Lymphoma (iNHL) (CHRONOS-3) [Internet]. Bayer. 2019. p. ClinicalTrials.gov Identifier: NCT02367040. Available from:
<https://clinicaltrials.gov/ct2/show/NCT02367040?term=Copanlisib&draw=2>
159. ClinicalTrial.gov. Phase III Copanlisib in Rituximab-refractory iNHL (CHRONOS-2) [Internet]. Bayer. 2019. p. ClinicalTrials.gov Identifier: NCT02369016. Available from:
<https://clinicaltrials.gov/ct2/show/NCT02369016?term=Copanlisib&draw=2>
160. ClinicalTrial.gov. Study of Copanlisib in Combination With Standard Immunochemotherapy in Relapsed Indolent Non-Hodgkin's Lymphoma (iNHL) (CHRONOS-4) [Internet]. Bayer. 2019. p. ClinicalTrials.gov Identifier: NCT02626455. Available from:
<https://clinicaltrials.gov/ct2/show/NCT02626455?term=Copanlisib&draw=2>
161. ClinicalTrial.gov. BAY86-9766 Plus Gemcitabine Phase I Study in Asian [Internet]. Bayer. 2018. p. ClinicalTrials.gov Identifier: NCT01764828. Available from:

- <https://clinicaltrials.gov/ct2/show/NCT01764828?term=BAY86-9766&rank=1>
162. ClinicalTrial.gov. Japanese BAY86-9766 Monotherapy Phase I Study [Internet]. Bayer. 2017. p. ClinicalTrials.gov Identifier: NCT01179295. Available from:
<https://clinicaltrials.gov/ct2/show/NCT01179295?term=BAY86-9766&rank=2>
 163. ClinicalTrial.gov. Refametinib (BAY86-9766) in Combination With Regorafenib (Stivarga, BAY73-4506) in Patients With Advanced or Metastatic Cancer [Internet]. Bayer. 2018. p. ClinicalTrials.gov Identifier: NCT02168777. Available from:
<https://clinicaltrials.gov/ct2/show/NCT02168777?term=BAY86-9766&rank=6>
 164. ClinicalTrial.gov. Effect of Ketoconazole on the Pharmacokinetics of Refametinib [Internet]. Bayer. 2014. p. ClinicalTrials.gov Identifier: NCT01925638. Available from:
<https://clinicaltrials.gov/ct2/show/NCT01925638?term=BAY86-9766&rank=7>
 165. ClinicalTrial.gov. Combination With Gemcitabine in Advanced Pancreatic Cancer (BAGPAC) [Internet]. Bayer. 2018. p. ClinicalTrials.gov Identifier: NCT01251640. Available from:
<https://clinicaltrials.gov/ct2/show/NCT01251640?term=BAY86-9766&rank=8>
 166. ClinicalTrial.gov. RDEA119 and Sorafenib Combination Dose Escalation Study [Internet]. Bayer. 2016. p. ClinicalTrials.gov Identifier: NCT00785226. Available from:
<https://clinicaltrials.gov/ct2/show/NCT00785226?term=BAY86-9766&rank=10>
 167. ClinicalTrial.gov. Assessing BAY86-9766 Plus Sorafenib for the Treatment of Liver Cancer. (BASIL) [Internet]. Bayer. 2013. p. ClinicalTrials.gov Identifier: NCT01204177. Available from:
<https://clinicaltrials.gov/ct2/show/NCT01204177?term=BAY86-9766&rank=3>
 168. ClinicalTrial.gov. Refametinib(BAY86-9766) in RAS Mutant Hepatocellular Carcinoma (HCC) [Internet]. Bayer. 2017. p. ClinicalTrials.gov Identifier: NCT01915589. Available from:
<https://clinicaltrials.gov/ct2/show/NCT01915589?term=BAY86-9766&rank=5>
 169. ClinicalTrial.gov. Refametinib in Combination With Sorafenib in RAS Mutant Hepatocellular Carcinoma (HCC) [Internet]. Bayer. 2017. p. ClinicalTrials.gov Identifier: NCT01915602. Available from:
<https://clinicaltrials.gov/ct2/show/NCT01915602?term=BAY86-9766&rank=9>

170. Clinical Trials [Internet]. NIH U.S. National Library of Medicine. [cited 2018 Feb 1]. Available from:
<https://clinicaltrials.gov/ct2/results?cond=&term=refametinib&cntry=&state=&city=&dist=>
171. Oken, Martin; Creech, Richard; Tormey, Douglass; Horton J. Toxicity and response criteria of the Eastern Cooperative Oncology Group. *Am J Clin Oncol.* 1982;5(6):649–56.
172. Desitter, Isabelle; Guerrouahen, Bella S; Benali-furet, Naoual; Wechsler, Janine; Jänne, Pasi A; Kuang Y et al. A New Device for Rapid Isolation by Size and Characterization of Rare Circulating Tumor Cells. *Anticancer Res.* 2011;31:427–41.
173. Vona, Giovanna; Sabile, Abdelmajid; Louha, Malek; Sitruk, Veronique; Romana, Serge; Schütze K et al. Isolation by Size of Epithelial Tumor Cells. *Am J Pathol.* 2000;156(1):57–63.
174. De Giorgi, Vincenzo; Pinzani, Pamela; Salvianti, Francesca; Panelos, John; Paglierani, Milena; Janowska A et al. Application of a filtration- and isolation-by-size technique for the detection of circulating tumor cells in cutaneous melanoma. *J Invest Dermatol.* 2010;130(10):2440–7.
175. Pinzani, Pamela; Scatena, Cristian; Salvianti, Francesca; Corsini, Elisa; Canu, Letizia; Poli G et al. Detection of Circulating Tumor Cells in Patients With Adrenocortical Carcinoma: A Monocentric Preliminary Study. *J Clin Endocrinol Metab.* 2013;98(9):3731–8.
176. Broad Institute of MIT and Harvard. Cancer Cell Line Encyclopedia (CCLE) [Internet]. [cited 2014 Sep 10]. Available from:
<https://portals.broadinstitute.org/ccle>
177. Promega. CellTiter96 AQueous One Solution Cell Proliferation Assay protocol. 2012.
178. Shields, L; Vega-Carrascal, I; Singleton, S; Lyng, FM; McClean B. Cell survival and DNA damage in normal prostate cells irradiated out-of-field. *Radiat Res.* 2014;182(5):499–506.
179. Smith, A M; Watson SA. Gastrin and gastrin receptor activation : an early event in the adenoma-carcinoma sequence. *Gut.* 2000;47:820–4.
180. Rajput, Ashwani; Greenbaum, Alissa; Lee, Ji-hyun; Ness, Scott A; Salud, De; Heber, Reginald; Hall F. Mutant-Allele Tumor Heterogeneity (MATH) Scores Correlate with Risk of Metastases in Colon Cancer. *Clin Colorectal*

- Cancer. 2017;16(3):1–13.
181. ProteinPaint. APC [Internet]. St.Judes. Available from: <https://pecan.stjude.cloud/proteinpaint/APC#>
 182. Sinicrope, Frank A.; Rego, Rafaela L.; Halling, Kevin C.; Foster, Nathan; Sargent, Daniel J.; La Plant B et al. Prognostic Impact of Microsatellite Instability and DNA Ploidy in Human Colon Carcinoma Patients. *Gastroenterology*. 2006;131(3):729–37.
 183. Samowitz, W S; Curtin, K; Ma, K N; Schaffer, D; Coleman, L W; Leppert, M; Slattery ML. Microsatellite instability in sporadic colon cancer is associated with an improved prognosis at the population level. *Cancer Epidemiol Biomarkers Prev*. 2001;10(9):917–23.
 184. Gafa, R; Maestri, I; Matteuzzi, M; Santini, A; Feretti, S; Cavazzini, L; Lanza G. Sporadic colorectal adenocarcinomas with high-frequency microsatellite instability. *Cancer*. 2000;89(10):2025–37.
 185. Thibodeau, SN; Bren, G; Schaid D. Microsatellite instability in cancer of the proximal colon. *Science* (80-). 1993;260(5109):816–9.
 186. The cancer genome atlas. Comprehensive molecular characterization of human colon and rectal cancer. *Nature*. 2012;487(7407):330–7.
 187. Briggs, Sarah; Tomlinson I. Germline and somatic polymerase ϵ and δ mutations define a new class of hypermutated colorectal and endometrial cancers. *J Pathol*. 2013;230:148–53.
 188. Olsen, Renate S.; Lindh, Mikael; Vorkapic, Emina; Andersson, Roland E.; Zar, Niklas; Löfgren S et al. CD93 gene polymorphism is associated with disseminated colorectal cancer. *Int J Colorectal Dis*. 2015;30(7):883–90.
 189. Shinada, Keisuke; Tsukiyama, Tadasuke; Sho, Takuya; Okumura F. RNF43 interacts with NEDL1 and regulates p53-mediated transcription. *Biochem Biophys Res Commun*. 2011;404(1):143–7.
 190. Pan, Huixing; Xu, Xiaojian; Wu, Deyao; Qiu, Qiaocheng; Zhou S. Novel somatic mutations identified by whole-exome sequencing in muscle-invasive transitional cell carcinoma of the bladder. *Oncol Lett*. 2016;11:1486–92.
 191. Li, Y; Zhou, Z; Alimandi, M; Chen C. WW domain containing E3 ubiquitin protein ligase 1 targets the full-length ErbB4 for ubiquitin-mediated degradation in breast cancer. *Oncogene*. 2009;28:2948–58.
 192. Wang, Qiang; Shi, Yan-long; Zhou, Kai; Wang, Li-li; Yan, Ze-xuan; Liu Y et al. PIK3CA mutations confer resistance to first-line chemotherapy in

- colorectal cancer. *Cell Death Dis.* 2018;9(7):739.
193. Lee, John T; Steelman, Linda S; Mccubrey JA. Phosphatidylinositol 3'-Kinase Activation Leads to Multidrug Resistance Protein-1 Expression and Subsequent Chemoresistance in Advanced Prostate Cancer Cells. *Cancer Res.* 2004;64(22):8397–404.
194. Eralp, Y; Derin, D; Ozluk, Y; Yavuz, E; Guney, N; Saip, P; Muslumanoglu, M; Igci, A; Ku S. MAPK overexpression is associated with anthracycline resistance and increased risk for recurrence in patients with triple-negative breast cancer. *Ann Oncol.* 2008;19(4):669–74.
195. COSMIC. KRAS - GRCh37 COSMIC v89 [Internet]. Available from: https://cancer.sanger.ac.uk/cosmic/gene/analysis?all_data=&coords=AA%3AAA&dr=&end=189&gd=&id=4&ln=KRAS&seqlen=189&sn=large_intestine&start=1#ts
196. Martellucci, Jacopo; Alemanno, Giovanni; Castiglione, Francesca; Bergami, Carlo; Valeri A. Role of KRAS mutation as predictor of pathologic response after neoadjuvant chemoradiation therapy for rectal cancer. *Updates Surg.* 2015;67(1):47–53.
197. Chow, Oliver S; Kuk, Deborah; Keskin, Metin; Smith, Joshua; Camacho N. KRAS and combined KRAS/TP53 mutations in locally advanced rectal cancer are independently associated with decreased response to neoadjuvant therapy. *Ann Surg Oncol.* 2016;23(8):2548–55.
198. Inoue, Yasuhiro; Saigusa, Susumu; Iwata, Eakashi; Okugawa Y. The prognostic value of KRAS mutations in patients with colorectal cancer. *Oncol Rep.* 2012;28(5):1579–84.
199. De Roock, Wendy; Jonker, Derek j; Di Nicolantonio, Federica; Sartore-Bianchi A. Association of KRAS p.G13D Mutation With Outcome in Patients With Chemotherapy-Refractory Metastatic Colorectal Cancer Treated With Cetuximab. *JAMA.* 2010;304(16):1812–20.
200. De Roock, Wendy ; Claes, Bart; Bernasconi, David; De Schutter, Jef; Biesmans B. Effects of KRAS, BRAF, NRAS, and PIK3CA mutations on the efficacy of cetuximab plus chemotherapy in chemotherapy-refractory metastatic colorectal cancer: a retrospective consortium analysis. *Lancet Oncol.* 2010;11(8):753–62.
201. Edkins, Sarah; O'Meara, Sarah; Parker, Adrian; Stevens, Claire; Reis, Marcelo; Jones S et al. Recurrent KRAS codon 146 mutations in human

- colorectal cancer. *Cancer Biol Ther.* 2006;5(8):928–32.
202. Cox, Adrienne D; Fesik, Stephen W; Kimmelman, Alec C; Luo, Ji; Der CJ. Drugging the undruggable RAS: mission possible? *Nat Rev Drug Discov.* 2015;13(11):828–51.
 203. Janakiraman, Manickam; Vakiani, Efsevia; Zeng, Zhaoshi; Pratilas, Christine A; Taylor BS. Genomic and biological characterization of exon 4 KRAS mutations in human cancer. *Cancer Res.* 2010;70(14):5901–11.
 204. Jones, Robert P; Sutton, Paul A; Evans, Jonathan P; Clifford, Rachel; Mcavoy, Andrew; Lewis J et al. Specific mutations in KRAS codon 12 are associated with worse overall survival in patients with advanced and recurrent colorectal cancer. 2017;116(7):923–9.
 205. Li, Wenbin; Qiu, Tian; Zhi, Wenxue; Shi, Susheng; Zou, Shuangmei; Ling Y et al. Colorectal carcinomas with KRAS codon 12 mutation are associated with more advanced tumor stages. *BMC Cancer.* 2015;15(340):1–9.
 206. Ikenoue, Tsuneo; Hikiba, Yohko; Kanai, Fumihiko; Tanaka, Yasuo; Imamura, Jun; Imamura T et al. Functional Analysis of Mutations within the Kinase Activation Segment of B-Raf in Human Colorectal Tumors. *Cancer Res.* 2003;63(23):8132–7.
 207. Heidorn, Sonja J; Milagre, Carla; Whittaker, Steven; Nourry, Arnaud; Niculescu-duvas, Ion; Dhomen, Nathalie; Hussain, Jahan; Reis-filho, Jorge S; Springer, Caroline J; Pritchard, Catrin; Marais R. Kinase-Dead BRAF and Oncogenic RAS Cooperate to Drive Tumor Progression through CRAF. *Cell.* 2010;140(2):209–21.
 208. Wan, Paul T C; Garnett, Mathew J; Roe, S Mark; Lee, Sharlene; Niculescu-duvaz, Dan; Good VM et al. Mechanism of Activation of the RAF-ERK Signaling Pathway by Oncogenic Mutations of B-RAF. *Cell.* 2004;116:855–67.
 209. Wu, Xiaowen; Yan, Junya; Dai, J I E; Ma, Meng; Tang, Huan; Yu J et al. Mutations in BRAF codons 594 and 596 predict good prognosis in melanoma. *Oncol Lett.* 2017;14:3601–5.
 210. Cremolini, C; Bartolomeo, M Di; Amatu, A; Antoniotti, C; Moretto, R; Berenato, R; Perrone F et al. BRAF codons 594 and 596 mutations identify a new molecular subtype of metastatic colorectal cancer at favorable prognosis. *Ann Oncol.* 2015;26:2092–7.
 211. Amaki-Takao, M; Yamaguchi, T; Natsume, S; Iijima, T; Wakaume R.

- Colorectal Cancer with BRAF D594G Mutation Is Not Associated with Microsatellite Instability or Poor Prognosis. *Oncology*. 2016;91:162–70.
212. Cathomas G. PIK3CA in Colorectal Cancer. *Front Oncol*. 2014;4(March):16–9.
 213. Day, Fiona L.; Jorissen, Robert N.; Lipton, Lara; Mouradov, Dmitri; Sakthianandeswaren, Anuratha; Christie M et al. PIK3CA and PTEN gene and exon mutation-specific clinicopathologic and molecular associations in Colorectal cancer. *Clin Cancer Res*. 2013;19(12):3285–96.
 214. COSMIC. APC - GRCh37 COSMIC v89 [Internet]. Available from: https://cancer.sanger.ac.uk/cosmic/gene/analysis?all_data=&coords=AA%3AAA&dr=&end=2844&gd=&id=923&ln=APC&seqlen=2844&sn=large_intestine&start=1#ts
 215. Donson, Andrew M; Birks, Diane K; Barton, Valerie N; Kleinschmidt-demasters, Bette K; Handler, Michael H; Waziri AE et al. Immune gene and cell enrichment is associated with a good prognosis in ependymoma. *J Immunol*. 2019;183(11):7428–40.
 216. Hu, Jing; Sun J. MUC16 mutations improve patients' prognosis by enhancing the infiltration and antitumor immunity of cytotoxic T lymphocytes in the endometrial cancer microenvironment. *Oncoimmunology*. 2018;7(10).
 217. Danan-Gotthold, Miri; Golan-Gerstl, Regina; Eisenberg, Eli; Meir, Keren; Karni, Rotem; Levanon EY. Identification of recurrent regulated alternative splicing events across human solid tumors. *Nucleic Acids Res*. 2015;43(10):5130–44.
 218. Tan, Fengbo; Zhu, Hong; Tao, Yiming; Yu, Nanhui; Pei, Qian; Liu H al. Neuron navigator 2 overexpression indicates poor prognosis of colorectal cancer and promotes invasion through the SSH1L / cofilin-1 pathway. *J Exp Clin Cancer Res*. 2015;34(117):1–12.
 219. Chang, Li-yun; Liu, Li-yu D; Roth, Don A; Kuo, Wen-hung; Hwa, Hsiao-lin; Chang K et al. The Major Prognostic Features of Nuclear Receptor NR5A2 in Infiltrating Ductal Breast Carcinomas. *Int J Genomics*. 2015;Article ID.
 220. Chen, Xin; Fu, Yufei; Xu, Hongfei; Teng, Peng; Xie, Qiong; Zhang Y. SOX5 predicts poor prognosis in lung adenocarcinoma and promotes tumor metastasis through epithelial-mesenchymal transition. *Oncotarget*. 2018;9(13):10891–904.
 221. Sun, Chuntao; Ban, Yunqing; Wang, K A I; Sun, Yanming; Zhao Z. SOX5

- promotes breast cancer proliferation and invasion by transactivation of EZH2. *Oncol Lett.* 2019;17(3):2754–62.
222. Micale, Lucia; Fusco, Carmela; Fontana, Andrea; Barbano, Raffaella; Augello, Bartolomeo; Nittis PD et al. TRIM8 downregulation in glioma affects cell proliferation and it is associated with patients survival. *BMC Cancer.* 2015;15(470):1–10.
 223. Liu, Lanxin; Kimball, Sarah; Liu, Hui; Holowatyj A. Genetic alterations of histone lysine methyltransferases and their significance in breast cancer. *Oncotarget.* 2014;6(4).
 224. Jung, Ah Ra; Eun, Young-gyu; Lee, Young Chan; Noh JK. Clinical Significance of CUB and Sushi Multiple Domains 1 Inactivation in Head and Neck Squamous Cell Carcinoma. *Int J Mol Sci.* 2018;19(12):1–11.
 225. Wood, Laura D; Parsons, D. Williams; Jones, Sian; Lin, Jimmy; Sjoblom T. The Genomic Landscapes of Human Breast and Colorectal Cancers. *Science (80-).* 2007;318(5853):1108–13.
 226. Li, Li; Fu, Luo-qin; Wang, Hui-ju; Yan, Zhi-long; Yu, Xiu-chong; Wang Y. FAT2 is a novel independent prognostic factor for the poor prognosis of gastric carcinoma. *Int J Clin Exp Pathol.* 2017;10(12):11603–9.
 227. Xia, Xiaochun; He, Chao; Wu, Anqing; Zhou, Jundong; Wu J. Microtubule-Associated Protein 4 Is a Prognostic Factor and Promotes Tumor Progression in Lung Adenocarcinoma. *Dis Markers.* 2018;2018.
 228. Jiang, Y-Y; Shang, L; Shi, Z-Z; Zhang, T-T; Ma, S; Lu C-C. Microtubule-associated protein 4 is an important regulator of cell invasion/migration and a potential therapeutic target in esophageal squamous cell carcinoma. *Oncogene.* 2016;15(35):4846–56.
 229. Yang, Qin; Zhu, Chunchao; Zhang, Yanli; Wang, Yangyang; Wang, Yahui; Zhu, Lei; Yang X. Molecular analysis of gastric cancer identifies genomic markers of drug sensitivity in Asian gastric cancer. *J cancer.* 2018;9(16):2973–80.
 230. Weng, Xingyue; Chen, Wei; Hu, Wangxiong; Xu, Kailun; Qi, Lina; Chen J et al. PTPRB promotes metastasis of colorectal carcinoma via inducing epithelial- mesenchymal transition. *Cell Death Dis.* 2019;10(352).
 231. Behjati, Sam; Tarpey, Patrick S; Sheldon, Helen; Martincorena, Inigo; Loo, Peter Van; Gundem G et al. Recurrent PTPRB and PLCG1 mutations in angiosarcoma. *Nat Genetics.* 2014;46(4):376–9.

232. Qiang, Wei; Zhao, Yuan; Yang, Qi; Liu, Wei; Guan, Haixia; Lv, Siqing; Ji M. ZIC1 Is a Putative Tumor Suppressor in Thyroid Cancer by Modulating Major Signaling Pathways and. *J Clin Endocrinol Metab.* 2014;99(7):1163–72.
233. Yan, Xiaotong; Wen, Xiajie; Zhao, Erjiang; Qian, Xiangjun; Lu, Weiquan; Lv Q et al. Elevated apolipoprotein B predicts poor postsurgery prognosis in patients with hepatocellular carcinoma. *Onco Targets Ther.* 2019;12:1957–64.
234. Shibamoto, Misako; Hirata, Hidenari; Eguchi H. The loss of CASP4 expression is associated with poor prognosis in esophageal squamous cell carcinoma. *Oncol Lett.* 2017;13(3):1761–6.
235. Yavorski, John M; Stoll, Rebecca J; Samy, Mohammad D; Mauro, James A; Blanck G. Identification of Sets of Cytoskeletal Related and Adhesion-related Coding Region Mutations in the TCGA Melanoma Dataset that Correlate with a Negative Outcome. *Curr Genomics.* 2017;18:287–97.
236. Marín, I González-gascón; Hernández, J A; Martín, A; Alcoceba, M; Sarasquete, M E; Heras C et al. Mutation Status and Immunoglobulin Gene Rearrangements in Patients from Northwest and Central Region of Spain with Chronic Lymphocytic Leukemia. *Biomed Res Int.* 2014;Article ID.
237. Cheng, Yuen Yee; Kirschner, Michaela B; Cheng, Ngan Ching; Gattani, Sumedha; Klebe, Sonja; Edelman JJB et al. ZIC1 Is Silenced and Has Tumor Suppressor Function in Malignant Pleural Mesothelioma. *J Thorac Oncol.* 2013;8(10):1317–28.
238. Mroz, Edmund, A; Rocco JW. MATH, a novel measure of intratumor genetic heterogeneity, is high in poor-outcome classes of head and neck squamous cell carcinoma. *Oral Oncol.* 2013;49(3):211–5.
239. Mroz, Edmund; Tward, Arron; Pickering, Curtis; Myers, Jeffrey N; Ferris RL. High intra-tumor genetic heterogeneity is related to worse outcome in head and neck squamous cell carcinoma. *Cancer.* 2013;119(16):3034–42.
240. Mandard, AM; Dalibard, F; Mandard, JC; Marnay, J; Henry-Amar M. Pathologic assessment of tumor regression after preoperative chemoradiotherapy of esophageal carcinoma. Clinicopathologic correlations. *Cancer.* 1994;73(11):2680–6.
241. Abdalmassih, Michael; Sivananthan, Gokulan; Raizman, Zachary; Lambert, Pascal; Wirtzfeld, Debrah; Bashir B et al. Prognostic markers of recurrence

- and survival in rectal cancer treated with neoadjuvant chemoradiotherapy and surgery. *Color cancer*. 2018;7(1).
242. Wu, Guangdong; Zhu, Rongrong; Li, Yatong; Zhao, Yupei; Dai M. Prognostic significance of circulating tumor microemboli in patients with pancreatic ductal adenocarcinoma. *Oncol Lett*. 2018;15:7376–82.
 243. Chandra, Anurag; Guerrero, Thomas M; Liu, Helen; Tucker, Susan L; Liao Z. Feasibility of using intensity-modulated radiotherapy to improve lung sparing in treatment planning for distal esophageal cancer. *Radiother Oncol*. 2005;77(3):247–53.
 244. Li, Yi-yang; Lin, Hai-qun; Zhang, Lu-lu; Feng, Ling-ling; Niu S. Intensity-modulated radiotherapy has superior outcomes to three-dimensional conformal radiotherapy in patients with stage IE-IIIE extranodal nasal-type natural killer / T-cell lymphoma. *Oncotarget*. 2017;8(36):60504–13.
 245. Xu, Dandan; Li, Guowen; Li, Hongfei; Jia F. Comparison of IMRT versus 3D-CRT in the treatment of esophagus cancer. *Medicine (Baltimore)*. 2017;96(31):1–7.
 246. Christensen, Troels Dreier; Spindler, Karen-lise Garm; Palshof, Jesper Andreas; Nielsen DL. Systematic review : brain metastases from colorectal cancer — Incidence and patient characteristics. *BMC Cancer*. 2016;16(260):1–14.
 247. Inhestern, Johanna; Oertel, Katrin; Stemmann, Viola; Schmalenberg, Harald; Dietz, Andreas; Rotter N et al. Prognostic Role of Circulating Tumor Cells during Induction Chemotherapy Followed by Curative Surgery Combined with Postoperative Radiotherapy in Patients with Locally Advanced Oral and Oropharyngeal Squamous Cell Cancer. *PLoS One*. 2015;1:1–13.
 248. Martin, Olga A; Anderson, Robin L; Russell, Prudence A; Cox, R. Ashely; Ivashkevich, Alesia; Swierczak A. Mobilization of Viable Tumor Cells Into the Circulation During Radiation Therapy. *Int J Radiat Oncol*. 2014;88(2):395–403.
 249. Toor, Omer M; Ahmed, Zaheer; Bahaj, Waled; Boda, Urooge; Cummings, Lee S; McNally ME et al. Correlation of Somatic Genomic Alterations Between Tissue Genomics and ctDNA Employing Next-Generation Sequencing : Analysis of Lung and Gastrointestinal Cancers. *Mol Cancer Ther*. 2018;17(5):1123–32.

250. Chen, Inna; Raymond, Victoria M; Geis, Jennifer A; Collisson, Eric A; Benny, V; Hermann KL et al. Ultrasensitive plasma ctDNA KRAS assay for detection , prognosis , and assessment of therapeutic response in patients with unresectable pancreatic ductal adenocarcinoma. *Oncotarget*. 2017;8(58):97769–86.
251. Campbell, Ian G; Russell, Sarah E; Choong, David Y H; Montgomery, Karen G; Ciavarella, Marianne L; Hooi CSF et al. Mutation of the PIK3CA Gene in Ovarian and Breast Cancer. *Cancer Res*. 2004;64(21):7678–81.
252. Bader, Andreas G; Kang, Sohye; Vogt PK. Cancer-specific mutations in PIK3CA are oncogenic in vivo. *Proc Natl Acad Sci U S A*. 2006;103(5):1475–9.
253. Zhao, Li; Vogt PK. Helical domain and kinase domain mutations in p110 α of phosphatidylinositol 3-kinase induce gain of function by different mechanisms. *Proc Natl Acad Sci U S A*. 2008;105(7):2652–7.
254. Carson, Jeffrey D; Aller, Glenn V A N; Lehr, Ruth; Sinnamon, Robert H; Kirkpatrick, Robert B; Auger KR et al. Effects of oncogenic p110 α subunit mutations on the lipid kinase activity of phosphoinositide 3-kinase. *Biochem J*. 2008;409(2):519–24.
255. Iverson, Cory; Larson, Gary; Lai, Chon; Yeh, Li-tain; Dadson, Claudia; Weingarten P et al. RDEA119 / BAY 869766 : A Potent , Selective , Allosteric Inhibitor of MEK1 / 2 for the Treatment of Cancer. *Cancer Res*. 2009;69(17):6839–48.
256. Lim, Ho Yeong; Merle, Philippe; Weiss, Karl Heinz; Yau, Thomas; Ross, Paul; Yen CJ et al. Phase II Studies with Refametinib or Refametinib plus Sorafenib in Patients with RAS -mutated Hepatocellular Carcinoma. *Clin cancer Res*. 2018;24(19):4650–61.
257. Van Laethem, Jean-Luc; Reiss, Hanno; Jassem J. Phase I/II study of Refametinib (BAY 86-9766) in combination with Gemcitabine in advanced pancreatic cancer. *Target Oncol*. 2017;12(1):97–109.
258. Lim HY. Phase II Study of Refametinib, a MEK Inhibitor, as Second-line Treatment in Advanced Biliary Tract Adenocarcinoma [Internet]. *ClinicalTrials.gov*. [cited 2018 Sep 11]. p. *ClinicalTrials.gov* Identifier: NCT02346032. Available from: <https://clinicaltrials.gov/ct2/show/NCT02346032>
259. Liu, N; Haegebarth, A; Puehler, F; Scholz, A; Hoffmann, J; Dubowy R et al.

- Combination of PI3K inhibitor BAY 80-6946 and allosteric MEK inhibitor BAY 86-9766 (RDEA119) is a promising approach for the treatment of colorectal cancers Combination of PI3K inhibitor BAY 80-6946 and allosteric MEK inhibitor BAY 86-9766 (RDEA119) i. In: 22nd EORTC-NCI-AACR symposium. Berlin, Germany;
260. Clarke, Paul A; Roe, Toby; Swabey, Kate; Hobbs, Steve M; Mcandrew, Craig; Tomlin K et al. Dissecting mechanisms of resistance to targeted drug combination therapy in human colorectal cancer. *Oncogene*. 2019;38(25):5076–90.
 261. Wee, Susan; Wiederschain, Dmitri; Maira, Sauveur-michel; Loo, Alice; Miller, Christine; Stegmeier F et al. PTEN-deficient cancers depend on PIK3CB. *Proc Natl Acad Sci U S A*. 2008;105(35):13057–62.
 262. Samuels, Yardena; Diaz, Luis A; Schmidt-kittler, Oleg; Cummins, Jordan M; Delong, Laura; Cheong I et al. Mutant PIK3CA promotes cell growth and invasion of human cancer cells. *Cancer Cell*. 2005;7(6):561–73.
 263. Jing, Junping; Greshock, Joel; Holbrook, Joanna Dawn; Gilmartin, Aidan; Zhang, Xiping; Mcneil E et al. Comprehensive Predictive Biomarker Analysis for MEK Inhibitor GSK1120212. *Mol Cancer Ther*. 2012;11(3):720–9.
 264. Rice, Kenneth D; Aay, Naing; Anand, Neel K; Blazey, Charles M; Bowles, Owen J; Bussenius J et al. Novel Carboxamide-Based Allosteric MEK Inhibitors: Discovery and Optimization Efforts toward XL518 (GDC-0973). *ACS Med Chem Lett*. 2012;3(5):416–21.
 265. Choo, Edna; Ng, Chee M; Berry, Leanne; Belvin M. PK-PD modeling of combination efficacy effect from administration of the MEK inhibitor GDC-0973 and PI3K inhibitor GDC-0941 in A2058 xenografts. *Cancer Chemother Pharmacol*. 2013;71(1):133–43.
 266. Cheon, Seul-ki; Kim, Hwang-phill; Park, Ye-lim; Jang, Jee-eun; Lim, Yoojoo; Song S et al. Macrophage migration inhibitory factor promotes resistance to MEK blockade in KRAS mutant colorectal cancer cells. *Mol Oncol*. 2018;12(8):1398–409.
 267. Okabe, Seiichi; Tauchi, Tetsuzo; Tanaka, Yuko; Sakuta, Juri; Ohyashiki K. Combination therapy with copanlisib and ABL tyrosine kinase inhibitors against Philadelphia chromosome-positive resistant cells. *Oncotarget*. 2016;7(33):53116–26.
 268. Dewert, Nadin; Schneider, Philine; Liu, Ningshu; Emmert S. A novel

- selective small-molecule PI3K inhibitor is effective against human multiple myeloma in vitro and in vivo. *Blood Cancer J.* 2013;3(9).
269. Mckenna, W Gillies; Muschel, Ruth J; Gupta, Anjali K; Hahn, Stephen M; Eric J. The RAS signal transduction pathway and its role in radiation sensitivity. *Oncogene.* 2003;22(37):5866–75.
 270. Sklar MD. The ras Oncogenes Increase the Intrinsic Resistance of NIH 3T3 Cells to Ionizing Radiation. *Science* (80-). 1988;239(4840):645–7.
 271. Gupta, Anjalil K; Cerniglia, George J; Mick, Rosemarie; Ahmed M. Radiation sensitization of human cancer cells in vivo by inhibiting the activity of PI3K using LY294002* 1. *Int J Radiat Oncol Biol Phys.* 2003;56(3):846–53.
 272. Gupta, Surbhi; Ramjaun, Antoine R; Haiko, Paula; Wang, Yihua; Warne PH et al. Binding of Ras to Phosphoinositide 3-Kinase p110 a Is Required for Ras- Driven Tumorigenesis in Mice. *Cell.* 2007;129(5):957–68.
 273. Gupta, Anjali K; Bakanauskas, Vincent J; Cerniglia, George J; Cheng, Yi; Bernhard, Eric J; Muschel, Ruth J; Mckenna WG. The Ras Radiation Resistance Pathway 1. *Cancer Res.* 2001;61(10):4278–82.
 274. Wee, Susan; Jagani, Zainab; Kay, Xiaoqin Xiang; Loo, Alice; Dorsch, Marion; Yao YM et al. PI3K pathway activation mediates resistance to MEK inhibitors in KRAS mutant cancers. *Cancer Res.* 2009;69(10):4286–93.
 275. Gryffe, Robert; Kim, Hyeja; Hsieh, Eugene T.K.; Aronson MD. Tumour microsatellite instability and clinical outcome in young patients with colorectal cancer. *N Engl J Med.* 2000;342(2):69–77.
 276. Domingo, Enric; Freeman-mills, Luke; Rayner, Emily; Glaire, Mark; Briggs, Sarah; Vermeulen L et al. Somatic POLE proofreading domain mutation , immune response , and prognosis in colorectal cancer : a retrospective , pooled biomarker study. *Lacet Gastroenterol Hepatol.* 2016;1(3):207–16.
 277. Innocenti, Federico; Ou, Fang-Shu; Qu, Xueping; Zemla, Tyler J; Niedzwiecki D. Mutational Analysis of Patients With Colorectal Cancer in CALGB/SWOG 80405 Identifies New Roles of Microsatellite Instability and Tumor Mutational Burden for Patient Outcome. *J Clin Oncol.* 2019;37(14):1217–27.
 278. Morris, Van K.; Overman, Michael J.; Jiang, Zhi-Qin; Garrett, Chris; Agarwal S. Progression-Free Survival Remains Poor Over Sequential Lines of Systemic Therapy in Patients with BRAF-mutated Colorectal Cancer. *Clin Colorectal Cancer.* 2014;13(3):164–71.

279. Yoshifumi, S; Mu, Yusuke; Masayuki, N; Ichika H. BRAF V600E and SRC mutations as molecular markers for predicting prognosis and conversion surgery in Stage IV colorectal cancer. *Sci Rep.* 2019;9(1):1–10.
280. Bonetti, Luca Reggiani; Barresi, Valeria; Maiorana, Antonino; Manfredini, Samantha; Caprera, Cecilia; Bettelli S. Clinical Impact and Prognostic Role of KRAS / BRAF / PIK3CA Mutations in Stage I Colorectal Cancer. *Hindawi.* 2018;2018:Article ID 2959801.
281. Shen, Yinchen; Han, Xiaohong; Wang, Jianfei; Wang, Shuai; Yang, Hongying; Lu, Shih-hsin; Shi Y. Prognostic impact of mutation profiling in patients with stage II and III colon cancer. *Nat Publ Gr.* 2016;(April):1–7.
282. Ahmad, Abrar; Mannan, Abdul; Hahn-strömberg V. Kras , Braf , PIK3CA and EGFR Gene Mutations are Associated with Lymph Node Metastasis and Right Sided Colon Carcinoma. *J cancer Sci Ther.* 2016;5(May):122–9.
283. Yang, Shifeng; Yu, Xinmin; Fan, Yun; Shi, Xun; Jin Y. Clinicopathologic characteristics and survival outcome in patients with advanced lung adenocarcinoma and KRAS mutation. *J Cancer.* 2018;9(16):2930–7.
284. Li, Weihua; Liu, Yi; Cai, Shaoxin; Yang, Changshun; Lin, Zhizun; Zhou, Liyuan; Liu L. Not all mutations of KRAS predict poor prognosis in patients with colorectal cancer. *Int J Clin Exp Pathol.* 2019;12(3):957–67.
285. Fu, Xin-hui; Chen, Zhi-ting; Wang, Wen-hui; Fan, Xin-juan; Huang, Yan; Wu X et al. KRAS G12V Mutation is an Adverse Prognostic Factor of Chinese Gastric Cancer Patients. *J cancer.* 2019;10(4):821–8.
286. Renaud, Stephane' Flacoz; Pierre-Emmanuel; Schaeffer, Mickael; Guenot, Dominique; Romain, Benoit; Olland A. Prognostic value of the KRAS G12V mutation in 841 surgically resected Caucasian lung adenocarcinoma cases. *Br J Cancer.* 2015;(113):1206–15.
287. Thierry, Alain R; Mouliere, Florent; El Messaoudi, Safia; Mollevi, Caroline; Lopez-Crapez, Evelyne; Rolet F. Clinical validation of the detection of KRAS and BRAF mutations from circulating tumor DNA. *Nat Med.* 2014;20(4):430–5.

Appendices

Gene	Role	Diseases associated with mutation
APC	Tumour suppressor Cell migration and adhesion Transcription Apoptosis Required for MM9 up-regulation through the JNK pathway in CRC cells.	Familial adenomatous polyposis (FAP)
TP53	Tumour suppressor Transcription DNA binding Cell cycle arrest Apoptosis DNA repair	Range of cancers including Li-Fraumeni syndrome
SYNE1	May be involved in nuclear centrosome attachment	
PRKDC	Encoded protein is a member of the PI3K family. DNA double break strand repair Transcription	
TTN	Forms striated muscle	
KRAS		Multiple forms of cancer incl CRC
LRP2	Reuptake of multiple ligands including MAPK scaffold proteins and JNK interacting proteins Cell-signalling	

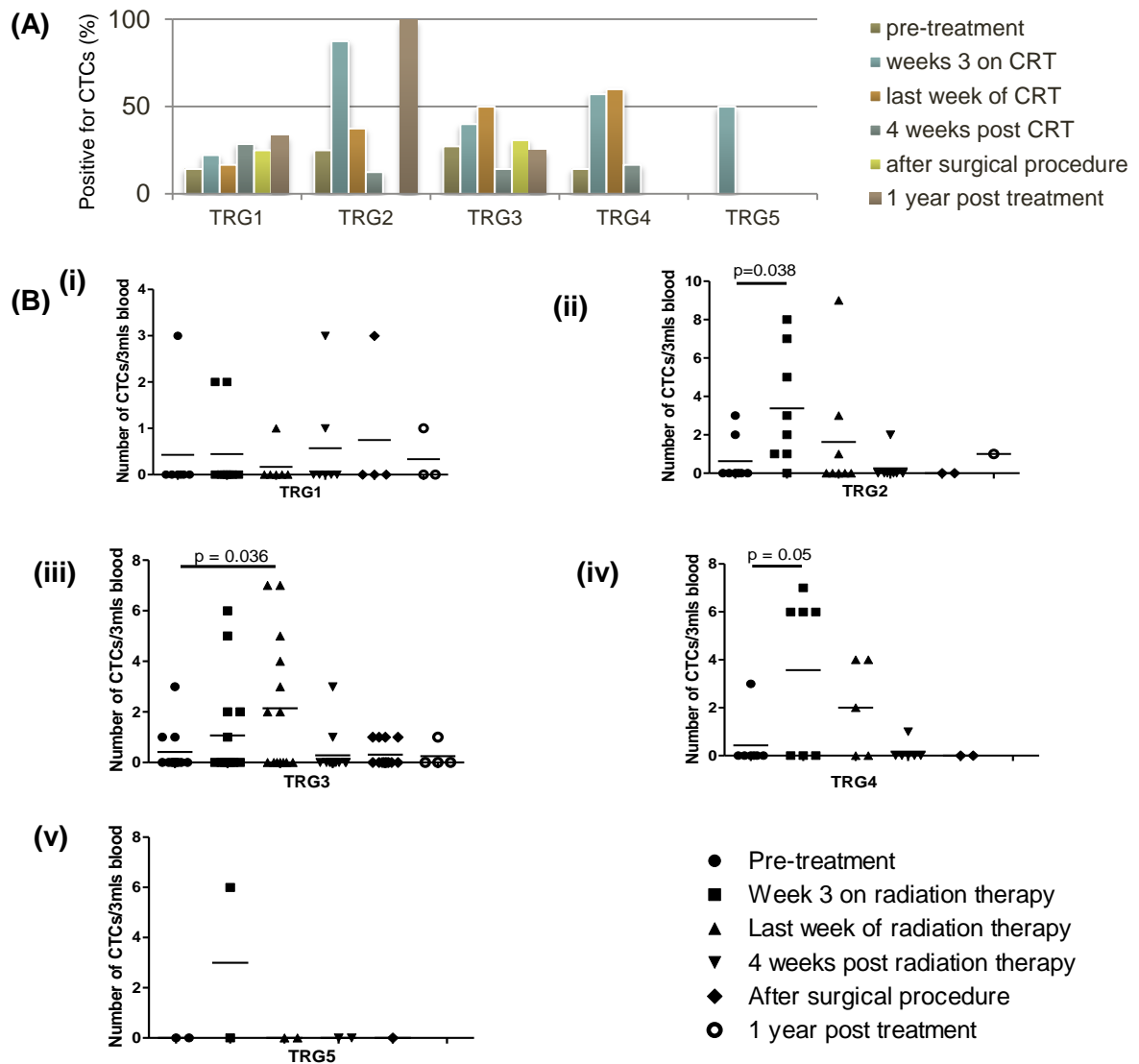
Supplementary table 1: Roles and diseases associated with genes commonly mutated in LARC patient samples in whole-exome sequencing study.

Gene	Role
ALG10	Translation
CEP290	Associated with cancer
GRK4	Phosphorylation of G-protein coupled receptors Activation of signal transduction pathways Associated with PI3K pathway
KMT2C	Transcription Associated with cancer
MROH2A	Intracellular transport
NAV2	Cellular growth and migration Associated with cancers
NOLC1	Ribosomal processing and modification GTPase and ATPase activity
PDE11A	Associated with cancer
PGAP1	Translation
PTPRJ	Cellular growth and migration Differentiation Proliferation (negative regulator) Cell adhesion Mitosis Oncogenic formation Vascular development Tyrosine phosphatase Associated with PI3K and MAPK pathways Associated with CRC
SOX5	Transcription
TCF20	Transcription (PI3K pathway – including JUN and SP1) (MAPK pathway including PAX6 and ETS1) Associated with cancer Associated with PI3K and MAPK pathways
TRIM8	Cell trafficking DNA repair Associated with cancer Cell signalling
TSC22D1	Transcription Tumour suppression
ZNF275	Transcription

Supplementary table 2: Roles associated with good responders to NACRT in whole-exome sequencing study.

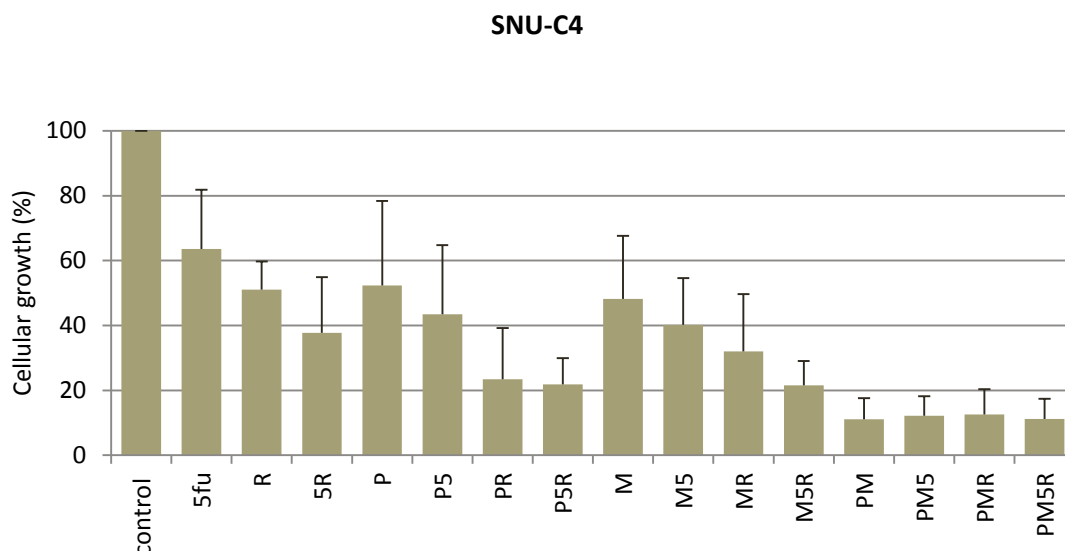
Gene	Function
APOB	Main apolipoprotein for chylomicrons and low-density lipoprotein. Occurs in 2 main isoforms Apo-B48 (synthesized in the gut), and APO-B100 (synthesized in the liver).
CASP4	Apoptosis, Necrosis Inflammation
CD93	Intercellular adhesion Clearance of apoptotic cells.
DSCAM	Central and nervous system development. Intracellular signalling of MAPK pathway
IGHV3-11	Participates in antigen recognition.
PCDHA12	Cell-cell connections in the brain
PZP	Inhibits the activity of all four classes of proteinases
RANBP2	Control a variety of cellular functions through its interactions with other proteins.
TCTE1	
ZIC1	Transcription Neurogenesis. Important in early stage of development of the central nervous system.

Supplementary table 3: Roles associated with poor responders to NACRT in whole-exome sequencing study



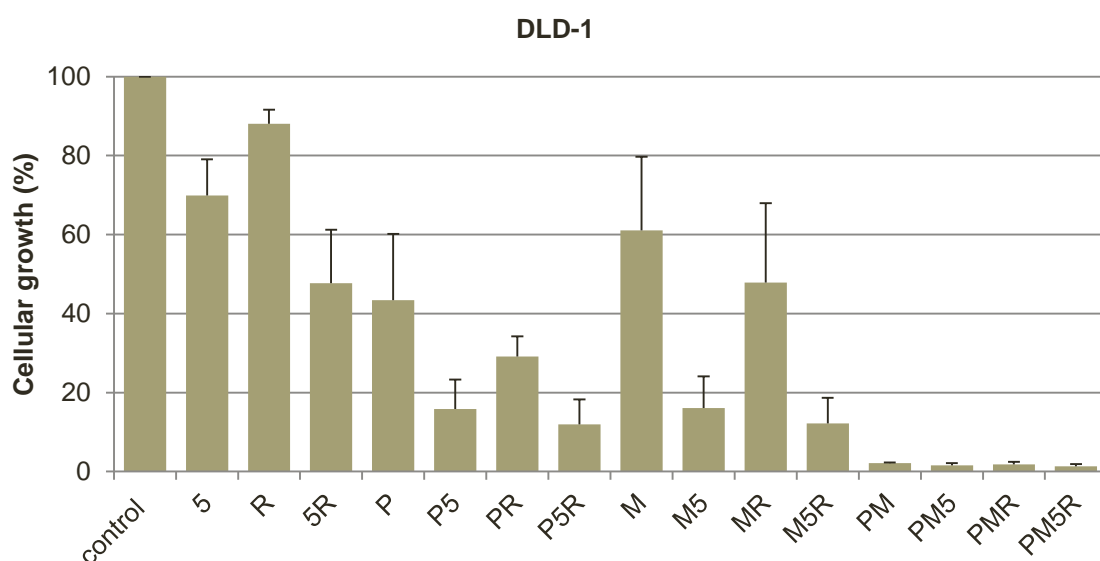
Supplementary figure 1: The relationship between serial circulating tumour cell (CTC) counts and TRG status (A) Percentage of samples positive for CTCs according to time-point and TRG grade. (B) Number of CTCs identified in 3mls blood per sample in (i) TRG1, (ii) TRG2, (iii) TRG3, (iv) TRG4, and (v) TRG5 patients.

LARC patients (n=66) were enrolled into a clinical trial. Blood was drawn at 6 time-points before, during and after chemoradiation therapy (CRT). Blood (3mls) was filtered through a ScreenCell CY device and stained with haematoxylin and eosin to detect CTCs. (A) Bar chart represents the percentage of samples which tested positive for CTCs at each of the 6 time-points in patients subdivided by TRG status. (B) Scatter plots depict the number of CTCs/3mls blood at each time-point. Each dot is representative of a sample. Mean values are represented as a bar. Significant differences ($p < 0.05$) are indicated. F-tests for two sample variances were used to calculate F and F-critical values, and the corresponding t-test was carried out.



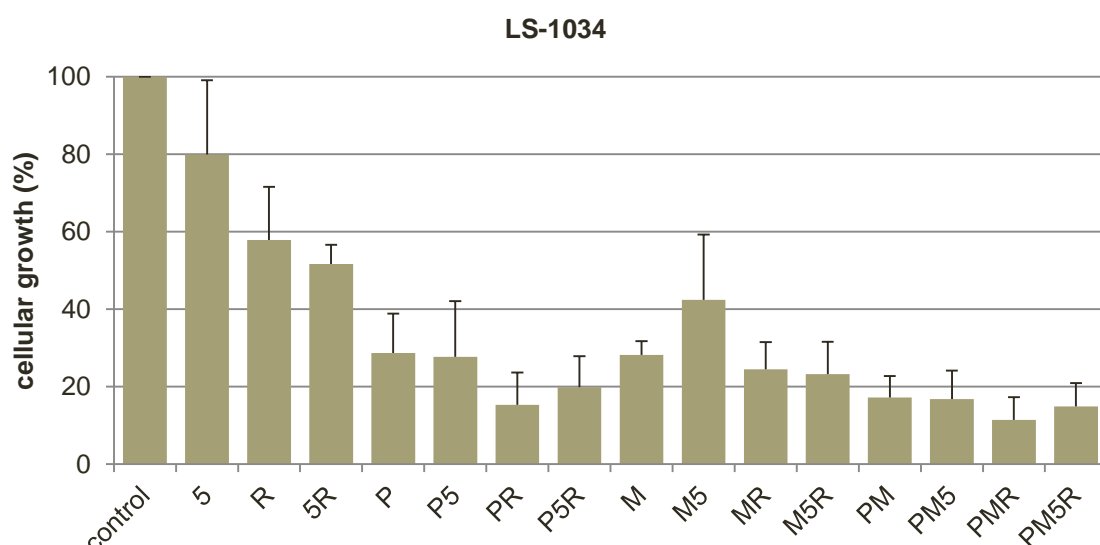
Supplementary figure 2: Cellular growth of PIK3CA^{mut} SNU-C4 cell line in clonogenic assays.

2,000 PIK3CA^{mut} CRC cells (SNU-C4) were plated in T25 flasks (20mls per flask) and incubated for 24 hours. Cells were treated with PI3K inhibitor copanlisib (P) (3.1nm), MEK inhibitor refametinib (M) (4.4nm), 5-FU chemotherapy (5) (130nm) and radiation (R) (2Gy). Cells were incubated until colony formation (2 weeks). Cells were fixed and stained with 0.1% crystal violet. Wells were rinsed with 1ml acetic acid to remove crystal violet, which was subsequently diluted (1:5), and the staining intensity was read on a plate reader at 595nm. Error bars represent the standard deviation, with experiments run in triplicate. Data are representative of the mean and standard deviation of 3 independent experiments. *p<0.05 compared to control, **P<0.05 compared to 5-fu chemoradiotherapy (5R). Representative clonogenic assays are shown in panel B (4x magnification) and C (macroscopic view of the flask).



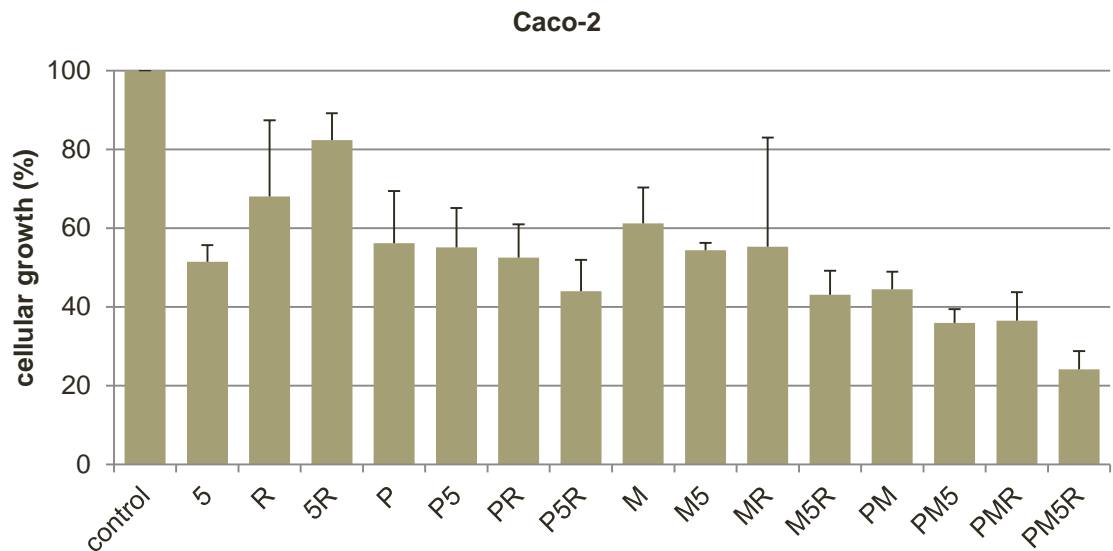
Supplementary figure 3: Cellular growth of PIK3CA-KRAS^{mut} DLD-1 cell line in clonogenic assays.

1,000 PIK3CA-KRAS^{mut} CRC cells (DLD-1) were plated in T25 flasks (20mls per flask) and incubated for 24 hours. Cells were treated with PI3K inhibitor copanlisib (P) (50nm), MEK inhibitor refametinib (M) (500nm), 5-FU chemotherapy (5) (730nm) and radiation (R) (2Gy). Cells were incubated until colony formation (2 weeks). Cells were fixed and stained with 0.1% crystal violet. Wells were rinsed with 1ml acetic acid to remove crystal violet, which was subsequently diluted (1:5), and the staining intensity was read on a plate reader at 595nm. Error bars represent the standard deviation, with experiments run in triplicate. Data are representative of the mean and standard deviation of 3 independent experiments. * $p < 0.05$ compared to control, ** $P < 0.05$ compared to 5-fu chemoradiotherapy (5R). Representative clonogenic assays are shown in panel B (4x magnification) and C (macroscopic view of the flask).



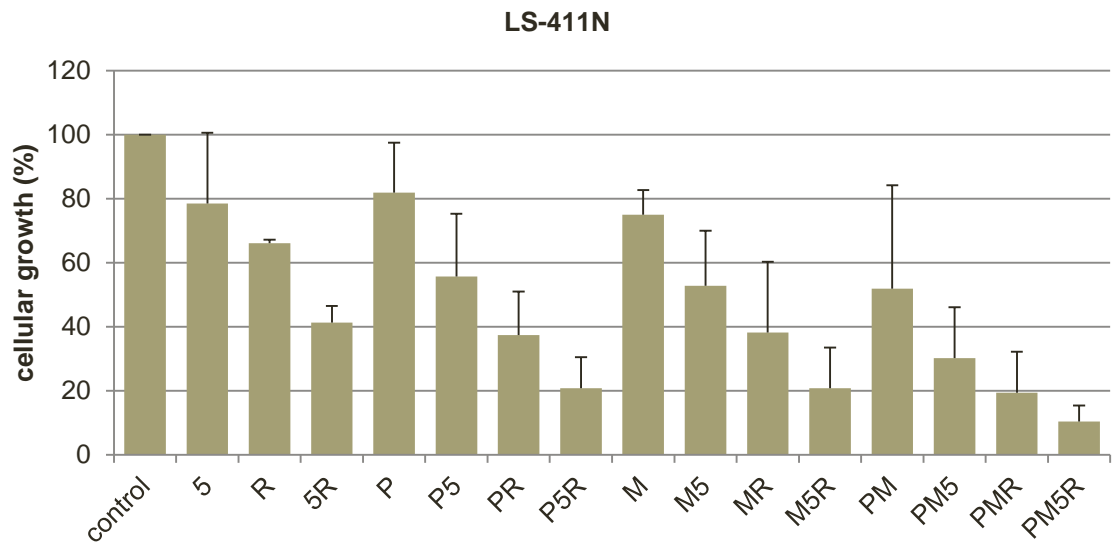
Supplementary figure 4: Cellular growth of KRAS^{mut} LS-1034 cell line in clonogenic assays.

3,000 KRAS^{mut} CRC cells (LS-1034) were plated in T25 flasks (20mls per flask) and incubated for 24 hours. Cells were treated with PI3K inhibitor copanlisib (P) (8.6nm), MEK inhibitor refametinib (M) (33nm), 5-FU chemotherapy (5) (60nm) and radiation (R) (2Gy). Cells were incubated until colony formation (2 weeks). Cells were fixed and stained with 0.1% crystal violet. Wells were rinsed with 1ml acetic acid to remove crystal violet, which was subsequently diluted (1:5), and the staining intensity was read on a plate reader at 595nm. Error bars represent the standard deviation, with experiments run in triplicate. Data are representative of the mean and standard deviation of 3 independent experiments. * $p < 0.05$ compared to control, ** $P < 0.05$ compared to 5-fu chemoradiotherapy (5R). Representative clonogenic assays are shown in panel B (4x magnification) and C (macroscopic view of the flask).



Supplementary figure 5: Cellular growth of wild-type Caco-2 CRC cell line in clonogenic assays.

50,000 wild-type CRC cells (Caco-2) were plated in T25 flasks (20mls per flask) and incubated for 24 hours. Cells were treated with PI3K inhibitor copanlisib (P) (6.1nm), MEK inhibitor refametinib (M) (250nm), 5-FU chemotherapy (5) (130nm) and radiation (R) (2Gy). Cells were incubated until colony formation (2 weeks). Cells were fixed and stained with 0.1% crystal violet. Wells were rinsed with 1ml acetic acid to remove crystal violet, which was subsequently diluted (1:5), and the staining intensity was read on a plate reader at 595nm. Error bars represent the standard deviation, with experiments run in triplicate. Data are representative of the mean and standard deviation of 3 independent experiments. * $p < 0.05$ compared to control, ** $P < 0.05$ compared to 5-fu chemoradiotherapy (5R) *** $p < 0.05$ compared to P5R or M5R. Representative clonogenic assays are shown in panel B (4x magnification) and C (macroscopic view of the flask).

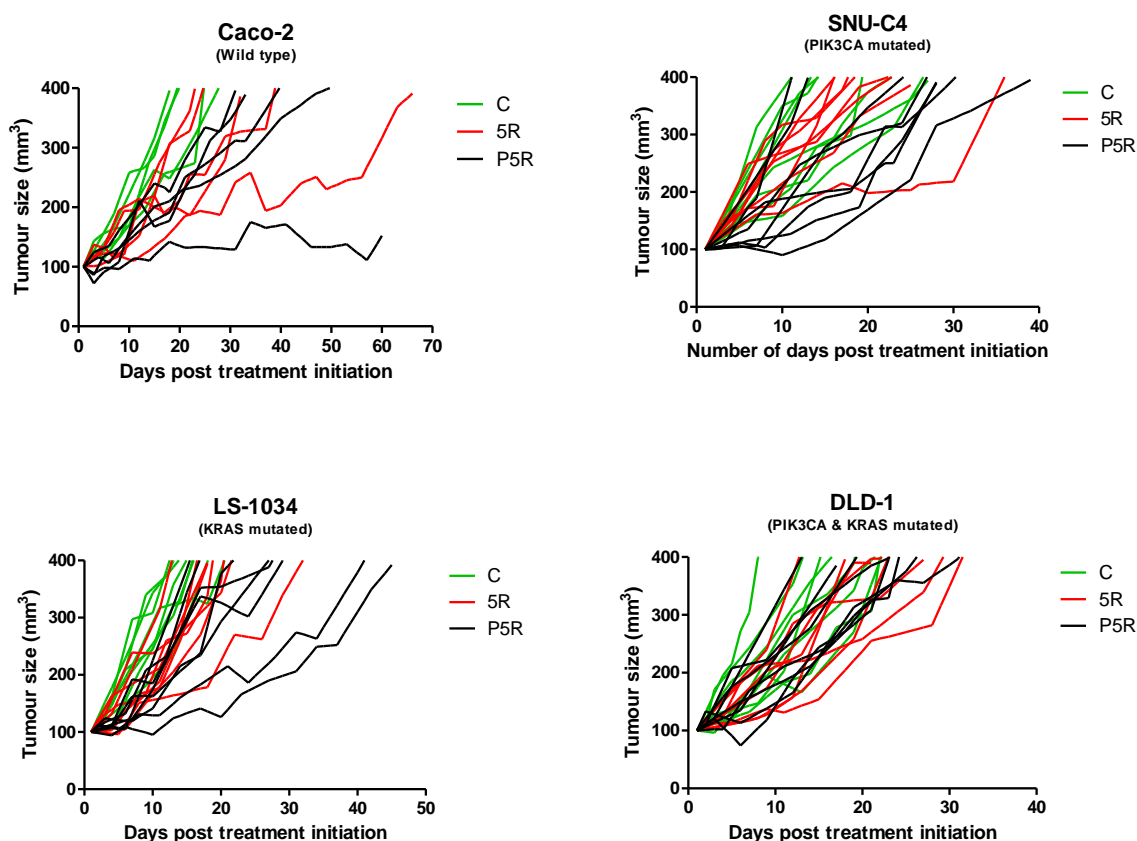


Supplementary figure 6: Cellular growth of BRAF^{mut} LS-411N in clonogenic assays.

5,000 BRAF^{mut} CRC cells (LS-411N) were plated in T25 flasks (20mls per flask) and incubated for 24 hours. Cells were treated with PI3K inhibitor copanlisib (P) (100nm), MEK inhibitor refametinib (M) (4.6nm), 5-FU chemotherapy (5) (290nm) and radiation (R) (2Gy). Cells were incubated until colony formation (2 weeks).

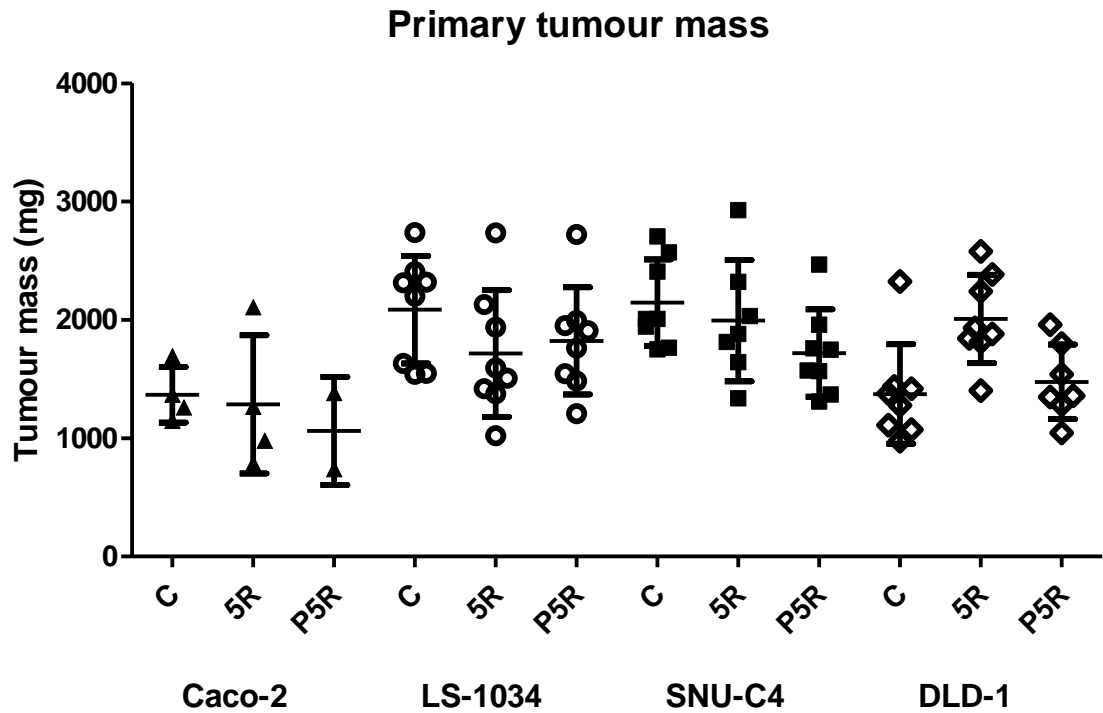
Cells were fixed and stained with 0.1% crystal violet. Wells were rinsed with 1ml acetic acid to remove crystal violet, which was subsequently diluted (1:5), and the staining intensity was read on a plate reader at 595nm. Error bars represent the standard deviation, with experiments run in triplicate. Data are representative of the mean and standard deviation of 3 independent experiments. * $p < 0.05$ compared to control, ** $p < 0.05$ compared to 5-fu chemoradiotherapy (5R).

*** $p < 0.05$ compared to P5R or M5R. Representative clonogenic assays are shown in panel B (4x magnification) and C (macroscopic view of the flask).



Supplementary figure 7: Tumour growth for each wild-type (Caco-2), PIK3CA (SNU-C4), KRAS (LS-1034) and PIK3CA-KRAS (DLD-1) xenograft model.

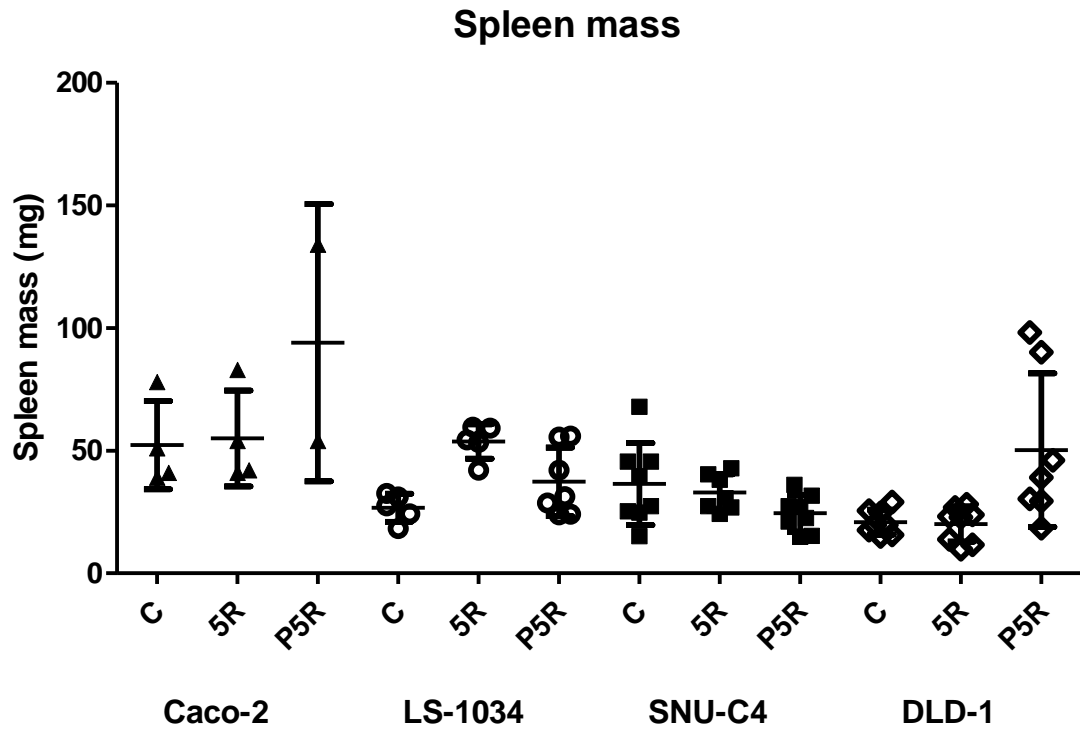
Colorectal cancer cells ($PIK3CA^{mut}$ (SNU-C4), $n = 2.5 \times 10^6$ cells/100ul; $KRAS^{mut}$ (LS-1034), $n = 2.5 \times 10^6$ cells/100ul; $PIK3CA-KRAS^{mut}$ (DLD-1), $n = 2.5 \times 10^6$ cells/100ul; wild-type (Caco-2), $n = 3.5 \times 10^6$ cells/100ul) were implanted in the right flank of 6-8 week old BALB/C SCID mice. When tumours reached 100mm³, mice were randomised into untreated control (C) (green), 5-fluorouracil (5-FU) chemoradiotherapy (5R) (red) and copanlisib plus chemoradiotherapy (P5R) (black) treatment arms. Copanlisib (7mg/kg) was administered intravenously twice a day on days 1 and 2. 5-FU chemotherapy (20mg/kg) was administered intraperitoneally, and mice were subsequently radiated in a Faxitron CP 160 x-ray generator at 1.8Gy on days 1, 3 and 5. Tumour measurements were taken every third day until tumours reached 400mm³, when mice were sacrificed. The grey box indicates the 5 days whilst treatment was ongoing. Error bars are representative of standard deviations in each treatment group. Mice whose survival rates were above or below the mean $\pm 2 \times$ s.d. were removed from the analysis.



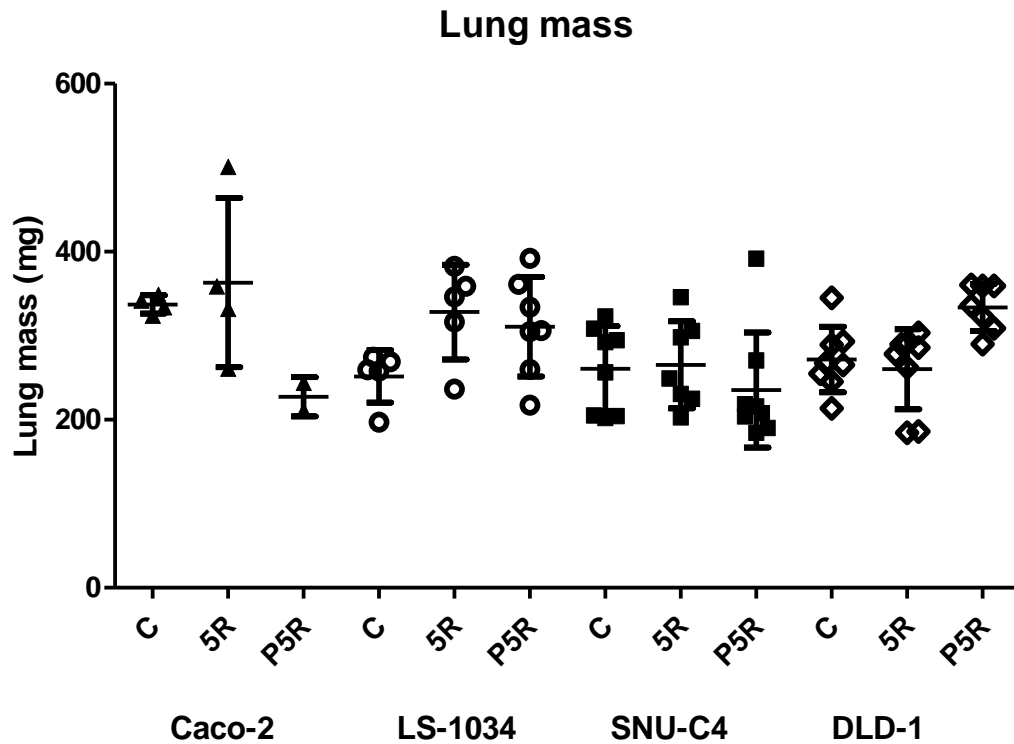
Supplementary figure 8: Scatter plot depicting tumour mass (mg) excised from wild-type (Caco-2 = ▲), KRAS mutated (LS-1034 = ○), PIK3CA mutated (SNU-C4 = ■) and PIK3CA-KRAS mutated (DLD-1 = ◇) xenograft models.

Cell line derived xenograft models were divided into control (C), chemoradiation (5R) or copanlisib-chemoradiation (P5R) treatment cohorts. Tumours were allowed to develop to 100mm³, at which time mice were administered intravenous copanlisib (14mg/kg/day) for 2 days, intraperitoneal chemotherapy (20mg/kg) and radiated (1.8Gy) on days 1, 3 and 5. Mice were sacrificed when tumours reached 400mm³; and tumour, liver, lungs and spleen were excised.

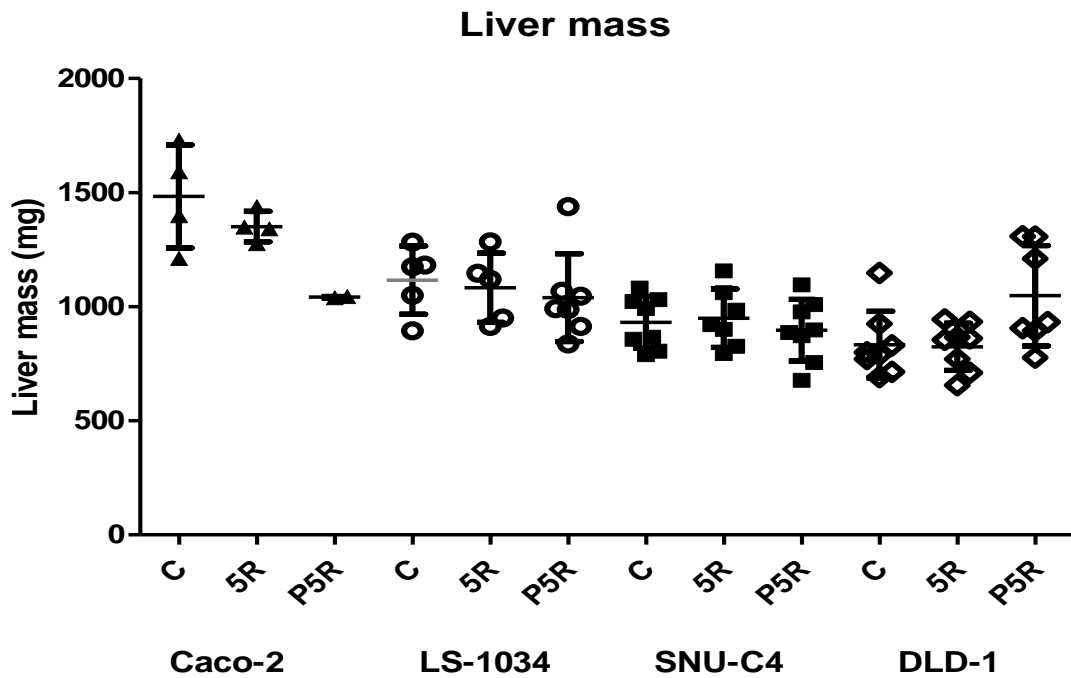
Error bars are representative of the mean and standard deviations per treatment group.



Supplementary figure 9: Scatter plot depicting spleen mass (mg) excised from wild-type (Caco-2 = ▲), KRAS mutated (LS-1034 = ○), PIK3CA mutated (SNU-C4 = ■) and PIK3CA-KRAS mutated (DLD-1 = ◇) xenograft models. Cell line derived xenograft models were divided into control (C), chemoradiation (5R) or copanlisib-chemoradiation (P5R) treatment cohorts. Tumours were allowed to develop to 100mm^3 , at which time mice were administered intravenous copanlisib (14mg/kg/day) for 2 days, intraperitoneal chemotherapy (20mg/kg) and radiated (1.8Gy) on days 1, 3 and 5. Mice were sacrificed when tumours reached 400mm^3 ; and tumour, liver, lungs and spleen were excised. Error bars are representative of the mean and standard deviations per treatment group.



Supplementary figure 10: Scatter plot depicting lung mass (mg) excised from wild-type (Caco-2 = ▲), KRAS mutated (LS-1034 = ○), PIK3CA mutated (SNU-C4 = ■) and PIK3CA-KRAS mutated (DLD-1 = ◇) xenograft models. Cell line derived xenograft models were divided into control (C), chemoradiation (5R) or copanlisib-chemoradiation (P5R) treatment cohorts. Tumours were allowed to develop to 100mm³, at which time mice were administered intravenous copanlisib (14mg/kg/day) for 2 days, intraperitoneal chemotherapy (20mg/kg) and radiated (1.8Gy) on days 1, 3 and 5. Mice were sacrificed when tumours reached 400mm³; and tumour, liver, lungs and spleen were excised. Error bars are representative of the mean and standard deviations per treatment group.



Supplementary figure 11: Scatter plot depicting liver mass (mg) excised from wild-type (Caco-2 = ▲), KRAS mutated (LS-1034 = ○), PIK3CA mutated (SNU-C4 = ■) and PIK3CA-KRAS mutated (DLD-1 = ◇) xenograft models. Cell line derived xenograft models were divided into control (C), chemoradiation (5R) or copanlisib-chemoradiation (P5R) treatment cohorts. Tumours were allowed to develop to 100mm³, at which time mice were administered intravenous copanlisib (14mg/kg/day) for 2 days, intraperitoneal chemotherapy (20mg/kg) and radiated (1.8Gy) on days 1, 3 and 5. Mice were sacrificed when tumours reached 400mm³; and tumour, liver, lungs and spleen were excised. Error bars are representative of the mean and standard deviations per treatment group.